



**This electronic thesis or dissertation has been downloaded from the University of Bristol Research Portal, <http://research-information.bristol.ac.uk>**

*Author:*

**Zampetakis, Ioannis**

*Title:*

**Cactus Based Solids**

**General rights**

Access to the thesis is subject to the Creative Commons Attribution - NonCommercial-No Derivatives 4.0 International Public License. A copy of this may be found at <https://creativecommons.org/licenses/by-nc-nd/4.0/legalcode>. This license sets out your rights and the restrictions that apply to your access to the thesis so it is important you read this before proceeding.

**Take down policy**

Some pages of this thesis may have been removed for copyright restrictions prior to having it been deposited on the University of Bristol Research Portal. However, if you have discovered material within the thesis that you consider to be unlawful e.g. breaches of copyright (either yours or that of a third party) or any other law, including but not limited to those relating to patent, trademark, confidentiality, data protection, obscenity, defamation, libel, then please contact [collections-metadata@bristol.ac.uk](mailto:collections-metadata@bristol.ac.uk) and include the following information in your message:

- Your contact details
- Bibliographic details for the item, including a URL
- An outline nature of the complaint

Your claim will be investigated and, where appropriate, the item in question will be removed from public view as soon as possible.

# CACTUS BASED SOLIDS

---

Ioannis Zampetakis

A dissertation submitted to the University of Bristol in accordance with the  
requirements for award of the degree of Doctor of Philosophy in the Faculty of  
Engineering,

Submitted September 2019

~43000 words

## ABSTRACT

---

Biological materials have always been on the forefront of the development of novel materials either through the use of the biological material itself or *via* the development of bioinspired materials that mimic the structures observed in nature. Plant fibres specifically have demonstrated significant application potential in the automotive industry through their use as composite reinforcements while their interesting structures have prompted the development of superior bioinspired materials. The focus of this thesis is to further investigate the morphological properties and application potential of the fibres obtained from the biological material of cactus species *Opuntia ficus indica*. Initially, in Chapter 4, the morphology of these cactus fibres is investigated in order to gain a better understanding of the mechanical properties they demonstrate. A fractal geometry characterization methodology is developed in an attempt to explain the hierarchical structure characteristics present while the morphology is compared to other commonly used natural fibres. The morphological information obtained is then utilized in Chapter 5 for the development of cactus bioinspired materials *via* 3D printing. The developed materials are mechanically characterized, and their mechanical properties are compared to those of the original cactus fibres to determine whether the morphology present is directly related to the mechanical behaviour. Moreover, the application potential of these 3D printed analogues is assessed *via* mechanical comparison with other 3D printed structure as well as dynamic mechanical testing. In Chapter 6, the last results chapter, the cactus fibres are used as a biological material for the development of novel thermoplastic and hydrogel composite materials. The materials developed are compared with other natural fibres in terms of mechanical properties to determine the mechanical benefits obtained *via* the use of the cactus fibres. Additionally, a bone tissue engineering application route is followed utilizing the cactus fibres as a natural reinforcement for a hydrogel bioink for tissue engineering application providing a novel approach to mechanically reinforce scaffolds for biomedical applications.

## ACKNOWLEDGEMENTS

---

I would like to thank and acknowledge the following people for all their support and help for the completion of this thesis. First and foremost, I would like to thank my parents, my siblings and all my family for their endless support throughout this process making this work possible. I would also like to thank my friends Iakwbos, Marios, Manolis, Ioannis K. Elia, and my partner Elena for their patience and continued support throughout the completion of this work.

I would also like to acknowledge my two supervisors Prof. Fabrizio Scarpa and Prof. Adam Perriman. They both believed in me and gave me an opportunity to pursue this work while always helping me with great ideas important support and always encouraging me to develop my skills further. Thanks to their guidance and mentorship I was able to understand what it means to be a scientist and how I can achieve my dream to be one. I would also like to thank Dr. Ben Woods for all the insightful conversations help on completing this work.

I would also like to acknowledge Yousef Dobah for all his help and various conversations in understanding various techniques that were new to me. Also, Carl Marsh, Graham Day and Bethany Hickton for their help and **support** throughout this process. Moreover, I would also like to thank the ACCIS Office and Perriman Group for all the support. Specifically, Dr. Weinjin Xiao for all her help in the stem cell techniques training. Also, Dr. Dong Liu for her help in obtaining µCT measurements *in situ* with 3-point bending tests.

Last but not least I would like to acknowledge the ACCIS Lab support, ACCIS office support and the ACCIS Lab technicians for all their help with all the logistics and training required to carry out this work specifically Steven Rae, Katie Smith, Ian Chorley & Allison McIntosh-Smith.

## **DECLARATION**

---

I declare that the work in this dissertation was carried out in accordance with the requirements of the University's Regulations and Code of Practice for Research Degree Programmes and that it has not been submitted for any other academic award. Except where indicated by specific reference in the text, the work is the candidate's own work. Work done in collaboration with, or with the assistance of, others, is indicated as such. Any views expressed in the dissertation are those of the author.

SIGNED: ..... DATE: .....

# **Research Output**

---

## **Publications:**

Billon K, **Zampetakis I**, Scarpa F, Ouisse M, Sadoulet-Reboul E, Collet M, et al. Mechanics and band gaps in hierarchical auxetic rectangular perforated composite metamaterials. Composite Structures. 2017;160:1042-50.

Deller RC, Carter BM, **Zampetakis I**, Scarpa F, Perriman AW. The effect of surface charge on the thermal stability and ice recrystallization inhibition activity of antifreeze protein III (AFP III). Biochemical and Biophysical Research Communications. 2018;495(1):1055-60.

Deller RC, Richardson T, Richardson R, Bevan L, **Zampetakis I**, Scarpa F, et al. Artificial cell membrane binding thrombin constructs drive *in situ* fibrin hydrogel formation. Nature Communications. 2019;10(1):1887.

## **Conference Papers:**

**Zampetakis Ioannis**, Hetherington Alistair, Perriman Adam & Scarpa Fabrizio (2018) ‘Cactus-Based Solids And Bio-Composites For Energy Dissipation In Defence And Biomedical Applications.’ 18<sup>th</sup> European Conference on Composite Materials-ECCM 18, Athens, Greece, 24-28th June 2018, 1594-512

## **Manuscripts in Review:**

**Zampetakis I**, Dobah Y, Liu D, Woods B, Bezazi A, Perriman A.W, Scarpa F, **Abnormal stiffness behaviour in artificial cactus-inspired reinforcement materials**, Submitted to *Advanced Materials*, 2019

Dobah Y, **Zampetakis I**, Ward C, Scarpa F, **Thermoformability characterisation of flax reinforced polypropylene composite materials**, Submitted to *Composites Part B*, 2019

## **Undergraduate Student Supervision:**

Dissertation: Cactus bone: a new bioink for osteogenic tissue engineering

Edward Blackburn

Date Submitted: 08/03/2018

# Table of Contents

---

Abstract.....	2
Acknowledgements.....	3
Declaration.....	4
Research Output.....	5
Table of Contents.....	6
List of Figures.....	10
List of Tables.....	18
1. Preface-Thesis Overview.....	19
2. Introduction.....	21
2.1 Background and Applications of Opuntia Ficus Indica.....	21
2.2 Fractals.....	23
2.2.1 Brief Theoretical Background.....	23
2.2.2 Applications.....	25
2.3 Biological & Bioinspired Materials.....	26
2.3.1 Biological Materials Through Literature .....	26
2.3.2 Bioinspiration and Biomimicry leads to Novel Synthetic Materials.....	28
2.3.3 3D Printing & bioinspired 3D Printed Materials.....	30
2.4 Composites.....	32
2.4.1 Composites Theoretical Background.. .....	32
2.4.2 Filler Based Composites.....	34
2.4.3 Natural Fibre Composites.....	35
2.5 Hydrogels & Composite Hydrogels.....	38
2.6 Applications.. .....	40
2.6.1 Defence Related Applications.....	40
2.6.2 Tissue Engineering.....	43
2.6.2.1 Bone & Bone Tissue Engineering.....	45
2.6.2.2 Bone tissue Engineering & Bioprinting.....	47
2.7 Thesis Aims.. .....	48
3. Materials & Methods.....	50
3.1 Theoretical Backround on Material Characterization Techniques.....	50
3.1.1 Mechanical Properties.....	50

3.1.2 Microcomputed Tomography ( $\mu$ CT) imaging in materials and biomaterials....	51
3.2 Extraction of Cactus Fibres.....	52
3.3 Ball Mill.. .....	52
3.4 Fractal Morphology Characterization.....	52
3.4.1 Optical Microscopy.....	52
3.4.2 Scaning Electron Microscopy (SEM).....	53
3.4.3Analytical & Algorithmic Procedures.. .....	53
3.4.4 User Defined Thresholding.. .....	54
3.4.5 MATLAB graythres () function.....	55
3.4.6 Bradley Thresholding Method.....	55
3.4.7 Hausdim.m.....	55
3.4.8 Boxcount.m.....	56
3.4.9 Edge_Detection_approach.m.....	56
3.4.10 Multifractal.m.....	56
3.4.11 Microcomputed Tomography ( $\mu$ CT) measurements.....	57
3.4.12 Mechanical Testing.. .....	57
3.5 Artificial Cactus Inspired Reinforcement Materials.....	58
3.5.1 Microcomputed Tomography ( $\mu$ CT) measurements.....	58
3.5.2 Polylactic Acid (PLA) 3D Printing.....	58
3.5.3 Stereolithography (SLA) 3D Printing.....	58
3.5.4 Specimen Manufacturing.. .....	58
3.5.5 Mechanical Testing & Analysis.....	59
3.5.6 Normalization Formulas.....	59
3.5.7 Finite Element Model.. .....	60
3.6 Cactus Based Thermoplastic and Hydrogel Composites.....	61
3.6.1 Fourier-Transform Infrared Spectroscopy.....	61
3.6.2 Thermoplastic Composites.....	61
3.6.3 Dynamic Mechanical Analysis (DMA). .....	61
3.6.4 Cell Culture.....	62
3.6.5 Hydrogel.. .....	63
3.6.6 Hydrogel Fibres.....	63
3.6.7 Rheology.. .....	63
3.6.8 Extrusion & Crosslinking.....	64
3.6.9 Compression Testing.....	64

3.6.10 Cell Viability & Cytotoxicity.....	64
3.6.11 Stem Cell Differentiation.....	65
3.6.12 Alkaline Phosphatase (ALP) Assay.....	65
3.6.13 Histological Analysis.....	65
3.6.14 Critical Point Drying for Scanning Electron Microscopy of Hydrogels.....	66
3.6.15 Roughness Measurements.....	66
3.7 Microcomputed tomography ( $\mu$ CT) for Hydrogels and Composites.....	66
3.7.2 Thermoplastic Composites Microcomputed tomography ( $\mu$ CT).....	66
3.6.17 Hydrogel & Hydrogel Composites Microcomputed tomography ( $\mu$ CT) with differentiated stem cells.....	67
4. Fractal Morphology Characterization.....	68
4.1 Chapter Overview.....	68
4.2 Results & Discussion.....	69
4.2.1 Fractal Characterization of Cacti Fibres.....	69
4.2.2 Fractal Characterization of Natural Fibres & Comparisons.....	74
4.2.3 Multifractal Characterization of the Cacti Fibres.....	82
4.2.4 Fractal Characterization of Synthetic Fibres & Comparisons.....	85
4.3 Conclusions.....	88
5. Artificial Cactus Inspired Reinforcement Materials.....	89
5.1 Chapter Overview.....	89
5.2 Results & Discussions.....	91
5.2.1 Development of 3D rendered models.....	91
5.2.2 Manufacturing & Testing of 3D Printed Specimens.....	92
5.2.3 Comparison of Cactus 3D Printed Analogues with Control Equivalent Beam..	96
5.2.4 Finite Element Simulation Results.....	102
5.3 Conclusions.....	109
6. Cactus Based Thermoplastic and Hydrogel Composites.....	111
6.1 Chapter Overview.....	111
6.2 Results & Discussion.....	112
6.2.1 Natural Fibre Characterization.....	112
6.2.2 Natural Fibre Hydrogel bioink composites.....	113
6.2.3 Thermoplastic natural fibre composites.....	117
6.2.4 Alicona Surface Measurements.....	120
6.2.5 Bioink Morphological Characterization.....	121

6.2.6 Cell Viability and Cytotoxicity.....	123
6.2.7 Bone Tissue Engineering Evaluation.....	127
6.2.8 Osteogenic Potential of Composite Bioinks.....	133
6.3 Conclusions.....	135
7. Conclusions.. ..	136
8. Future Work.....	139
9. Bibliography.....	143
APPENDIX.. ..	162

## List of Figures

---

<b>Figure #</b>	<b>Description</b>	<b>Pg #</b>
<b>Figure 2.1</b>	Overview figure demonstrating the wide research and application potential of <i>Opuntia Ficus Indica</i> .	22
<b>Figure 2.2</b>	Example of a fractal surface characterization using the box-counting method. Reproduced from guarino et.al <sup>21</sup> .	24
<b>Figure 2.3</b>	Schematic of 8 distinct structural motifs prevalent in natural materials <sup>41</sup>	27
<b>Figure 2.4</b>	Comparison between natural nacre (a-c) and artificial nacre. Figure is obtained from Finnmore et.al. <sup>181</sup>	29
<b>Figure 2.5</b>	Examples of Bioinspired 3D printed materials enabling to replicate the microstructure observed in nature. Figure is reproduced from Martin et. al <sup>63</sup>	31
<b>Figure 2.6</b>	Examples of Composite materials consisting of a matrix material and different types of reinforcing elements. d from Gibson. <sup>182</sup>	33
<b>Figure 2.7</b>	Demonstration of the inner structure of natural fibres as found in nature, demonstrating the presence of cellulose, hemicellulose and the other parts within the fibre. Reproduced from Pandey et.al. <sup>81</sup>	36
<b>Figure 2.8</b>	Examples of various natural fibre biocomposites using various different polyme matrices and natural fibre reinforcements. Reproduced from Bledzki et. al. <sup>183</sup>	37
<b>Figure 2.9</b>	Example of a composite hydrogel system using PCL microfibres as the mechanical reinforcement. Reproduced from Visser et.al <sup>115</sup>	39
<b>Figure 2.10</b>	Composite material design utilized for impact and energy absorption. Reproduced from Qiao et. al <sup>121</sup> .	42
<b>Figure 2.11</b>	Example of Aircraft wing shape morphing. Reproduced from Sofla et.al <sup>131</sup>	43
<b>Figure 2.12</b>	Representation of the process of bone tissue engineering based on a scaffold tissue engineering approach. Reproduced from Amini et. al <sup>146</sup>	46

<b>Figure 2.13</b>	Example of bioink system demonstrating internal porosity and structural fidelity for biomedical applications. Reproduced from Perriman et. al <sup>103</sup>	48
<b>Figure 3.1</b>	Demonstration of the user defined algorithm application. It is evident that from the histogram there is a distinct ‘peak’ (red box) of pixel intensity values and frequency. This peak signifies the pixel intensity of the object of interest and the rest the pixel values of the background thus in this case the threshold would be set as $I>100$ and $I<200$ where I is pixel intensity.	54
<b>Figure 3.2</b>	Cactus fibre specimen for X-Ray Micro-Computed Tomography ( $\mu$ CT) measurements	57
<b>Figure 3.3</b>	Mould Design for the manufacturing of the thermoplastic composite specimens	61
<b>Figure 4.1</b>	The fractal order of the above figures was maintained at 1.6 for the whole fibre sheets and the smaller piece.	70
<b>Figure 4.2</b>	The images displayed demonstrate the Micro-Computed Tomography ( $\mu$ CT) scan results of the structural subunit of the cactus fibre structure. The fractal order of these images was also estimated at 1.6.	70
<b>Figure 4.3</b>	Reconstructed image of the cactus fibre sheet from the Micro-Computed Tomography ( $\mu$ CT) data obtained. Fractal analysis revealed that the value of these images is also at 1.6.	71
<b>Figure 4.4</b>	Tensile testing of cactus piece (a) Force vs Displacement data and (b) Stress Vs Strain Data. All tests were carried out according to ASTM D638-14 (n=5)	72
<b>Figure 4.5</b>	3-Point Bending testing of cactus piece (a) Force vs Displacement data and (b) Stress Vs Strain Data. All tests were carried out according to ASTM D790-17 (n=5)	72
<b>Figure 4.6</b>	The pictures demonstrated show images obtained for the cactus natural fibre Sheet at: A, 0x. B, 5x. C, 10x. D, 20x. E, 50x	74
<b>Figure 4.7</b>	The images displayed A through D displayed demonstrate 4 Scanning Electron Microscopy (SEM) images of the natural fibres at different	74

magnifications. The fractal order determined from the images was estimated at:  $1.80 \pm 0.13$ .

- Figure 4.8** The resulting fractal dimension estimations are plotted for each magnification image and SEM images of the cactus fibre sheath after the values obtained from each algorithm are averaged. (\* shows significant difference), (ANOVA,  $p<0.05$ ,  $n=5$ ). 75
- Figure 4.9** The pictures demonstrated show images obtained for the cactus natural fibre in powder form at: A, 5x. B, 10x. C, 20x. D, 50x. E, 100x 75
- Figure 4.10** The resulting fractal dimension estimations are plotted for each magnification image of the cactus processed powder after the values obtained from each algorithm are averaged. (\* shows significant difference), (ANOVA,  $p<0.05$ ,  $n=5$ ). 76
- Figure 4.11** The pictures demonstrated show images obtained for the Eucalyptus natural fibre sheet at: A, 5x. B, 10x. C, 20x. D, 50x. 76
- Figure 4.12** The pictures demonstrated show images obtained for the Eucalyptus natural fibre in powder format after ball milling at: A, 5x. B, 10x. C, 20x. D, 50x. E, 100x 77
- Figure 4.13** The pictures demonstrated show images obtained for the Flax natural fibre sheet at: A, 5x. B, 10x. C, 20x. D, 50x. 77
- Figure 4.14** The pictures demonstrated show images obtained for the Flax natural fibre in powder format after ball milling at: A, 5x. B, 10x. C, 20x. D, 50x. E, 100x 78
- Figure 4.15** The pictures demonstrated show images obtained for the Hemp natural fibre sheet at: A, 5x. B, 10x. C, 20x. D, 50x. 78
- Figure 4.16** The pictures demonstrated show images obtained for the Hemp natural fibre in powder format after ball milling at: A, 5x. B, 10x. C, 20x. D, 50x. E, 100x 79
- Figure 4.17** The pictures demonstrated show images obtained for the Rice Husk natural fibre sheet at: A, 5x. B, 10x. C, 20x. D, 50x. 79

<b>Figure 4.18</b>	The pictures demonstrated show images obtained for the Rice Husk natural fibre in powder format after ball milling at: A, 5x. B, 10x. C, 20x. D, 50x. E, 100x	80
<b>Figure 4.19</b>	The images displayed (A through D) demonstrate 4 Scanning Electron Microscopy (SEM) images of the natural fibres specifically: A, Eucalyptus. B, Flax. C, Hemp. D, Rice Husk.	80
<b>Figure 4.20</b>	The resulting fractal dimension estimations from the described algorithmic approach for each magnification of the optical microscope (OM) and Scanning electron Microscopy (SEM) images for all the natural fibres sheets. (* shows significant difference), (ANOVA, $p<0.05$ , $n=5$ ).	81
<b>Figure 4.21</b>	The resulting fractal dimension estimations from the described algorithmic approach for each magnification of the optical microscope (OM) and Scanning electron Microscopy (SEM) images for all the natural fibres powders after ball milling. (* shows significant difference), (ANOVA, $p<0.05$ , $n=5$ ).	81
<b>Figure 4.22</b>	The resulting multifractal spectra after applying the multifractal analysis algorithm on the cactus fibre sheet images for the three different thresholding techniques. A, User Defined Thresholding. B, MATLAB graythres () function. C, Bradley Thresholding Method.	83
<b>Figure 4.23</b>	The resulting multifractal spectra after applying the multifractal analysis algorithm on the cactus fibre powder images for the three different thresholding techniques. A, User Defined Thresholding. B, MATLAB graythres () function. C, Bradley Thresholding Method.	84
<b>Figure 4.24</b>	The pictures demonstrated show images obtained for the Glass Fibre synthetic fibre sheet at: A, 5x. B, 10x. C, 20x. D, 50x.	85
<b>Figure 4.25</b>	The pictures demonstrated show images obtained for the Carbon Fibre synthetic fibre sheet at: A, 5x. B, 10x. C, 20x. D, 50x.	85
<b>Figure 4.26</b>	The resulting fractal dimension estimations from the described algorithmic approach for each magnification of the optical microscope (OM) images for all the natural fibres and synthetic fibre sheets. (* shows significant difference), (ANOVA, $p<0.05$ , $n=5$ ).	86

<b>Figure 4.27</b>	Example of our fractal estimation algorithm being implemented in a Koch Snowflake image yielding a fractal order value of 1.27 (1.2682) which is very close to the known fractal value of the Koch snowflake at 1.26.	87
<b>Figure 5.1</b>	The process from obtaining the imaging data of the cactus structure and those being used for the generation of 3D rendered models for mechanical testing of the bioinspired cactus structure.	91
<b>Figure 5.2</b>	Tensile testing of cactus bioinspired 3D printed PLA analogues at 100% infill (a) Force vs Displacement data and (b) Stress Vs Strain Data. All tests were carried out according to ASTM D638-14 (n=5)	92
<b>Figure 5.3</b>	3-Point Bending testing of cactus bioinspired 3D printed Polylactic Acid (PLA) analogues at 100% infill (a) Force vs Displacement data and (b) Stress Vs Strain Data. All tests were carried out according to ASTM D790-17 (n=5)	93
<b>Figure 5.4</b>	Tensile testing of cactus bioinspired 3D printed Polylactic Acid (PLA) analogues at 10% infill (a) Force vs Displacement	93
<b>Figure 5.5</b>	3-Point Bending testing of cactus bioinspired 3D printed Polylactic Acid (PLA) analogues at 10% infill (a) Force vs Displacement data and (b) Stress Vs Strain Data. All tests were carried out according to ASTM D790-17 (n=5)	93
<b>Figure 5.6</b>	Tensile testing of cactus bioinspired 3D printed Stereolithography analogues (a) Force vs Displacement data and (b) Stress Vs Strain Data. All tests were carried out according to ASTM D638-14 (n=5)	94
<b>Figure 5.7</b>	3-Point Bending testing of cactus bioinspired 3D printed Stereolithography (SLA) analogues (a) Force vs Displacement data and (b) Stress Vs Strain Data. All tests were carried out according to ASTM D790-17 (n=5)	94
<b>Figure 5.8</b>	Graphic representation of the control equivalent beam used for comparisons for the cactus 3D printed analogue structure.	96
<b>Figure 5.9</b>	Comparison of 3D printed Polylactic Acid (PLA) control equivalent beam specimens with cactus 3D printed analogue specimens at 10% infill in 3-Point Bending Flexural Modulus. ASTM D790-17 (n=5)	96

<b>Figure 5.10</b>	Comparison of 3D printed Polylactic Acid (PLA) control equivalent beam specimens with cactus 3D printed analogue specimens at 100% infill in 3-Point Bending Flexural Modulus. ASTM D790-17 (n=5)	97
<b>Figure 5.11</b>	Comparison of 3D printed Stereolithography (SLA) control equivalent beam specimens with cactus 3D printed Stereolithography (SLA) analogue specimens in 3-Point Bending Flexural Modulus. ASTM D790-17 (n=5)	97
<b>Figure 5.12</b>	Comparison of 3D printed Polylactic Acid (PLA) control equivalent beam specimens with cactus 3D printed analogue specimens at 10% infill in 3-Point Bending Specific Flexural Modulus. ASTM D790-17 (n=5).	98
<b>Figure 5.13</b>	Comparison of 3D printed Polylactic Acid (PLA) control equivalent beam specimens with cactus 3D printed analogue specimens at 100% infill in 3-Point Bending Specific Flexural Modulus. ASTM D790-17 (n=5)	99
<b>Figure 5.14</b>	Comparison of 3D printed Stereolithography (SLA) control equivalent beam specimens with cactus 3D printed Stereolithography (SLA) analogue specimens in 3-Point Bending Flexural Modulus. ASTM D790-17 (n=5)	99
<b>Figure 5.15</b>	Graphic Representation of the Specific Flexural modulus of the control and cactus specimen demonstrating there is no significant difference between the different manufacturing methods used. (one tailed t-test, $p<0.05$ * demonstrates significant difference)	100
<b>Figure 5.16</b>	Tensile Stress Vs Strain (a) and Flexural Stress Vs Flexural Strain graphs (b) for the control equivalent PLA 10% & SLA specimens to determine the bending to axial stiffness ratio (n=5).	101
<b>Figure 5.17</b>	ANSYS modelling finite element simulations for the 3 Point Bending Testing Specimens of the cactus 3D printed Polylactic Acid (PLA) & SLA analogue structures at different infills.	103
<b>Figure 5.18</b>	Micro-Computed Tomography ( $\mu$ CT) scans showing the internal and macro porosity of the Cactus 3D Printed PLA Specimens justifying the porosity of the ANSYS finite element simulation.	104

<b>Figure 5.19</b>	ANSYS modelling finite element simulations for the Tensile Testing Specimens of the cactus 3D printed Polylactic Acid (PLA) & SLA analogue structures at different infills.	105
<b>Figure 5.20</b>	Comparison of Ideal simulation (100% Infill) and Experimental data for Cactus 3D Printed Polylactic Acid (PLA) analogues in axial loading.	105
<b>Figure 5.21</b>	Comparison of Ideal simulation (100% Infill) and Experimental data for Cactus 3D Printed Polylactic Acid (PLA) analogues in 3 Point Bending.	106
<b>Figure 5.22</b>	Comparison of Ideal simulation (100% Infill) and Experimental data for Cactus 3D Printed Stereolithography (SLA) analogues in axial loading.	106
<b>Figure 5.23</b>	Comparison of Ideal simulation (100% Infill) and Experimental data for Cactus 3D Printed Stereolithography (SLA) analogues in 3 Point Bending.	107
<b>Figure 5.24</b>	In situ Micro-Computed Tomography ( $\mu$ CT) scans and flexural bending of cactus fibres demonstrating swarming effect of fibrils.	108
<b>Figure 6.1</b>	The Fourier Transform Infrared Spectroscopy (FTIR) results of all the natural fibres used for this work demonstrating that there is no chemical modification present as all natural fibres present peaks in the same regions.	112
<b>Figure 6.2</b>	Storage Modulus (a), loss Modulus (b) and viscosity (c) of all the hydrogel and hydrogel composites to ensure the extrudability of the cactus-based gels ( $n=5$ ).	115
<b>Figure 6.3</b>	Compressive modulus comparison between control hydrogels and different hydrogel composites.	116
<b>Figure 6.4</b>	Micro-Computed Tomography ( $\mu$ CT) results of the PLA thermoplastic composites manufactured.	118
<b>Figure 6.5</b>	In situ 3 point bending tests of PLA and PLA cactus composites. It is observed that mechanical reinforcement is achieved in flexural loading at a significantly low weight percent of cactus fibre filler at 3% w/w. The mechanical reinforcement is attributed to the presence	119

of the cactus filler increasing the material strength both in compression and tensile loading.

- Figure 6.6** Storage Modulus Dynamic Mechanical Aanalysis (DMA) results of PLA and PLA natural fibre composites in 3 point bending. 119
- Figure 6.7** (a)Cactus and (b) Hemp Alicona surface measurements results demonstrating the differences in roughness demonstrated by these two types of natural fibres 120
- Figure 6.8** Comparison of Scanning Electron Microscopy (SEM) Micrographs between Control Hydrogels and Cactus Hydrogel composites. 122
- Figure 6.9** Confocal Images demonstrating the interaction of the cactus fibres with stem cells showing no effect on cell viability (Day 7). 124
- Figure 6.10** Confocal images assessing the cell viability at Day 7 on (a) Control Hydrogels, (b) Cactus Hydrogel Composites, (c) Hemp Hydrogel Composites extruded through a 21- gauge needle via a syringe. 126
- Figure 6.11** Histology results for Control (a), Cactus Hydrogel Composites (b) and Hemp Hydrogel composites (c) after 21 days of differentiation. 128
- Figure 6.12** Micro-Computed ( $\mu$ CT) results for Non-cell containing Hydrogel (a) and Cell containing Cactus hydrogel after 21 days of differentiation (b). 130
- Figure 6.13** Compressive modulus comparison between control hydrogels and different hydrogel composites differentiated and undifferentiated. 132
- Figure 6.14** Alkaline Phosphatase (ALP) assay results comparison between tissue culture plastic (control) cactus fibres and hemp fibres 133
- Figure 6.15** Alkaline Phosphatase (ALP) assay results comparison between the hydrogel and the cactus composite hydrogel. 134

## LIST OF TABLES

---

Table #	Description	Pg #
<b>Table 4.1</b>	Axial and Flexural Modulus of the cactus fibre Piece and their ratio	73
<b>Table 5.1</b>	Tensile Testing Specimen Dimensions for Analysis	92
<b>Table 5.2</b>	Bending Testing Specimen Dimensions for Analysis	92
<b>Table 5.3</b>	Axial Modulus, Flexural Modulus and Ratios for all 3D printed specimens	94
<b>Table 5.4</b>	Mass, Volume, Density Characteristics of the Cactus and Control 3D Printed Specimens.	98
<b>Table 5.5</b>	Cummulative Results of Flexural Moduli and Specific Flexural Moduli for all control and cactus analogue specimens	100
<b>Table 5.6</b>	Axial Modulus, Flexural Modulus and Ratios for control 3D printed specimens.	102
<b>Table 5.7</b>	ANSYS 100% Infill Model Predicted moduli and ratios	107
<b>Table 6.1</b>	Flow indexes calculated <i>via</i> the Ostwald–de Waele relationship.	115
<b>Table 6.2</b>	Roughness Profile of Cactus and Hemp determined by Alicona surface measurements. The quantitative information obtained from the roughness profile demonstrated in the figure above	121

## 1. Preface-Thesis Overview

---

The aim of this thesis was to investigate the potential of cactus fibres in **a fibre sheet and fibre powder format** as well as a form of bioinspiration for the development of novel materials for energy dissipation and biomedical applications.

In Chapter 2 an extensive literature review is presented focusing on the main scientific areas that the current work is applied on and highlighting some of the gaps in the scientific knowledge that prompted the idea of pursuing this project. Chapter 3 includes an extensive description of the various methodologies and techniques utilized to obtain the experimental results required to reach the conclusions presented in the following chapters.

In chapter 4 the focus was maintained on acquiring a better understanding of the cactus fibre morphology to understand further the interesting mechanical properties observed on the cactus fibre sheath. Various imaging modalities were utilized to obtain information on the morphology of cactus fibres **both in sheath and powder format** across different scales to investigate the existence of a hierarchical structure that is prevalent in natural materials. The ability to obtain information across various scales combined with the traits of self-similarity observed prompted the idea to utilize fractal geometry for the characterization of the structure. An algorithm for the characterization of the fractal dimension of a structure through the use of various images was developed to achieve this goal.

The wealth of morphological information obtained from the fractal characterization of the structure prompted the pursuit of a bioinspiration and biomimicry approach to generate cactus structure analogue materials with **novel** mechanical properties, in chapter 5. Through the imaging analysis it was made possible to generate 3D rendered models of the cacti fibre structure that were utilized both for 3D printing of analogue materials as well as for finite element simulations. The novel cactus-based 3D printed analogue materials were mechanically characterized and compared to their biological material analogues to determine how their mechanical properties are maintained. The finite element simulations on the other hand enabled a further understanding of the mechanical behaviour of the cactus structure and how it can be manipulated. Besides the generation of novel fully characterize, materials based on the

inspiration of the cactus structure, this biomimicry approach served to provide additional evidence required for the fractality of the cactus observed.

In chapter 6, the cactus fibre as a biological material was utilized for the generation of novel biocomposite materials. The cactus fibre was implemented as a structural reinforcement of a hydrogel bioink system as well as a thermoplastic matrix, and the mechanical benefits obtained were compared to other natural fibres commonly used. Moreover, the biomedical application of the cactus fibres as filler reinforcement was assessed with preliminary bone tissue engineering work. To the author's knowledge this was the first attempt of utilizing directly obtained plant natural fibres as hydrogel structural reinforcement as well as the first attempt at implementing natural plant fibres for tissue engineering applications.

The thesis is then concluded in chapter 7 and chapter 8 where the main findings are summarized while the future work required is also presented.

## 2. Introduction

---

### 2.1 Background and Applications of *Opuntia Ficus Indica*

*Opuntia ficus indica*, shown in Fig. 2.1, is a plant that flourishes in various climates from temperate, to subtropical as well as cold regions due to its unique carassulacean acid metabolism, leaf tissue and cuticular waxes<sup>1</sup>. The *opuntia ficus Indica* plant and its fruit the prickly pear has been prevalent and in direct relationship with humans and animals for more than 2000 years<sup>2</sup>. The stems are comprised of a core tissue, called white parenchyma and the chlorophyll containing cortex tissue that enables photosynthetic procedures to take place<sup>226,227</sup>. It has also been reported that the cactus stems and fruits containing various low and high molecular weight compounds including minerals, vitamins, sugars and even amino acids, making them excellent candidates for the development of various food supplements and medical applications<sup>226,227</sup>. It has been shown that it is able to provide water for animals in desert and semi desert regions while recently it has found various applications<sup>3</sup>. This species of cactus plant has found its way as a biofuel with a recent company, Nopalmix, using the cactus plant as a direct biofuel for cars<sup>3</sup>. Furthermore, it has been shown in literature that the fruits and branches of this plant have significant medicinal effects ranging from anticancer and anti-diabetic effects<sup>1</sup> to wound healing in vivo by accelerating the reepithelialization and remodelling process<sup>5</sup>. Those medicinal applications are usually attributed to the abundance of sugars existing in the cladodes and the mucilage of the leaves of this plant<sup>6</sup>. These properties clearly demonstrate the potential that these natural fibres have as tissue engineering and regenerative materials since they have been shown to have positive effects on serious diseases as well as assisting the remodelling of tissue which is a primary goal of regenerative medicine. Therefore, the choice of this material as part of the composite material network bodes well for achieving a novel bone tissue engineering scaffold.

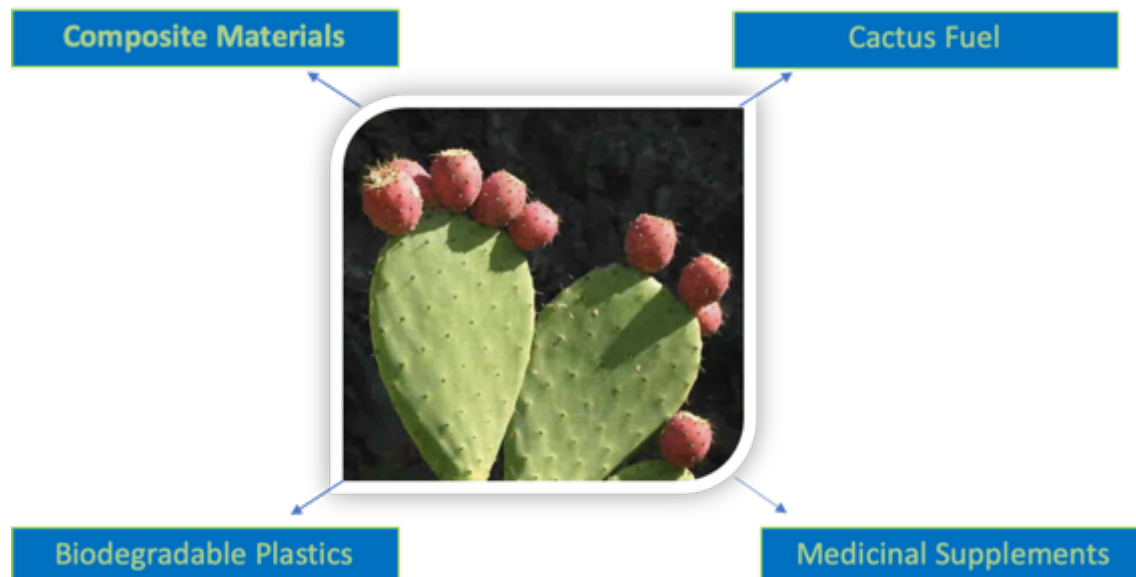


**Fig. 2.1** Overview figure demonstrating the wide research and application potential of *Opuntia Ficus Indica*.

The reason this specific fibre is the primary interest of this project is because composites fabricated with these cacti fibres demonstrate unique mechanical properties that are essential for impact and bone tissue engineering applications<sup>7-10</sup>. It has been shown that the introduction of *opuntia ficus indica* natural fibres in thermoplastic nanocomposites with styrene and butyl acetate yielded, unsurprisingly, materials with improved tensile modulus as the concentration of the fibres increased while showing good matrix entanglement and improvement of the thermal stability of the initial polymers<sup>8</sup>. In another study biocomposites generated with this natural fibre and PLA demonstrated that the interlaminar shear strength of the components was very high and that resulted in an improvement of the fatigue and toughness characteristics, while the flexural behaviour of the material was improved showing that such composites could find applications as semi-structural components, such as a bone tissue scaffold<sup>9</sup>. Moreover, natural fibre powder generated from the fibre sheaths of the *opuntia ficus indica* plant demonstrated significant increase in the tensile modulus when implemented as a PLA natural filler reinforcement<sup>10</sup>. Specifically with regards to impact and energy absorbing applications it has been reported<sup>9</sup> that biocomposites made from *opuntia ficus indica* fibres and polyester demonstrate a significantly higher flexural modulus compared to other composites as well as large energy dissipation under cyclic loading which is a very promising result in order to generate a composite material with interest in the field of impact energy absorbing materials and applications. This property is believed to have originated from the need of the plant to protect itself from herbivores, reflection of light and shading of the stem to reduce water loss, and those biological survival needs have given rise to these mechanical properties observed<sup>9,226,227</sup>. Moreover, additional applications of this natural fibre were pursued specifically focusing on tissue engineering and biomedical applications as a significant gap in plant fibre usage in tissue engineering was observed in the literature. The initial step of the

investigation focused on explaining the mechanical properties present on the cactus fibres and how they are related to its morphology through pursuing a fractal geometric analysis.

## 2.2 Fractals

### 2.2.1 Brief Theoretical Background

Benoit Mandelbrot is widely considered as the father of fractal geometry and he defined fractals as: ‘Beautiful, damn hard, increasingly useful. That’s fractals.’ Fractals have been an emerging field due to the fact that they have the ability to describe complex structures that Euclidean Geometry is unable to analyse while enabling the correct estimation of length and other quantities **of shapes like coastlines**<sup>11-13</sup>. As far as what defines a fractal, it is a complex object which when divided in parts each part is a smaller copy of the whole initial object<sup>11-13</sup>. This definition encloses the two main principles of fractal objects which are: i) self-similarity and self-affinity and ii) scale invariance<sup>11-13</sup>. Self-similarity and self-affinity are directly implied in the definition since a fractal object is essentially a multiple copy of itself. In this sense a fractal can be described as an infinite amount of repetitive self-similar patterns. With regards to scale invariance it is evident that since the object is manufactured of patterns that are repeated across all scales, no matter the scale of interest, the geometrical pattern of the fractal should be identical. Fractals are divided into two categories deterministic and random fractals<sup>13,14</sup>. Deterministic fractals are described and generated by a mathematical formula which means that they are produced through an infinitely repeated and iterative process<sup>13</sup> which ensures their identical self-similarity across scales. Random fractals are the type of fractals that are also most commonly found in nature and they do not have the same degree of self-similarity as deterministic fractals<sup>13</sup>. Rather they demonstrate a statistical self-similarity and a dilatational symmetry across a finite range of scales in the sense that enlargement of details have the same statistical distributions of the whole set<sup>13,14</sup>. We hypothesized that the cactus fibres belong in the random fractal category and their fractality is part of the reason of their interesting mechanical properties and we pursued this initial route for morphological characterization. One of the most important elements of fractal geometry, besides being able to characterize complex structures, is the fact that it is quantifiable through the definition of the fractal dimension. The fractal dimension is a real number (usually not an integer) that describes the complexity of a structure<sup>11-14</sup>. An easier way to grasp the meaning of the fractal dimension definition follows this paradigm<sup>12</sup>: let us consider an object and an element of this object is to be surrounded with a sphere of a given radius R and count the amount of object elements ‘r’ inside the sphere. The measure of ‘r’ can be arbitrary. This method is usually defined as the box counting method for

the estimation of the fractal order of an object, and an example of its application is shown in Fig. 2.2<sup>15,16</sup>.

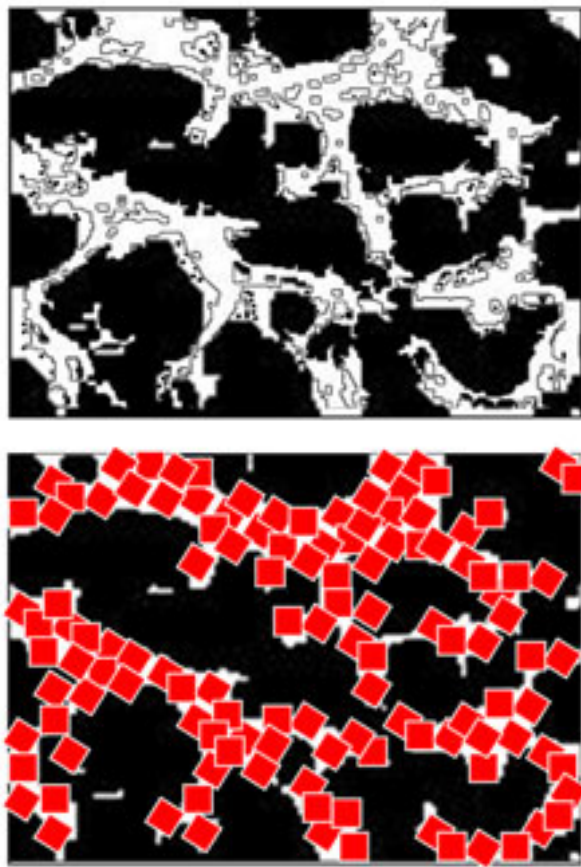


**Fig. 2.2** Example of a fractal surface characterization using the box-counting method. Reproduced from Guarino et.al<sup>21</sup>.

The box counting algorithm has been used successfully to characterize deterministic fractal orders of well-known fractal shapes such as the Cantor set (0.6) the Koch snowflake (1.26)<sup>15-17</sup>. There are other methods utilized for the estimation of the fractal dimension however in this thesis the focus was on the box counting algorithm as it is the simplest and most widely used method for the estimation of fractal orders in the literature<sup>18,19</sup>. There are also cases when complex structures have more than one self-similar pattern across scales in that case the object is characterized as a multifractal system and in that scenario a single fractal dimension is not enough to characterize its morphology, but a spectrum of fractal dimensions is utilized<sup>20</sup>. Now that a theoretical framework of fractals is established, it is evident why this approach was determined the best course of action for assessing the morphological characteristics of the *Opuntia ficus Indica* fibres since their morphology is too complex for a Euclidean characterization. The cellular morphology present within the cactus fibres<sup>11</sup> eludes to the presence of a hierarchy that could be self-affine and the investigation of this morphology is an essential aim of this study.

## **2.2.2 Applications**

Fractal geometry as described above can be a useful tool in quantifying the unique morphologies of structures that are not easy to characterize with conventional methods thus, they have started to gain more scientific interest in various application sectors including material characterization and biomedical applications<sup>22-31</sup>. Initially, fractal geometry has been used extensively to characterize the microstructure of bone<sup>22,27</sup>. It has been demonstrated that bone consists of a hierarchical fractal like structure that starts from the nanoscale and repeats itself all the way to the macroscale<sup>27</sup>. Through imaging across scales it was observed that there are helical motifs that are present through the bone structure across 9 to 10 orders of magnitude<sup>27</sup> signifying that there is prevalent self-affinity which as described is the fundamental characteristic for the presence of a fractal morphology<sup>11-13</sup>. Moreover, it was established that the fractality of the bone material is one of the fundamental reasons for its demonstrated unique mechanical properties<sup>27</sup>. Other applications were fractal characterization has been successfully utilized is in the biomedical sector where it has been used to distinctly characterize the size of tumours in the body for the assessment of imminent danger to the patient<sup>28</sup>. However, the field with the most applications of fractal characterization is that of material science<sup>23,26,29,30</sup>. It has been demonstrated that composites with a fractal microstructure demonstrate more efficient damping behaviour compared to composites with a random microstructure present, concluding that fractal microstructures are more efficient as a matrix toughening mechanism<sup>29</sup>. Furthermore, it has been shown that metamaterials with fractal implemented design have led to the generation of materials with significantly enhanced mechanical properties similarly in the case of fractal like honeycombs where a fractal morphology approach enabled the optimal design for function for the materials<sup>30,31</sup>. It is also important to note that the mechanical enhancement of materials due to a fractal microstructure is not affected by whether the fractal present is deterministic or random as we are only focusing at a few scales of the material microstructure. The fractal pattern prevalent at those few scales (which is not enough evidence to characterize the fractal as random or deterministic) leads to the improvement in the mechanical behaviour. Cellular materials have also found interesting applications in the medical sector due to their unique mechanical properties making them ideal candidates for angioplasty as well as novel lumbar fusion cages<sup>211-213</sup>. The properties and morphology of the *Opuntia Ficus Indica* fibres utilized in composites manufacturing hint at the existence of the prevalence of a hierarchical fractal like structure present<sup>9</sup>. One of the aims of this work is to initially develop a methodology for the characterization of a fractal structure based on the work that has been implemented<sup>31</sup>. Once the methodology was established a focus

was maintained on evaluating whether a fractal structure can be identified and at which scales is present, using the estimation of the fractal order as a tool, and if the prevalence of the fractal structure is correlated with the mechanical properties observed.

## ***2.3 Biological & Bioinspired Materials***

### ***2.3.1 Biological Materials Through Literature***

Nature's material designs have been evolving over large periods of time and tend to feature superior and robust functionalities depending on the specific needs of each organism<sup>32-34</sup>. Great examples of biological and natural materials that have no direct synthetic counterpart are bone, wood and bamboo. Over the years many attempts have been made to explain and justify the chemical, structural and morphological elements of these biological materials with their unusual properties<sup>34,35</sup>. One of the unique advantages of most natural materials is the fact that they are part of a living organism, and they are therefore able to constantly adapt and evolve depending on the environmental context in which they operate; a task that their synthetic counterparts are unable to perform. Nature is able to achieve superior and robust functions with very simple constituent materials. The three main reasons generally given in open literature about the optimization and robustness of natural materials lie in the interphase chemistry, the structural motifs and the functionality across length scales<sup>34,36</sup>. In terms of the interphase chemistry, it has been shown that nature combines hard and soft materials in a single interphase and thus is able to more efficiently adapt in various loading conditions<sup>37</sup>.

As far as structural architectures are concerned, there are eight distinct structural motifs, also presented in Fig. 2.3: i) fibrous, ii) helical, iii) gradient. iv) layered, v) tubular, vi) cellular, vii) suture and viii) overlapping structures<sup>38,41</sup>.

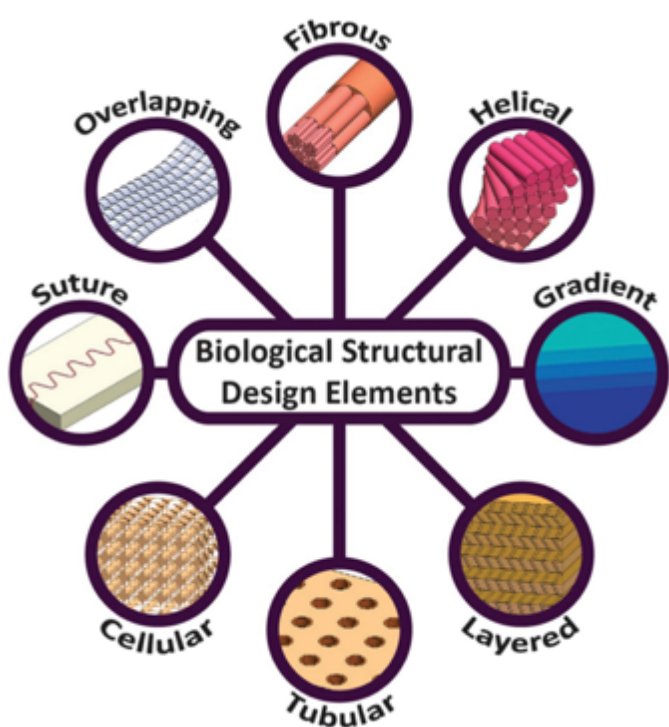


**Fig. 2.3** Schematic of 8 distinct structural motifs prevalent in natural materials<sup>41</sup>.

Biological materials have the ability to combine and adjust those structural gradients across various scales while using multiple ones in order to optimize functionalities to manage efficiently the different environmental loading scenarios. The chemical interphase and structural motifs that provide natural materials with their unique structural, mechanical and multi-functional properties, have also been observed in various synthetic materials and are common across many material manufacturing methods. The mechanism that potentially provides the most critical contribution in the development of the intrinsic properties of the biological materials is the presence of functionality across scales, as well as the multiscale structural characteristics<sup>32-34</sup>. Advances in imaging techniques have provided a unique insight on the multiscale structural elements of natural materials<sup>38</sup>, with an improved understanding of the underlying mechanisms and deformations associated to each structural element at different scales. These imaging techniques have highlighted the fact that through evolution nature performs a continuous **optimization of the morphologies and materials present in biological materials**. Through the use of various imaging modalities, it is evident that through evolution and continuous design cycles, nature has optimized the structure of biological materials across scales that are appropriate to their functionality. For instance, the continuous evolution of the highly porous hierarchical design of bone and bamboo has provided those materials with a high stiffness with significantly low weights<sup>34</sup>. **The information obtained via further studying and imaging biological materials**, provided further insight into the natural mechanisms enabling the use of simple and abundant materials to develop multifunctional and superior materials with unique properties, as is the example of bioinspired nacre-like materials that demonstrate unique toughness and strength combinations<sup>37</sup>. In particular, an in-depth analysis of biological materials across scales reveals the existence of very interesting

architectural features and the prevalence of hierarchical and self-similar structures<sup>32-38</sup>, the latter being an attribute of fractal geometry. The existence of hierarchy and self-similarity has been directly related to the mechanical and structural properties of various natural materials. The most common examples explored are those of bone<sup>39</sup>, nacre<sup>37</sup> and bamboo<sup>40</sup>, where it is demonstrated that the inherent hierarchy that exists within the structure leads to global unusual properties. As evident, there is a wealth of information regarding how the morphology and the synthesis of biological materials enable them to exhibit their intrinsic properties. As the OFI fibres are a biological material it was important to understand how other biological materials have been studied to understand the blueprint utilized, to develop a methodology to characterize the properties of these cactus fibres. Thus, we hypothesized in this thesis that there is a hierarchy present in the morphology of the OFI fibres that leads to its high bending to axial stiffness ratio. The fractal approach utilized did provide unique insight in the morphology and hierarchy present however it was determined that a better understanding of the mechanical behaviour of the cactus present would be achieved *via* generating cactus structure analogues and studying them experimentally. Thus, a bioinspiration and biomimicry approach was developed to be able to replicate the cactus structure with different materials to determine its mechanical behaviour.

### **2.3.2 Bioinspiration and Biomimicry leads to Novel Synthetic Materials**

Albert Einstein once said, ‘look deep into nature, and then you will understand everything better’. The opportunity to deeply understand the phenomena behind the unusual characteristics of natural materials has led to a significant interest in the field of bioinspiration and biomimicry. The word biomimetics first appeared in Webster’s dictionary in 1974 and is defined as ‘the study of the formation, structure or function of biologically produced substances and materials (as enzymes or silk) and biological mechanisms and processes (as protein synthesis or photosynthesis) especially for the purpose of synthesizing similar products by artificial mechanisms which mimic natural ones’<sup>42</sup>. Bioinspiration and biomimicry have always been one of the pillars of material development for humanity since ancient times. Some of the most famous successful results of the use of these techniques in the development of novel technologies include Velcro and airplanes. Airplanes were generated through in depth investigation of the mechanisms of bird flying since the Da Vinci days. Velcro on the other hand originates from the 1940s and to this day is one of the most fundamental and widely used material adhesives and it was discovered by the simple study of the mechanisms that cockle burs stick to objects<sup>43</sup>. Since then various approaches have been attempted to create materials with chemical morphological and structural features emulating the ones observed in nature

with similar successes being achieved both in research and industry<sup>37,44-48</sup>. As an example, hierarchy is one of the topological reasons behind the ‘brick and mortar’ structure of nacre that generates the large viscoelastic energy dissipation at the organic mineral level that favours local scale sliding and therefore increase energy absorption and toughness, as depicted in Fig. 2.4<sup>37,44,45</sup>. In an attempt to understand the design principles that enable nacre to present such interesting properties further studies concluded that those properties are attributed to nacre’s hierarchical structure<sup>37,44,45</sup>.

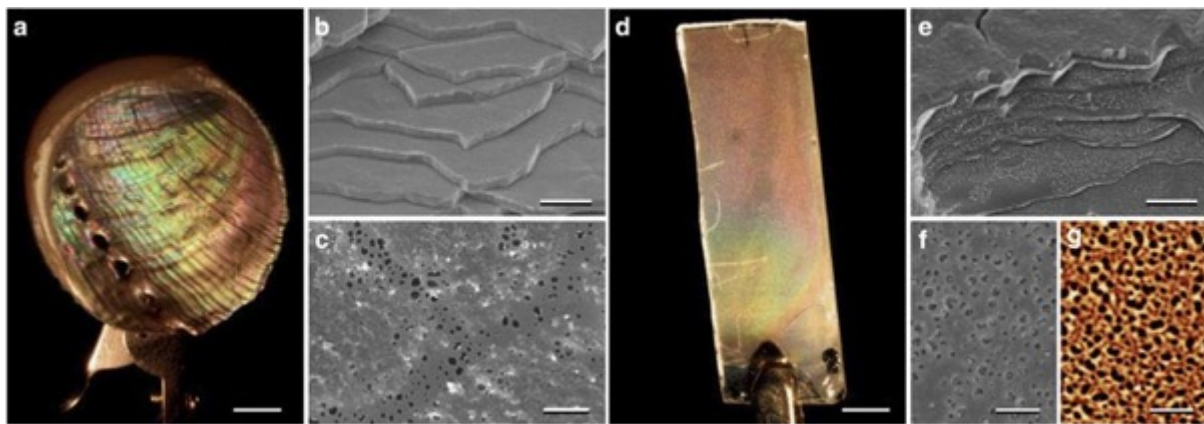


**Fig. 2.4** Comparison between natural nacre (a-c) and artificial nacre. Figure is obtained from Finnmore et.al.<sup>181</sup>

Specifically, nacre consists of 86% vol aragonite that is bonded by thin layer of organic material while exhibiting impressive toughness<sup>37</sup> due to hierarchical architecture enabling viscoelastic energy dissipation at the organic layer mineral bridge rupture and sliding of the aragonite layers in its unique multiscale ‘brick and mortar’ structure<sup>37,44</sup>. This understanding of the intrinsic hierarchical characteristics of nacre enabled the formation of novel techniques for the bioinspired materials with impressive strength toughness from brittle constituents demonstrating the potential of biomimicry and bioinspiration. There are multiple examples of bioinspired materials that yield significantly improved properties by simply changing the architecture to emulate a natural design while keeping the same constituents ranging from improving the properties of glass to generating novel biocatalytic materials<sup>46,47,49</sup>. Various architectures have been achieved with various synthetic routes however some of the more prevalent technique used for the generation of bioinspired materials has been additive manufacturing<sup>50</sup>. As evident, bioinspiration and biomimicry has enabled the development of novel materials with exciting mechanical properties that can revolutionize the field of material science. To that spirit, our idea was to utilize a similar approach to develop novel materials through this cactus fibre structure and determine the properties achieved. The use of

bioinspiration in this thesis was twofold. Being able to create cactus biomimetics would initially enable a better understanding of the cactus fibre behaviour and serve to explain how the properties present can be explained. Moreover, cactus bioinspired materials could be a novel material class with various applications in energy dissipation and morphing applications. If our hypothesis that the structure is responsible for the properties present, it could lead to the generation of a material independent platform that would have as significantly wide applications space as the properties would be present irrespective of material or manufacturing method.

### **2.3.3 3D Printing & Bioinspired 3D Printed Materials**

Additive manufacturing was originally developed in the mid 1980s when the first references of layer-by-layer addition for 3D material generation were developed, and the first original patent for layer by layer material addition *via* stereolithography was filed<sup>51</sup>. Additive manufacturing is defined according to the ISO/ASTM 52900:2015 standard as: ‘process of joining materials to make parts from 3D model data, usually layer upon layer as opposed to subtractive manufacturing and formative manufacturing methodologies’. It originates from the idea of building a material *via* a bottom up approach and replacing the top down approach. Since the conception of the first layer by layer additive manufacturing methodology there has been a significant increase in the field of 3D printing with the development of various 3D printing modalities and significant applications space. According to ASTM standards there are 7 categories of 3D printing methodologies: i) Binder jetting where material particles are joined *via* a bonding agent, ii) Direct energy deposition where heat is applied to material substrate to melt the part into shape iii) Material extrusion where the material is coming out through a nozzle at constant pressure and fully solidifies on a substrate, iv) Material jetting where liquid droplets are deposited sequentially on the working platform to solidify the desired part, v) Powder bed fusion where an energy source cause particle fusion before a roller smooths the surface for an additional layer to be added, vi) Sheet lamination where materials sheets are combined *via* the use of ultrasound or laser cutting vii)Vat photopolymerization in which photocurable materials are exposed to a laser to solidify and generate the additive manufactured part<sup>52</sup>. **Material extrusion, which is the primary method utilized in this thesis has a great selection of materials to be utilized and is cost effective, however, it demonstrates poor resolution.**

This significant increase in the options for 3D printing manufacturing methods has led to the development of an increasingly expandable library of 3D printable materials which has led to the implementation of 3D printing in various material fields. One of the emerging fields that

has directly originated from 3D printing methods and the availability of materials is the field of 4D printing where multi-material interphases can react to environmental stimuli and change their properties<sup>53</sup>. Furthermore, 3D printing methodologies have led to significant advances in the field of electrical material fabrication where electrically active materials can be directly 3D printed on various substrates and add novel functionality and topological control of that functionality<sup>54</sup>. In the composite sector recently, there has been a significant academic interest in the development of composite structures through the multi-material and topology control of 3D printing methods generating composite materials with specific mechanical properties at specific locations<sup>55</sup>. Last but not least, the biomaterials sector has received great benefits from the rapid development of additive manufacturing technologies. Initially the architectural and design control enabled by additive manufacturing provides significant benefits in the fields of bioinspiration and biomimicry where there have been various examples of generating bio-based materials with interesting properties modelling the structures observed in nature<sup>50</sup> as evidenced in Fig. 2.5.

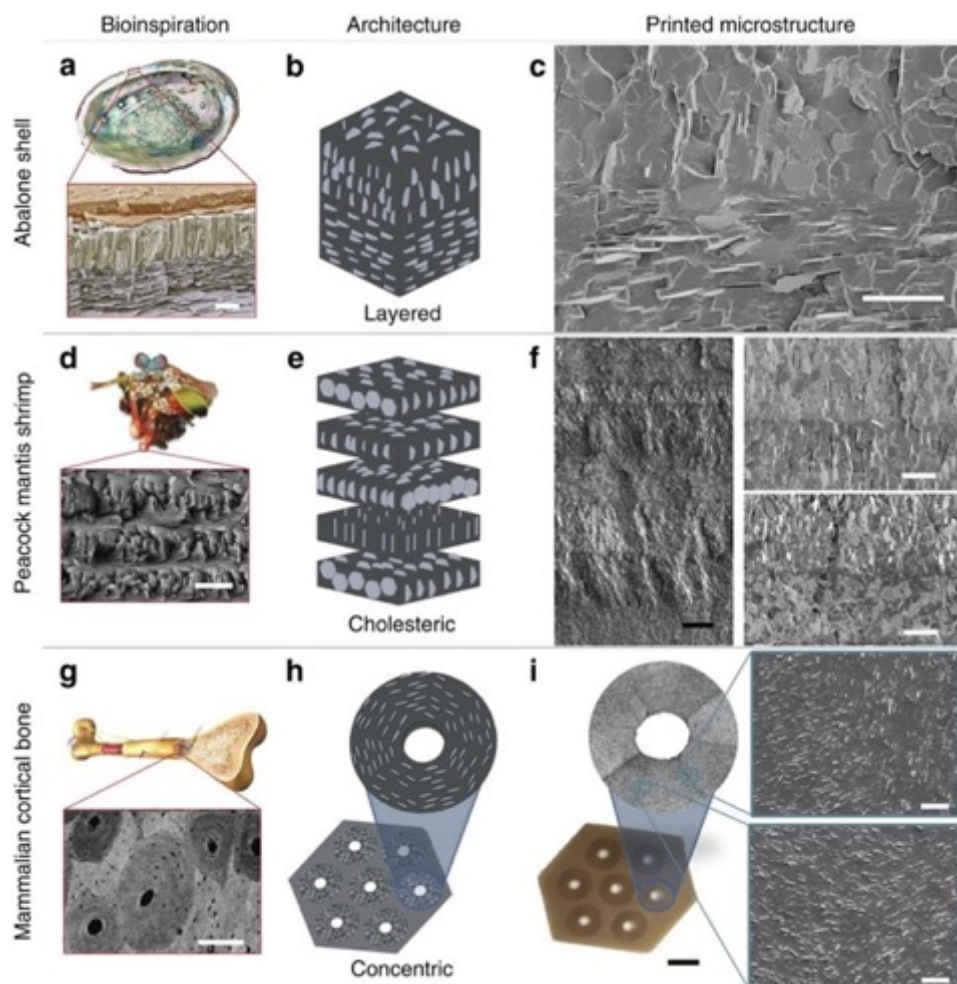


**Fig. 2.5** Examples of Bioinspired 3D printed materials enabling to replicate the microstructure observed in nature. Figure is reproduced from Martin et. al<sup>63</sup>

The additional levels of manufacturing control introduced through the invention of 3D printing make this technique an ideal candidate for the successful replication of the unique structures observed in nature, since complicated structures at different scales can be generated resembling the hierarchical motifs that are most common in biological materials. The continued evolution of the different techniques and approaches to 3D printing has given a significant rise into the development of bioinspired and biomimetic structures through the implementation of additive manufacturing<sup>56-64</sup>. For example, composite materials inspired by the inner structure of osteons, nacre and mantis shrimp have been manufactured *via* 3D printing. With the bioinspired fibre orientations and placements used, these materials have shown a clear dependence between their macro-mechanical properties and the microarchitecture from 3D print builds<sup>63</sup>. Recently, the unique microstructure of wood consisting of helical microfibril composites has been observed and reproduced *via* 3D printing<sup>64</sup>. Moreover, biomimicry also provided additional understanding of the mechanical properties of wood and how the structure has been optimized by nature for the adaptability of wood under various loads, providing unique insight into the properties of biological materials<sup>64</sup>. Additive manufacturing has already contributed significantly in the field of biomimicry and bioinspired materials as it has provided the ability to develop unique architectures across scales in a hierarchical fashion to mimic closer the unusual structures observed in natural materials. These developments have not only enabled scientists to develop novel materials with unique properties from simple constituents, but also provided a unique insight into the structural and architectural elements of biological materials that give rise to these characteristic properties. The focus of this thesis has been on utilizing 3D printing for the development of cactus structure biomimetics. Material extrusion of PLA was utilized for the manufacturing of the cactus biomimetics for their study as bioinspired materials while stereolithography SLA printing was also utilized to investigate the effect manufacturing methods incur in the development of the cactus bioinspired specimens.

## 2.4 Composites

### 2.4.1 Composites Theoretical Background

Composite materials have been used for generations with reports leading back to the early 1500 BC when early composites materials were utilized for building houses as well as weapons combining wood with bones and other materials to enhance their mechanical properties. Composites are defined as materials that are generated by the combination of at least two different materials usually with different properties for the production of a novel material with improved properties as demonstrated in Fig 2.6<sup>65,66</sup>. Their manufacturing procedure usually

indicates that composite materials are anisotropic and inhomogeneous materials with their properties mainly relying on the properties of the matrix and reinforcement material as well their interphase<sup>65,66</sup>. There are various classes of composite materials ranging from nanocomposites to hybrid and polymer composites. Composite materials have dominated multiple industry sectors including aerospace automotive and have recently entered the biomedical sector as well<sup>67-69</sup>. The reason behind the wide implementation of composite materials in all these industries is due to the design capabilities they provide while also enabling interesting combinations of lightweight and strong materials<sup>65,66</sup>.

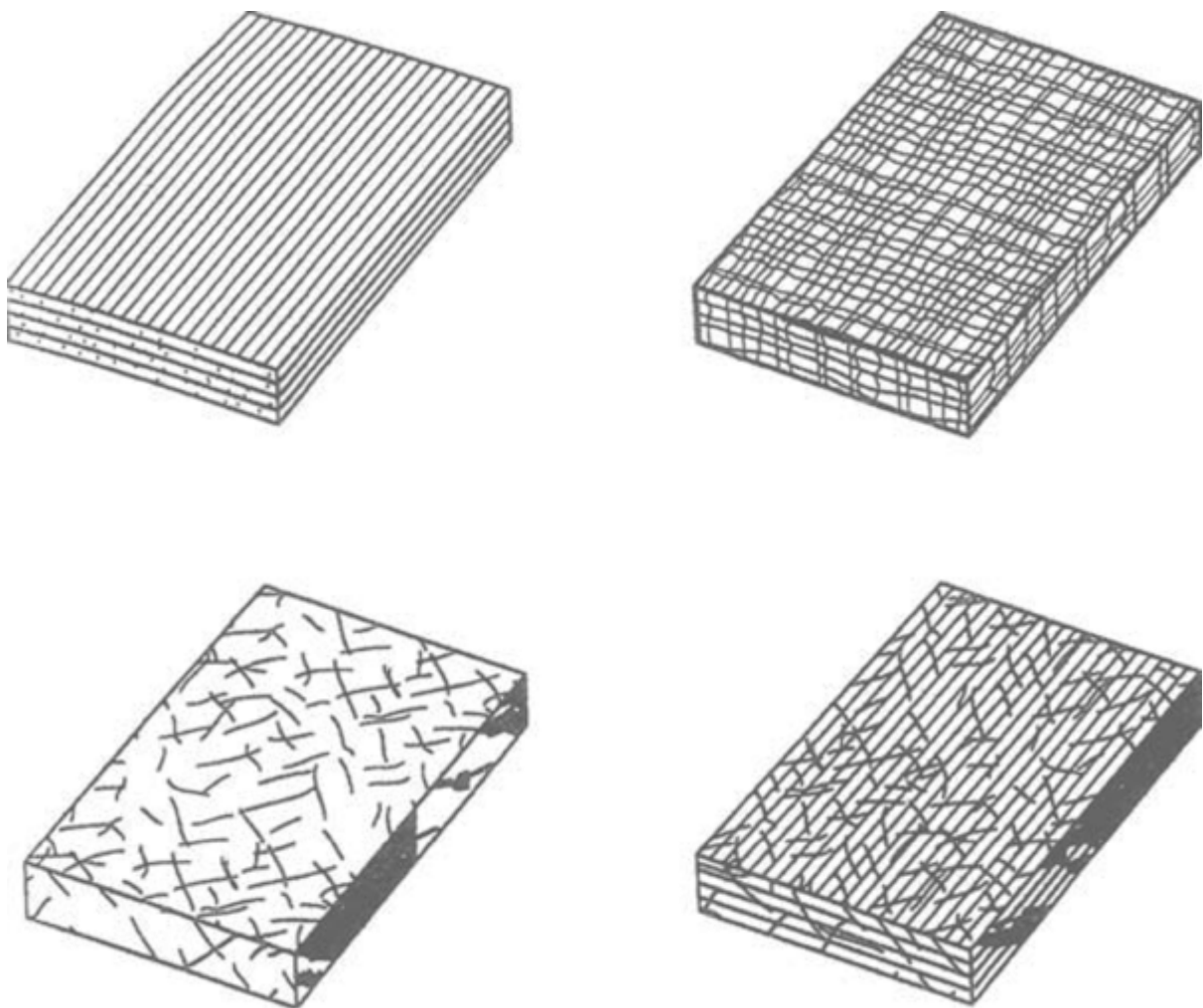


**Fig. 2.6** Examples of Composite materials consisting of a matrix material and different types of reinforcing elements. Reproduced from Gibson.<sup>182</sup>

The most commonly reinforcing elements of matrices in the composites industry have been carbon and glass fibres<sup>70,71</sup>. Carbon in various formats including carbon nanotubes, graphene, carbon fibres have been an instrumental reinforcing element in the composite material industry yielding materials that have found applications in all sectors and materials with very intriguing

and unique properties<sup>67,70</sup>. Glass fibre composites have been also one of the oldest and most widely used class of composite materials with their first applications leading back to the ancient times, while since the 1930s they have found applications across industries due to their excellent mechanical properties and high interphase matching with various matrices<sup>71</sup>. Despite their numerous benefits in terms of material development traditional composites also present significant drawbacks. Specifically, they incur a high cost for the manufacturing of the glass and glass fibres and a low rate of reuse and recyclability, while also incurring a significant environmental cost that recent legislation has focused on alleviating. **Over the past 20 years there has been a shift in the reinforcing materials utilized as composite reinforcements.** Significant research interest has been devoted to the implementation of natural fibres as composite material reinforcements since they have been shown to provide significant benefits<sup>72</sup> and are the main focus of this work. In terms of matrix materials two classes of polymeric materials that have been predominantly investigated for the incorporation of natural fibres: thermosets and thermoplastics. Thermosets are materials where the curing of the composite occurs *via* chemical crosslinking and there are two main manufacturing routes for the fabrication of such thermoset composite materials including sheet moulding and resin transfer moulding<sup>72</sup>. In the case of thermoplastics the curing of the material occurs *via* heat application and those composite structures can be fabricated *via* compression moulding, extrusion, injection moulding and long fibre thermoplastic direct (LFT-D) method<sup>72</sup>. The main focus on this thesis is on thermoplastic matrices as well as hydrogel networks for the generation of composite materials with natural fibre reinforcements.

#### **2.4.2 Filler Based Composites**

A more specific subcategory of composite materials concerns the use of fillers as the reinforcing element of a polymer matrix. A particulate filler is defined as a material that has been processed to a powder format, usually at a size of 100 µm and it is implemented in a polymer matrix with the aim to improve its properties<sup>73</sup>. There is a wide array of properties that the introduction of fillers aims to achieve within a composite material including<sup>73</sup>: i) Increase heat resistance, ii) Improve mechanical properties, iii) Reduce creep, iv) Change electrical properties, v) Reduce flammability. Filler materials can be implemented across various matrix materials including thermosets, thermoplastics and elastomers. It has been previously reported that with regards to thermoplastic matrices, that is the main focus of this thesis, the introduction of fillers yields significant benefits in terms of its mechanical properties<sup>74-77</sup>. In most cases the filler is introduced in the thermoplastic polymer matrix *via* thermomixing at high temperatures enabling for the polymers to melt and ensure thorough mixing and good dispersion between

the filler and the polymer matrix<sup>74-78</sup>. In terms of specific natural fibre fillers there are significant examples demonstrating that natural fibres have the potential to generate fillers that can provide significant benefits when implemented as the reinforcing element of a polymer matrix. It has been demonstrated that rice husk flour<sup>74</sup> bamboo powder<sup>75</sup> and coconut shell<sup>76</sup> powder have generated composite materials with significantly reinforced mechanical properties in all cases, providing us with the inspiration to utilize the cactus fibre as a filler matrix reinforcement.

#### **2.4.3 Natural Fibre composites**

Composite materials are an ever-evolving industry with continuous research and academic interest with applications across various industries. Natural fibres over the past twenty years have found their way in the composite materials forefront due to their cost effectiveness, biodegradability and abundance combined with their interesting mechanical properties<sup>72, 78-82</sup>. The automotive and structural industries have been the initial beneficiaries of the revolution taking place in the field of natural composites. Over the past 20 years automotive manufacturing giants such as Mercedes and Audi have started utilizing natural fibre composites for the manufacturing of their automotive interiors<sup>83,84</sup>. Moreover, there have been initial reports of initial utilization of natural fibre composites in parts of bridge manufacturing as well as window panels and decks<sup>83,84</sup>. It is important to understand the chemical and structural characteristics that enable natural fibres present their benefits and drawbacks as a composite manufacturing tool. Natural fibres are primarily comprised of cellulose, hemicellulose, lignin and various waxes, at different ratios, with each playing a significant role in the natural fibres properties<sup>81,85,86</sup>. Hemicellulose and lignin are the two components that are mostly responsible for the thermal degradation, UV degradation and moisture absorption of the natural fibres which is the reason why most treatments aim to remove these elements from the fibres<sup>81</sup>. Cellulose is the component of the natural fibres that is responsible for their mechanical properties. Cellulose is a hydrophilic glucan polymer consisting a linear chain of beta-1,4 – bonded anhydroglucose units which contains alcoholic hydroxyl groups that form hydrogen bonds between cellulose macromolecules to generate cellulose microfibres within the natural material<sup>82</sup>. The natural fibres are considered a hollow matrix of cellular fibres with a thin primarily wall making the matrix comprised of hemicellulose and lignin. The secondary wall consisting of cellulose fibrils which are **embedded in the hemicellulose and lignin matrix as demonstrated in Fig. 2.7**<sup>81,82</sup>. The thick layer of the secondary wall that consists of cellulose fibrils that determines the mechanical properties of the fibres (Fig.2.7)<sup>81,82</sup>.

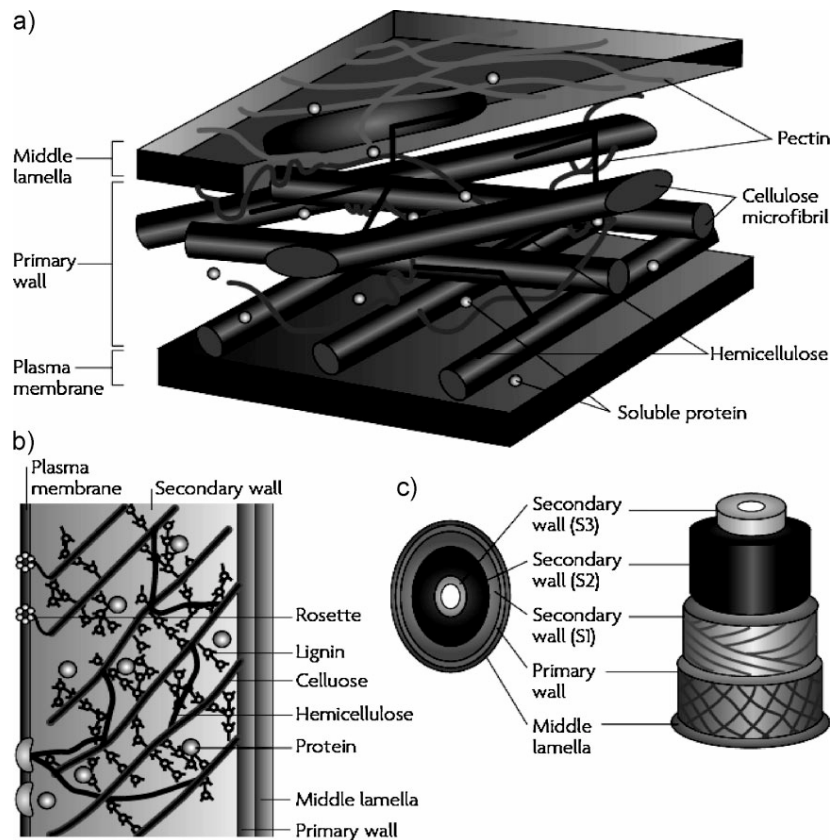


**Fig. 2.7** Demonstration of the inner structure of natural fibres as found in nature, demonstrating the presence of cellulose, hemicellulose and the other parts within the fibre. Reproduced from Pandey et.al.<sup>81</sup>

The combination of all these elements and their distribution in the internal structure of each plant fibre provides them with their tensile and flexural mechanical properties at low weights. However, it is important to mention that the natural fibres do also have some significant drawbacks attributed to their chemical and structural unique characteristics in terms of their use in composite manufacturing. Specifically, due to the fact that natural fibres are grown and not produced there is great batch to batch variability combined with sensitivity to water and UV absorption<sup>80</sup>. However, there are ways circumvent these drawbacks through chemical and physical modifications<sup>87,88</sup> and there have been a multitude of studies comparing the reinforcement achieved with natural and synthetic fibres<sup>79,89-91</sup> as shown in Fig. 2.8.

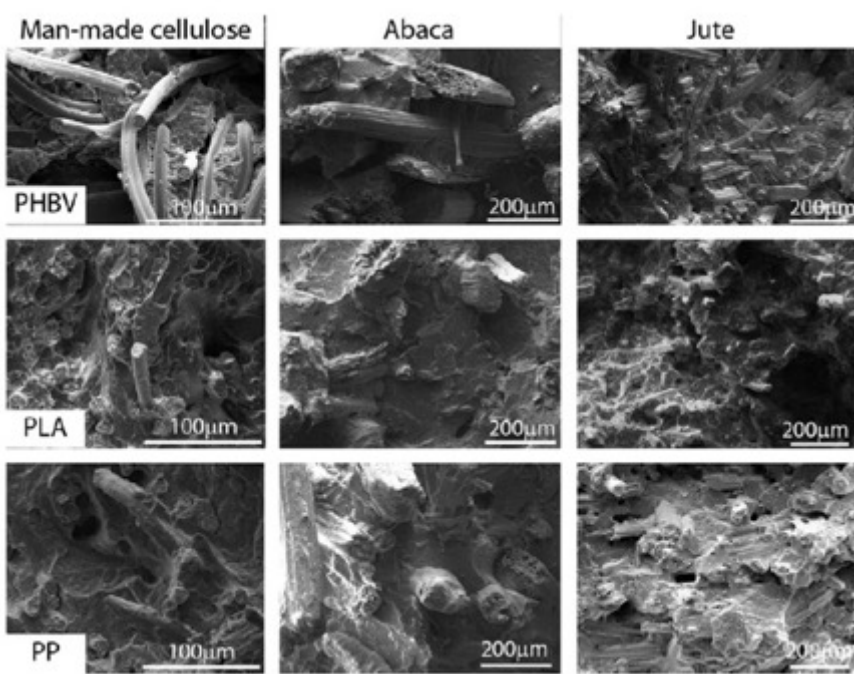


**Fig 2.8** Examples of various natural fibre biocomposites using various different polymer matrices and natural fibre reinforcements. Reproduced from Bledzki et. al.<sup>183</sup>

Another key factor in the successful **application** of the natural fibres in composite systems is the manufacturing methods implemented. The most common manufacturing methods **implemented for natural fibre introduction in a composite matrix** include injection moulding, compression moulding and hot pressing as well as resin transfer moulding. Injection moulding and resin transfer moulding are based on forcing matrix into specific mould cavities to generate the composite materials<sup>92</sup>. Compression moulding and hot pressing is based on applying a combination of pressure and temperature in a mould in order to generate the mixing between the fibre and the matrix<sup>92</sup>. In the case of this work a similar approach to hot pressing was utilized as the cactus fibre composites were thermoformed into a mould due to the fact that the natural fibres were implemented as a particulate filler reinforcement, a procedure described in detail in chapter 3. The main characteristics that affect the mechanical properties of the natural fibres have been identified as<sup>80</sup>: i) the microfibrillar angle, ii) cell dimensions and iii) chemical composition of the natural fibres. That is why such variability is present between the mechanical characteristics of the natural fibres with values ranging from 1.5 GPa (Pineapple fibres) to 70 GPa (Hemp fibres) in terms of Young's modulus<sup>80</sup>. It has been shown that natural fibres can compare favourably with glass fibres providing equivalent composite reinforcement at significant smaller weights<sup>90</sup>. Most commonly used industrially fibres such as hemp<sup>89</sup>, flax<sup>93</sup> and bamboo<sup>94</sup> have been shown to demonstrate **mechanical benefits** when implemented as matrix reinforcements yielding composite materials with significantly enhanced mechanical properties specifically **enhancing their modulus and their toughness**. The success of those original natural fibre usage has led to **remarkable** research interest in discovering new classes natural fibres that can be used as novel composite reinforcements. **There has been an increasing number of studies** ranging from the use of banana fibres<sup>95</sup>, pineapple<sup>96</sup> and date palm fibres<sup>97</sup>

that have demonstrated that natural fibres from a huge variety of plants can lead to the **development** of novel composite materials with emergent properties. One of those cases are the natural fibres from the cactus species of *Opuntia ficus indica* which are also the focus of this thesis. Previous work demonstrated that these cacti fibre sheaths are able to introduce **mechanical benefits in terms of flexural modulus and fatigue resistance** when implemented as a polyester matrix reinforcement yielding materials with significantly increased energy dissipation properties<sup>9</sup> while also **improving** the tensile behaviour or thermoplastic matrices when implemented in powder format<sup>10</sup>.

## 2.5 *Hydrogels & Composite Hydrogels*

Over the past 30 years, hydrogels have been used in various applications ranging from packaging in the food industry to dressing and device development in the biomedical sector <sup>99-101</sup>. There are many materials that can be used to form hydrogels, and these can be separated into two main categories: natural and synthetic<sup>102</sup>. Some of the most commonly used natural materials for the generation of hydrogels include alginate<sup>103</sup>, hyaluronic acid<sup>104</sup>, fibrin<sup>105</sup>, gelatin<sup>106</sup>, collagen<sup>107</sup> and cellulose<sup>108</sup>. The hydrogels generated from these natural biogenic materials **provide benefits** in terms of low cytotoxicity as they contain naturally derived biomacromolecules. However, one of their main drawbacks is their mechanical properties. It has been shown that their modulus is significantly lower from the threshold for various applications for instance most hydrogels compressive moduli is in the kPa range whereas bone tissue is in the MPa and GPa range<sup>109</sup>. In terms of the synthetic materials used for the generation of chemical hydrogels, some of the most common hydrogel precursors are derived from polyethylene glycol (PEG)<sup>110</sup> and polyvinyl alcohol (PVA)<sup>111</sup> and their respective hydrogels provide **added advantages** in terms of mechanical stability, however, their manufacturing usually is more demanding with steps that could introduce cytotoxicity on cells such as photo- and chemical crosslinking. In this work, the focus was on using alginate as the gelation constituent. As discussed above, a major drawback of natural gels is their low mechanical properties, specifically for alginate gels which limit their application space. There have been major attempts in literature to structurally reinforce natural hydrogels with the introduction of additional materials generating composite hydrogels with improved mechanical properties<sup>112-117</sup>. One of the most common approaches to reinforce hydrogels is *via* mixing of natural and synthetic materials for the generation of hybrid hydrogels that allow for better mechanical properties and cytocompatibility for biomedical applications<sup>112,113</sup>. For example, Xu et. al<sup>113</sup> utilized a combination of a thiol crosslinked collagen with a polymer (OAC-PEG-OAC)

for the generation of hydrogels to create a more versatile platform for cardiac tissue engineering combining the natural effects of the collagen with the mechanical property control provided by the polymer component. In terms of generating composite hydrogels, where the hydrogel serves as the composite matrix and fibres are introduced for the structural reinforcement, there have been various examples where carbon nanomaterials and graphene that have generated hydrogels with astonishing mechanical properties almost as close as the modulus values observed in the biological tissue<sup>118,119</sup>, however, there are still cytotoxicity issues that need to be resolved and optimized, as graphene needs to go through additional functionalization steps to become biocompatible<sup>114</sup>. Polycaprolactone (PCL) fibres have also been implemented successfully as a hydrogel reinforcing fibres as demonstrated in Fig 2.9<sup>115</sup>. Perhaps the most successful implementation of a reinforcing fibres implemented in hydrogel matrices has been *via* the integration of silk and cellulose fibres<sup>116,117</sup>. Silk and cellulose have very interesting mechanical properties due their protein structural motif while being highly biocompatible<sup>116,117</sup>.

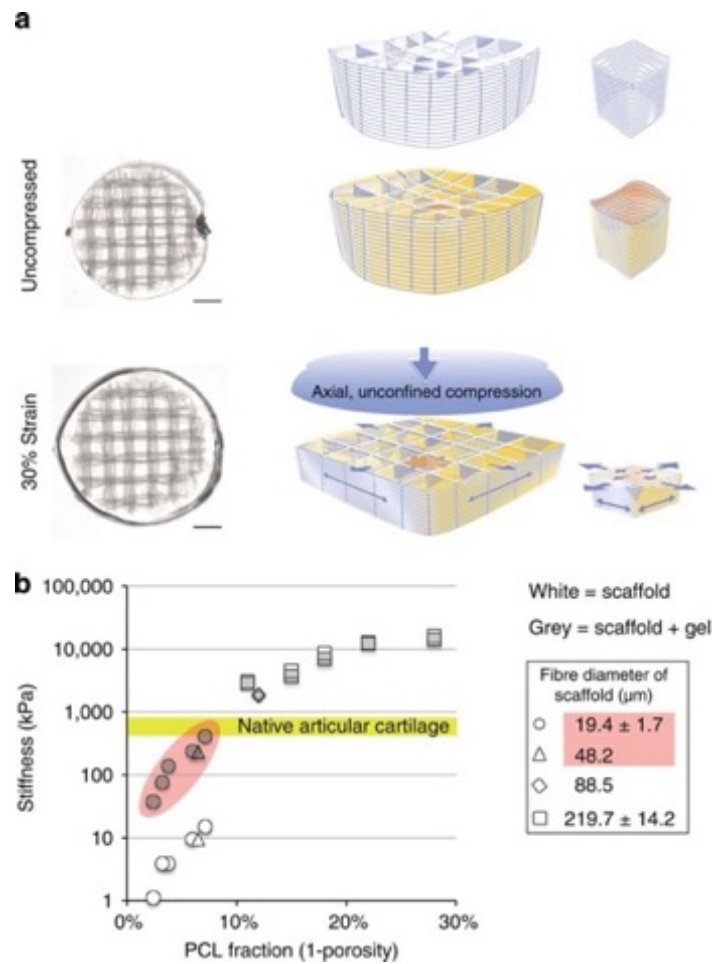


**Fig. 2.9** Example of a composite hydrogel system using PCL microfibres as the mechanical reinforcement. Reproduced from Visser et.al<sup>115</sup>

Once implemented as a hydrogel reinforcing elements, the mechanical properties of hydrogels are significantly improved while tunability of those properties is also achieved. Despite this huge variability in attempts to generate composite hydrogel systems using various fillers and structural reinforcing fibres, there have not been any known attempts of introducing plant fibres in hydrogel systems to assess the mechanical and biomedical potential of these systems. Accordingly, one of the objectives in this work is to compare and contrast the performance of alginate hydrogel composites stabilised with natural plant fibres from different plant species, with a special emphasis on the cactus fibres from *Opuntia ficus indica*, which has demonstrated interesting composite reinforcement properties.

## 2.6 Applications

### 2.6.1 Defence Related Applications

Since this was a project that was funded through a government defence organization it was important to keep the military and defence applications in perspective, along with civilian applications, while pursuing the potential of a cactus-based solids as a novel material. Impact and energy absorption applications are two of the fundamental fields in the area of engineering and composite materials research. There is a constant need for the development of materials with enhanced impact energy absorption properties since they are of special interest in the aerospace and automotive industry as well as in military and defence applications. Impact strength of a material is defined as the magnitude of stress at high speed that a material can resist before failure and it is directly related to its toughness and interlaminar strength<sup>120</sup>. Impact resistance is the quantifiable ability that assesses the impact strength of a material and it is measured by the total energy dissipated before catastrophic failure of the material occurs<sup>120</sup>. The phenomenon of impact is comprised by the simultaneous occurrence of multiple physical phenomena that depict its complexity including: elastic shock, plastic wave propagation, fracture, fragmentation, perforation, and spallation<sup>121</sup>. This multi-component nature of impact demonstrates the large number of considerations that need to be taken into account when designing an impact energy absorbing material for industrial and commercial applications. Traditional requirements for materials used for impact absorbing applications include high strength and high ductility<sup>122</sup> while the energy dissipating mechanisms that will allow the absorption of the impact's kinetic energy need to be considered. The main mechanisms that allow for this process to take place include<sup>122</sup>: i) formation of interlaminar cracks, ii) breakage of fibres, iii) shear away of lamina bundles and debris and iv) plastic deformation. There is a large variety of materials that are currently being developed for energy dissipating applications

ranging from magnetorheological fluids and metal alloys<sup>122</sup> to polymeric structural foams<sup>124</sup>. Composites, however, are perhaps the most widely researched class of energy dissipating materials in the field<sup>122,125,126</sup>, which has resulted in applications across a wide range of industries. Energy dissipating materials need to be characterized and understood from a dynamic perspective in order to determine their properties and evaluate their potential for impact applications. Specifically, mechanical experiments need to be designed and applied that are focused on assessing the dynamic response, the contact dynamics of the material on static and impact conditions, the effect of anisotropy on the material structure as well as the magnitude of the impact damage and the failure point<sup>122</sup>. In depth studies of impact damage can be divided into three main categories that need to be characterized and understood for impact dissipating applications<sup>123</sup>: i) impact dynamics and damage dynamics, ii) post-impact residual property characterization, iii) damage resistance improvements. It is also important however, to grasp how the impact occurrence is portrayed on composite networks and what are the specific design considerations necessary to generate an impact dissipating material<sup>127</sup>: i) the strain energy absorbing capacity of the fibres is one of the most important parameters in determining the impact resistance of a composite structure, ii) high interlaminar strength and toughness are very important design characteristics for good impact properties, iii) the fibre and matrix adhesion can be adapted depending on the properties of the impact for optimization of impact energy absorbance, iv) the fibre stacking sequence and orientation play a key role and have a direct relationship with the elastic energy absorption properties of the composite and v) geometrical considerations in the composite fabrication are important for optimization of the impact absorption properties of the composite structure **as evidenced in Fig. 2.10.**

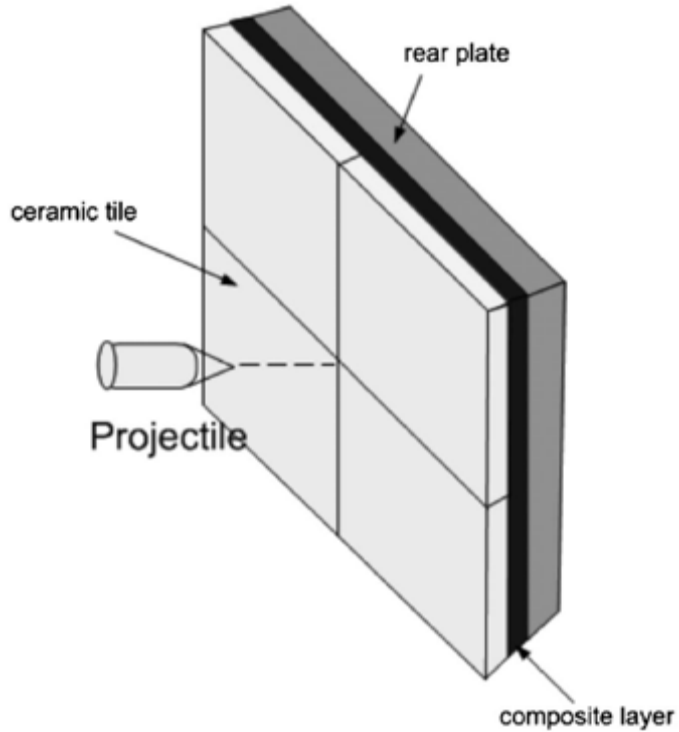


**Fig. 2.10** Example of a composite material design utilized for impact and energy absorption applications. Reproduced from Qiao et. al<sup>121</sup>.

These criteria and considerations provide a design framework for the manufacturing of composite materials for impact absorbing applications. A specific mechanism of composites that is significant in energy dissipation, is the damping mechanism of the structures which is one of the main factors for determining their dynamic behaviour. There are three main sources of energy dissipation in fibre reinforced composites and they are all directly related to damping<sup>128</sup>: i) Frictional Damping which occurs due to the slippage between the fibres and the matrix, ii) Viscoelastic and Viscoplastic damping which usually occurs in specific regions of the fibres within the matrix and iii) Thermoelastic damping which occurs due to the heat flow between the compressive stress regions and the tensile stressed regions at the occurrence of the impact. It is paramount to consider these damping mechanisms when studying the energy dissipation properties of composite structures. It is evident that impact and energy absorbing materials represent an intriguing and emerging field with significant application potential across various industries. Natural fibre composites, that are the focus of this project, have shown excellent potential in the field and have already found some applications in the automotive industry<sup>129</sup>, and show great potential as novel platforms for the development of impact and energy absorbing materials with unique impact dissipation characteristics. **Besides the material characteristics that need to be considered for the production of energy absorption materials, geometric design considerations need to be also taken into account to accommodate for specific applications.** The cactus structure does demonstrate properties with potential in

terms of energy dissipation due to its bending to axial stiffness ratio property observed previously<sup>9</sup>. This property could suggest that there are different strain energy mechanisms present in the same architecture something that could lead to the specific design for energy dissipation depending on the loading direction<sup>130,131</sup>. The emergence of natural fibre composites in energy dissipation and damping applications combined with the unique structural properties of the cactus were provided key ideas for this thesis in terms of material characterization. Another potential application field of the cactus properties is shape morphing applications as demonstrated in Fig. 2.11. Shape morphing in aerospace applications, is used to identify aircraft that are able to undergo geometrical changes to adapt more efficiently to their specific missions<sup>132</sup>. Shape morphing provides significant benefits in terms of energy saving as it increases the efficiency of flight significantly and can have a significant positive impact on both military and civilian applications.

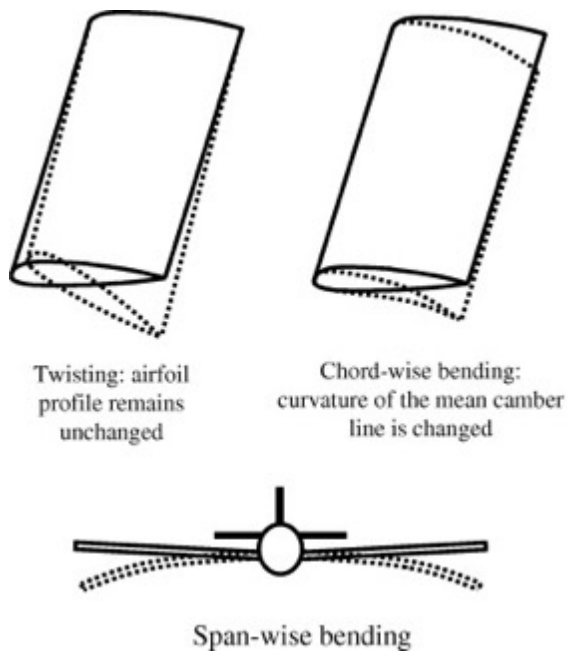


**Fig. 2.11** Example of Aircraft wing shape morphing. Reproduced from Sofla et.al<sup>131</sup>

It has been shown that a high bending to axial stiffness ratio is a critical design requirement and highly beneficial for morphing applications, since the materials need to be able to adapt to twist bending and axial stretching simultaneously in different directions<sup>131</sup> which makes the cactus fibre structure an ideal candidate for this field.

## 2.6.2 Tissue engineering

Tissue engineering was recognized as the civilian application of this work focusing on the development of novel cactus-based solids for biomedical applications. The origins and definition of tissue engineering can be traced back to the early 1980s were for the first time the term of engineering of tissues was utilized to describe the need for the development of the

methodology to generate tissues from cells originating from the human body<sup>133,134</sup>. From the onset and the foundation of this new scientific field it was evident that successful tissue engineering would only be achieved *via* an interdisciplinary scientific approach<sup>133-135</sup>. Initially, it was important to identify how the human tissue and the human body have the ability to regenerate themselves to understand the factors and key components that enable human tissue regeneration. It was observed that various human tissues have an extraordinary ability of self-regeneration and the common factor present in most of those cases is the existence of stem cells<sup>133-135</sup>. Stem cells are also prevalent and of significant importance in the early stages of the embryo growth<sup>133-136</sup>. A stem cell is defined as a progenitor cell with the potential to self-renew and mature into mature cell types that comprise human tissue<sup>137</sup>. There are several **types** of stem cells that are directly related to various tissues of the human body **however on this thesis human mesenchymal stem cells (hMSCs) were utilized**<sup>137</sup>. Mesenchymal stem cells are adult stem cells that can be found in various tissues and organs of the body and have had great scientific interest due to their easy isolation and expansion in vitro as well as their therapeutic potential<sup>133-137</sup>. Stem cells are a fundamental building block of the field of tissue engineering and are widely used for the development of novel regenerative medicine approaches for clinical applications. There are two different schools of thought when it comes to tissue engineering namely the scaffold free tissue engineering<sup>138</sup> and the scaffold-based tissue engineering<sup>139</sup>. Scaffold free tissue engineering refers to platforms where tissue engineering is achieved without the use of an exogenous three-dimensional material to serve for cell seeding and there are various successful examples of the utilization of this approach<sup>138-142</sup>. **Since a scaffold was used for the preliminary bone tissue engineering work presented in this thesis, the focus on this introduction will be on the scaffold-based systems.** Scaffold materials need to be biocompatible materials that will closely resemble the native human tissue in terms of structure, mechanical properties as well as biochemical signals<sup>133-136,143</sup>.

Usually the biochemical signals can be supplemented in the scaffold in various formats but from a material science perspective it is essential that the scaffold mechanically and structurally resembles native tissue in terms of stiffness, porosity and hierarchy<sup>143</sup>. Once a scaffold material is established, it is usually seeded with stem cells and then it is in vitro cultured along with any necessary biochemical growth factors and other signals to assess its tissue engineering potential for the tissue of interest<sup>139</sup>. There are various successful examples of that approach being implemented clinically with the most prevalent ones the case of artificial skin and the **artificial bone constructs**<sup>133</sup> demonstrating the potential of the scaffold tissue engineering in clinical applications. There have also been significant developments in the field of cardiac tissue

engineering in recent years. The development of novel polymer nanocomposite materials has yielded novel scaffold materials with excellent mechanical and biocompatible properties for potential implementation as synthetic heart valves<sup>214-216</sup>. However, scaffold-based tissue engineering does also introduce some disadvantages namely the limited porosity achieved, the homogenous distribution of stem cells within the scaffolds, and the limited mechanical properties<sup>144</sup>. One of those disadvantages can be mitigated through the use of biofabrication which is a technique that uses 3D printing for the development of scaffolds that include stem cells in every layer of the scaffold material enabling for better distribution as well as higher structural and mechanical control<sup>144</sup>, which will be discussed further in section 2.6.2.2 as it was primarily used for the work presented.

### **2.6.2.1 Bone & Bone Tissue Engineering**

Bone serves some fundamental functions within the body, which is why bone tissue regeneration is a rapidly emerging field in modern medicine. These functions include<sup>146</sup>: i) The foundation for bodily locomotion, ii) The load-bearing capacity of our skeleton and protection for our internal organs, iii) The housing of the biological elements required for haematopoiesis, iv) The sequestration of dangerous metals (i.e., lead), and v) The maintenance of the homeostasis of key electrolytes via calcium and phosphate ion storage. Besides the importance of bone from a physiological point of view, bone is one of the most intriguing natural materials. Bone is a structural composite material with a laminated structure present that through the manipulation of porosity and hierarchy is able to achieve unparalleled mechanical and structural properties<sup>147,148</sup>. Current approaches for bone trauma are based on allografts and autografts, but they provide limited benefits for the patients due to immunorejection, donor scarcity and frequency of revision surgeries concerns. Bone grafts are the most transplanted tissue in the clinic second only to blood and an example of the tissue engineering process is depicted in Fig. 2.12<sup>145</sup>. Thus, the field of bone tissue engineering has seen a significant research and industrial interest in recent years<sup>149-151</sup>. Due to the unique physiology and mechanical hierarchical structure present in the bone tissue a specific set of requirements are usually implemented for various bone tissue engineering scaffolds: i) three dimensional and highly porous with an interconnected pore network for cell growth and flow transport of nutrients and metabolic waste, ii) biocompatible and bioresorbable with a controllable degradation and resorption rate to match cell/tissue growth, iii) suitable surface chemistry for cell attachment proliferation and differentiation, iv) mechanical properties to match these of those of the tissues at the site of implantation<sup>146,149-151</sup>.

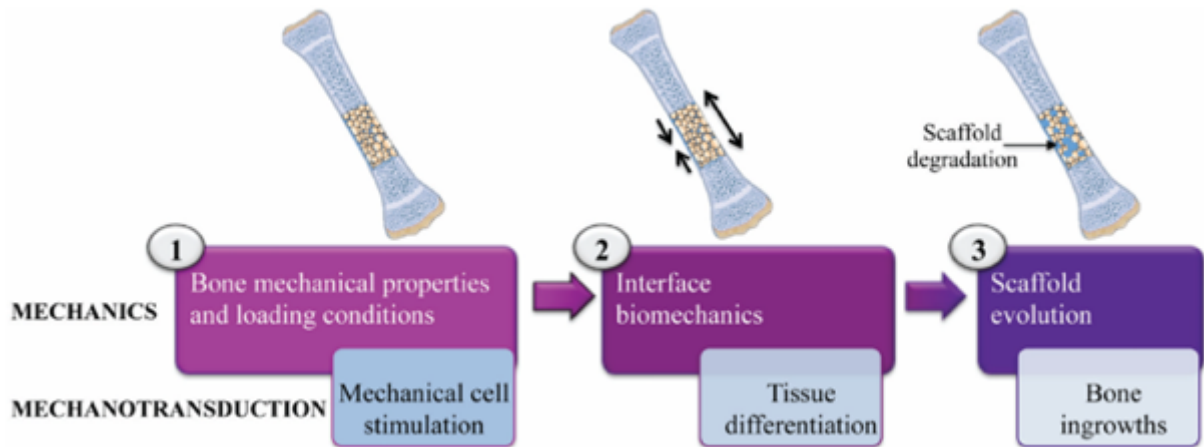


**Fig. 2.12** Representation of the process of bone tissue engineering based on a scaffold tissue engineering approach. Reproduced from Amini et. al<sup>146</sup>

From a material science perspective, the development of materials with the above properties is still a significant scientific challenge, but there have been some successes in the open literature. Some of the most common examples of scaffold materials used for bone tissue engineering include the use of calcium phosphate materials in composite formulations since they include one of the main materials that exists in bone as well as exhibiting mechanical properties that can be comparable to native bone tissue<sup>152</sup>. Another additional benefit from introducing calcium phosphate in bone tissue engineering scaffolds is that it has been proven that the calcium phosphate presence leads to the scaffold presenting osteoinductive properties<sup>152</sup>. Osteoinduction is defined as the property of a material to induce bone formation without the presence of osteogenic factors that are usually implemented to achieve tissue regeneration<sup>153</sup>. For instance, composite scaffolds generated with PLGA and hydroxyapatite particles showed significant osteogenic potential and remarkable mechanical properties demonstrating its potential for bone tissue engineering applications<sup>154</sup> while similar results have been obtained via nanohydroxyapatite-polyamide scaffolds<sup>155</sup> and gelatin apatite scaffolds<sup>156</sup>. Hydroxyapatite composite materials are not the only ones implemented for bone tissue engineering applications with other materials such as polymers and hydrogels successfully finding their way in the bone tissue engineering industry<sup>157</sup>. For instance, the utilization of 3D printing for the generation of lumbar fusion cages with superior compressive properties demonstrating a novel methodology that can be utilized for the generation of patient specific implants<sup>212</sup>. Despite the plethora of material options existing for bone tissue engineering scaffolds, there is still a lot of room for improvement of the materials utilized in the field to enhance the properties of the material scaffolds for their clinical application. As described above, natural fibre composite materials

are able to provide significant mechanical benefits in terms of material specifications at various formats. However, there is a significant gap in the literature for the use of plant obtained fibres in biomedical applications especially as a structural reinforcement element for biomedical materials such as hydrogels and other scaffolds. This prompted the idea of expanding the focus of natural fibre composites to include biomedical applications and here we present the first attempt of utilizing unprocessed plant fibres directly as bone tissue engineering scaffolds with a specific focus on the natural fibre of interest in this thesis, the *Opuntia ficus indica*.

### **2.6.2.2 Bone tissue engineering & Bioprinting**

As it is evident from the requirements for the ideal bone engineering scaffold hydrogels present an excellent candidate as they are biocompatible, biodegradable and can have internal porosity and be structurally reinforced and thus there have been multiple attempts using hydrogels for bone tissue engineering applications<sup>158,159</sup>. One of the disadvantages of using hydrogels for bone tissue engineering is the lack of control of the precise structure of the scaffolds, since with most methods the gels will randomly assemble in the vessel where the reaction and the cross linking will take place. Rheological analysis of most hydrogel networks revealed that these gels are shear thinning which means that they can be extruded which prompted the idea of 3D printing using these hydrogels as the inks for the generation of scaffolds<sup>109,160</sup>. Additionally, since these gels are biocompatible, and it has been demonstrated that small amounts of shear stress do not damage human cells novel bioinks have been formulated for 3D bioprinting where cell containing hydrogels are directly printed on a substrate following specific patterns designed by the user<sup>160,161</sup>. This has led to the successful generation of various bioinks with various internal porosities and unique structures that have provided significant benefits in bone tissue engineering and other tissue regeneration fields<sup>103,106,117</sup>. There have also been developed interesting composite bioink systems that demonstrate the potential of composite systems for tailoring of the mechanical properties of hydrogels widening their application space<sup>117,162-164</sup>. The system of focus on this work is a fugitive ink based on alginate and Pluronic F-127 where a sol gel transition and subsequent removal of the Pluornic enables the generation of macro porosity<sup>103</sup> as demonstrated in Fig.2.13.

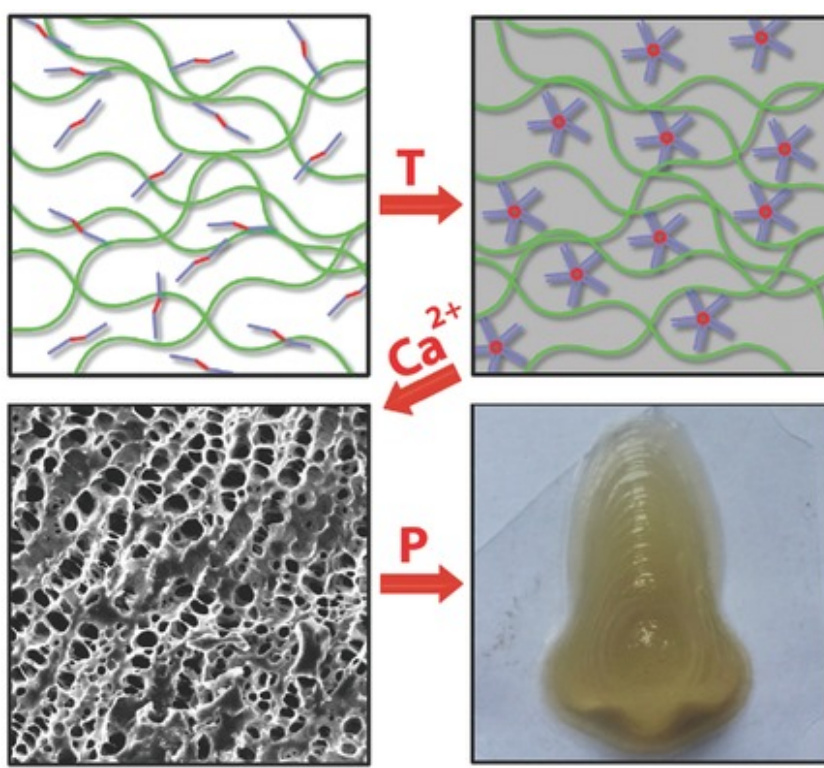


**Fig. 2.13** Example of bioink system demonstrating internal porosity and structural fidelity for biomedical applications. Reproduced from Perriman et. al<sup>103</sup>

We aim to incorporate natural plant fibres as a novel structural reinforcement of the hydrogel system that will enable us to tailor the mechanical properties of the hydrogel systems for a specific application in our case bone tissue engineering.

## 2.7 Thesis Aims & Objectives

As it has been presented through the introduction, the aim of this work was centred around the understanding of the mechanical properties of *Opuntia Ficus Indica* fibres and the development of novel materials based on these natural fibres. The specific objectives to achieve this aim described below were the main focus of this work:

- The initial aim of this work is the analysis of the morphological characteristics present in the structure of the cactus fibres. To that end, a hypothesis that the structure presents hierarchical characteristics that can be directly correlated to the fibre's mechanical properties was formulated, and a fractal geometry characterization approach was developed to characterize the structure of the cactus fibre. The methodology developed and the results of the analysis are described in detail in chapters 3 & 4.
- After the morphological characterization was carried out, the second aim of this work was the utilization of the morphological information obtained for the development of cactus fibre structural analogues and finite element simulations. The data obtained from the various imaging modalities applied allowed us to achieve a morphological evaluation of the structure while enabling the production of artificial 3D printed analogues and a simplified finite element model simulation of the cactus structure. This

enabled a better understanding of the mechanical properties present in the cactus fibres and allowed for the development of novel cactus-based materials with high bending to axial stiffness ratios. The methodology and the results are thoroughly discussed in chapters 3 & 5.

- Besides, focusing on the characterization, understanding and biomimicry of the cactus fibres, the last aim of this work focused on utilizing the cactus fibres themselves for the development of novel cactus composites. To that aim, a methodology was developed for the generation of thermoplastic and hydrogel composites using a cactus fibre powder as the reinforcing element with the latter being utilized for bioprinting for bone tissue engineering applications. The methodology and the results are presented in chapters 3 & 6.

### **3. Materials and Methods**

---

#### ***3.1 Theoretical Background on Material Characterization Techniques***

##### ***3.1.1 Mechanical Properties***

Material science is always an ever-evolving scientific field with new materials constantly being developed and produced. Proper material characterization is of fundamental importance in the field while common routes of evaluation of material performance have been developed. The mechanical performance of a novel material are perhaps the most fundamental properties that need to be characterized<sup>165-169</sup>. Irrespective of the materials size, shape and scale it is always important to evaluate how the material behaves under mechanical stresses. In terms of mechanical properties there is a wide range of properties that can be characterized<sup>165-169</sup> however in this thesis the properties focused concerned the tensile, flexural and compressive properties of the novel materials developed and thus this review will focus on those. The tensile properties reveal how the material behaves when a force is applied in tension<sup>170,171</sup>. They are crucial for material characterization as they provide the necessary information to assess fundamental properties of materials including the modulus of elasticity, tensile modulus, tensile strain, yield strength and elongation at break which are important to understand the application potential of materials<sup>170,171</sup>. It is also important to note that specific ASTM standards have been developed to correctly characterize the tensile properties of each material class using specific tensile testing methods and it is important to follow the right one depending on the synthesis of a material. The second property that was the focus of this thesis was that of the flexural modulus. Flexural properties of a material are determined when a material is subjected to a bend load while being usually supported at two points<sup>172,173</sup>. It is widely used in the composite industry to assess composite stiffness as in most isotropic materials the tensile and flexural modulus are equivalent<sup>172,173</sup>. In the case of the cactus fibre composites it was observed that there is a significant difference between the tensile and flexural moduli of the materials manufactured based on the OFI fibres<sup>9</sup> and that is why further investigation was carried out on this type of fibres in this thesis. The last mechanical property evaluation methodology that was followed was concerning the compressive stiffness of hydrogels. Compression testing has been a staple for the mechanical characterization of biomaterials as in most cases in the open literature unconfined compression testing is utilized to evaluate the modulus of biomaterials<sup>174,175</sup>.

### **3.1.2 Micro-CT imaging in materials and biomaterials**

Besides the mechanical property characterization of a novel material when developed its morphological characterization is of equal importance to assess the application potential of any material. There are various techniques commonly used to assess the morphology of various materials mainly focusing on electron microscopy<sup>176,177</sup>. However, this technique usually provides two-dimensional information and that two-dimensional information is interpolated to obtain information for the 3D architecture of a material<sup>176,177</sup>. This approach does incur limitations, specifically the surface information obtained cannot be always correctly correlated into volume information while also leading to false conclusions due to the presence of artefacts<sup>176,177</sup>. That is why tomography has been an emerging technique being utilized in material science providing 3D information of novel materials<sup>178,179</sup>. X-Ray radiography is the basis of X-ray Tomography where an X-Ray beam is directed towards the sample and the transmitted beam is recorded on a camera<sup>176-179</sup>. According to the Beer Lamber attenuation law the ratio of the emitted and incident electrons of the material are correlated to the integral attenuation coefficient and the electron path followed along the material<sup>176-179</sup>. Following this principle a 3D image projection of a structure can be obtained and thus if radiographs are taken from different angles of a specimen usually from 0 to 180 degrees using the filtered back projected algorithm to obtain volume information of a specimen<sup>176-179</sup>. There are various modes and options using X-Ray tomography for material evaluation where usually a compromise between the resolution required and the software abilities needs to be achieved<sup>176-179</sup>. The implementation of X-ray CT in material science has provided significant benefits in understanding material morphology and structure better widening the understanding of material behaviours at various scales<sup>179</sup>. Initially the implementation of CT imaging in composite materials has led to a better understanding of the distribution of the fibres within the matrix due to the difference in their attenuation coefficient<sup>178</sup>. Moreover, CT evaluation of tested material specimens enables to understand how the microstructure behaves under stress while assessing the areas where failure occurred within the material to find ways to further improve the material mechanical behaviour<sup>178,179</sup>. Furthermore, the ability to get a 3D volume reconstruction of materials has enabled the full assessment of porosity and pore interconnectivity in cellular materials and bio scaffolds<sup>178-180</sup>. Additionally, it has enabled the hierarchical evaluation of biological materials enabling a further understanding of the structural uniqueness present in nature while expanding the field of biomimicry and bioinspiration for the generation of materials with unusual properties<sup>179</sup>. Last but not least, material tomography has provided significant benefits in terms of finite element simulations of novel materials<sup>178-</sup>

,<sup>180</sup>. Through the ability to obtain 3D volume information of a material structure scientists have been able to generate finite element models that can describe and predict the mechanical behaviour of materials more accurately even for challenging structures such as those of cellular materials<sup>179,180</sup>. It is evident that X-Ray tomography presents various benefits in terms of material characterization and it is a technique that has been implemented throughout this thesis.

### **3.2 Extraction of Cactus Fibres**

The cactus fibres were extracted as described before<sup>9</sup>. Briefly, Opuntia Ficus Indica trunks were buried in sand-less soil 30 cm deep for 15 days with the average outside temperature being at 27°C where the fermentation process taking place enables the facile removal of the cactus fibre layers. The trunks were then washed with water and left to air dry with outdoor exposure for at least two days at an average temperature of 27°C. These extracted cactus fibres demonstrating a tree like fibril structure were used for all the analysis described in this work.

### **3.3 Ball Mill**

For the purpose of this work the cactus fibre were utilized both in a sheet and a powder format for the development of filler-based cactus fibre composites. The mill used for the processing of the fibres was a Retsch® Mixer Mill MM 400, a rotary mill with steel balls and all experiments were carried out at room temperature, 22°C. Initially small fragments of the fibre sheet were cut and placed inside the mill vessels. There were 2 vessels used at each run both of which had the same mass, so the ball mill was balanced at all times. The optimized setting to achieve complete powderization of the fibres was rotating the mill at 30 Hz for 15 minutes. Optical and SEM microscopy were then utilized to assess the properties of the powder particles generated.

### **3.4 Fractal Morphology Characterization**

As described in the introduction section 2.2 fractal geometry is a well-established methodology for the geometrical characterization of complex non-Euclidean geometries. In the case of the cactus fibre morphology due to its geometrical features we determined to develop a fractal geometry characterization methodology based on obtaining images from the cactus fibres across scales <sup>13,31</sup>.

#### **3.4.1 Optical Microscopy**

Optical microscopy images were obtained for both the OFI fibre sheet as well as the processed OFI fibre powders using a Carl Zeiss Microscope at magnifications of: 5x, 10x, 20x, 50x and 100x under Bright Field Light, Dark Field Light and Polarized Light settings. Those images were then analysed following the analytic and algorithmic procedures described below in order

to determine their fractal dimension and investigate whether multifractal characteristics are present.

### **3.4.2 Scanning Electron Microscopy (SEM)**

SEM images of the fibres were obtained for assessing the morphology and fractal order of the natural fibres with higher resolution at a closer magnification. The fibre fragments were initially silver coated *via* sputtering to ensure the conductivity of the surfaces for proper imaging.

### **3.4.3 Analytical & Algorithmic Procedures**

Obtaining images through various imaging modalities, was the first step in determining the fractal characteristics of the cactus structure. The next step involved developing an algorithmic procedure to enable the generation of the fractal dimension based on those images, in a MATLAB environment. As described in the introduction section 2.2, the most commonly accepted fractal dimension (FD) estimate is the Hausdorff-Besicovitch dimension D which is defined as the logarithmic ratio between the number N of an object's internal homotheties and the reciprocal of the common ratio R of this homothety<sup>31</sup>. There are various algorithmic approaches in estimating D ranging from the box-counting methods and its derivatives, to wavelet-based methods and Fourier transform methods. All the different algorithmic approaches usually use three similar steps in determining the value of the Fractal Dimension<sup>31</sup>:

1. Measure the quantities of an object using various step sizes
2. Plot log (measured quantities) versus log (step sizes) and fit a least-squares regression line through the data points
3. Estimate FD as the slope of the regression line

The most common approach used in estimating the fractal dimension is the box-counting approach which is used in this analysis. In this case the homotheties used are boxes and a number of boxes N of size R are assumed to cover the entire shape and using these methods after a various iteration the fractal dimension value can be determined following the steps outlined above. It is important to note that the box-counting method works only for binary signals and images therefore some image processing procedures had to be employed in order to utilize this algorithmic approach.

In the analytical approach implemented the programming environment that was used was MATLAB R2018b. In order to get results that are as accurate and precise as possible we applied three different MATLAB R2018b scripts that utilize the box-counting method with slight modifications in the ways each script is applied on an image. This allowed to estimate the

fractal order with confidence as well as determine the variability obtained by using different MATLAB R2018b scripts of the same method. Since the algorithm used could only be applied in binary images the images obtained had to be binarized initially through image processing methods, specifically thresholding. Thresholding is a common image processing approach that allows to distinguish the object of interest from the background of an image based on pixel intensity. The image is then separated in the background pixels that now have a value of 0 and the object pixels that will have a value of 1. There are multiple ways to perform this operation and in this case three different thresholding approaches were utilized and compared in order to ensure the robustness of the algorithms in determining the fractal order:

#### **3.4.4 User defined thresholding**

In this case the image was transformed into a grayscale image and then a histogram of the pixel intensity was generated. The regions of the histogram that have a high number of similar pixel intensities belong to the same region of the image therefore the regions with the highest number of pixels of the same intensity belong to the object and sparse pixel intensities belong to the background. Therefore, looking at the histogram the ‘peaks’ belong to the objects and the ‘valleys’ to the background. When there is a single peak region on the histogram there is certainty that those pixel intensities belong to the object so the Threshold values can be set around that region making the pixels of the object 1s and the pixels of the background 0s allowing for the successful implementation of the box counting method. An example of how this technique can be applied is shown in Figure 3.1.

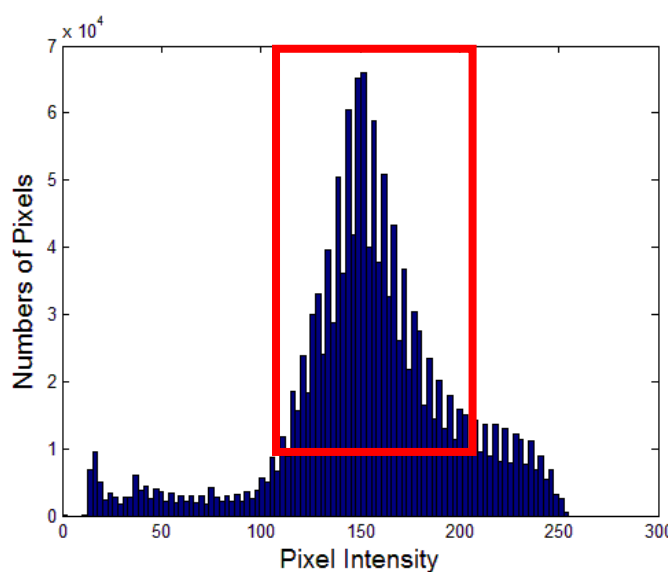


**Fig. 3.1** Demonstration of the user defined algorithm application. It is evident that from the histogram there is a distinct ‘peak’ (red box) of pixel intensity values and frequency. This peak signifies the pixel

intensity of the object of interest and the rest the pixel values of the background thus in this case the threshold would be set as  $I > 100$  and  $I < 200$  where  $I$  is pixel intensity.

Human error in this case plays a big part in this threshold estimation and could potentially be a major source of error in our estimation. Thus, to enhance the reproducibility and robustness of our approach, other mechanisms of thresholding were used in this analysis. MATLAB provides its own functions for generating binary images from image sets and some of those built in functions were utilized to minimize the error in the generation of the binary images necessary for the fractal box counting algorithms. Below are the detailed descriptions of these thresholding algorithms for the binarization of the data as well as a detailed description of the fractal box counting algorithms.

#### **3.4.5 MATLAB graythres () function:**

Computes a global threshold (LEVEL) that can be used to convert an intensity image to a binary image with IM2BW. LEVEL is a normalized intensity value that lies in the range [0, 1]. graythresh uses Otsu's method, which chooses the threshold to minimize the intraclass variance of the thresholded black and white pixels.

#### **3.4.6 Bradley Thresholding Method**

Bradley.m: Contributed by Jan Motl ([jan@motl.us](mailto:jan@motl.us)): performs local thresholding of a two-dimensional array IMAGE with the Bradley method. The key idea of the algorithm is that every image's pixel is set to black if its brightness is T (threshold value) percent lower than the average brightness of surrounding pixels in the window of the specified size, otherwise it is set to white.

Once the thresholding approaches were established various scripts that apply the box counting method for the estimation of the fractal dimension and for multifractal analysis were implemented in the images obtained from the microscopes and are described in detail below.

#### **3.4.7 Hausdim.m**

This method has been adjusted based on previous studies<sup>17,31</sup>. After the image is thresholded and binarized successfully the algorithm is implemented. The algorithm was provided by: Alceu Ferraz Costa email: [alceufc@icmc.usp.br](mailto:alceufc@icmc.usp.br) and it follows the following steps:

1. Pad the image with background pixels so that its dimensions are a power of 2.
2. Set the box size 'e' to the size of the image.
3. Compute  $N(e)$ , which corresponds to the number of boxes of size 'e' which contains at least one object pixel.
4. If  $e > 1$  then  $e = e / 2$  and repeat step 3.

5. Compute the points  $\log(N(e)) \times \log(1/e)$  and use the least squares method to fit a line to the points.
6. The returned Haussdorff fractal dimension D is the slope of the line.

#### **3.4.8 Boxcount.m**

The algorithm was provided by Frederic Moisy<sup>220</sup>: Counts the number N of D-dimensional boxes of size R needed to cover the nonzero elements of C. The box sizes are powers of two, i.e.,  $R = 1, 2, 4 \dots 2^P$ , where P is the smallest integer such that  $\text{MAX}(\text{SIZE}(C)) \leq 2^P$ . If the sizes of C over each dimension are smaller than  $2^P$ , C is padded with zeros to size  $2^P$  over each dimension (e.g., a 320-by-200 image is padded to 512-by-512). The output vectors N and R are of size P+1. For a RGB colour image (m-by-n-by-3 array), a summation over the 3 RGB planes is done first.

#### **3.4.9 Edge Detection approach.m**

This is a slight different algorithmic approach for determining the fractal order compared to the MATLAB R2018b scripts described above. In this approach none of the thresholding approaches described above are utilized to generate a binary image to apply the box-counting method. Instead in this case an edge detection method is used where the algorithm is detecting all the edges existing in the image, which can distinguish the object from the blank background, and then converting into a binary image where all the edges enclose the surface of the object. Then the box counting method can be applied and in this case any box that contains a pixel of an edge part is included in the calculation of the Fractal Dimension. This is an interesting approach since it enables to assess the structures from a surface point of view giving a different perspective in the estimation of the fractal dimension.

#### **3.4.10 Multifractal.m**

This algorithm was used based on the previous work by Posadas et al.<sup>20</sup>, where a detailed description of the theoretical background of this algorithm can be found. Multifractals allow for the characterization of complex spatial arrangements with respect to mass since local densities can be resolved<sup>10</sup>. It enables for characterization of different fractal patterns simultaneously providing a range of fractal dimension spectra that characterizes in more detail the surface pattern of complex structures, if there is an evident variability in the objects of interest. In order to determine if the OFI fibres do depict a multifractal character this algorithm was applied in the images obtained for the OFI fibres. This algorithm again is based on the box counting method, so the images had to be binarized for its application through the three

different thresholding approaches described above, in order to test the robustness and reproducibility of this algorithm.

#### **3.4.11 Microcomputed tomography ( $\mu$ CT) measurements**

A small piece of length of 2.5 cm and width of 2.5 cm and thickness of 0.1 cm (see figure 3.2) was cut from the cactus natural fibre sheet and was placed in the Nikon XTH225ST CT Scanner with a 3 micron focal spot size at 35kV (Fig. 3.2).



**Fig. 3.2** Cactus fibre specimen for X-Ray Micro-Computed Tomography ( $\mu$ CT) measurements

X-ray computed micro-tomography scan ( $\mu$ -CT) was performed on a portion of the cactus sheath (2.5 cm X 2.5 cm X 0.1 cm - Fig. 2) using a Nikon XTH225ST CT Scanner. The scanning voltage was 35 kV and a 3 X 3  $\mu$ m voxel size was achieved. Projections were acquired over 360° rotation and the images were reconstructed and viewed using the VG Studio MAX 3.3 software. Measurements obtained with the help of Katie Smith.

#### **3.4.12 Mechanical Testing**

Since the fractal argument implies the presence of self-similarity across scales we wanted to see if the properties of the cactus structure are maintained if a small subsection of the cactus fibre sheet was mechanically tested. If the high bending to axial stiffness ratio were to be maintained our fractal hypothesis would be reinforced. The same pieces described above and demonstrated in Fig 3.2 with a length and width of 2.5 cm and a thickness of 0.1 cm were used to perform 3 point bending and tensile testing tests according to ASTM D790-17 and ASTM D638-14 standards using a Shimadzu testing machine fitted with a 1kN load cell. For both tests a crosshead speed of 1mm/min was utilized and in the tensile test case no grips were utilized as we aimed to characterize the mechanical properties of the structure directly without other materials present. All results are reported as an average with a standard deviation error (n=5)

## **3.5 Artificial Cactus Inspired Reinforcement Materials**

### **3.5.1 Microcomputed tomography ( $\mu$ CT) measurements & model extraction**

The  $\mu$ CT measurements were obtained as described in section 3.4.12 using the same specimen depicted in Fig. 3.2, while further manipulation was carried out in VG studio max 3.3 in order to obtain the .stl files. The  $\mu$ CT data were exported in a tetrahedron mesh .stl from the VG studio MAX software interface using the Polygonal surface Extraction mode; in this study, the iso-gray-value-surface extraction through the auto detect grayvalue method was implemented. The extracted .stl file was then manipulated in Meshlab 2017 to remove non manifold edges and vertices, and also reduce the size of the file by applying the polygon reduction filter via Quadric edge collapse (QEC). This polygon reduction filter was used to significantly reduce the number of polygons in our mesh, since the extraction form the  $\mu$ CT resulted in the extracted mesh having  $10^7$  polygons, while the printer used in this work could only operate with a maximum of  $10^5$  polygons. The filter had the option set for the target amount of  $10^5$  polygons, while maintaining the quality threshold value to 1 for minimizing the modifications made to the overall shape of our model .stl file (a value between 0 to 1 is selected in the filter; the higher the value, the lower the amount of modifications made to the original shape). The use of the polygon reduction filter enabled us to manipulate our .stl file model to generate the 3D printed manufactured specimens. Five additional  $\mu$ CT measurements were performed on the 3D Printed cactus analogue specimens to assess their internal porosity. Measurements obtained with the help of Katie Smith.

### **3.5.2 Polylactic Acid (PLA) 3D Printing**

All the samples were printed on Raise 3D N1-V2 Hot End printer using a single roll of Raise 3D Premium filament red. The printer settings were at: 10% and 100% infill, using full supports and raft material. Additionally, a 0.2 mm layer height was used at a 30 mm/s speed for the infill and a 60mm/s for the support while the right extruder was used for all prints at 225°C and a heated bed at 65°C.

### **3.5.3 Stereolithography (SLA) 3D Printing**

All the samples were printed on a Form 2 SLA printer using Clear Resin V2. All the supports were used at a layer thickness of 0.1 mm and the post processing was carried out as instructed by the manufacturer.

### **3.5.4 Specimen Manufacturing**

Once the .stl files and the 3D rendered models were optimized and a cactus analogue structure could be produced, specimen manufacturing became of key importance. Initially the material

selection was limited to the range of materials that can be 3D printed. However, since our hypothesis is that the geometry is maintained and that the architectural features are responsible for the 7:1 bending to axial stiffness ratio then the phenomenon should be observed irrespective of material; thus PLA filament was used. The aim was to generate specimens in agreement with the ASTM standard requirements. Thus, our 3D analogues would need to have a substantially larger thickness than the one observed in the biological material. In order to be able to provide a fair mechanical assessment of the cactus structure, our analysis included appropriate normalizations through calculating the specific flexural moduli of the cactus analogues including density measurements. Moreover, the 3D printed cactus analogues were compared against the ASTM standard controls and also against the equivalent beams, which would be a more appropriate comparison of the cactus structure potential, since the size of the geometrical characteristics of the cactus structure are taken into account. Thus, four categories of specimens were generated:

Cactus ASTM: L=200 mm, W=50 mm (maximum width), T=4 mm

Bending Equivalent Beam ASTM: L=200 mm, W=50mm, T= 4 mm

Cactus Tensile ASTM-with grips: L= 165 mm, W=19mm, T= 4 mm

Tensile ASTM-with grips : L= 165 mm, W=19 mm, T= 4 m

### **3.5.5 Mechanical Testing & Analysis**

All the mechanical tests performed according to ASTM standards. Specifically, ASTM D638-14 was followed for the tensile testing and ASTM D790-17 for the 3 point bending tests. Five (n=5) specimens were tested for each of the cases described above and all data is reported as an average with a standard deviation error. The tests were carried out using a Shimadzu testing machine fitted with 1 kN and 10 kN load Cells at crosshead speeds of 1 mm/min. The specimen dimensions are described in section 3.5.4.

### **3.5.6 Normalization Formulas**

In order to compare the mechanical properties between the cactus analogues and the equivalent control beams a density normalization was implemented to generate the specific moduli of the specimens. The formula used was:

$$\text{Specific Modulus (MPa/(g/cm³))} = \frac{\text{Flexural Modulus}}{\text{Density}}$$

where the Flexural Modulus is calculated according to ASTM D790-17. To estimate density in our case we used the mass of each control and cactus specimen, and we assumed the volume of the control and cactus specimens to be the same as the control beams were designed to mirror the dimensions of the cactus structure.

### **3.5.7 Finite Element Model**

Finite element simulations are in general instrumental in providing further understanding of the mechanisms present in the structure responsible for the mechanical properties observed. In this work we were focusing on the stiffness of a larger scale representation of the cactus structure manufactured with an isotropic material (PLA) and directly compared to an equivalent beam. A linear elastic beam element model representing the distribution of the moment of inertia of the beam was therefore deemed as a reasonable approach to carry out simulations focused on the stiffness characteristics, especially at small strains. A full-scale model representing the complexity of the cactus structure via the wealth of the morphological data obtained from the  $\mu$ CT measurements was initially developed, however computing power available and convergence issues did not enable the meshing of the whole cactus structure. By observing the structure of the 3D printed manufactured cactus specimens, it is evident that the major structural element that is varied across the structure is the cross-sectional area of the specimens. Thus, sections were obtained from the cactus specimen structure to recreate a varying cross-sectional area beam reproducing the same distributions of cross sections observed in the cactus 3D printed specimens. The model developed could be considered in a sense emulating a coarse-graining approach for the recreation of the structure with the finite element environment. The generation of the Finite element (FE) model was carried out in an ANSYS environment. Initially, morphological information of the 3D printed cactus analogues was obtained in Meshlab 2017, in which sections were obtained and the morphological information of each used for the generation of the equivalent beam. Sections of the cactus configurations were therefore used for the generation of a reduced order model finite element beam, with the number of sections optimized to obtain an acceptable convergence of the model with the experimental data. A non-linear Newton-Raphson solver was used for the bending and tensile loading simulations. It is important to note that only linear elastic properties of the PLA polymer were used here for the FE material selection. Those properties were evaluated *via* a ASTM D638-14 tensile test and it was determined that the experimental values matched closely the elastic properties specified by the manufacturer. The finite element model had the two ends represented by clamps (i.e., no translational or rotational degrees of freedom allowed). To account for the macro-porosity present in the cactus structure, an infill factor was introduced in the material constants of the model to account for the effective porosity present due to the 3D printing infill and also the complexity of each cross section utilized.

## 3.6 Cactus Based Thermoplastic and Hydrogel composites

### 3.6.1 Fourier-transform Infrared Spectroscopy

Ball milled natural fibres were analysed using Spectrum One FTIR spectrometer with data collected from 600-4200 cm<sup>-1</sup> and the blank background collected was subtracted.

### 3.6.2 Thermoplastic Composites

Thermoplastic composites were initially manufactured using the natural biopolymer Polylactic acid (PLA) Ingeo 4043D grade that was supplied by NatureWorks LLC. The composites were manufactured using a thermoforming approach. In the aluminium mould **shown in Fig. 3.3 were placed** 6g of PLA pellets in the mould with 3% w/w of the natural fibres of interest and they were hand mixed. The mixtures were placed in an oven at 200°C for 2 hours for the composite specimens to be thermoformed and then the temperature was reduced to 90°C for 4 hours and the specimens were removed from the mould and left inside the oven overnight to cool down naturally as the oven was also shut down. It is important to note that the mould dimensions were based on the dimensions of the Dynamic Mechanical Analysis (DMA) Viscoanalyzer MetraVib DMA 400+ for the 4-point bending specimen holder.

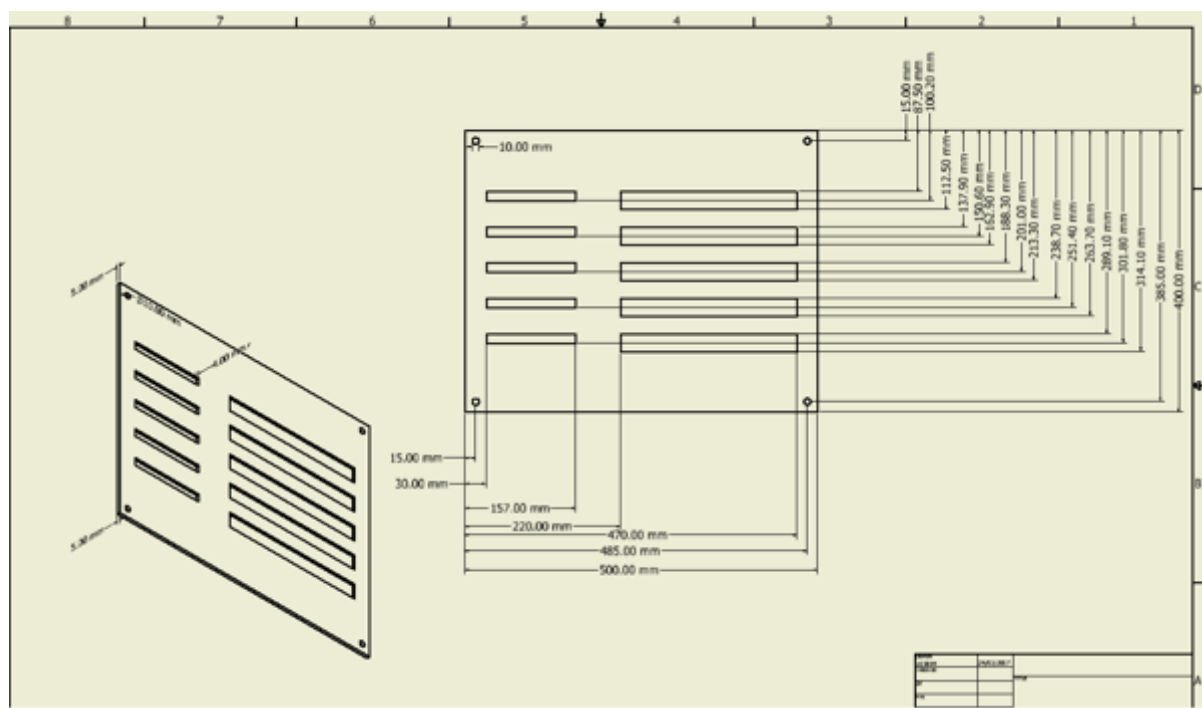


**Fig. 3.3** Mould Design for the manufacturing of the thermoplastic composite specimens

### 3.6.3 Dynamic Mechanical Analysis (DMA)

As previously described<sup>185</sup> The rationale for focusing on DMA measurements for the determination of storage loss modulus, loss modulus and damping characteristics was due to the lightweight nature of natural fibre powders that meant that for significant weight

percentages to be introduced the amount of the PLA to be used had to be minimal. We did manufacture specimens of thickness of 4 mm as it has been previously described by Wielage et. al<sup>185</sup> to determine the differences between the behaviour of PLA specimens and the various natural fibre composites. This enabled us to directly compare the mechanical behaviour observed between the PLA specimens and the composites. In this case all the measurements were carried out at room temperature in order to evaluate the mechanical properties of those composite specimens and compare them and the frequency used was 5 Hz and the static amplitude was 50 µm. Single cantilever clamps were used for the 3-point bending measurements and the specimens as described in the mould above were 155 mm in length, 15 mm in width and 4 mm in thickness.

#### **3.6.4 Cell Culture**

Human Mesenchyma Stem cells (hMSCs) were obtained from the proximal femur bone marrow of patients undergoing total hip replacement surgery, in full accordance with Bristol Southmead Hospital Research Ethics Committee guidelines (reference #078/01) and having received informed consent from all patients. hMSCs were cultured at 37 °C and 5% carbon dioxide environment and the medium use for expansion was low glucose Dulbecco's Modified Eagle's Medium (DMEM) supplemented with:

i) 100 units mL<sup>-1</sup> penicillin/100 mg mL<sup>-1</sup> streptomycin (Sigma Aldrich,

UK)

ii) 2 × 10<sup>-3</sup> m GlutaMAX (Invitrogen, USA),

iii) 10% (v/v) foetal bovine serum (FBS),

A working expansion medium formulation had the following:

- 450 ml low glucose DMEM
- 50 ml FBS
- 5ml P/S
- 5 ml GlutaMAX

Before every cell media change 5 ng mL<sup>-1</sup> basic human fibroblast growth factor (Peprotech, USA) was freshly supplemented.

Once the desired confluence was achieved cells, were obtained using Dulbecco's phosphate buffered saline (Sigma Aldrich, UK) and trypsin/ethylenediaminetetraacetic acid solution (Sigma Aldrich, UK) and centrifuged for 5 minutes at 5000 rpm into a pellet. The pellet was

resuspended in low glucose fully supplemented phenol free media at a small volume of 50  $\mu$ l and were then counted and introduced to the hydrogel specimens for cell bioprinting.

### **3.6.5 Hydrogel**

The methodology for the preparation of the hydrogel formulation has been previously described<sup>103</sup> and has been utilized by the laboratory since then. In brief the aim is to make a hybrid hydrogel formulation comprised of alginate and pluronic F-127. Initially stock solutions of the Pluronic F-127 (Sigma Aldrich, UK) in low glucose phenol free DMEM (Sigma Aldrich, UK) was prepared at 40% and this sterile solution was used for four weeks. To make working gel formulations the Sodium Alginate powder (Sigma Aldrich, UK) was sterilized under UV irradiation for 1 hour. The working gel formulation contains 6 wt% Sodium alginate and 13 wt% Pluronic F-127, thus to generate the 2 ml of gel initially 120 mg of sterile sodium alginate powder was dissolved in 1.2 ml low glucose phenol free DMEM followed by the addition of 0.675  $\mu$ l of the sterile Pluronic F-127 solution prepared. For the mixing of the gel a DAC 150.1 FVZ Speedmixer™ was used, which meant that the gel was prepared on the custom-made DAC pots provided by the manufacturer. Initially the gel was mixed at 1500 rpm for 5 minutes followed by 3500 rpm for 15 minutes in 5 minute intervals. Once the gels were prepared, they were transferred to a sterile 5ml syringe (Thermo Corporation, Japan) where they were extruded via an 18 gauge needle. For the cell-containing gels  $5 \times 10^5$ /ml hMSCs were introduced in the gel and were hand-mixed before the cell containing gel was transferred in the syringe for extrusion.

### **3.6.6 Hydrogel Fibres**

The natural fibres were ball milled as described above and were sterilized under UV irradiation for 1 hour. The working gel formulations contained 6 wt% Sodium alginate a natural fibre range of 0.625 wt%, 1.25 wt% and 2.5 wt% and 13 wt% Pluronic F-127. To generate 2 ml of gel in this case 120 mg of sterile sodium alginate powder and 50 mg of sterile natural fibre powder (for the 2.5 wt% case) were initially dissolved in 1.2 ml low glucose phenol free DMEM followed by the addition of 0.675  $\mu$ l of the sterile Pluronic F-127 solution prepared. The procedure then is exactly the same as the one described above.

### **3.6.7 Rheology**

From previous work<sup>103</sup> it has been demonstrated that the hybrid gel exhibits shear thinning behaviour and viscoelastic behaviour making it ideal for bioprinting applications. Since the natural fibre reinforced hydrogel composites are nearly identical to the original hybrid gel described it was expected that a similar behaviour would be observed. Thus, the methodology utilized for the measurements was identical and only focused on the uncross-linked systems as

those are the one being extruded. Briefly, Small amplitude oscillatory measurements were performed on the specimens at 37 °C with a TA Discovery HR-1 Hybrid Rheometer. The uncross-linked hydrogels were placed on the rheometer plate and the test geometry was lowered at 500 µm and the excess hydrogels from the side were removed. A linear viscoelastic region strain was used at 0.1% and a frequency sweep was performed from 0.1 to 10 Hz which was used to determine the G' and G'' while a shear rate range of 0.1 to 10 Hz was utilized to determine the flow index using the Ostwald-de Waele relationship. All measurements were performed at 37 °C as those are the conditions of the extrusion of the gels due to the fact that the cells encapsulated within the hydrogel need to remain at 37 °C. Due to the mechanism of the formation of this hybrid gel where micelle formation of the Pluronic F-127 at 37°C leads to greater variability in the rheometry measurements as the micelle formation directly affects the rheological properties of the gels.

### **3.6.8 Extrusion & Crosslinking**

In our experimental design the hydrogel and the hydrogel composites were extruded from an 18-gauge needle by hand and they were placed in a 96-well plate that acted like a mould for the hydrogel specimen. The extruded gels were crosslinked with 100 mM Calcium Chloride in fully supplemented expansion low glucose phenol free overnight where the crosslinker was supplied from the top. The next day the media was replaced with 5 mM Calcium Chloride for the amount of time required for each experiment, specifically for 21 days in the cases of both cell free and cell containing hydrogels that were differentiated for bone tissue engineering.

### **3.6.9 Compression Testing**

All mechanical testing was performed on a STARRET FMS-500-L2 Force Measurement System (The L.S. Starrett Company Limited, UK) fitted with a 100 N load cell at room temperature. The hydrogels were scooped with a spatula from each well and the thickness and diameter of each gel was measured with the use of a calliper. Each sample was then mounted onto a PLA stage and subjected to destructive compression testing at a rate of 1 mm min<sup>-1</sup>. The compressive modulus (kPa) of each sample was then calculated with the values reported representing the mean (n = 9) ± standard deviation.

### **3.6.10 Cell Viability & Cytotoxicity**

Hydrogel and Hydrogel composites were intermixed with cells at 5 x 10<sup>5</sup> ml<sup>-1</sup> and were extruded in 96-well plates at small volumes. The extruded gels were crosslinked with 100 mM Calcium Chloride low glucose phenol free fully supplemented DMEM overnight and then cultured in 5mM Calcium Chloride low glucose phenol free fully supplemented DMEM for up to 7 days. On the day of the cell viability experiment the specimen media was supplemented

with a commercial live/dead stain kit consisting of Calcein AM and ethidium bromide. These samples were imaged on an SP8 confocal fluorescence microscope (Leica, UK) using a 10× objective lens and the cell viability measurements were made using Image J software.

### **3.6.11 Stem Cell Differentiation**

Cell Containing hydrogel and hydrogel natural fibre composites were extruded in 96 well plates as described above. For osteogenic differentiation the cells were stimulated for 21 days in differentiation media (Gibco<sup>TM</sup>) according to the manufacturer's instructions. The differentiation media was supplemented with 100 mM Calcium Chloride for the first 24 hours and then with 5 mM Calcium Chloride for the rest of the 21 days. Media was changed 7 times a week (**every 24 hours**) due to the thickness required for the samples to be tested under mechanical compression to failure.

### **3.6.12 Alkaline Phosphatase (ALP) Assay**

ALP activity was determined by a biochemical colorimetric assay using an alkaline phosphatase kit (Gene Tex, Irvine, USA) after 7 days of culturing cell containing hydrogel and hydrogel composites in normal expansion medium DMEM without any osteogenic factors present to assess the osteo-inductive potential of these hydrogels. ALP is an early genetic indicator of osteogenesis thus this assay enables the assessment of the potential of materials to induce osteoinduction without the presence of osteogenic growth factors.

### **3.6.13 Histological Analysis**

The histology experiments carried out followed the same procedures developed before<sup>103</sup> for the histological characterization of the hybrid bioink. Briefly, after 21 days of differentiation the hydrogels and the hydrogel natural fibre composites were submerged in fixation buffer (BioLegend, USA) for 2 h and then they were transferred in 70% v/v ethanol solution and were submitted and then submitted to Histology Services Unit (University of Bristol). **After the initial preparation and the fixation in ethanol which was carried out by me, the next steps for the sample preparation were carried out by the Histology Services Unit (University of Bristol).** The specimens were embedded in paraffin and were cut in 10 um sections and then were fixed in polysine microscope slides (VWR, UK) where the samples were rehydrated using 2-minute immersions in xylene, 100% ethanol, 70% (v/v) ethanol and Deionized water successively. Calcium staining were immersed in 2% Alizarin Red S for 5 minutes and then excess stain was cleared by 20 dips in acetone, 50:50 acetone:xylene solution and in xylene successively. Von Kossa staining was used for phosphate staining were the slide were immersed for 90 minutes in 5% solution of silver nitrate (Sigma Aldrich, UK) with the container covered in foil and illuminated using a lamp. The slides were then washed four times with deionized water,

immersed for 3 min in 5% sodium thiosulphate (Sigma Aldrich, UK), washed twice with deionized water, and then dehydrated using 2 min immersions in 90% (v/v) ethanol and 100% ethanol. For collagen staining, slides were immersed in 0.1% Sirius Red (Sigma Aldrich, UK) for 1 h at room temperature, briefly washed in two changes of 0.5% (v/v) acetic acid and then dehydrated using 2 min immersions in 70% (v/v) ethanol, 90% (v/v) ethanol, and 100% ethanol. For glycosaminoglycan staining, slides were briefly washed with acetic acid (pH 2.3), stained for 2 min using 0.1% Safranin O (pH 2.3), dipped in 95% (v/v) 20 times, 100% ethanol ten times and then immersed for 2 min in xylene. All the slides were imaged with a Carl Zeiss Microscope using a 5x objective lens.

#### **3.6.14 Critical Point Drying for Scanning Electron Microscopy of Hydrogels**

Small sections of the hydrogel and the hydrogel natural fibre composite specimens were obtained and were submerged successively for 20 minutes in, 10% v/v, 20% v/v, 50% v/v, 60% v/v, 70% v/v, 80% v/v, 90% v/v, 100% v/v ethanol solution. Then the samples were critically point dried mounted on SEM stubs and sputter coated with silver using High Resolution Sputter Coater (Agar Scientific, UK). Samples were imaged using a JSM IT300 Scanning Electron Microscope (Jeol Ltd., Japan).

#### **3.6.15 Roughness Measurements<sup>186</sup>**

An Alicona InfiniteFocus microscope was used for the evaluation of the surface roughness of the natural fibres. Briefly, the Alicona measurements are based on principle of focus variation where the microscope recreates a three-dimensional image based on the vertical focusing on the object. The microscope obtains images as the vertical focusing is changed through the image and generates a composite image of all the layers allowing for the characterization of the surface topography.

### **3.7 micro-CT ( $\mu$ CT) for Hydrogels And Composites**

All measurements were carried out in a Nikon XTH225ST CT Scanner with a 3-micron focal spot size at 35 kV. Projections were acquired over 360° rotation and the images were reconstructed and viewed using the VG Studio MAX 3.3 and AVIZO 2018 software.

#### **3.7.1 Thermoplastic Composites micro-CT**

$\mu$ CT measurements were obtained of 25x25x4 mm sections of the specimen manufactured to assess the distribution of the cactus fibre particles within the matrix, while in situ bending tests revealed information of the mechanical properties of those composites in bending loading scenarios. Measurements obtained with the help of Dr. Dong Liu.

### **3.7.2 Hydrogel & Hydrogel Composites micro-CT with differentiated stem cells**

The bioink samples that were differentiated for 21 days and were embedded in paraffin for histology were also used for  $\mu$ CT measurements to determine the calcium phosphate present within the differentiated samples of the hydrogels and the hydrogel cactus composites. Samples that did not contain any cells were also fixed in paraffin and sliced in 10 um sections and were imaged for control comparison purposes. Measurements obtained with the help of Olie Nixon Pearson.

## 4 Fractal Morphology Characterization

---

### Relevant Publication:

Billon K, **Zampetakis I**, Scarpa F, Ouisse M, Sadoulet-Reboul E, Collet M, et al. **Mechanics and band gaps in hierarchical auxetic rectangular perforated composite metamaterials.** Composite Structures. 2017;160:1042-50.

### *4.1 Chapter Overview*

The aim of this chapter was to assess and characterize the morphology of the cactus fibre through fractal geometry in an effort to gain a better understanding of the mechanical properties observed and how can those be related to the fibres' hierarchical structure. Images through various imaging modalities and at various scales were obtained to evaluate this morphology and a fractal geometry approach was pursued to characterize the cactus structure. The fractal geometry characterization was achieved through the development of an algorithm utilizing the images obtained of the fibres and traits of self-similarity were observed. The fractal characterization approach was also utilized on 3D rendered models of the cactus structure that were developed through the morphological information observed in order to further verify and validate the hierarchical and morphological characteristics maintained in the cactus fibre structure.

## **4.2 Results & Discussion**

### **4.2.1 Fractal Characterization of Cacti Fibres**

The initial stage of the project included a morphological evaluation of the *Opuntia ficus indica* (OFI) fibres. The purpose of this analysis was to gain an understanding of the unique architecture of this type of natural fibres across multiple scales in order to determine the effect that these characteristics have on their unusual mechanical properties<sup>9,10</sup>. It was established initially that traditional Euclidean geometry would not provide the required framework for a correct analysis and assessment of the natural fibres, so the focus steered towards alternatives that would provide a better scheme for successful morphological evaluation. It was decided that fractal geometry was the tool to provide a better understanding of the properties of the fibres. A fractal geometry analysis provides a better morphological evaluation of these natural fibres since it is a quantifiable measure of roughness<sup>11-13</sup>. Moreover, a fractal characterization of an object implies self-similarity across scales which would suggest that this unique morphology is maintained throughout scales<sup>11-17</sup> providing unique potential for composite fabrication. In order to perform this type of fractal analysis a method described previously was pursued where images at different scales can be obtained and analysed for the estimation of the fractal order<sup>3</sup>. The strategy followed in order to perform the fractal analysis of the fibres included obtaining images through an optical microscope at various magnifications for the OFI fibre sheet as well as from a processed powder form of the OFI fibres<sup>31</sup>. The images were evaluated on a MATLAB environment through image processing analysis and box counting methods for the estimation of the fractal dimension *Opuntia Ficus Indica* fibres<sup>17,31</sup>. Three different MATLAB scripts were utilized for the estimation of the fractal dimension to ensure reproducibility and accuracy of the results as well as three different thresholding techniques to assess the robustness of the algorithms themselves. It is important to note that all the algorithms implemented<sup>17,18,31</sup> were developed for the assessment of deterministic fractals with known fractal orders and thus have been validated for the characterization of these fractal estimations. They were then implemented for the fractal characterization of the cactus fibres where they have been used previously for the fractal characterization of other materials<sup>18,31</sup>. Initially, the fractal analysis was implemented on images of the whole cactus fibre sheath and a fractal order of 1.6 was established, Fig. 4.1, for the whole cactus structure. In order to initially test the fractality argument a much smaller section of the cactus fibre sheath was obtained, and the same algorithmic approach was applied while it was also imaged under µCT, see Fig. 4.2.

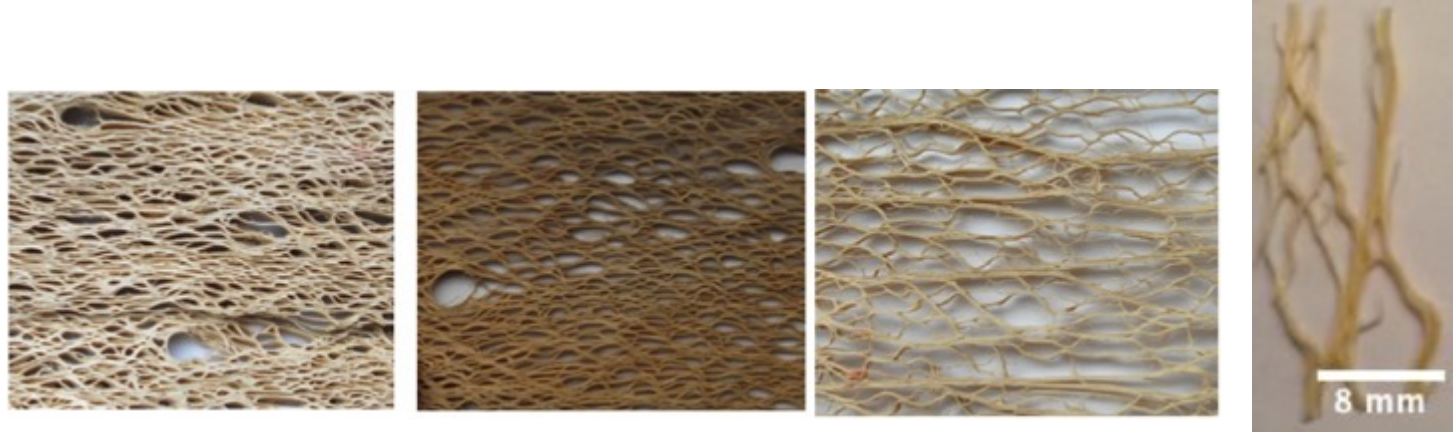


**Fig. 4.1** The fractal order of the above figures was maintained at 1.6 for the whole fibre sheets and the smaller piece.

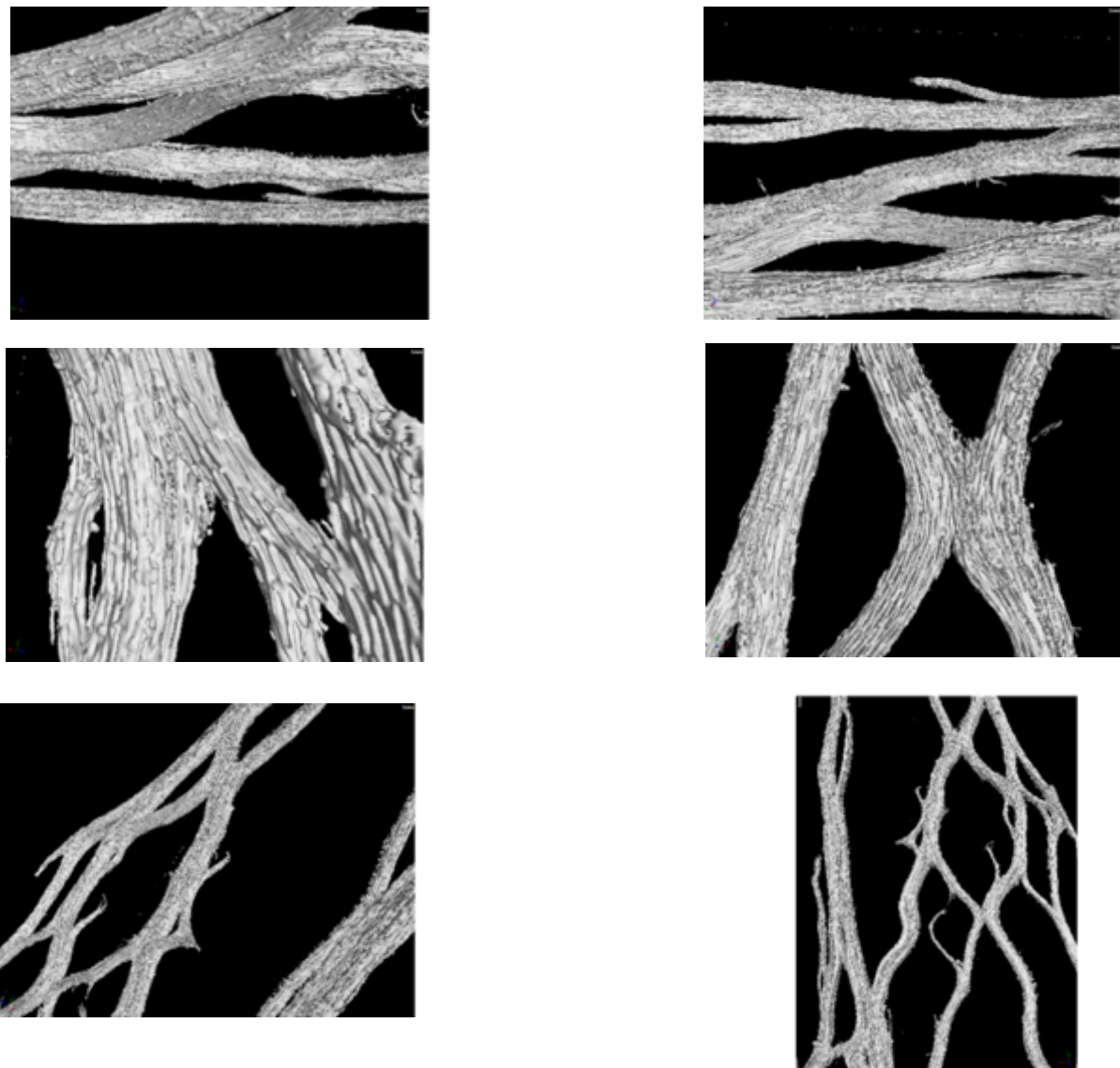


**Fig. 4.2** The images displayed demonstrate the Micro-Computed Tomography ( $\mu$ CT) scan results of the structural subunit of the cactus fibre structure. The fractal order of these images was also estimated at 1.6.

The fractal algorithm was initially implemented on the picture of the smaller piece of the cactus sheath and the fractal order was maintained at 1.6 while the same held true for the fractal order

of the  $\mu$ CT images shown. These results demonstrate the first elements of fractality being present in the cactus fibre sheath structure as a smaller structural subunit has the same fractal order as the whole cactus fibre sheath, verifying the assumption of self-similarity for fractal structures<sup>9</sup>. Moreover, the robustness of those results is empowered by the fact that the fractal order is maintained both in the image of the cactus fibre piece and the  $\mu$ CT results which means that the results are independent of the imaging modality utilized. To further research how the fractality present is maintained a reverse engineering approach was implemented. Obtaining a 3D rendered model of the cactus structural subunit we aimed to recreate the cactus fibre sheath by self-replicating that one structural subunit following the definition of a fractal as a self-repeating unit across scales<sup>11-13</sup>. Initially fractal characterization of the 3D rendered subunit revealed that it maintains a fractal order of 1.6 which is to be expected as it is directly exported from the  $\mu$ CT measurements obtained where the images maintain the fractality. The 3D rendered structural subunit was self-replicated to generate the artificial digital copy of the cactus fibre structure Fig. 4.3 and the fractal analysis implemented demonstrated that the fractal order remains at 1.6

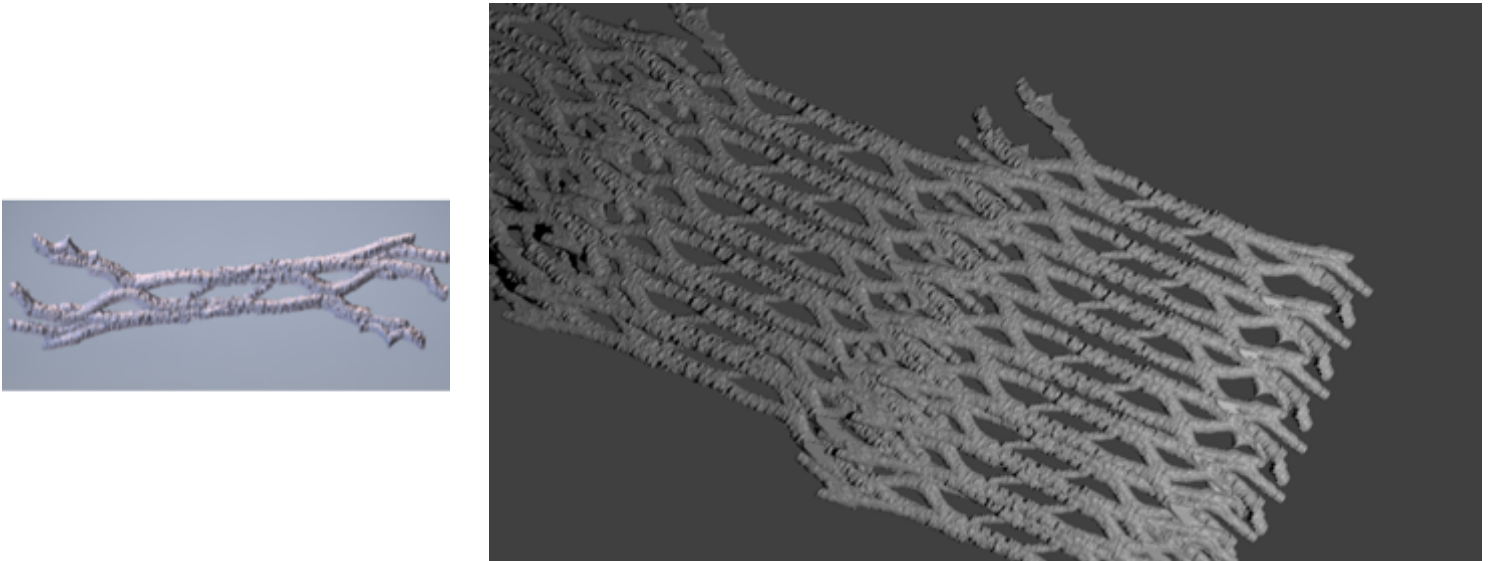


**Fig. 4.3** Reconstructed image of the cactus fibre sheet from the Micro-Computed Tomography ( $\mu$ CT) data obtained. Fractal analysis revealed that the value of these images is also at 1.6.

This is quite a significant result as it clearly demonstrates that there is fractality present in the cactus fibre sheath and the whole structure can be reduced to a singular significantly smaller subunit that maintains the morphology of the whole cactus fibre sheath. That argument holds true even if the cactus fibre sheath structure is reverse engineered from that singular subunit. To the author's knowledge this is the first attempt at the fractal characterization of a biological material at the macroscale with the ability to reverse engineer the structure from a single

structural subunit. The established fractality present on this natural structure could be directly related to the mechanical properties demonstrated by these fibres when implemented as polyester matrix reinforced where a bending to axial stiffness ratio of 7 to 1 was observed<sup>9</sup> as hierarchical self-similarity i.e. fractality has been previously related with interesting mechanical properties<sup>27,30,31</sup>. We hypothesized that since the morphology plays a key role in the mechanical properties observed by the cactus structure, and the morphology is maintained at a smaller subunit due to the fractality present, the mechanical properties would be maintained in the smaller cactus subunit. To that end, bending and tensile testing was performed on the smaller structural subunit for the cactus structure to determine whether the bending to axial stiffness ratio is maintained. As it is evident on Fig. 4.4, Fig. 4.5 and Table 4.1 the unusual mechanical properties were maintained even as the specimen tested was a significantly smaller structural subunit of the whole cactus fibre sheath.

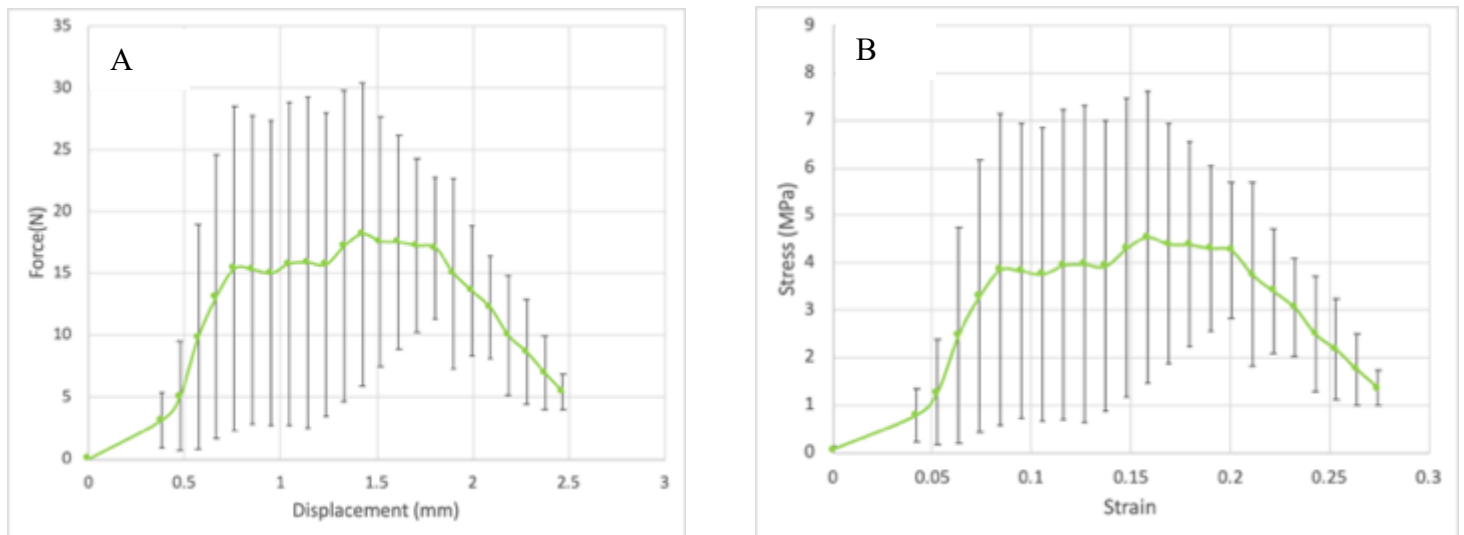


**Fig. 4.4** Tensile testing of cactus piece (a) Force vs Displacement data and (b) Stress Vs Strain Data.

All tests were carried out according to ASTM D638-14 (n=5)

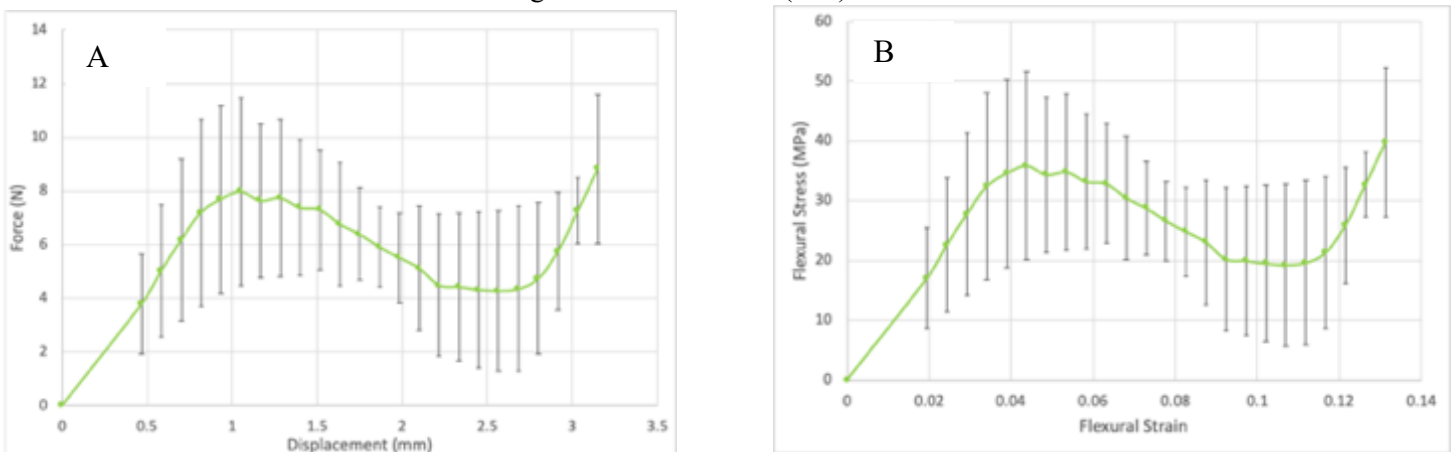


**Fig. 4.5** 3-Point Bending testing of cactus piece (a) Force vs Displacement data and (b) Stress Vs Strain Data. All tests were carried out according to ASTM D790-17 (n=3)

**Table 4.1** Axial and Flexural Modulus of the cactus fibre Piece and their ratio.

	Axial Modulus (MPa)	Flexural Modulus (MPa)	Ratio
Cactus_Fibre_Element_1	155.6	1513.9	9.7
Cactus_Fibre_Element_2	157.1	1482.3	9.5
Cactus_Fibre_Element_3	219.8	1695.9	7.7
Cactus_Fibre_Element Average	177.5 ± 36.6	1564.1 ± 115.3	8.8

This finding serves to verify our hypothesis that the structural characteristics are maintained across scales due to the fractal structure present in the cactus fibres, since it is observed that a significantly high bending to axial stiffness ratio is observed at the small structural subunit of the cactus. Thus, the existing fractality within the structure also ensures that the mechanical properties self-replicate across the scales that fractality is present. It is observed in Fig.4.4 that there is an initial non-linearity present which is attributed to the lack of grips while performing the tensile test to attribute the mechanical properties directly to the structure itself. This non-linearity was normalized and was not taken into account for the final calculations. It is important to note that the significant variability demonstrated in the samples is due to the fact that all the samples were randomly selected from various different cactus fibre sheaths to ensure the robustness of the results and conclusions drawn. In all cases of the testing however the ratio of bending to axial stiffness always remained significantly high and close to the one observed in the original work<sup>9</sup>. Once the fractality of the cactus structure was established up to the single structural subunit scale the focus shifted on determining across which scales the fractality is maintained and thus various imaging modalities were used on various fibres formats to determine the fractal order. Images were obtained using optical microscopy and SEM across various magnifications both for the cactus structural subunit piece and a cactus fibre powder format prepared via a ball milling method Fig.4.6, Fig. 4.7, Fig. 4.9.

#### ***4.2.2 Fractal Characterization of Natural Fibres & Comparisons***

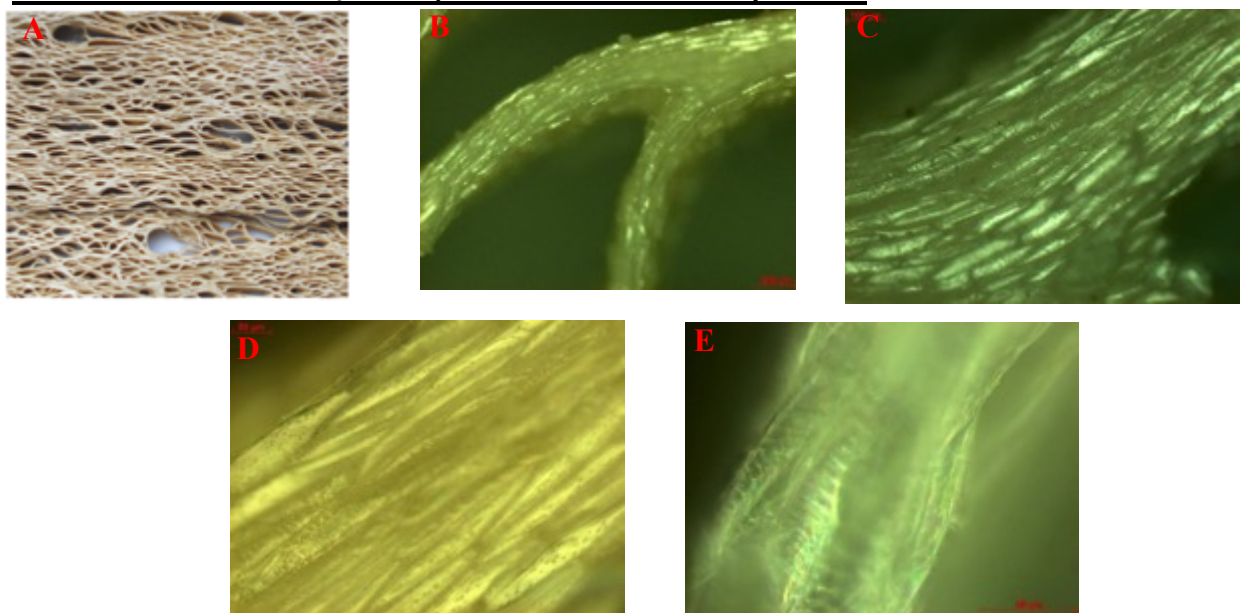


**Fig. 4.6** The pictures demonstrated show images obtained for the cactus natural fibre Sheet at: A, 0x. B, 5x. C, 10x. D, 20x. E, 50x

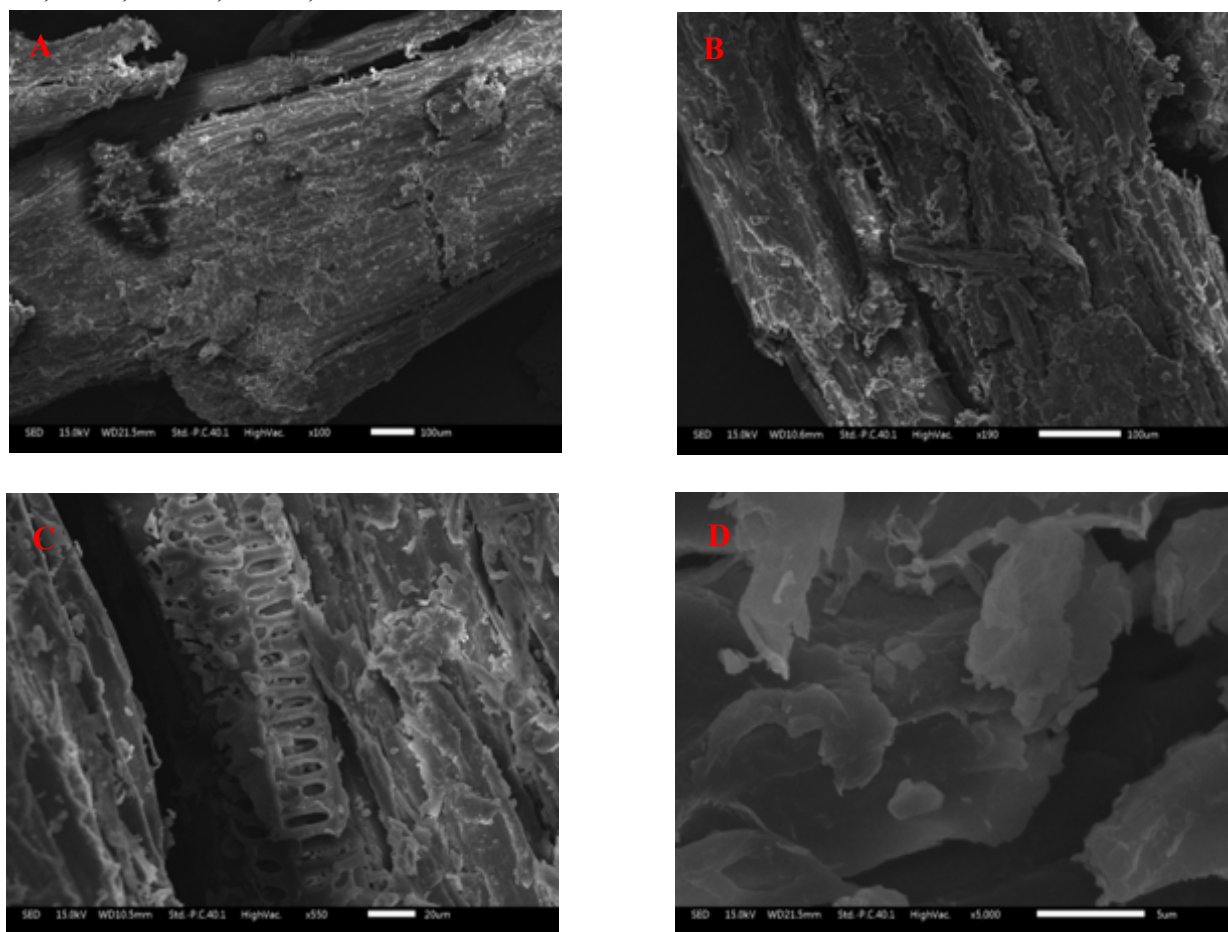


**Fig. 4.7** The images displayed A through D displayed demonstrate 4 Scanning Electron Microscopy (SEM) images of the natural fibres at different magnifications. The fractal order determined from the Scanning Electron Microscopy (SEM) images was estimated at:  $1.80 \pm 0.13$ .

As evident in Fig. 4.8 and fig. 4.10 it was revealed that the fractal order at those scales and as the format of the fibre is changed it has a new value of 1.8 that is significantly different from the fractal value of 1.6 observed in the cactus fibre sheath.

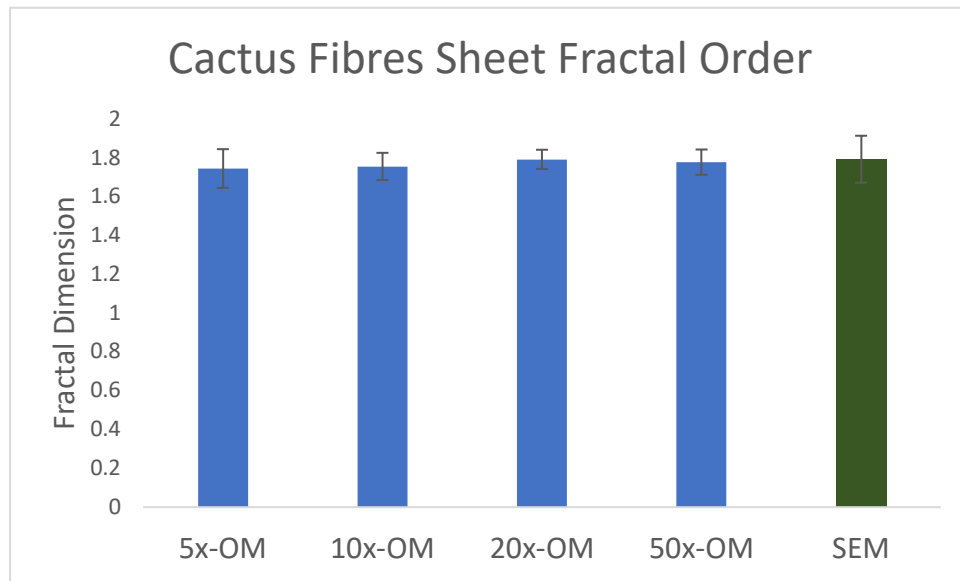


**Fig. 4.8** The resulting fractal dimension estimations are plotted for each magnification image and Scanning Electron Microscopy (SEM) images of the OFI sheath after the values obtained from each algorithm are averaged (\* shows significant difference), (ANOVA, p<0.05, n=5).

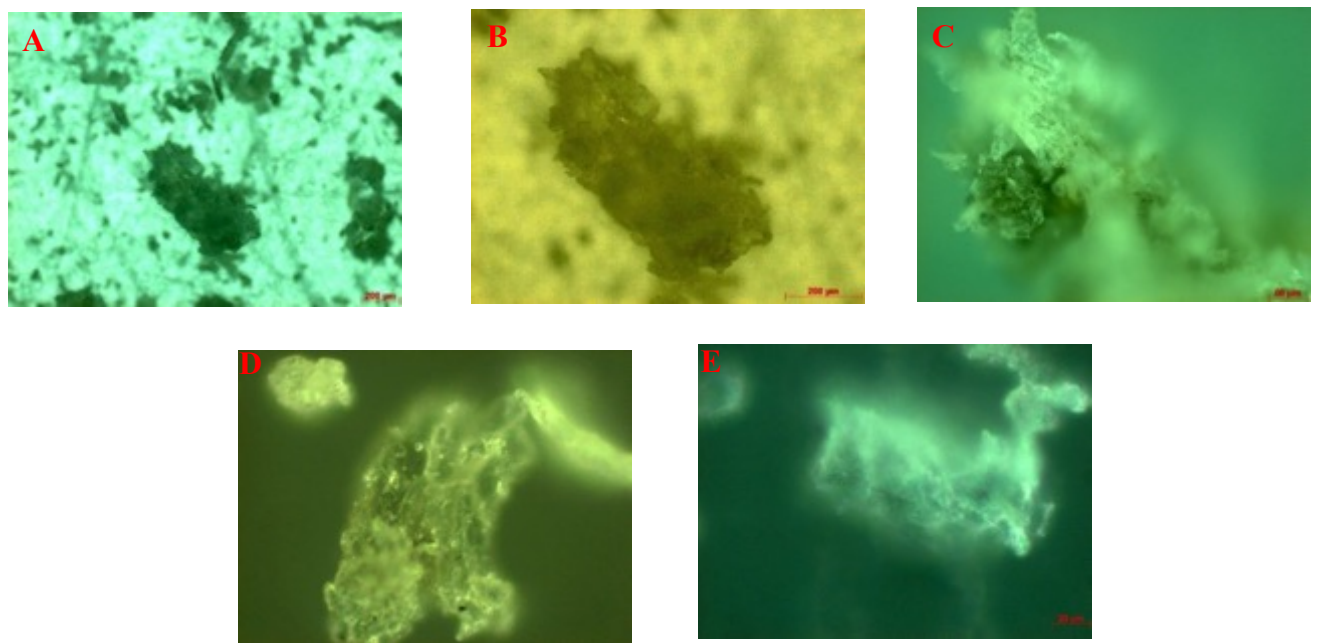


**Fig. 4.9** The pictures demonstrated show images obtained for the cactus natural fibre in powder form at: A, 5x. B, 10x. C, 20x. D, 50x. E, 100x.

## Fractal Order of OFI Fibres-Powder

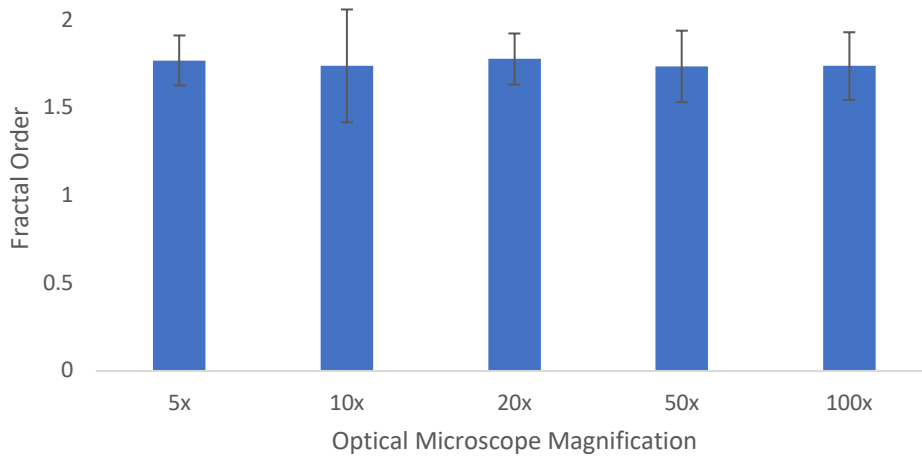


**Fig. 4.10** The resulting fractal dimension estimations are plotted for each magnification image of the OFI processed powder after the values obtained from each algorithm are averaged (\* shows significant difference), (ANOVA,  $p<0.05$ ,  $n=5$ ).

This demonstrates that the fractality is not maintained across all scales for the cactus fibres. The cactus fibres are a natural material that demonstrates a random fractal behaviour where the self-similarity is not maintained across all scales, but it is only maintained across some scales<sup>13,14</sup>. It was also important to assess whether the fractal order of 1.8 observed in the smaller scales of the cactus fibre pieces and particles is unique or is it the same as it is observed in other natural fibres in the same format. Thus, the same experimental and algorithmic approach was utilized to assess the fractal order of eucalyptus Fig. 4.11 & 4.12, flax Fig. 4.13 & 4.14, hemp Fig. 4.15 & 4.16 and rice husk Fig. 4.17 & 4.18 where images across scales were obtained of the fibres and their powders through optical microscopy and SEM in Fig. 4.19.

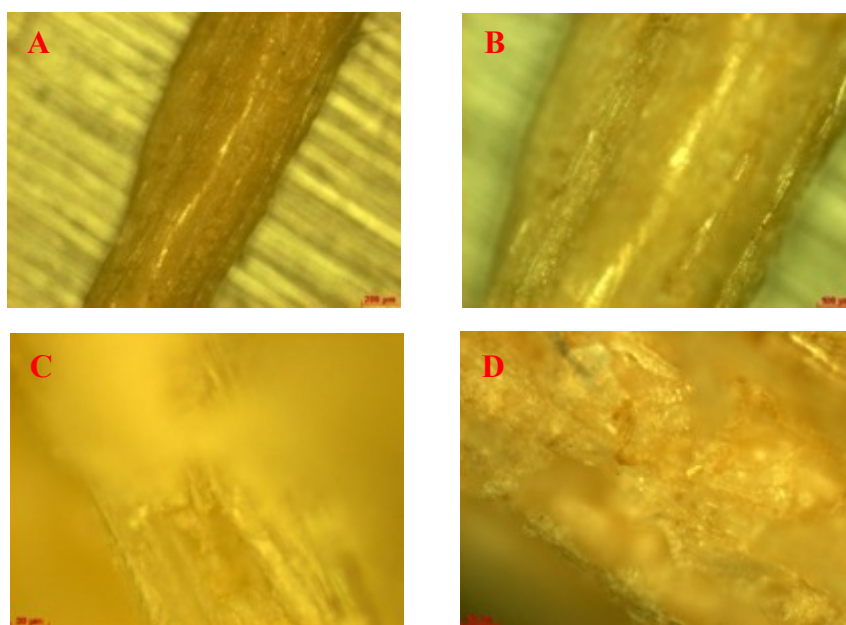


**Fig. 4.11** The pictures demonstrated show images obtained for the Eucalyptus natural fibre sheet at: A, 5x. B, 10x. C, 20x. D, 50x.

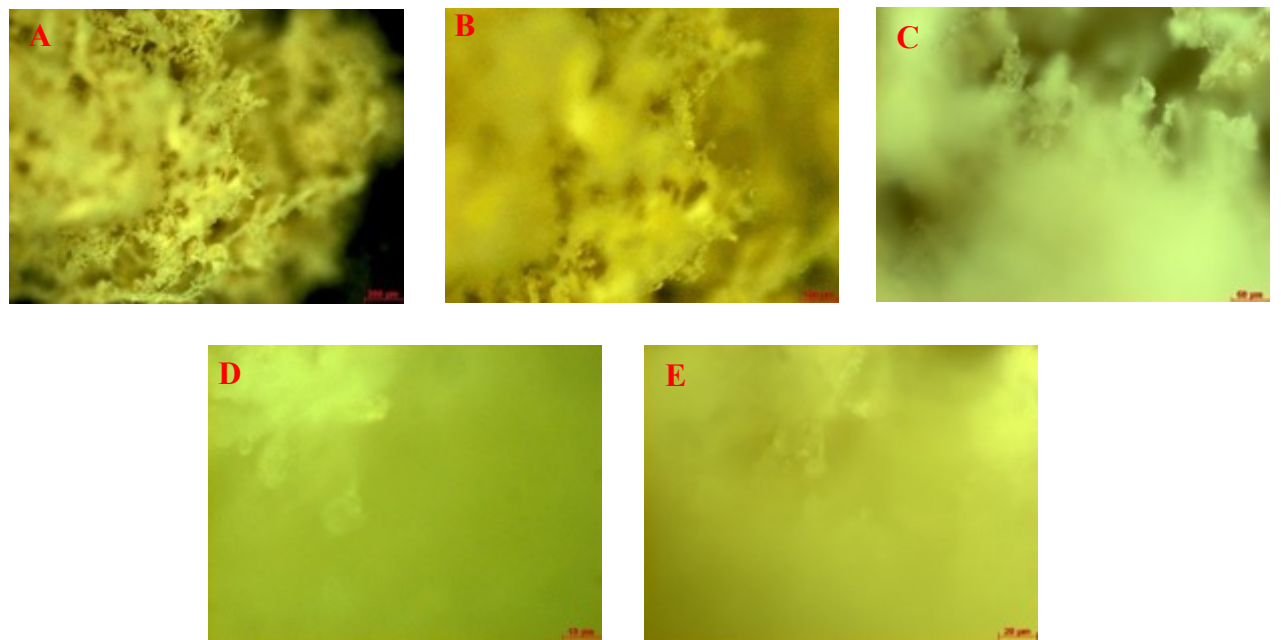


**Fig. 4.12** The pictures demonstrated show images obtained for the Eucalyptus natural fibre in powder format after ball milling at: A, 5x. B, 10x. C, 20x. D, 50x. E, 100x.

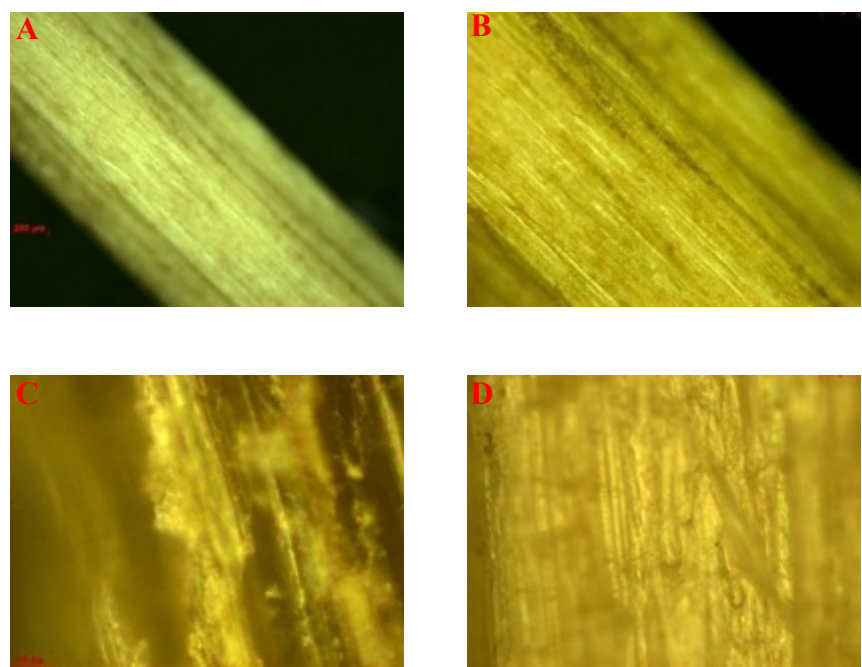


**Fig. 4.13** The pictures demonstrated show images obtained for the Flax natural fibre sheet at: A, 5x. B, 10x. C, 20x. D, 50x.

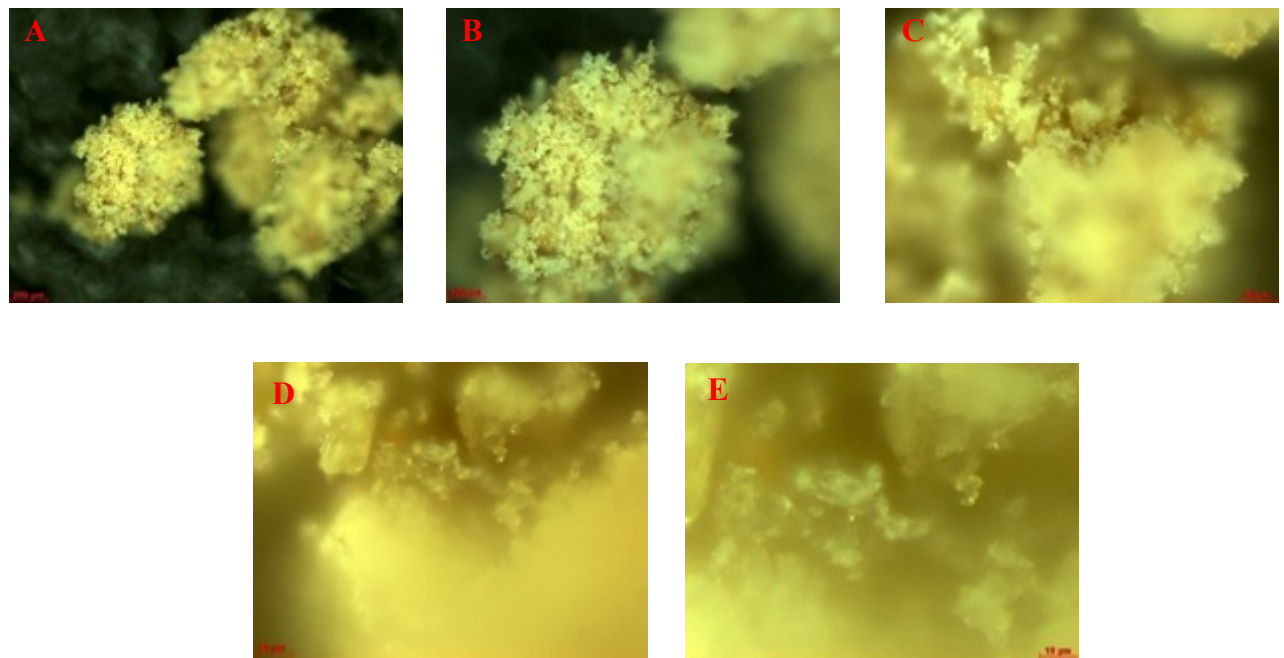


**Fig. 4.14** The pictures demonstrated show images obtained for the Flax natural fibre in powder format after ball milling at: A, 5x. B, 10x. C, 20x. D, 50x. E, 100x.

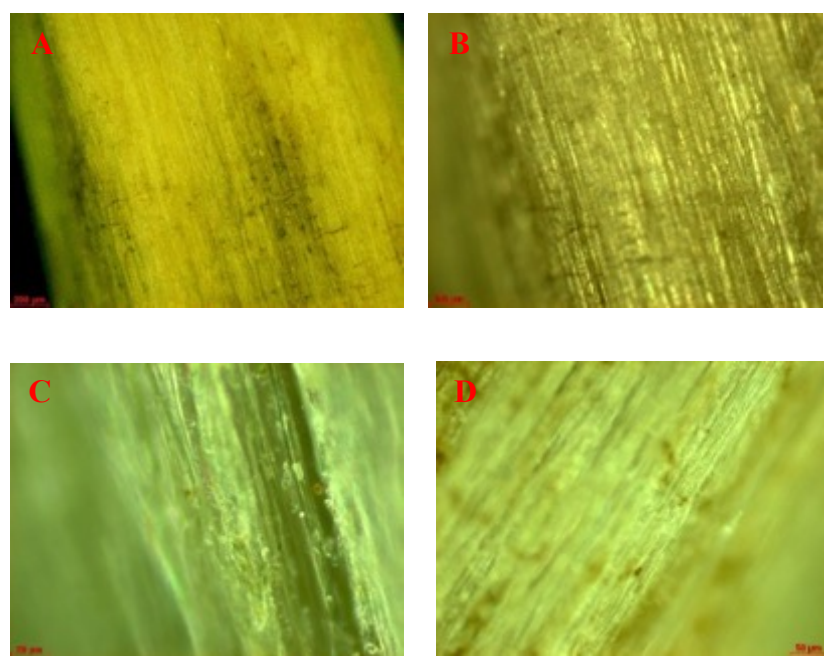


**Fig. 4.15** The pictures demonstrated show images obtained for the Hemp natural fibre sheet at: A, 5x. B, 10x. C, 20x. D, 50x.

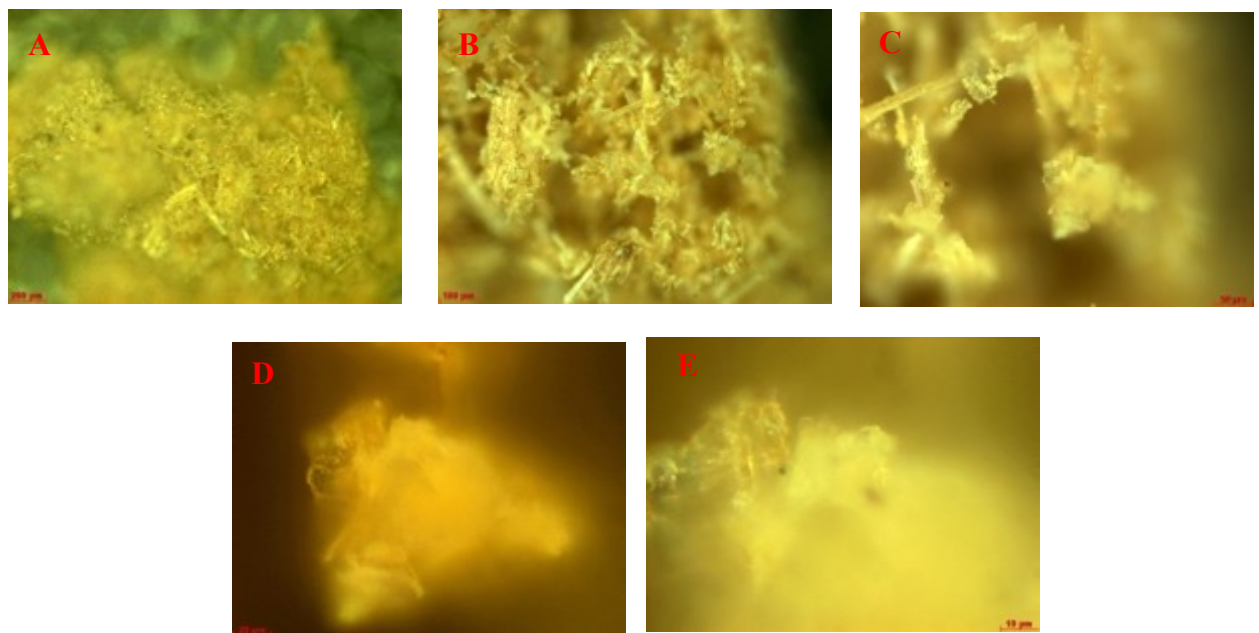


**Fig. 4.16** The pictures demonstrated show images obtained for the Hemp natural fibre in powder format after ball milling at: A, 5x. B, 10x. C, 20x. D, 50x. E, 100x.

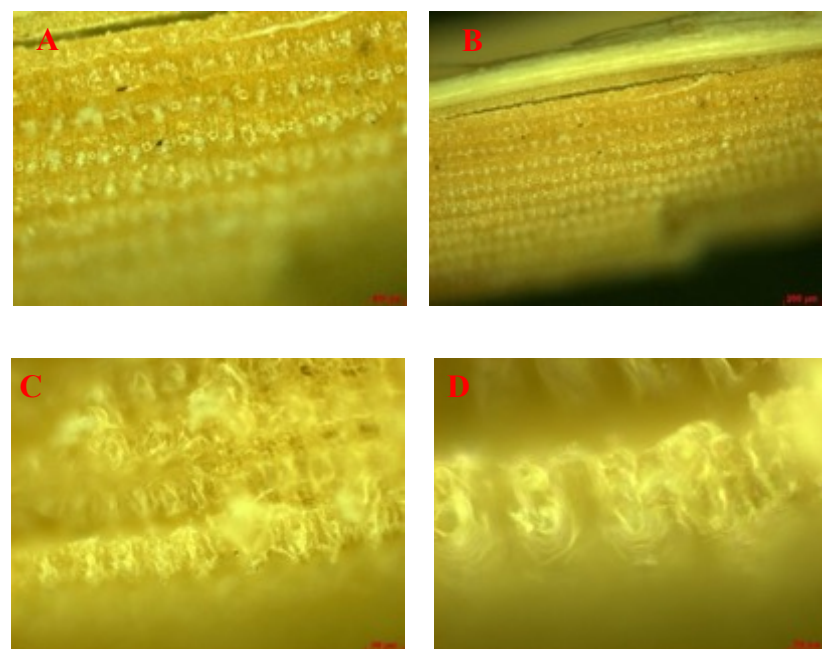


**Fig. 4.17** The pictures demonstrated show images obtained for the Rice Husk natural fibre sheet at: A, 5x. B, 10x. C, 20x. D, 50x.

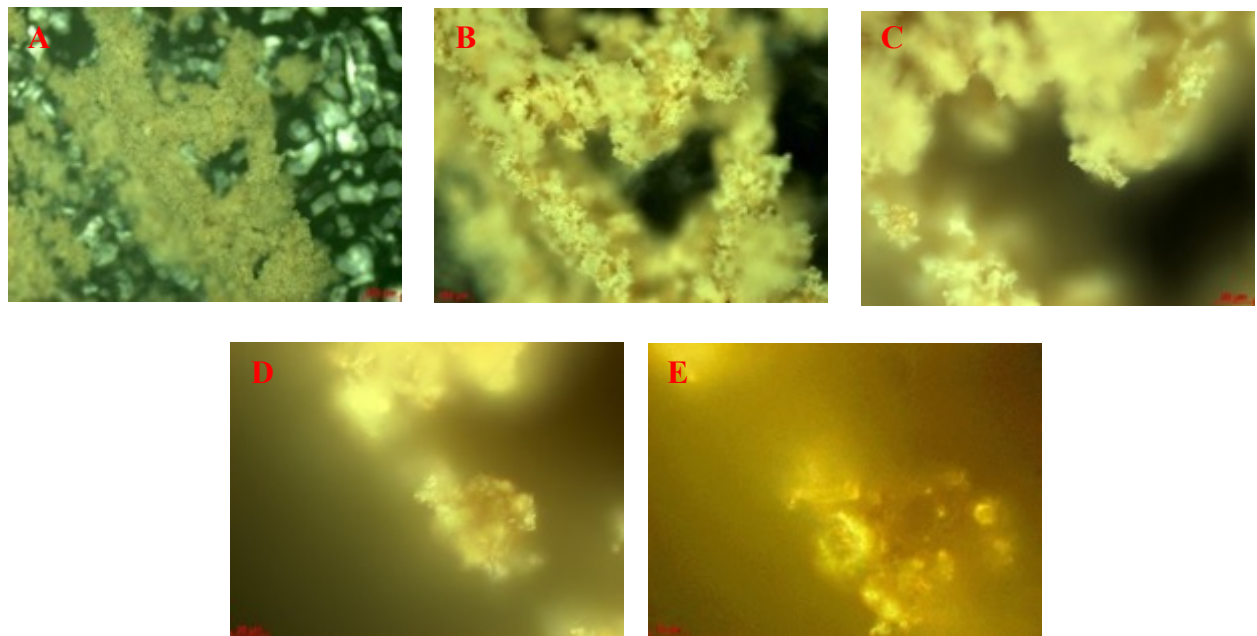


**Fig. 4.18** The pictures demonstrated show images obtained for the Rice Husk natural fibre in powder format after ball milling at: A, 5x. B, 10x. C, 20x. D, 50x. E, 100x.

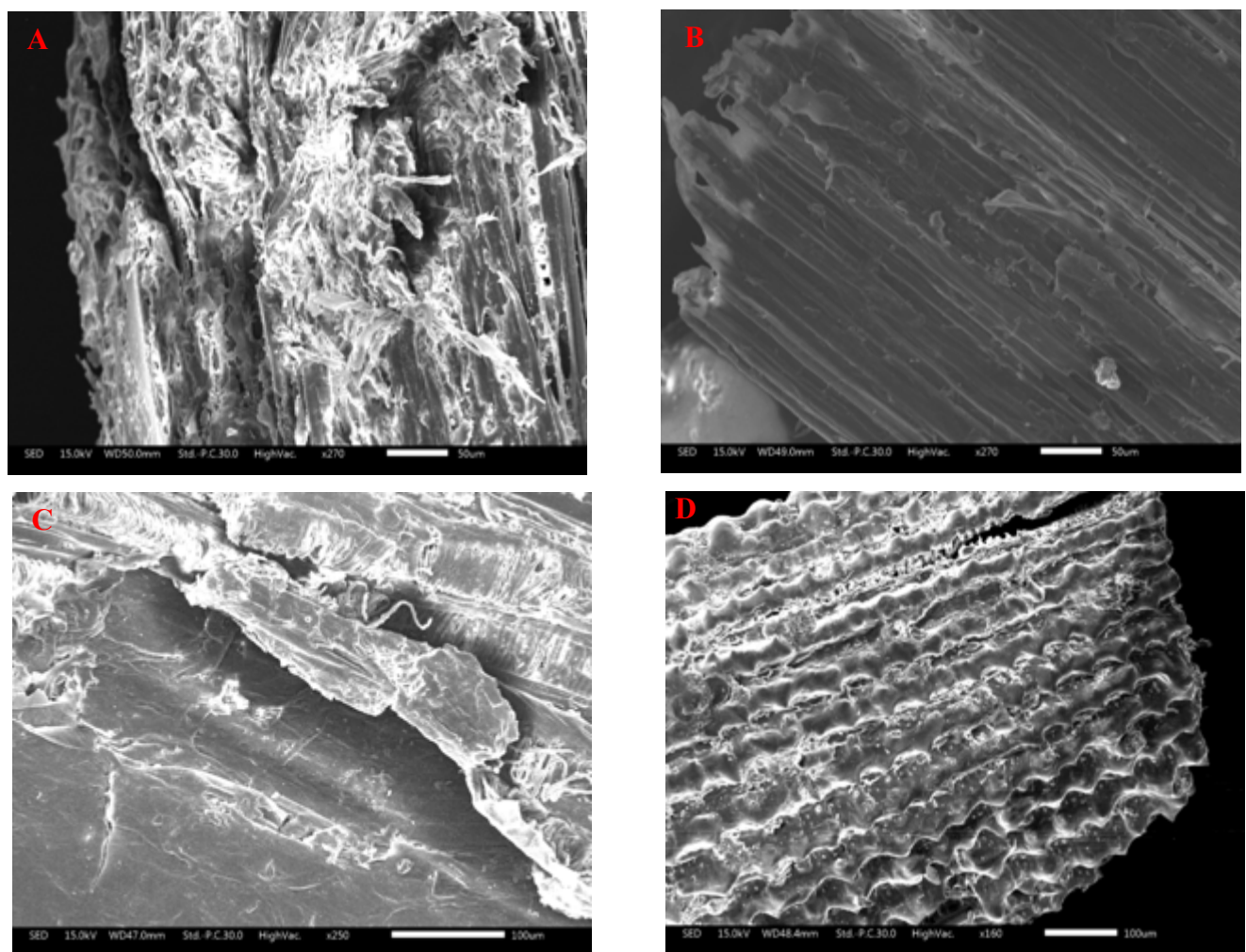


**Fig. 4.19** The images displayed (A through D) demonstrate 4 Scanning Electron Microscopy (SEM) images of the natural fibres specifically: A, Eucalyptus. B, Flax. C, Hemp. D, Rice Husk.

As evident in Fig. 4.20 & Fig. 4.21 the fractal order is the same across all the natural fibres both in their piece and their powder format which is to be expected as all natural fibres are comprised of similar chemical components<sup>187</sup>. The fractal information revealed about the natural fibres could be utilized to explain their ability to provide mechanical reinforcement in composite systems in various formats<sup>188,189</sup> as it shows that the natural fibres have a distinct morphological characteristic present.

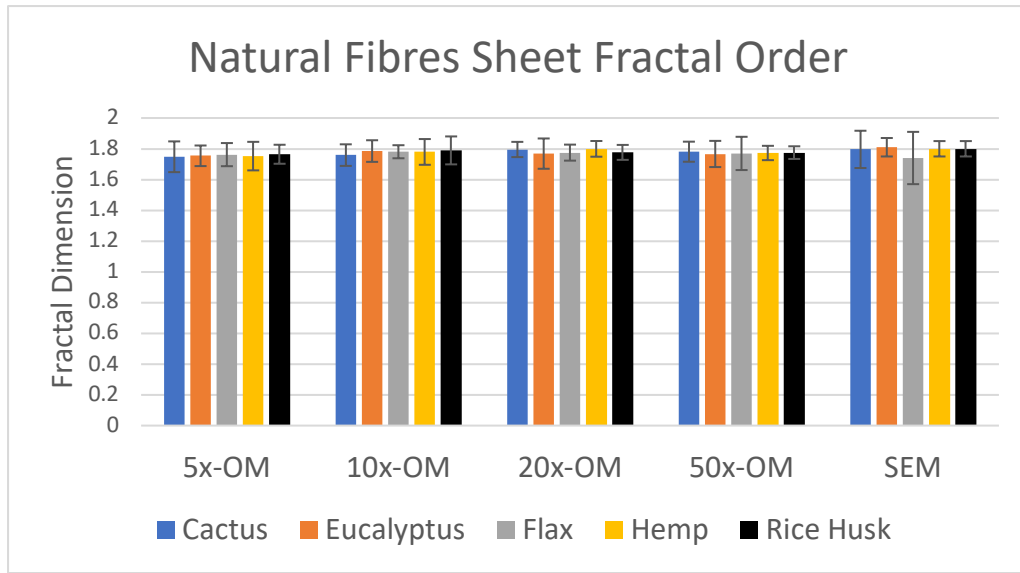


**Fig. 4.20** The resulting fractal dimension estimations from the described algorithmic approach for each magnification of the optical microscope (OM) and Scanning Electron Microscopy (SEM) images for all the natural fibres sheets. (\* shows significant difference), (ANOVA, p<0.05, n=5).

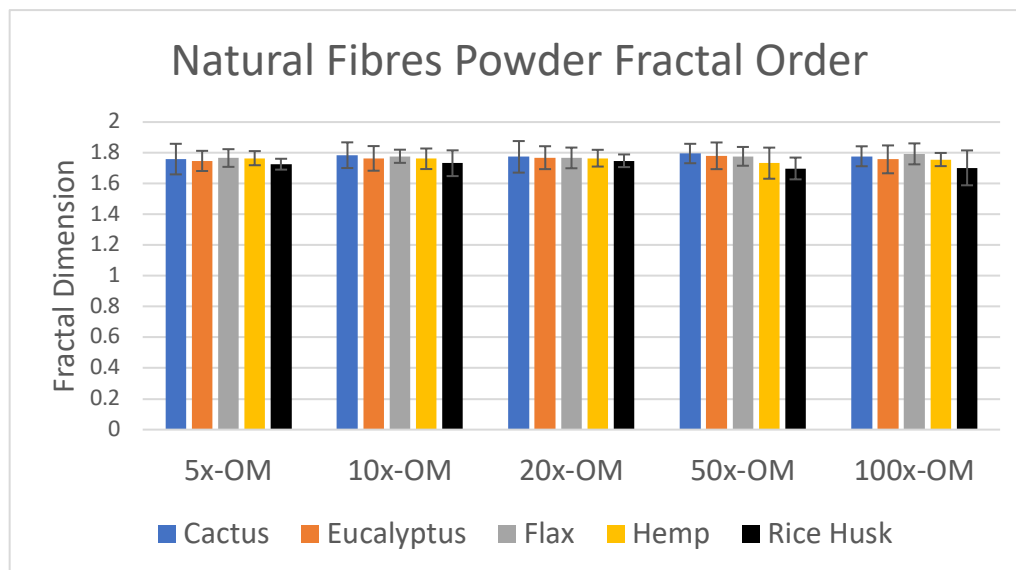


**Fig. 4.21** The resulting fractal dimension estimations from the described algorithmic approach for each magnification of the optical microscope (OM) and Scanning Electron Microscopy (SEM) images for all the natural fibres powders after ball milling. (\* shows significant difference), (ANOVA, p<0.05, n=5).

It is important to note that the fact that the cactus fibre piece and powder do not show any significant difference in their fractal order when compared to other natural fibres, further demonstrates that the fractality of the cactus fibres is primarily maintained at the macroscale and as the scale is reduced the material changes its morphological behaviour and loses its fractality. The fact that the fractality changes as the scales change prompted the idea of assessing whether a multifractal structure is present in the cactus fibre.

#### **4.2.3 Multifractal characterization of the Cacti Fibres**

A multifractal is an object where there are multiple fractal patterns and consequently a fractal order spectrum is present across scales. A multifractal assessment algorithm was implemented on the images to assess the multifractal potential of this structure<sup>20</sup>. As described in the method used, a fractal order spectrum in the form of a straight line signifies a system with no multifractal characteristics present<sup>20</sup>. A symmetrical spectrum signifies an object with some heterogeneity present and an asymmetrical spectrum a high heterogeneity, while both signifying multifractal objects. The three different spectra for the OFI natural fibre sheets are depicted in Figure 4.22 after applying the three different thresholding approaches. Even though it is evident that the spectra obtained is asymmetrical, which would signify a multifractal shape with high heterogeneity, looking at the values of the spectra it is evident that the change occurring in the values is insignificant, **with the dominant value centering at 1.95**, which conveys that there are no multifractal characteristics present but this is a homogeneous fractal system. **The limits of the algorithm are set between 1 and 2 since we are looking for a fractal value in a 2-dimensional fashion as our images are in 2D and two-dimensional fractals are expected to have a value between 1 and 2<sup>11-14</sup>.**

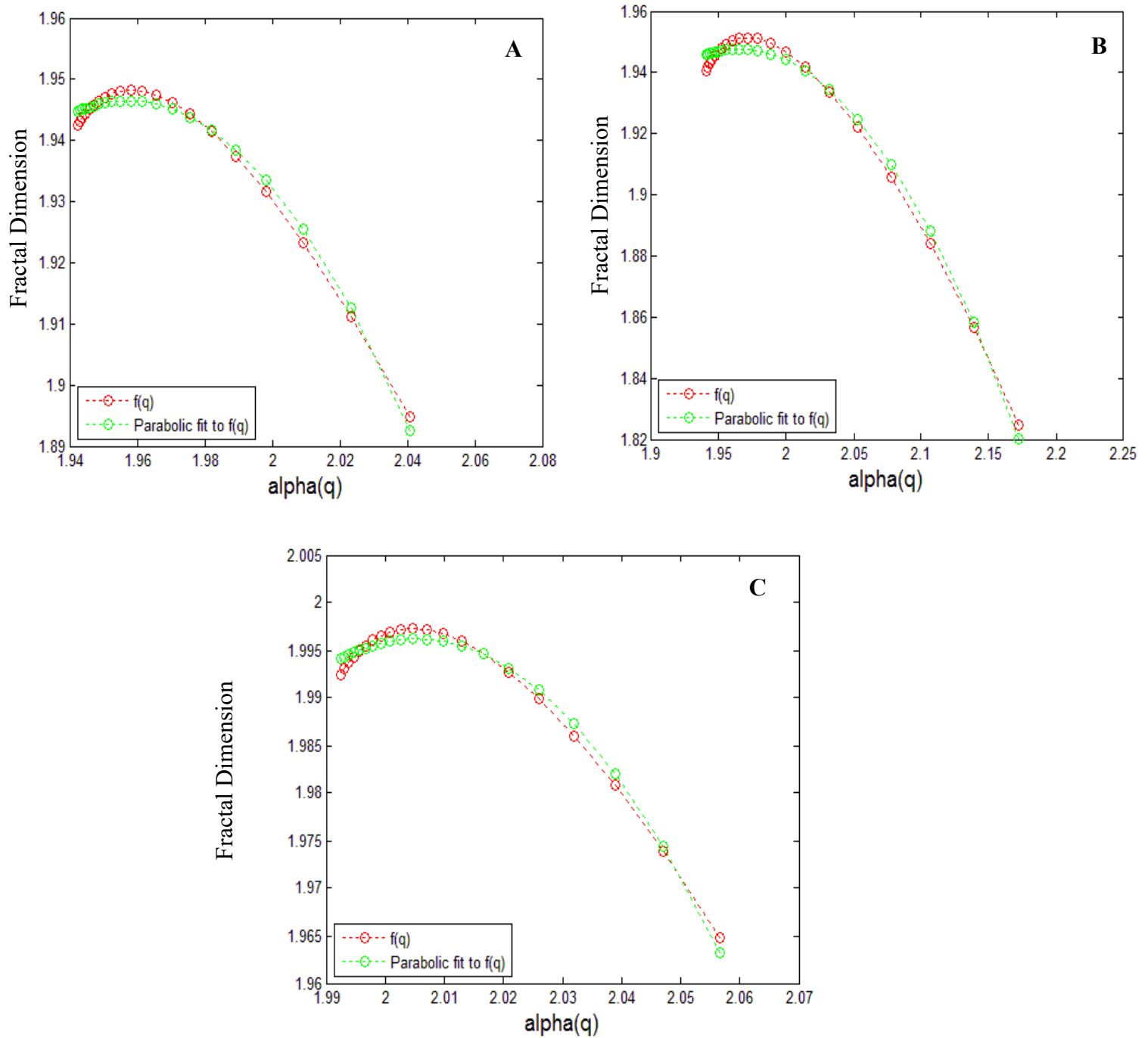


**Fig. 4.22** The resulting multifractal spectra after applying the multifractal analysis algorithm on the cactus fibre sheet images for the three different thresholding techniques. A, User Defined Thresholding. B, MATLAB graythres () function. C, Bradley Thresholding Method.

Similar conclusions can be drawn from Fig. 4.23 for the multifractal morphology of the processed powder form of the fibres, since again despite the asymmetrical property of the spectra the change in the values is insignificant to justify the presence of a multifractal shape.

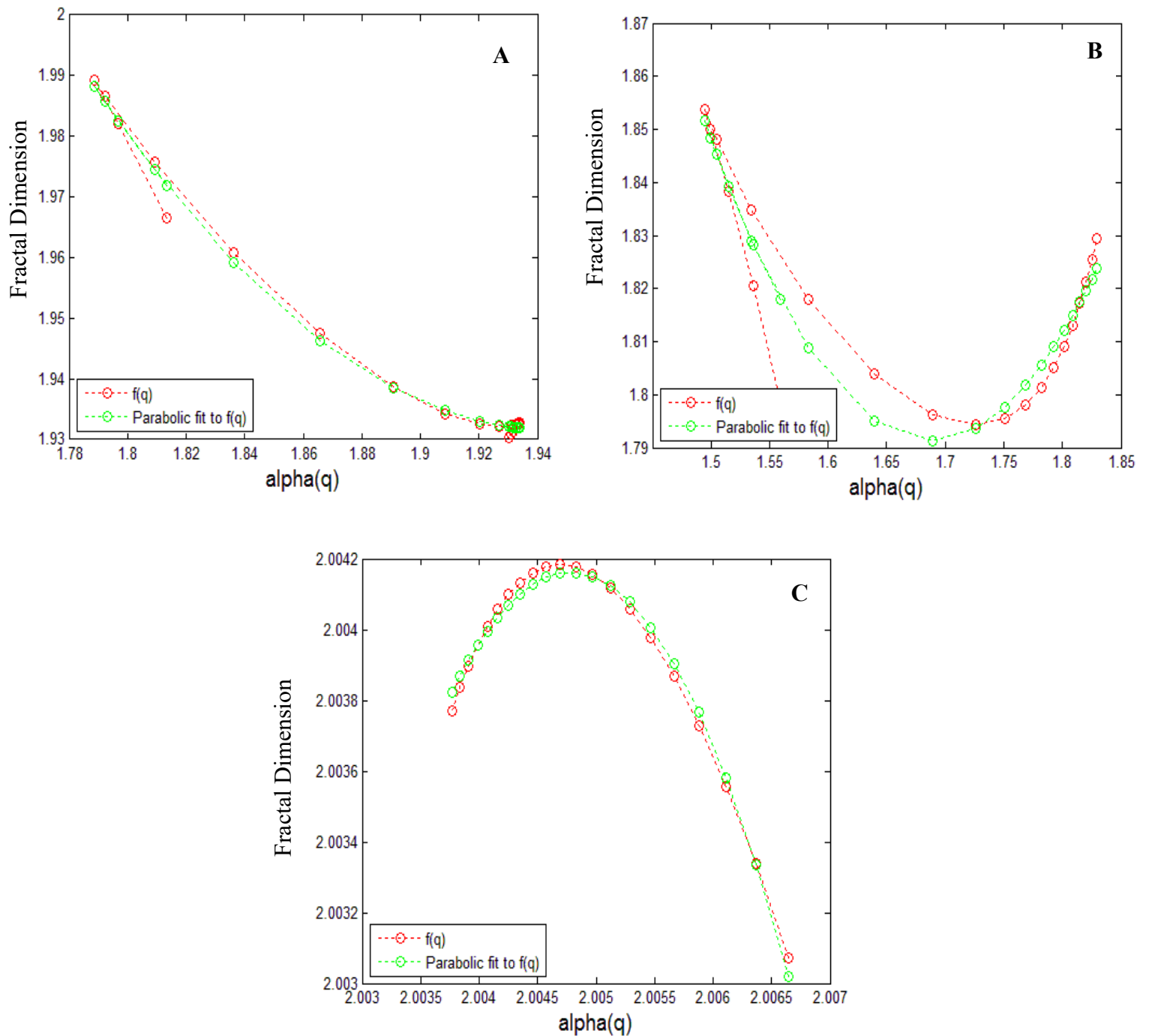


**Fig. 4.23** The resulting multifractal spectra after applying the multifractal analysis algorithm on the cactus fibre powder images for the three different thresholding techniques. A, User Defined Thresholding. B, MATLAB graythres () function. C, Bradley Thresholding Method.

Overall, it was determined that there is fractality present at the macroscale of the cactus fibres that can be directly correlated to the mechanical properties observed and the interesting high bending to axial stiffness ratio<sup>9</sup>. The structure can be reduced down to a singular structural subunit and this structural subunit demonstrates similar mechanical properties to the whole structure while it can be used to reverse engineer the entire cactus fibre. However, at smaller scales the fractality is not maintained and it is very similar to the fractality observed across natural fibres in nature which is to be expected due to their chemical and structural similarities. Once an investigation of the fractality of the cactus fibres was carried and the fractality was

compared to other natural fibres, it was also important to investigate the fractality of the most commonly used synthetic fibres glass and carbon fibres. This would enable us to compare the fractal order value of the natural fibres and how it relates to the one of the synthetic fibres and see if the natural fibres demonstrate a distinct morphological feature at these or if the fractal order of 1.8 estimated is maintained across fibres at those scales, being a characteristic of a fibrous structural motif.

#### **4.2.4 Fractal Characterization of Synthetic Fibres & Comparisons**

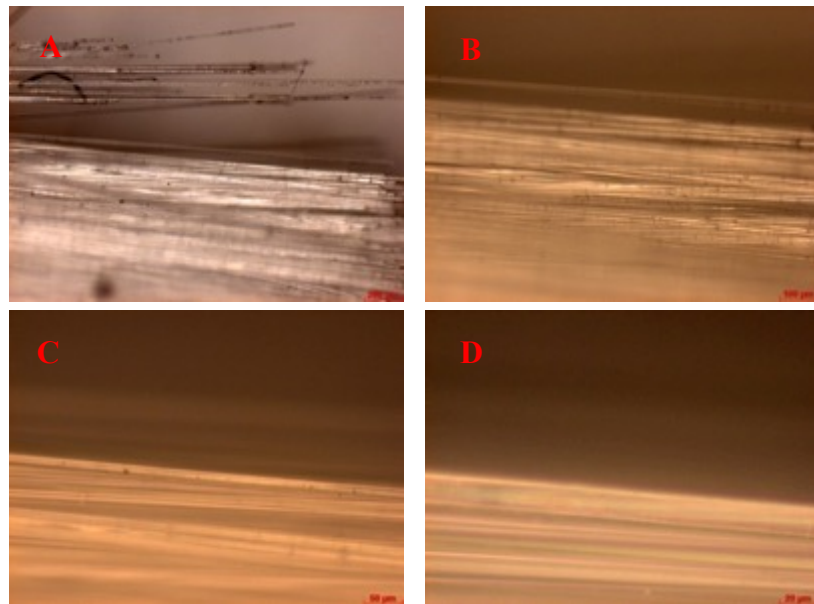


**Fig. 4.24** The pictures demonstrated show images obtained for the Glass Fibre synthetic fibre sheet at: A, 5x. B, 10x. C, 20x. D, 50x.

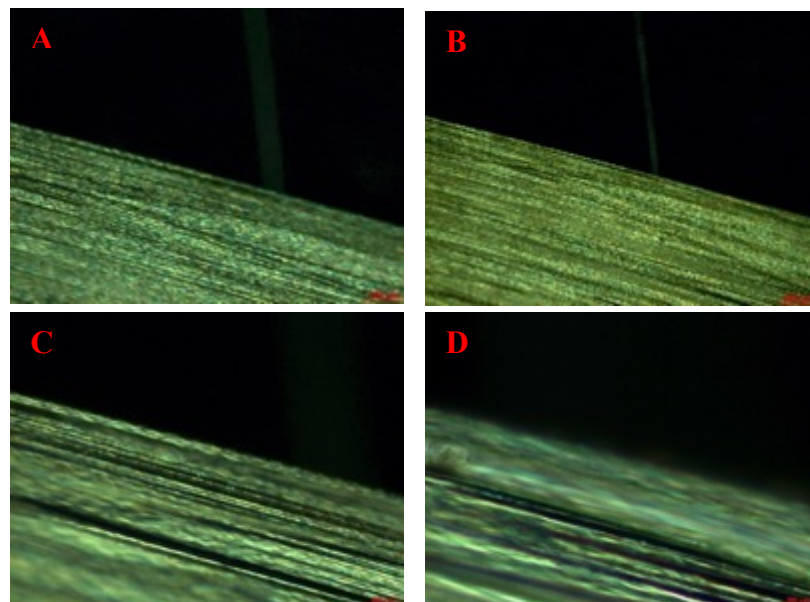


**Fig. 4.25** The pictures demonstrated show images obtained for the Carbon Fibre synthetic fibre sheet at: A, 5x. B, 10x. C, 20x. D, 50x.

As shown in Figures 4.24 & 4.25 the same methodology was applied were images of carbon and glass fibres were obtained via optical microscopy at increasing magnifications. Observing

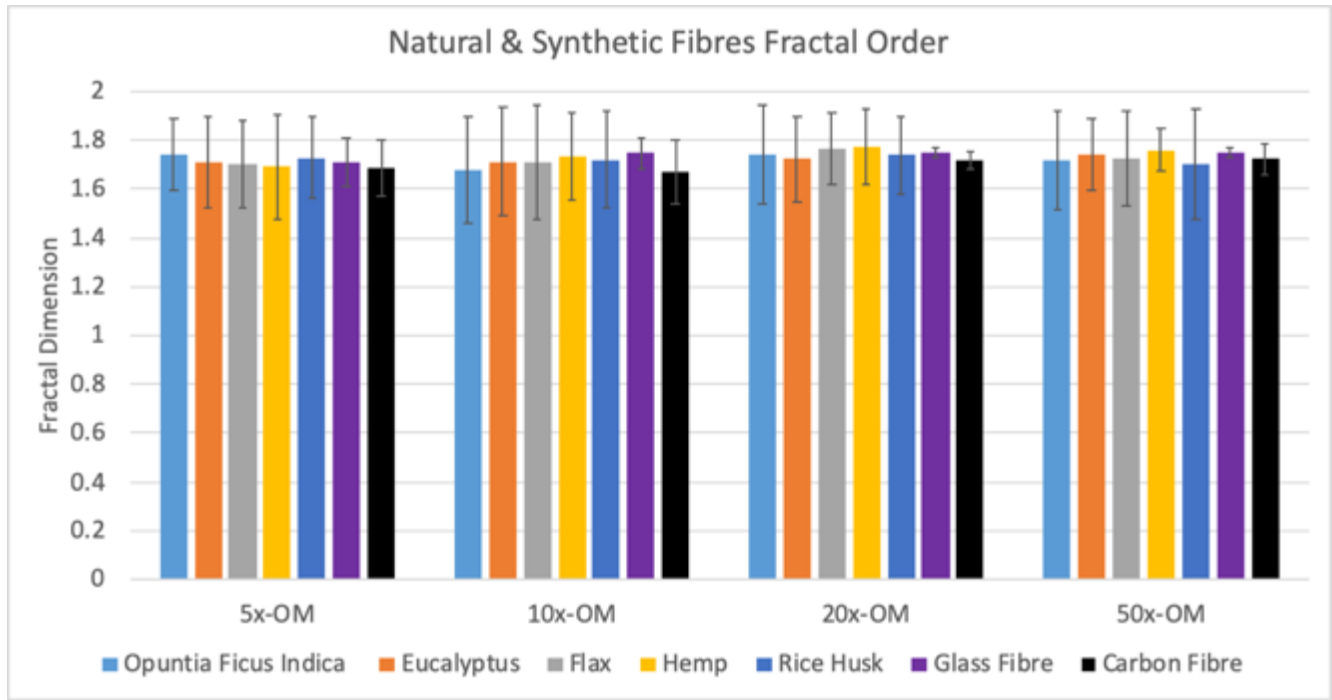


**Fig. 4.26** The resulting fractal dimension estimations from the described algorithmic approach for each magnification of the optical microscope (OM) images for all the natural fibres and synthetic fibre sheets (\* shows significant difference), (ANOVA,  $p<0.05, n=5$ ).

The MATLAB algorithmic approach was applied on those images as well and as evident in Figure 4.26 the fractality of the glass and carbon fibres is similar to the fractal value observed for all the natural fibres. This demonstrates that the fractal dimension observed at those scales is not a unique characteristic of natural fibres but it appears to be that fibrous morphologies demonstrate this fractal order of around 1.8 irrespective of their origin. This is an interesting result that more importantly serves to strengthen the robustness of the algorithm developed since morphologies that appear to have the same characteristics, in this case a fibrous motif, demonstrate the same fractal order. However, to ensure the robustness of our algorithm additional steps were taken. Initially, we tested our algorithm against shapes with known fractal values such as the Koch snowflake with a known fractal value of 1.26, and our algorithm returned a value of 1.27 (1.2682), as shown in Fig. 4.27, demonstrating that the algorithm developed is robust as it is able to characterize known fractals correctly.

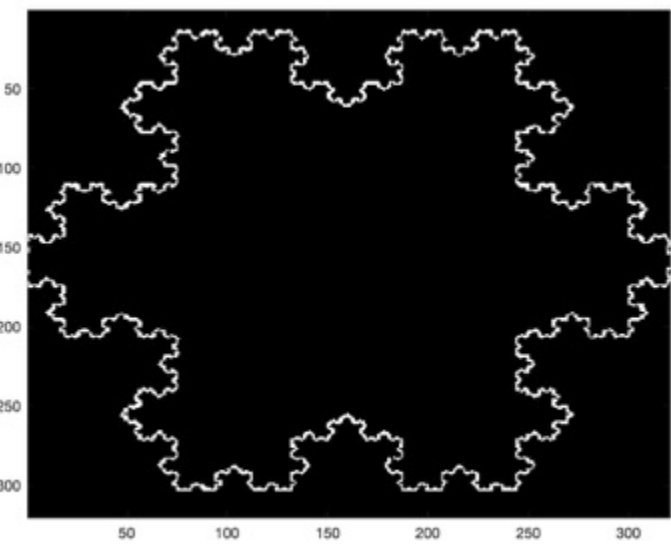
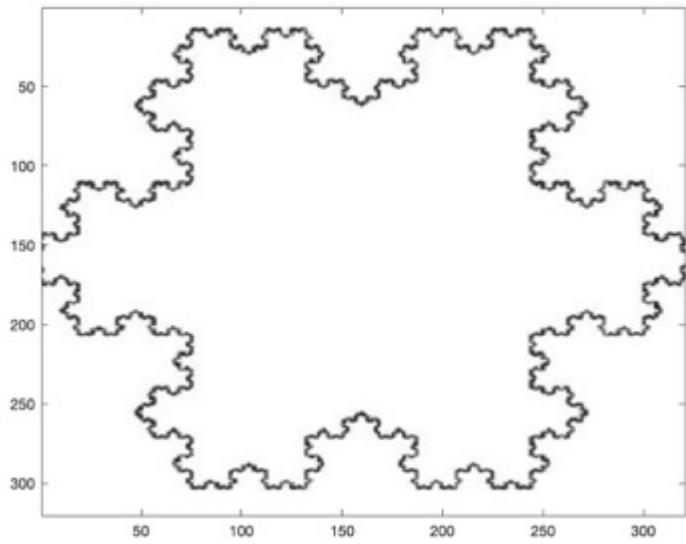


**Fig.4.27** Example of our fractal estimation algorithm being implemented in a Koch Snowflake image yielding a fractal order value of 1.27 (1.2682) which is very close to the known fractal value of the Koch snowflake at 1.26.

Additionally, in our recent publication<sup>31</sup> our algorithm was utilized successfully in the characterization of composite materials with hierarchical structures where the fractality was correlated with the mechanical properties present.

### **4.3 Conclusions**

The aim of this analysis was to investigate the morphological characteristics of the OFI natural fibres to obtain a better understanding of their unique structural and architectural characteristics that give them their interesting mechanical properties. It was determined that Euclidean geometry would not allow for a complete characterization of the unique morphology of the fibres, so a fractal geometric analysis was pursued as the best route in evaluating the structure and architecture of the natural fibres through a novel algorithm developed. Initial fractal characterization through the algorithm developed demonstrated that the cactus fibre sheath does present fractal behaviour and can be reduced to a single structural subunit with a fractal value of 1.6. The cactus structural subunit demonstrates the same fractal order as the cactus fibre sheath, similar mechanical properties and can be used to reverse engineer the cactus structure with the same fractality maintained at 1.6. In order to get a complete evaluation of the fractal characteristics of the structures the OFI fibres were analysed as sheets as well as in a processed powdered form that was obtained via a ball milling process. Optical microscopy images were obtained at various magnifications for both the fibre sheet and the powder and SEM images were obtained for fibre fragments. Those were used for the determination of the fractal dimension and multifractal characteristics of the OFI fibres across scales via MATLAB scripts utilizing the box-counting method. It was demonstrated that at lower scales and different formats the fractal order of the cactus fibre changes and it is similar to the fractal order observed by various natural fibres. Those results signified that at those lower scales and different formats the fractality of the cactus is no longer present while also demonstrating an interesting result for the fractality and self-similarity of natural fibres pieces and powders that seem to be morphologically equivalent. Multifractal analysis revealed that these structures are homogeneous fractal morphologies and do not present multifractal characteristics. It was determined that fractality is present at the macroscale of these cactus fibres and this morphological uniqueness could be one of the reasons behind their unique mechanical properties previously observed. To the author's knowledge this is the first attempt at the macro structural fractal characterization of a natural material that lead to the reduction of the structure to a single self-repeating subunit that maintains the structural and mechanical properties of the whole structure.

## 5 Artificial Cactus Inspired Reinforcement Materials

---

### **Relevant Publication:**

The work on artificial cactus inspired reinforcement materials was submitted and under review at the time of the thesis submission.

**Zampetakis I, Dobah Y, Liu D, Woods B, Bezazi A, Perriman A.W, Scarpa F, Abnormal stiffness behaviour in artificial cactus-inspired reinforcement materials,** Submitted to *Advanced Materials*, 2019

### **5.1 Chapter Overview**

The primary objective of this chapter is on developing a mechanical understanding and artificial reproduction of the dried cladodes of *Opuntia ficus indica* (OFI) and their interestingly high 7:1 bending to axial stiffness ratio that leads to significantly increasing the energy dissipation per volume matrix, observed experimentally<sup>9</sup>. Even though, the behaviour is somewhat expected due to the fact that the material is mainly concentrated away from the neutral axis, the fact that the ratio is high signifies that the morphology needs to be studied in further detail. The approach utilized for the morphological and mechanical characterization of the cactus structure was similar to a previous methodology utilized for the bamboo parenchyma characterization, where µCT imaging and 3D printing was utilized to explore the mechanical properties demonstrated by bamboo parenchyma<sup>27</sup>. Inspired from the properties demonstrated from the cactus fibre structure an effort to generate bioinspired analogues to evaluate their mechanical properties and assess their application potential was initiated. Initial morphological analysis provided unique information of the morphology of the cactus across scales revealing a hierarchical structure prevalent expanding our understanding of the mechanical properties observed. However, further evidence was necessary with regards to its mechanical properties. The wealth of morphological information obtained was utilized to generate cactus structure analogues via 3D printing using two different printing modalities for the evaluation of the reproducibility of the structure. The ability to replicate the cactus structure via 3D printing served great benefits for the understanding of the properties and how those are maintained at different structural subunits of the structure as a reduced cactus subunit was utilized for the 3D rendered models obtained. Furthermore, the 3D printed cactus analogue specimens granted the possibility to generate finite element simulations of the cactus structure to get an insight in its

mechanical behaviour while also assessing its potential as a bioinspired material platform. It was demonstrated that the cactus inspired 3D printed specimens demonstrate the same unusually high bending to axial stiffness ratios regardless of manufacturing method. Moreover, when compared to their equivalent beam analogues the cactus specimens demonstrated significant potential in terms of weight saving and specific flexural modulus. Overall, we present a novel bioinspired material that shows excellent reproducibility across manufacturing methods generating a platform of novel bioinspired materials for energy dissipation applications demonstrating high bending to axial stiffness ratios.

## 5.2 Results & Discussion

### 5.2.1 Development of 3D rendered models

In this work we have aimed at artificially reproducing and replicating the mechanical response of the cactus fibre cellular structures observed in nature, specifically their 7:1 bending to axial stiffness ratio, by using various materials and manufacturing methods. For this purpose, we have used various materials and manufacturing methods. Initially through  $\mu$ CT measurements we were able to generate 3D rendered models and export triangular meshes of the cactus structure. The size of the triangular meshes was then further reduced, from 10 million triangular meshes to five hundred thousand, to enable further manipulation of the files for the generation of 3D printing g-codes. The reduction of the size of the triangular meshes for the production of manageable STL files leads however to the loss of some structural information at the micro and meso scales. The structural integrity of the cactus structure at macro scale was however maintained Fig. 5.1.

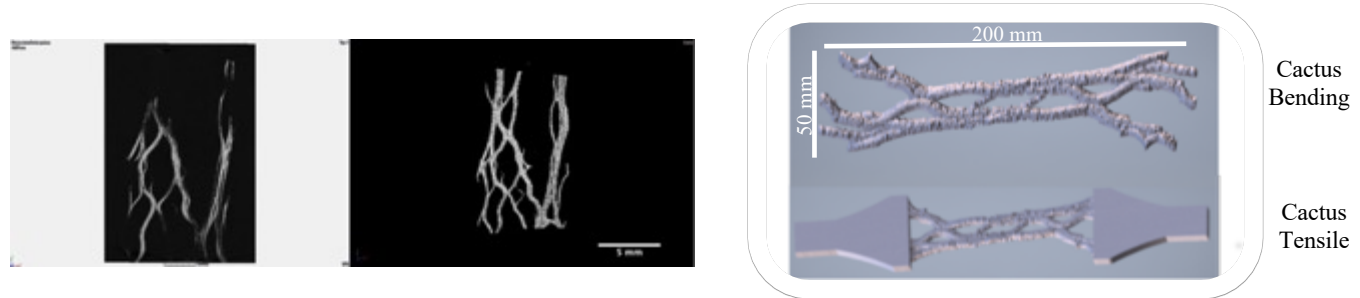


**Fig.5.1** The process from obtaining the imaging data of the cactus structure and those being used for the generation of 3D rendered models for mechanical testing of the bioinspired cactus structure.

Once the .stl files of the cactus structure were optimized for 3D printing through fixing all the nonmanifold edges and vertices, they were 3D printed with two different printing modalities. Initially the cactus structures were produced using a commercial FDM 3D printer Raise3D using commercial PLA filament (Raise3D premium) at two different infill ratios (10% and 100%). The different infills were used to determine their effect on the mechanical characteristics of the structure, as well as to understand if the bending to axial stiffness ratio would be maintained irrespectively of the amount of material used. It is also important to note that the specimens manufactured are at a much larger scale than the original cactus specimen as described in Tables 5.1 & 5.2. We hypothesized due to the fractality present as proven in chapter 4 it would be possible to reproduce and model the global behaviour of the cactus fibres based on a single portion of the cactus fibre structure.

### **5.2.2 Manufacturing & Testing of 3D Printed Specimens**

**Table 5.1** Tensile Testing Specimen Dimensions for Analysis

	Length (mm)	Width (mm)	Thickness (mm)	Gage Length (mm)
Control	165	20	4	57
Cactus	200	50	4	105

**Table 5.2** Bending Testing Specimen Dimensions for Analysis

	Length (mm)	Width (mm)	Thickness (mm)	Support Span (mm)
Control	200	50	4	64
Cactus	200	50	4	64

The purpose of doing this was twofold. Initially, our aim was to generate specimens that would conform with ASTM standards in order to be able to classify the cactus analogues among other materials while also being able to perform comparisons with control specimens of equivalent beams. The second justification behind the choice of making larger specimens was to verify the presence of any scale issue, and that the architectural and geometric structures present in the fibres are responsible for the unusual bending/axial ratio observed in nature. As evident from observing Fig. 5.2 to Fig. 5.7 and Table 5.3, the high bending to axial stiffness ratio in these artificial cactus fibre-inspired structures varies between 9.9:1 and 10:1 for the 10 % and 100% infill specimens, respectively.

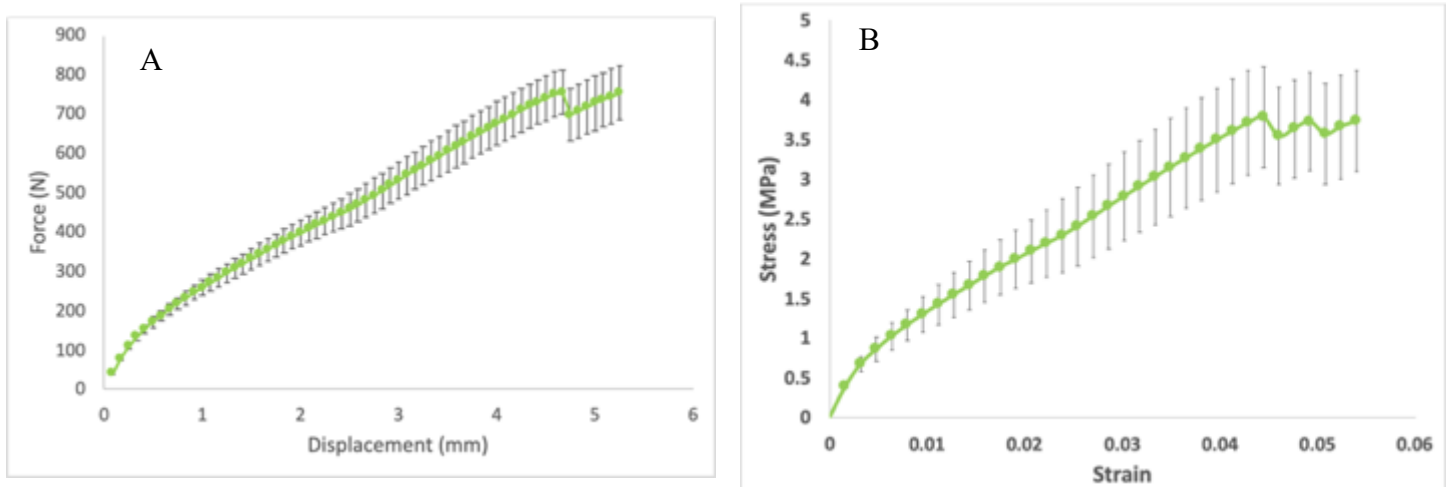


**Fig. 5.2** Tensile testing of cactus bioinspired 3D printed Polylactic Acid (PLA) analogues at 100% infill  
(a) Force vs Displacement data and (b) Stress Vs Strain Data. All tests were carried out according to ASTM D638-14 (n=5)

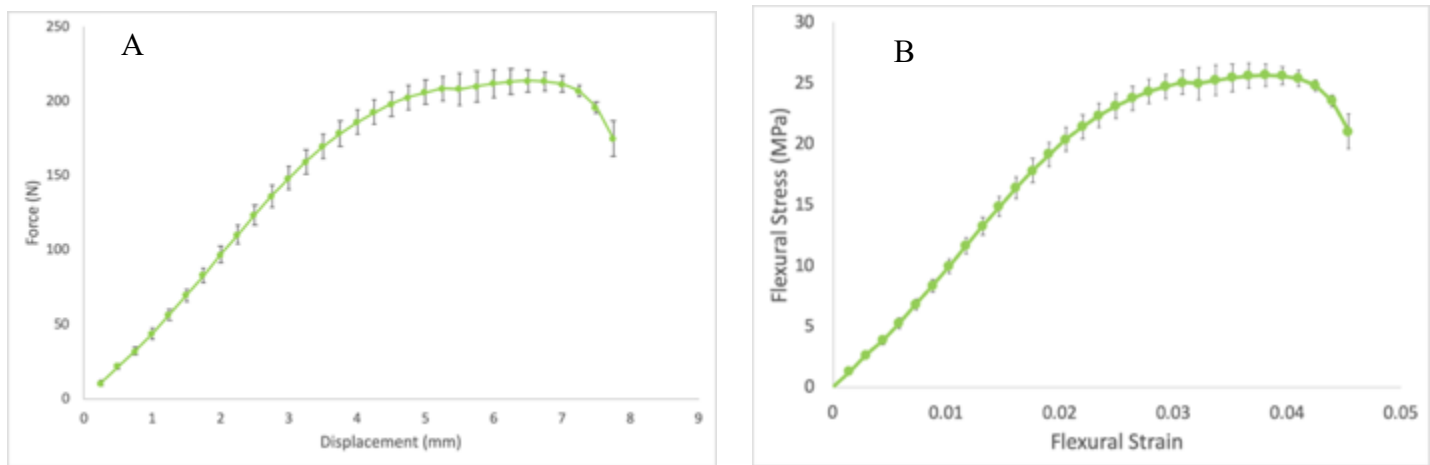


**Fig. 5.3** 3-Point Bending testing of cactus bioinspired 3D printed Polylactic Acid (PLA) analogues at 100% infill (a) Force vs Displacement data and (b) Stress Vs Strain Data. All tests were carried out according to ASTM D790-17 (n=5)

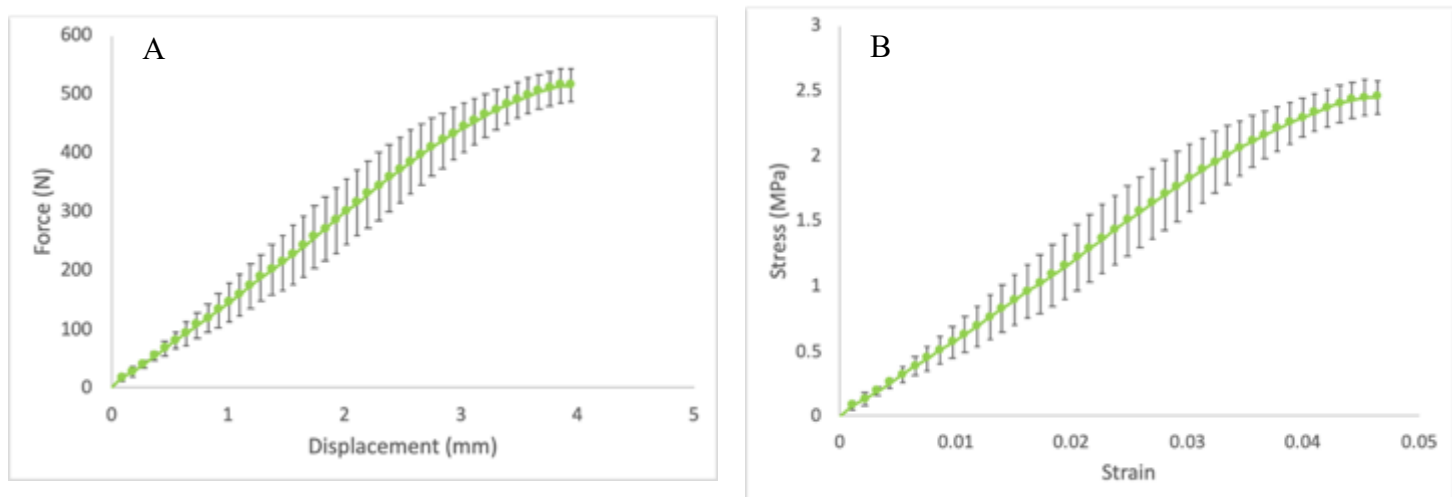


**Fig. 5.4** Tensile testing of cactus bioinspired 3D printed Polylactic Acid (PLA) analogues at 10% infill (a) Force vs Displacement data and (b) Stress Vs Strain Data. All tests were carried out according to ASTM D638-14 (n=5)

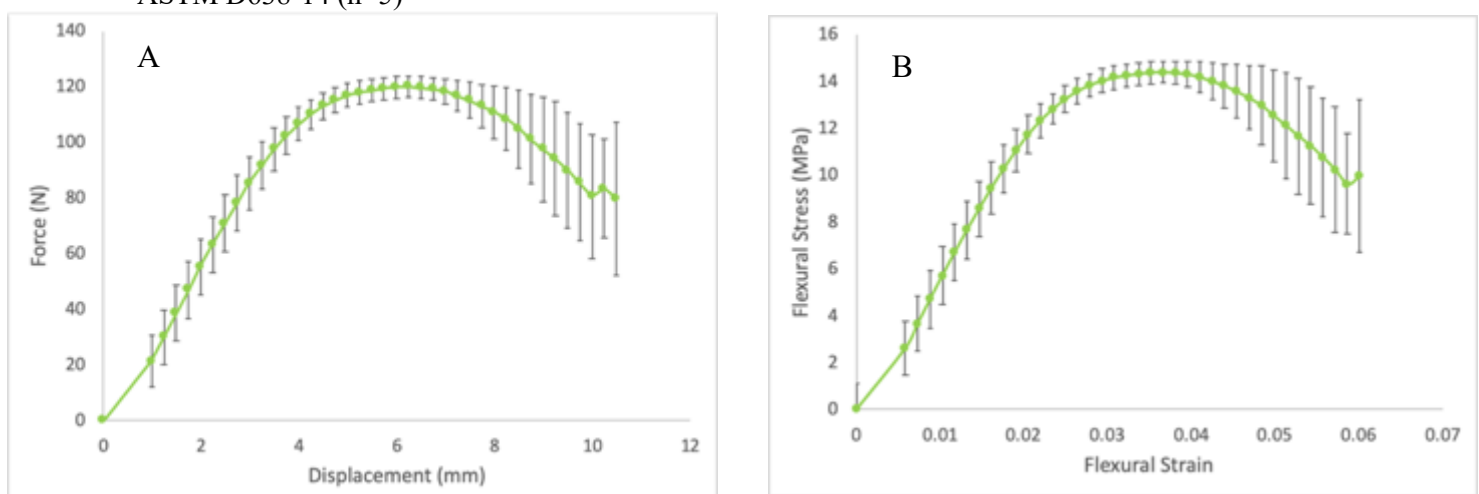


**Fig. 5.5** 3-Point Bending testing of cactus bioinspired 3D printed Polylactic Acid (PLA) analogues at 10% infill (a) Force vs Displacement data and (b) Stress Vs Strain Data. All tests were carried out according to ASTM D790-17 (n=5)

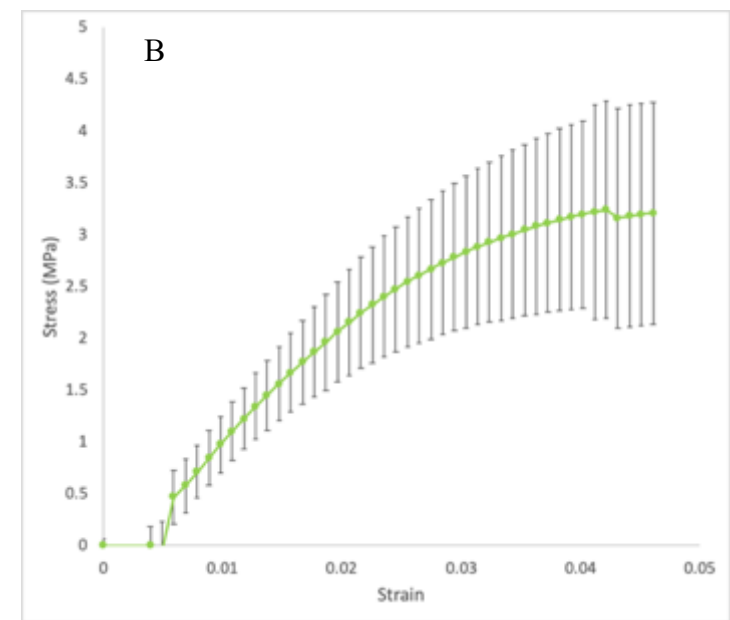
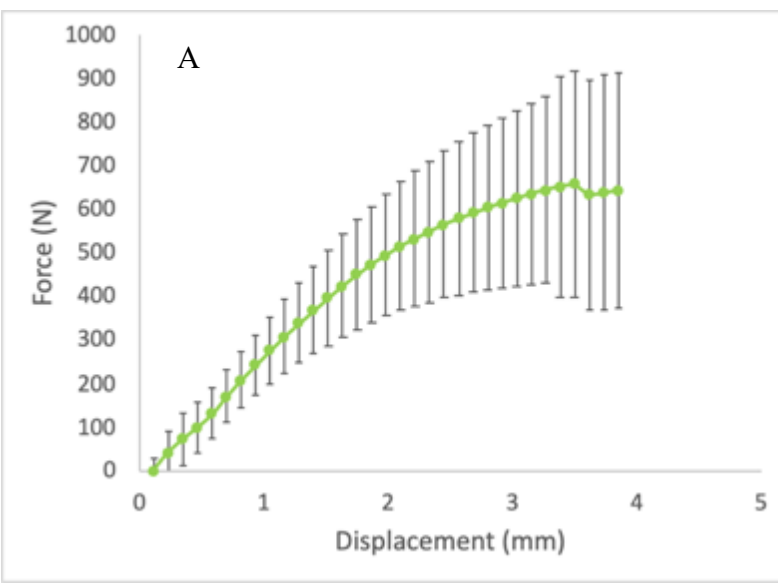


**Fig. 5.6** Tensile testing of cactus bioinspired 3D printed Stereolithography (SLA) analogues (a) Force vs Displacement data and (b) Stress Vs Strain Data. All tests were carried out according to ASTM D638-14 ( $n=5$ )

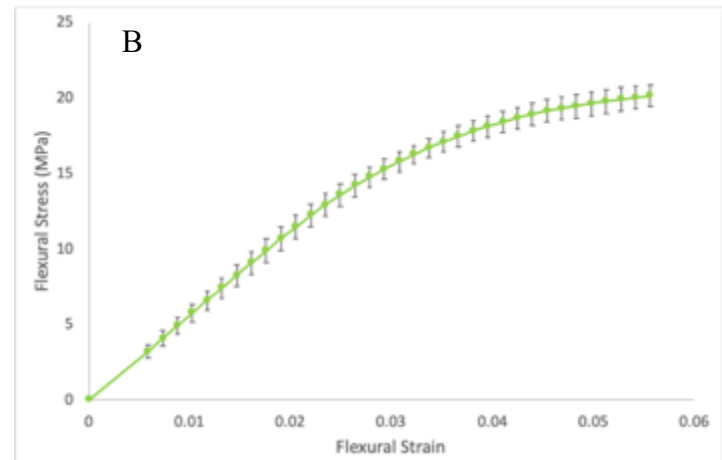
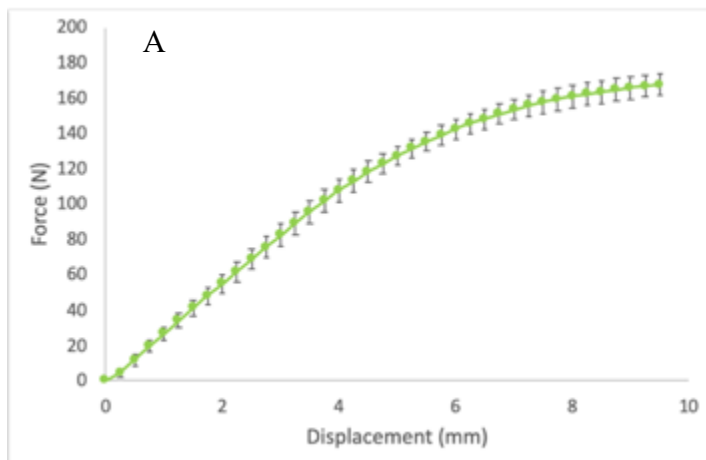


**Fig. 5.7** 3-Point Bending testing of cactus bioinspired 3D printed Stereolithography (SLA) analogues (a) Force vs Displacement data and (b) Stress Vs Strain Data. All tests were carried out according to ASTM D790-17 ( $n=5$ )

**Table 5.3** Axial Modulus, Flexural Modulus and Ratios for all 3D printed specimens

	Axial Modulus (MPa)	Flexural Modulus (MPa)	Ratio
Cactus_10%_PLA	$60.5 \pm 10.2$	$602.2 \pm 13.4$	9.9
Cactus_100%_PLA	$102 \pm 14$	$1025.5 \pm 44.3$	10
Cactus_SLA	$120.7 \pm 15.5$	$581.7 \pm 37.4$	5

It is important to note the nominal cross sectional area is utilized for the stress calculations while the initial non-linearity existing from strains 0.00 to 0.01 are not taken into account in the stiffness estimations as they are attributed to the initial slipping in the interaction of the

**mechanical probe to the specimen.** Those bending to axial stiffness ratios are slightly higher than the one observed in nature, however this can be also attributed to the added-on tabs of the specimens used for the gripping during the tensile tests; the grips could introduce a source of error on our measurements, together with a slightly higher degree of tensile compliance. To ensure the reproducibility of those results irrespective of the materials and manufacturing methods used, the same specimens were manufactured by stereolithography using a Form Labs 2 printer. The specimens manufactured with the SLA printing method were produced with the same specifications as the ones for the PLA printed specimens to investigate whether the same high ratio was still observed. Also in this case Fig. 5.6 & 5.7 and in Table 5.3 a high bending to axial stiffness ratio is observed, and this value is closer to the 7:1 observed in the biological material. This could be attributed to the higher printing resolution of the stereolithography method as compared to FDM<sup>190</sup>. **The difference in printing resolution between the two printing modalities can also be used to explain the difference in the ratios between them.** SLA printed specimens include a smaller number of artefacts within their structure as compared to their PLA counterparts. Additionally, the top down approach utilized in stereolithography generates a tighter bond between the specimens and the added-on grips, compared to the bottom up approach utilized in PLA printing, resulting in a significantly higher tensile stress in the SLA case resulting in a lower ratio being observed. This difference in the way the grips are added on the specimens in the two manufacturing routes can have a distinct impact on the tensile stress observed explaining the difference in the ratios. Further optimization needs to be carried out in the grip manufacturing on the specimens in order to eliminate these gripping effects on the tensile behaviour. Notwithstanding the manufacturing method used, the fact that the high bending to axial stiffness is present in all the specimens produced provides additional supporting evidence that the tree-like geometry characteristics of the cactus fibre sheaths are the primary driver behind the unusual bending to axial stiffness ratio behaviour. Hierarchical fractal-like configurations generate materials with significant mechanical benefits in comparison to non-hierarchical structures<sup>191</sup>, and the fractal-like configuration of the cactus fibre appears to provide another set of unusual mechanical properties. To the Author's knowledge this is the first structure that demonstrates this unusual deformation mechanism. There have been previously reported natural fibre biocomposites that do have significantly high bending to axial stiffness ratios with wood (4:1), arabaca (5:1) jute fibres (5:1) and carbon fibres (9:1) however this is due to the direction of loading with respect to the fibre alignment in the matrix<sup>192,193,194</sup>. **In the cactus structure case however, this behaviour is generated by a**

single component material and not a composite, demonstrating that the cellular fractal geometry present has a direct correlation with the mechanical properties observed.

### **5.2.3 Comparison of Cactus 3D Printed Analogues with Control Equivalent Beam**

A direct comparison with the control specimens in FDM and SLA, as manufactured based on Fig. 5.8, shows that those bulk solid samples demonstrate a significantly higher flexural modulus when compared to the cactus 3D printed analogues as it is evident in Fig. 5.9, 5.10, & 5.11. A direct comparison with the control specimens in FDM and SLA shows that those bulk solid samples demonstrate a significantly higher flexural modulus when compared to the cactus 3D printed analogues.

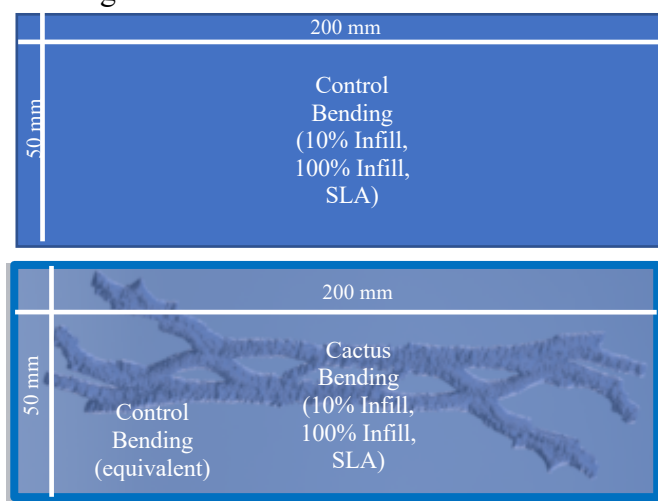


**Fig. 5.8** Graphic representation of the control equivalent beam used for comparisons for the cactus 3D printed analogue structure.

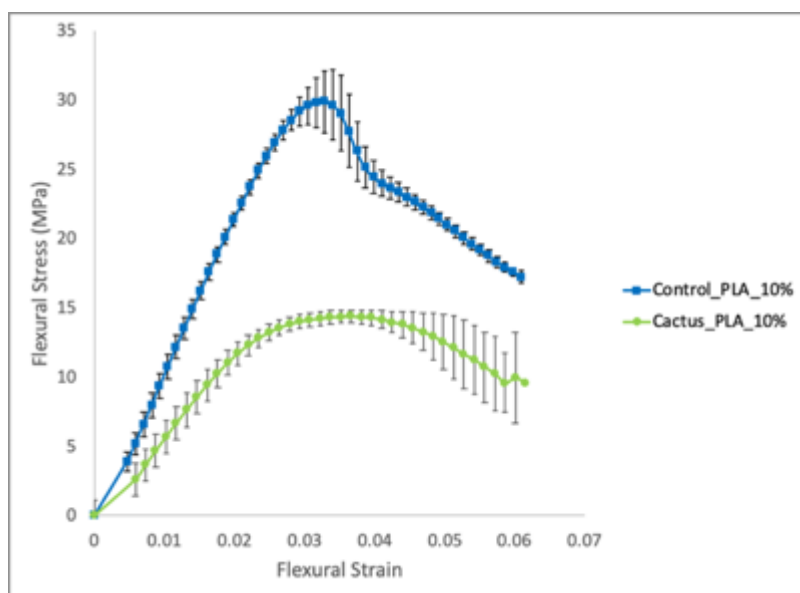


**Fig. 5.9** Comparison of 3D printed Polylactic Acid (PLA) control equivalent beam specimens with cactus 3D printed analogue specimens at 10% infill in 3-Point Bending Flexural Modulus. ASTM D790-17 (n=5)

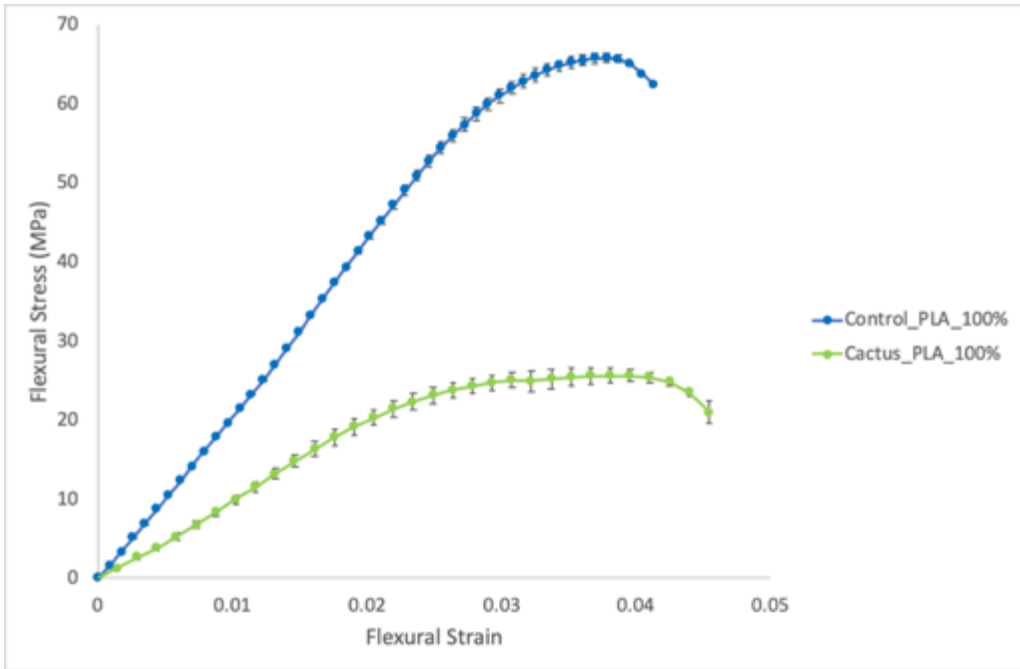


**Fig. 5.10** Comparison of 3D printed Polylactic Acid (PLA) control equivalent beam specimens with cactus 3D printed analogue specimens at 100% infill in 3-Point Bending Flexural Modulus. ASTM D790-17 (n=5)

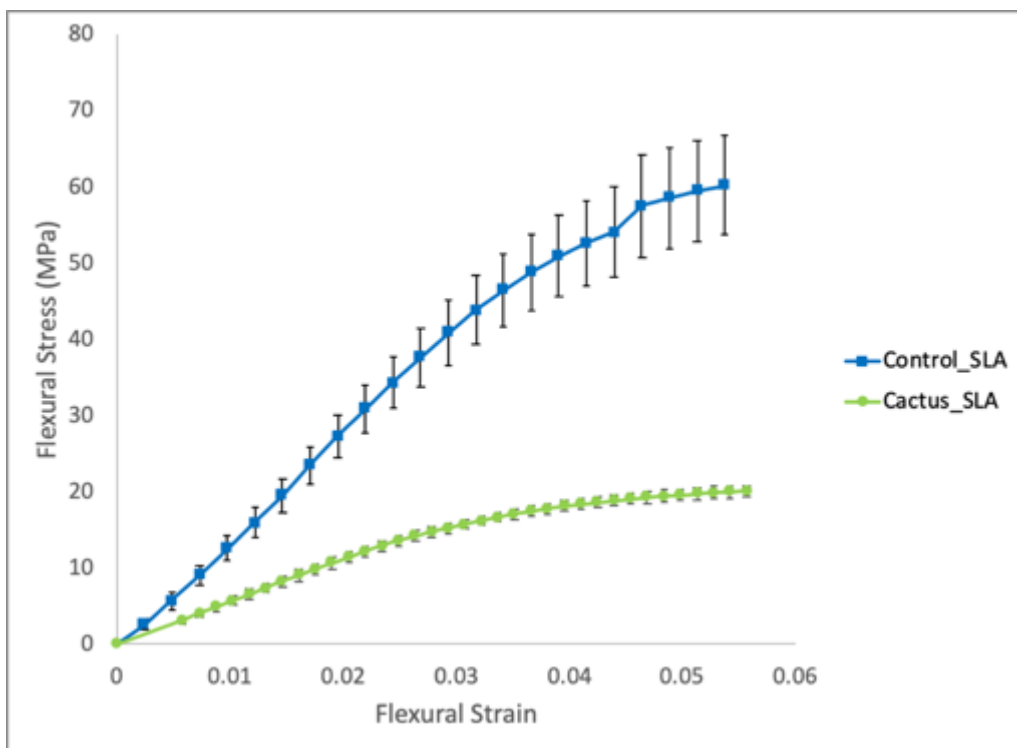


**Fig. 5.11** Comparison of 3D printed Stereolithography (SLA) control equivalent beam specimens with cactus 3D printed SLA analogue specimens in 3-Point Bending Flexural Modulus. ASTM D790-17 (n=5)

However, one of the biggest benefits of cellular materials is their macro porosity, which enables a weight reduction allowing some excellent mechanical performance in terms of specific (density averaged) stiffnesses<sup>195</sup>. Specific stiffnesses are defined as the stiffness of a material per unit density. Once the density normalization is performed Table 5.4 it is evident in Fig 5.12, 5.13 & 5.14 that the cactus specific flexural modulus is directly comparable to that of an equivalent beam.

**Table 5.4** Mass, Volume, Density Characteristics of the Cactus and Control 3D Printed Specimens.

	Mass (g)	Volume (cm <sup>3</sup> ) (Equivalent Beam)	Density (g/cm <sup>3</sup> )
Control_10%	22.2 ± 0.03	40	0.55
Cactus_10%	13.4 ± 0.02	40	0.34
Control_100%	47.6 ± .3	40	1.2
Cactus_100%	21.4 ± 0.1	40	0.54
Control_SLA	51.1 ± 0.2	40	1.3
Cactus_SLA	21.6 ± 0.3	40	0.54

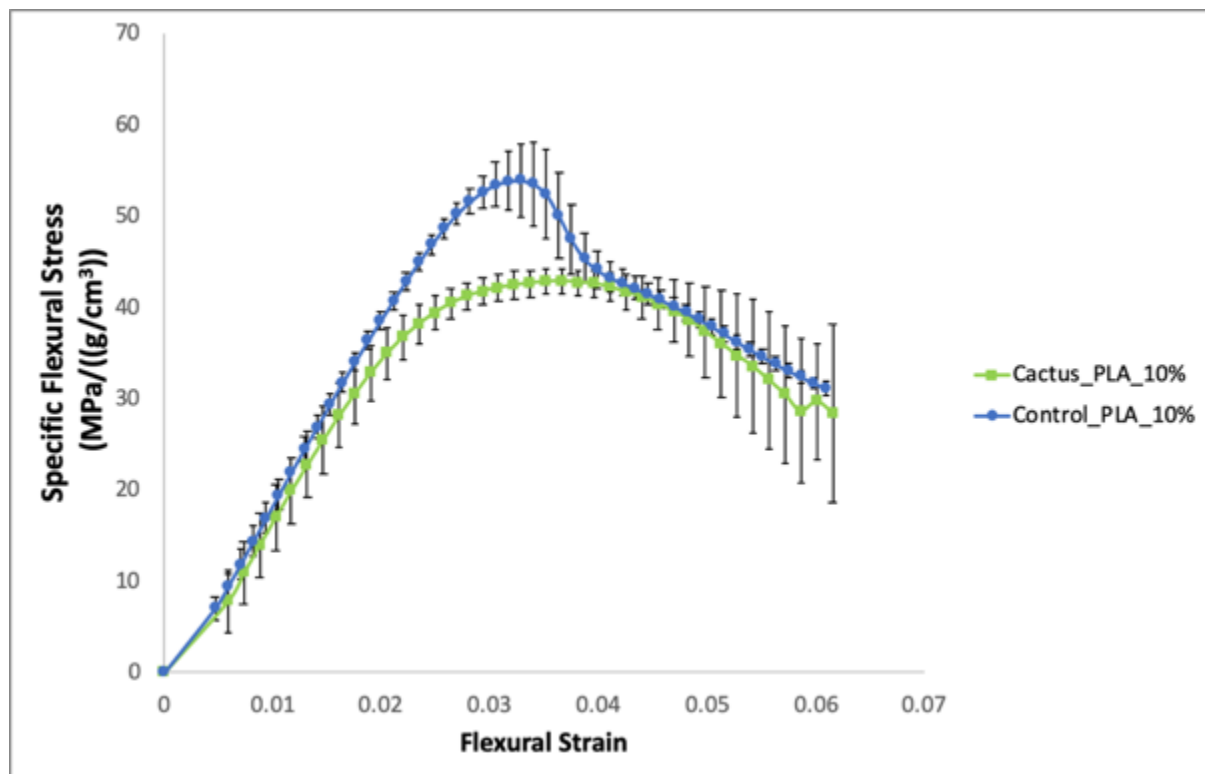


**Fig. 5.12** Comparison of 3D printed Polylactic Acid (PLA) control equivalent beam specimens with cactus 3D printed analogue specimens at 10% infill in 3-Point Bending Specific Flexural Modulus. ASTM D790-17 (n=5).

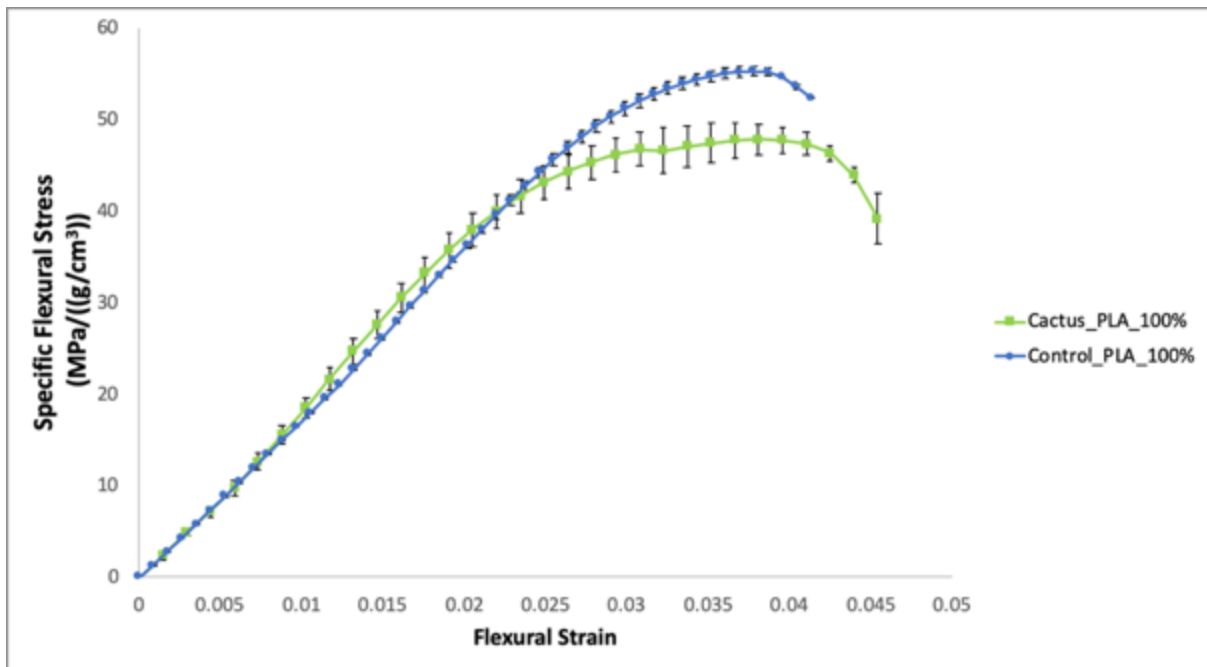


**Fig. 5.13** Comparison of 3D printed Polylactic Acid (PLA) control equivalent beam specimens with cactus 3D printed analogue specimens at 100% infill in 3-Point Bending Specific Flexural Modulus. ASTM D790-17 (n=5)

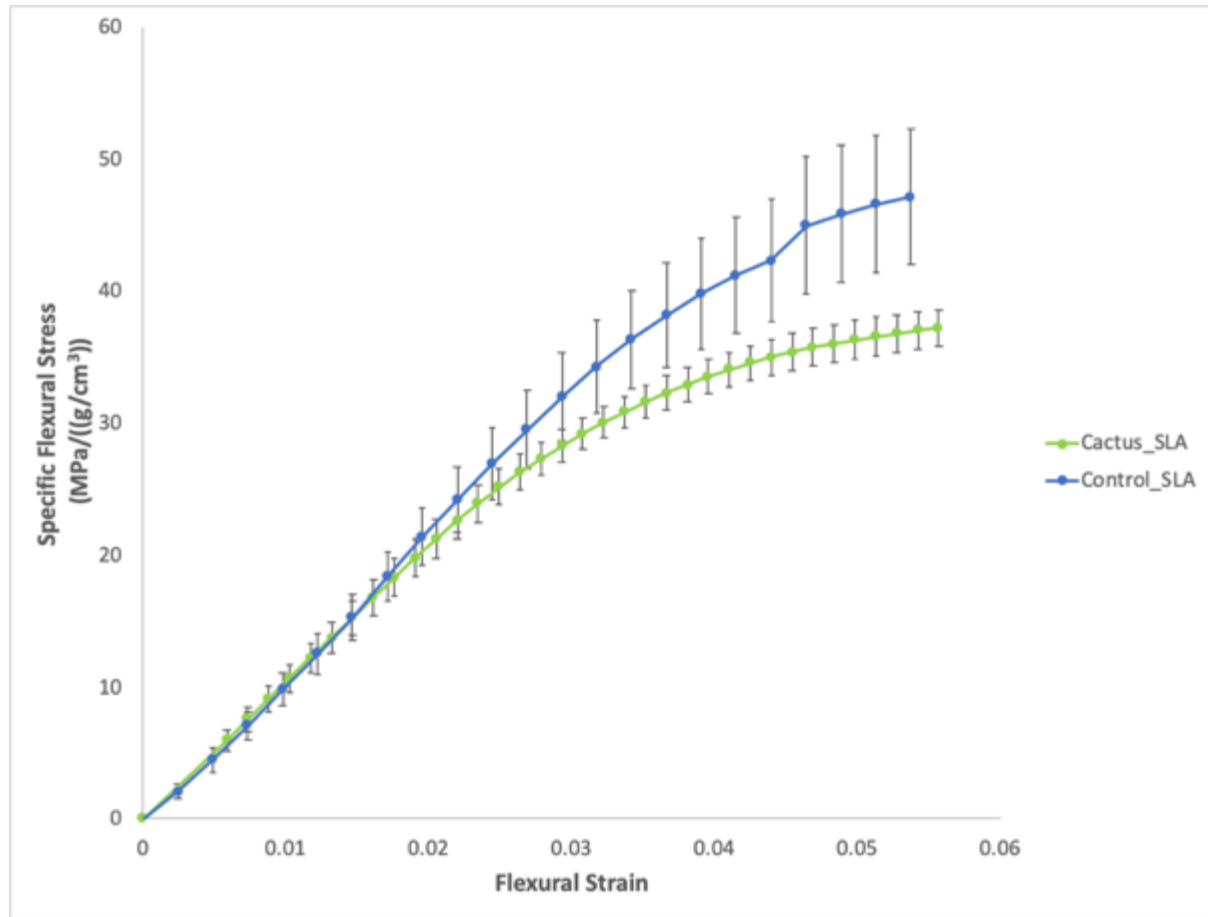


**Fig. 5.14** Comparison of 3D printed Stereolithography (SLA) control equivalent beam specimens with cactus 3D printed SLA analogue specimens in 3-Point Bending Flexural Modulus. ASTM D790-17 (n=5)

This demonstrates the significant potential of the cactus structure in applications where a high bending modulus is required. It is shown that the cactus structure, at half the weight of its equivalent beam (as an equal volume between cactus and equivalent beam was assumed for the density calculation), generates a directly comparable flexural modulus demonstrating that the architecture of the cellular structure is responsible for the properties observed as shown in Table 5.5 and Fig. 5.15. **It is observed that the cactus structure does not yield a better response as compared to the control beam when normalized.**

**Table 5.5** Cummulative Results of Flexural Moduli and Specific Flexural Moduli for all control and cactus analogue specimens

	Flexural Modulus	Specific Flexural Modulus
Control_10%_PLA	1079 ± 4	1944.3 ± 42.5
Cactus_10%_PLA	602.2 ± 13.4	1939.6± 55.1
Control_100%_PLA	2154.6 ± 27.8	1856.4± 54
Cactus_100%_PLA	1025.5 ± 44.3	1923.8± 94.3
Control_SLA	1194.9 ± 125	1132.7± 97.7
Cactus_SLA	581.7 ± 37.4	1045.4± 49.4

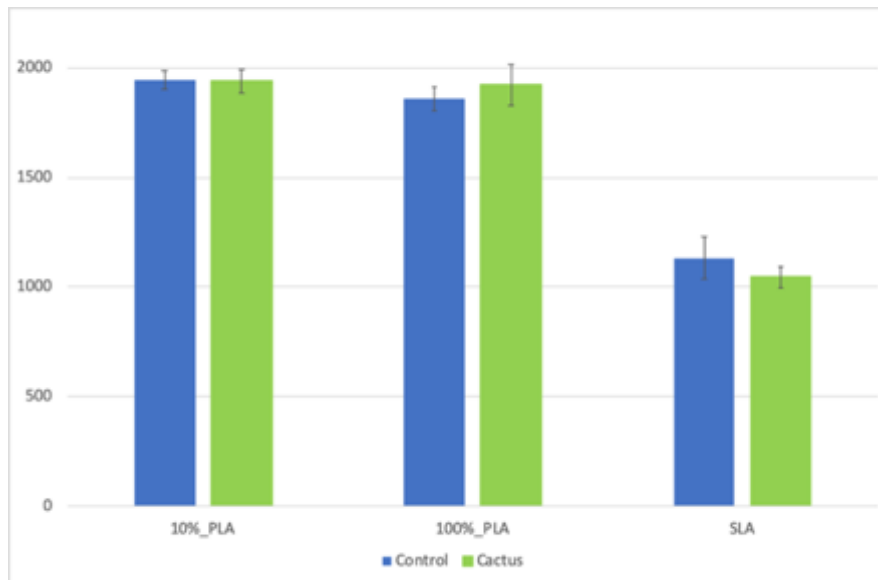


**Fig. 5.15** Graphic Representation of the Specific Flexural modulus of the control and cactus specimen demonstrating there is no significant difference between the different manufacturing methods used. (one tailed t-test,  $p<0.05$  \* demonstrates significant difference)

Since data for all the control specimens was also obtained to carry out the comparisons between those and the cactus equivalent specimens, we also calculated the bending to axial modulus

ratios of these specimens to demonstrate the significant morphological influence that the cactus structure has in the mechanical properties present. The results are presented below in Fig. 5.16 & Table 5.6. For material saving considerations and due to shortage of the PLA filament below the comparisons shown are only for the 10% PLA and the SLA specimens, however the results are expected to be similar for the 100% PLA specimens.

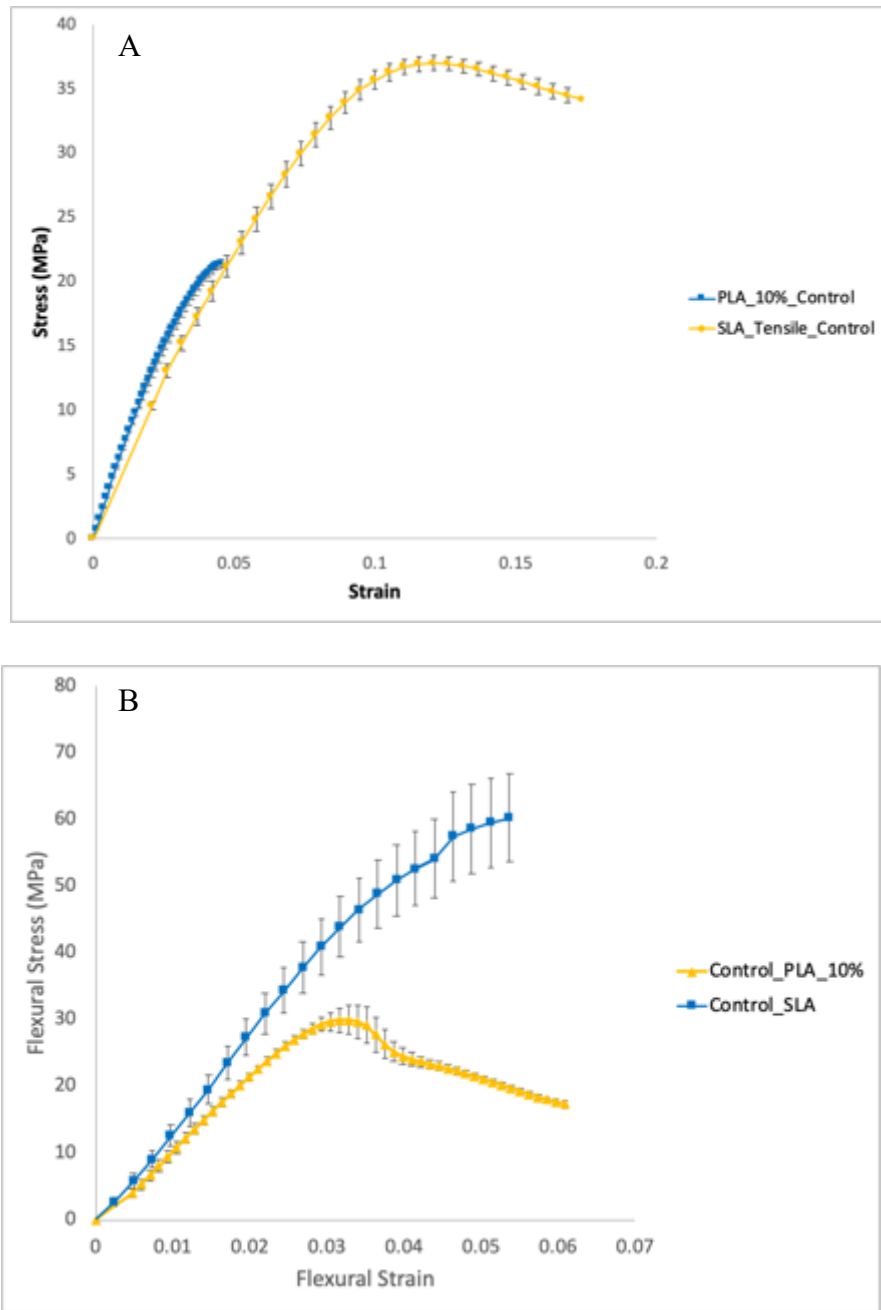


**Fig.5.16** Tensile Stress Vs Strain (a) and Flexural Stress Vs Flexural Strain graphs (b) for the control equivalent PLA 10% & SLA specimens to determine the bending to axial stiffness ratio (n=5).

**Table 5.6 Axial Modulus, Flexural Modulus and Ratios for control 3D printed specimens**

	Axial Modulus (MPa)	Flexural Modulus (MPa)	Ratio
Control_10%_PLA	$480.2 \pm 9.3$	$1079 \pm 4$	2.2
Control_SLA	$405.8 \pm 14.8$	$1194.9 \pm 125$	2.9

As it is expected the ratios observed in the case of the control equivalent beams are significantly smaller than the ones observed for the cactus 3D printed analogues. This is expected as the equivalent beams do not have the morphological features observed in the cactus structure, reinforcing our hypothesis that the cactus morphology is responsible for the high bending to axial stiffness ratio observed.

#### ***5.2.4 Finite Element Simulation Results***

A more in-depth understanding of the behaviour of these materials could however be only achieved through the development of mechanical simulations. In the original work on cactus fibre polyester composites<sup>9</sup> a modelling approach based on lattice beam constructions was adopted, with the assumption that the hierarchical structure of the cactus fibrils and bundles across scales enables the generation of these high bending to axial stiffness ratios. The model also pointed out that the ‘tree-like’ structure was responsible at the macro scale of the increased high bending modulus of the cactus fibre sheath. The 3D printed analogues of this work do not have a hierarchical structure present as they were manufactured through an additive manufacturing method in which the same layer is applied repeatedly to develop the final part. Moreover, the 3D printed analogues are not strictly speaking composite multiphase materials, since they have been developed using a single type of solid. Lastly, these bio-inspired artificial reinforcement materials have been generated using a small structural subunit from the whole cactus fibre sheath structure following the hypothesis of fractal geometry present within the biomaterial. For these reasons the 3D lattice hierarchical model implemented previously could not be used for the characterization of the 3D printed analogue specimens and a new approach was necessary. A reduced finite element beam that would replicate the cactus geometrical properties was therefore implemented for the simulations. By observing and studying the structure of the cactus stl file in Fig 5.1 used for the 3D printing of the 3D cactus analogue parts it is evident that the variability of the shape is mainly across the width of the structure. An equivalent beam that would replicate the structural elements of the cactus structure would therefore, at a very fundamental level, be a beam with a varied cross section area and moments of inertia. The FE beam model sections were taken from the .stl file in a Meshlab environment,

and for each section the cross-sectional area was determined. One of the key characteristics of the cactus analogue structure is its macro-porosity as evidenced in Fig 5.1 thus it was crucial to introduce a porosity factor to the equivalent mechanical properties of the material in the FE simulations, and this to cater for the effective porosity provided by the 3D printing infilling and the complexity of the cross-sections of the artificial cactus fibres. The infill factor implemented, Fig. 5.17, for both PLA and SLA, shows that this approach provides a good approximation of the bending of the cactus analogue, with the one given by the equivalent beam at an infill level of 40-50%.

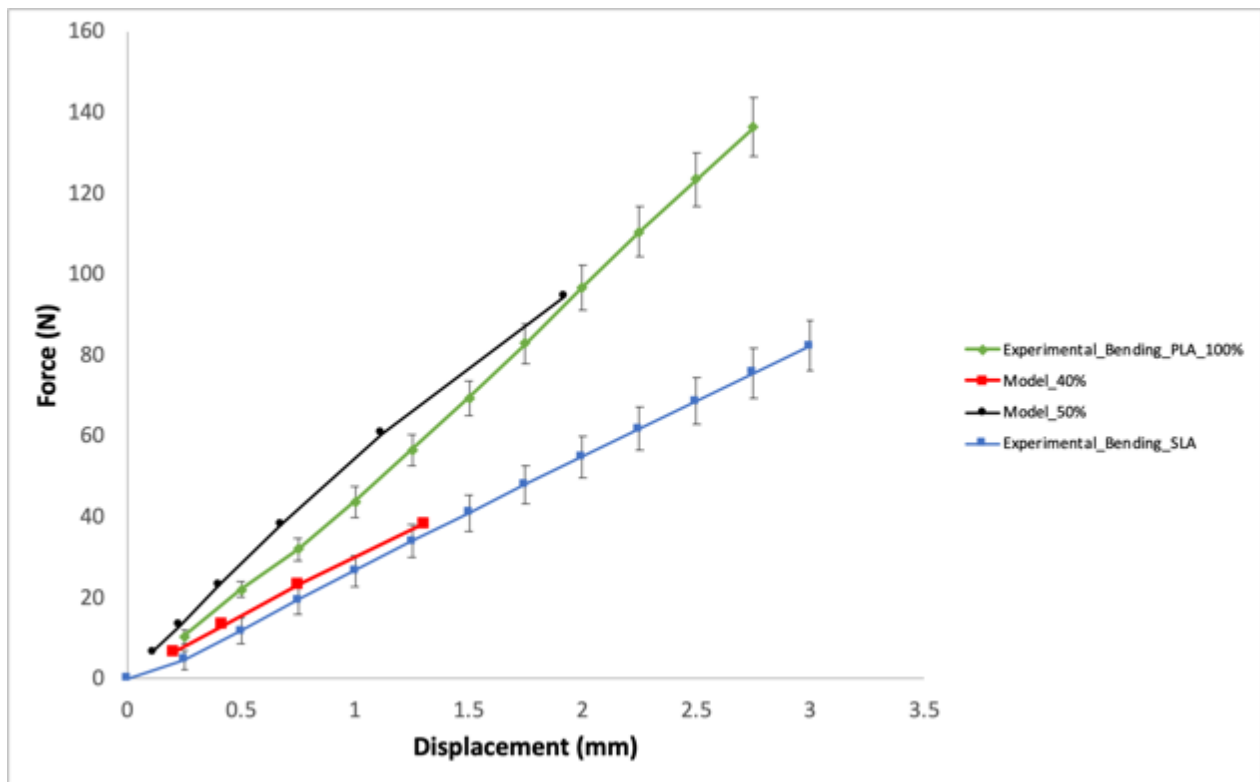


**Fig. 5.17** ANSYS modelling finite element simulations for the 3 Point Bending Testing Specimens of the cactus 3D printed Polylactic Acid (PLA) & SLA analogue structures at different infills.

Assuming that a solid equivalent beam would have an infill level of 100%, the infill level used of 40-50% translates into an effective porosity in the model of 50-60%. This result is to be expected; as observed in the cactus analogue structure of Fig. 5.1, the macro-porosity of the structure is evident. The mass of the cactus 3D printed analogues is also about half the mass of their equivalent beams generated to replicate the geometrical characteristics of the cactus structures of Table 5.4. Additional evidence of the porosity exhibited in the 3D printed cactus analogue specimen is shown in Fig 5.18 where a  $\mu$ CT scan of the 3D printed cactus analogue is presented.

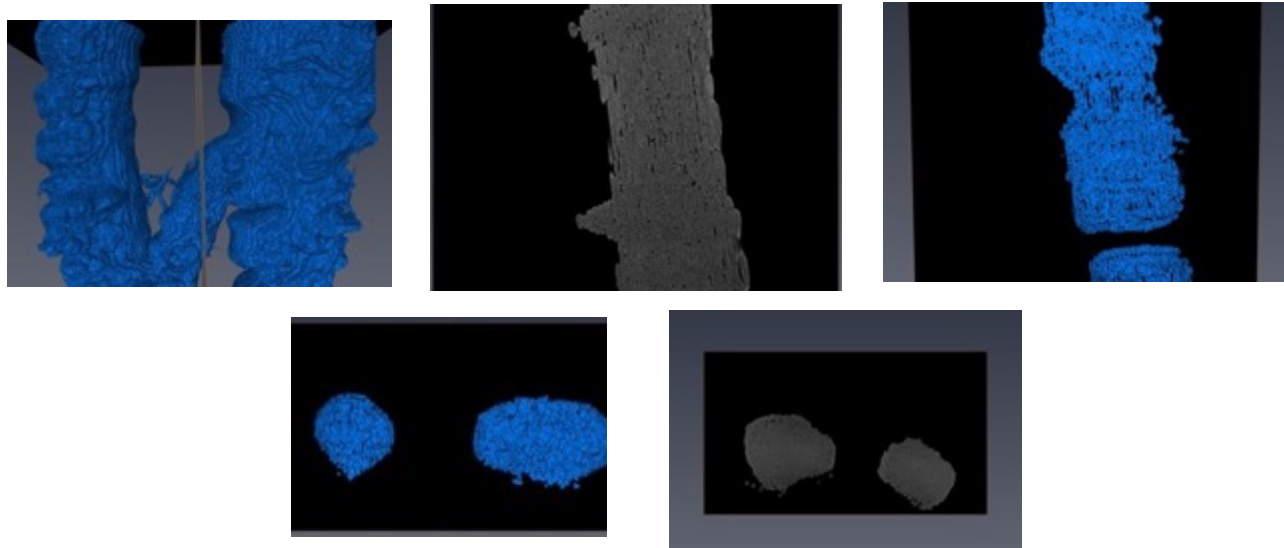


**Fig. 5.18** Micro-Computed Tomography ( $\mu$ CT) scans showing the internal and macro porosity of the Cactus 3D Printed PLA Specimens justifying the porosity of the ANSYS finite element simulation. It is evident that there is porosity throughout the structure, which was quantified at 5%. The internal porosity observed within the sections of the 3D printed specimen combined with the macro-porosity present in the cellular cactus structure explains the prediction from the model of the bending properties of the cactus structure at porosities between 50-60%. The more interesting results from the simulation however is in its prediction for the tensile behaviour of the cactus 3D printed analogues. As shown in Fig. 5.19 it is predicted that this tensile behaviour is expected from a cactus-equivalent beam at an infill of 20-30% i.e. with porosity of 70-80% which is very different than then porosity predicted from the bending simulations, **an observation that is more accurate in the SLA case**. It is also observed that even if the initial instant is taken into account on the PLA case, the 40% infill prediction (i.e. 60% porosity) is still a significant over-estimation of the tensile properties. Thus, the 20-30% infill range provides a reasonable estimate for the mechanical properties observed. It is also important to note that there is an initial non-linear behaviour observed in the case of the PLA samples that is not accurately modelled in our simulations, which is something that definitely will need to be taken into consideration in future analyses. For this analysis since such a non-linearity is not present in the SLA specimens, this characteristic was attributed to the gripping effects introduced in the FDM 3D printing and was not taken into account for the estimation of the mechanical properties present in the structure.

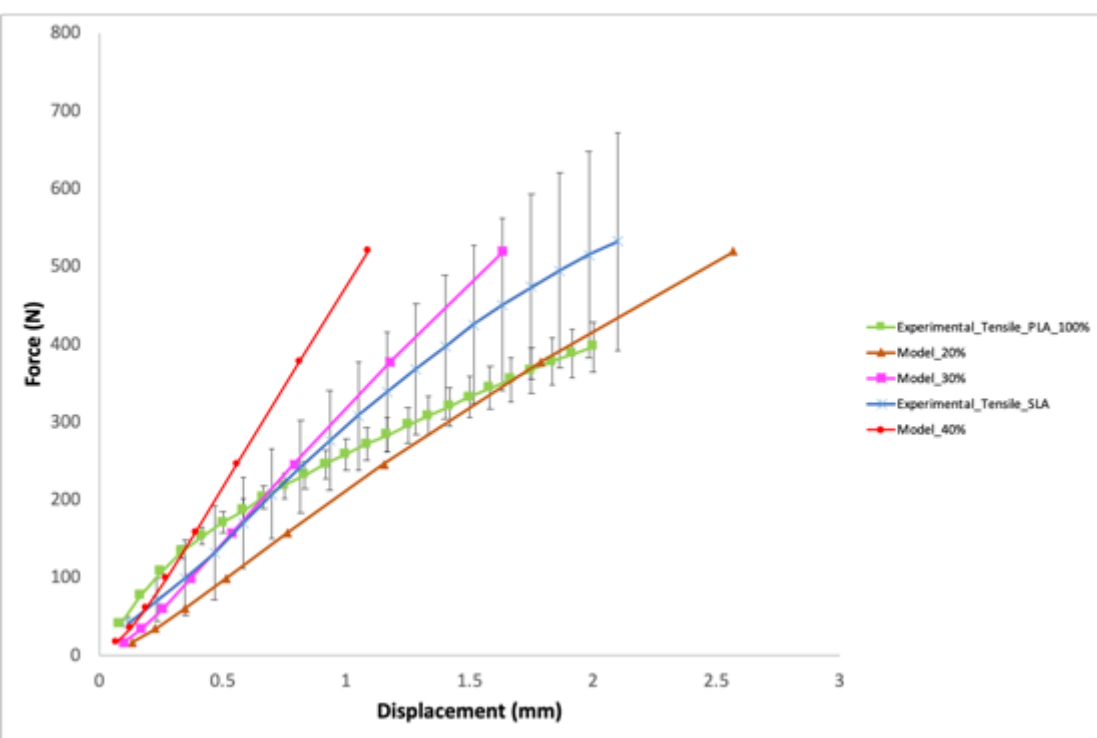


**Fig. 5.19** ANSYS modelling finite element simulations for the Tensile Testing Specimens of the cactus 3D printed Polylactic Acid (PLA) & SLA analogue structures at different infills.

The finite element simulations carried out demonstrate that the reduced order model approach alone is not adequate to predict the mechanical behaviour of the cactus structure. However, some useful information about the mechanical properties of the cactus configuration can still be obtained. To fully understand the information obtained from this simulation first it is essential to see what the bending to axial ratio predicted from the finite element simulation is. Looking at the results from the ideal scenario where the infill is 100% where there is no porosity present in the equivalent beam the bending to axial stiffness ratio is around 4 to 1 Fig.5.20 & 5.21 for PLA and Fig. 5.22 & 5.23 for SLA as well as in Table 5.7.

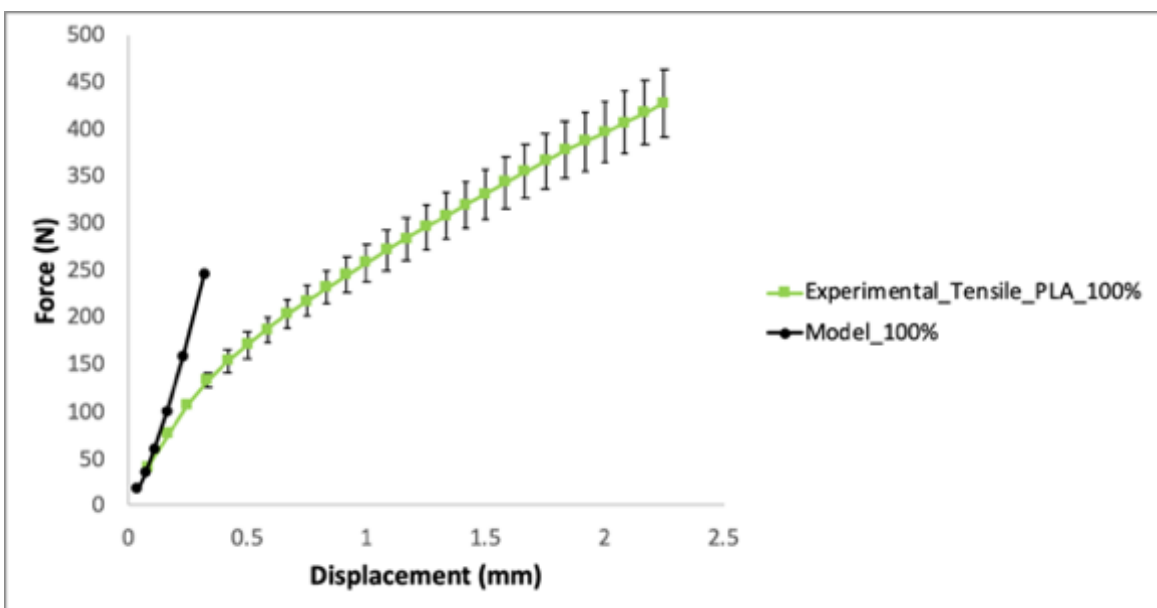


**Fig. 5.20** Comparison of Ideal simulation (100% Infill) and Experimental data for Cactus 3D Printed Polylactic Acid (PLA) analogues in axial loading.

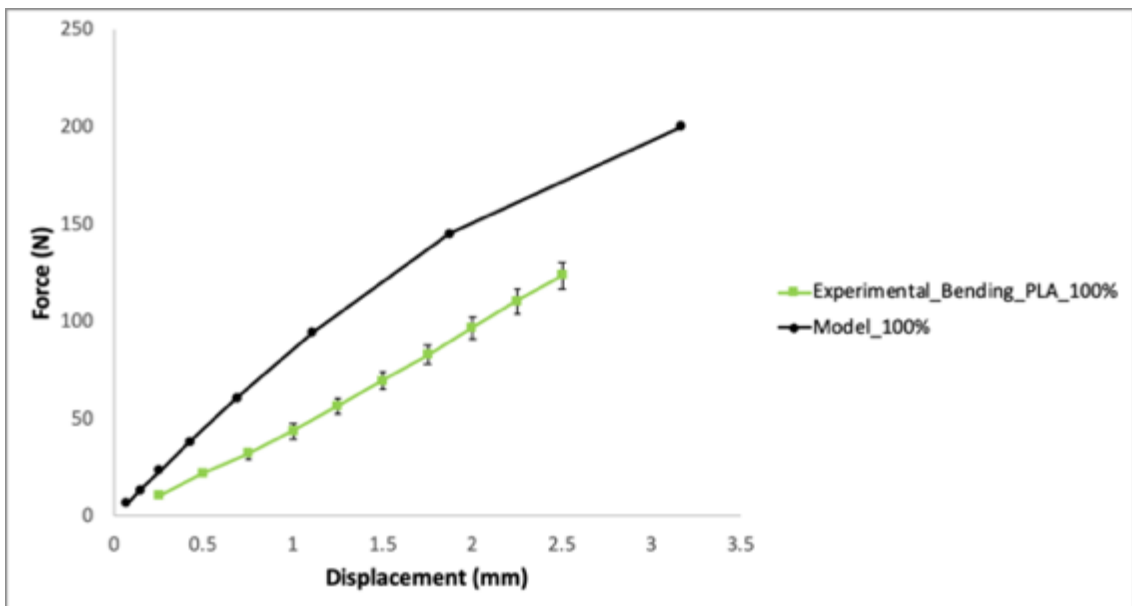


**Fig. 5.21** Comparison of Ideal simulation (100% Infill) and Experimental data for Cactus 3D Printed Polylactic Acid (PLA) analogues in 3 Point Bending.

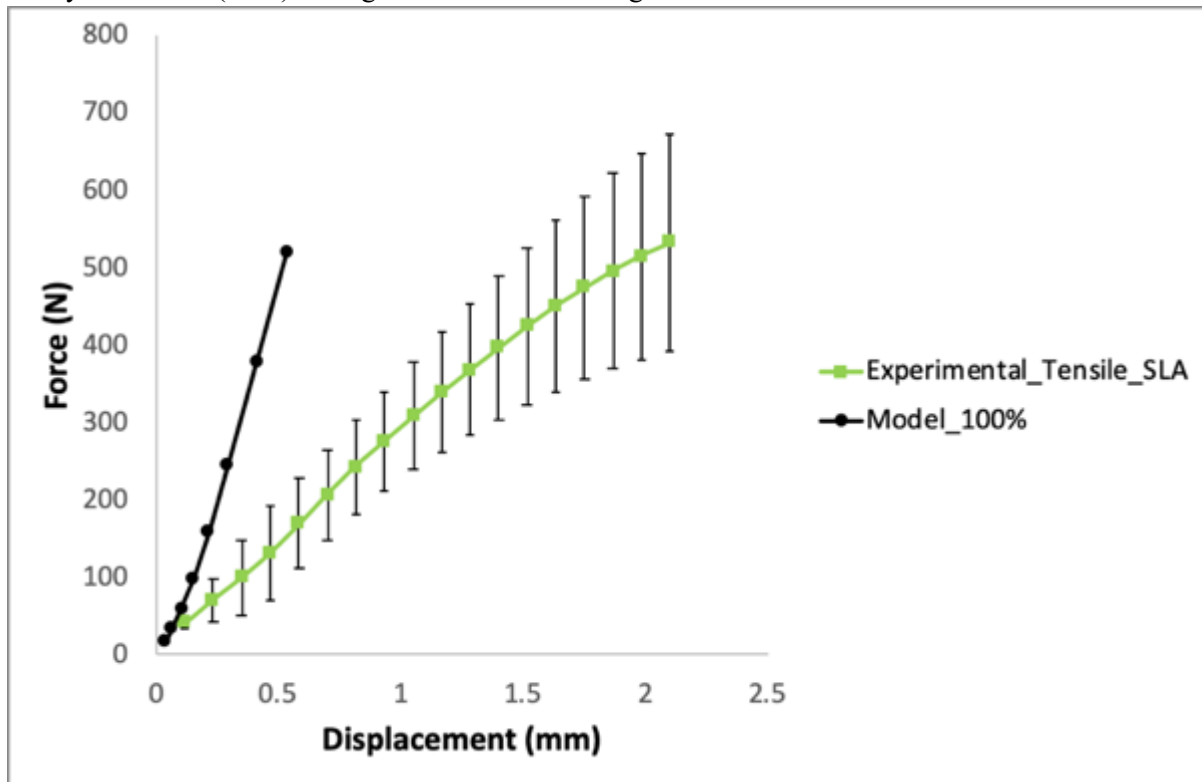


**Fig. 5.22** Comparison of Ideal simulation (100% Infill) and Experimental data for Cactus 3D Printed Stereolithography (SLA) analogues in axial loading.

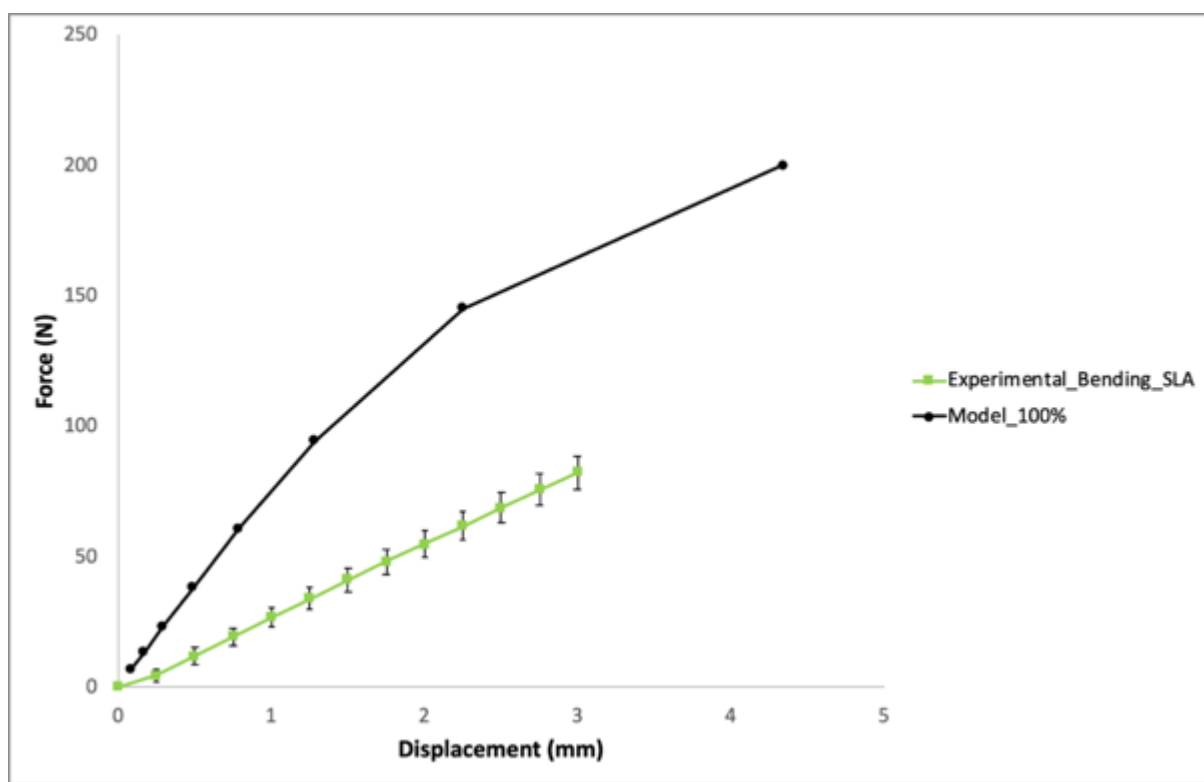


**Fig. 5.23** Comparison of Ideal simulation (100% Infill) and Experimental data for Cactus 3D Printed Stereolithography (SLA) analogues in 3 Point Bending.

**Table 5.7** ANSYS 100% Infill Model Predicted moduli and ratios

	Tensile Modulus (MPa)	Flexural Modulus (MPa)	Ratio
ANSYS_100%_PLA	377.3	1589.4	4.2
ANSYS_100%_SLA	414.3	1320.1	3.2

Even though this is still a significantly high bending to axial stiffness ratio it is still significantly lower than the one demonstrated by the cactus structure. It is important to note here that the simulations were not performed for the control specimens as for the material properties utilized the values were experimentally checked and matched the manufacturer specifications. Moreover, it is interesting to observe that the correct bending to axial stiffness ratio is achieved within the simulation once the porosity of the tensile testing is increased making the beam significantly weaker in tension as a result of the increased porosity. At the same time if the same porosity is used for the bending stiffness simulation the predicted modulus is significantly lower than the one of the experimental data. These observations demonstrate that this modelling approach fails at predicting the exact ratio observed experimentally demonstrating that there are additional factors that need to be accounted for to understand the cactus morphology and its mechanical properties observed. The fact that the structure in bending loading scenarios behaves significantly better than expected means that besides the varied cross-sectional area the architecture of the structure and the location of the pores existing play

a significant role for the mechanical properties observed as it can be seen in the in situ  $\mu$ CT 3 point bending test shown in Fig. 5.24.

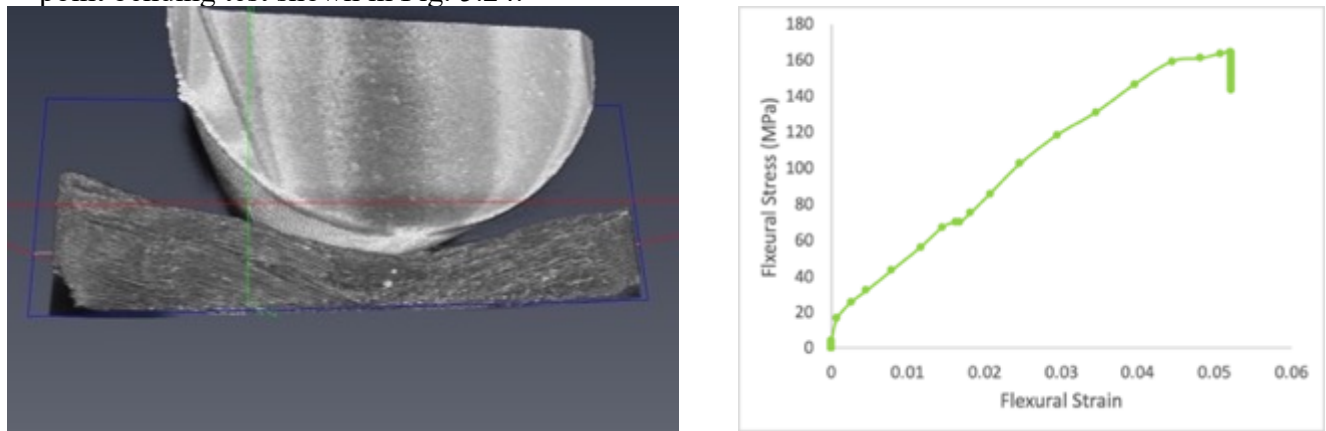


**Fig. 5.24** In situ Micro- Computed Tomography ( $\mu$ CT) scans and flexural bending of cactus fibres demonstrating how the fibrils within the structure behave under bending loading.

The porosity in the finite element simulation is distributed uniformly over the cross sections, whereas in the cactus structure the pores are localized in specific areas, with the outer surface of the samples showing a higher density. That would effectively generate hollow cross sections, with higher thickness close to the external surfaces and therefore higher moment of inertia. Moreover, in the tensile loading scenarios the topography of the porosity of the structure serves as a disadvantage, because cellular solids tend to be bending dominated from a mechanical perspective and are significantly more compliant in tension<sup>196</sup>. Although the reduced order finite element model shows some limits, it does however provide some insight on the architectural and morphological properties present in the cactus structure. The 4:1 ratio obtained by the models at 100% infilling suggests indeed that the geometry of the tree-like configuration provides unusual bending to axial stiffness behaviours, which could find applications in various fields. For example, a high bending to stiffness ratio would be useful in shape morphing applications in aerofoils, in which structures need to be stretched but the shape under bending needs to be preserved<sup>129</sup>. The different stiffnesses in stretching and bending also suggest different strain energy mechanisms being present in the same architecture; this could be used to design structures with tailored energy absorption capabilities that depend on the type of external loading provided<sup>130</sup>.

### **5.3 Conclusions**

Biological materials have always been on the forefront of scientific and industrial focus due to their mechanical properties and abundance, while bioinspiration through additive manufacturing has enabled the generation of novel biological based materials with unique properties expanding the material field significantly. Specifically, previous work on cactus fibres has demonstrated that the morphology and architectural characteristics of this fibre when implemented as a matrix reinforcement, yield composite materials with unusual high bending to axial stiffness ratios and a significant increase in energy dissipation per volume matrix. The ability to extensively image the cactus structure in an effort to fully understand its mechanical properties and explain the presence of this unusual high ratio led to the generation of 3D rendered models of a simplified cactus structure. Due to the data size and limitations the studies focused on a small structural subunit of the cactus structure that was hypothesized to maintain similar mechanical properties to the full cactus structure. Those 3D models of the cactus structure were 3D printed using two different additive manufacturing methods and the 3D cactus analogues were tested in 3-point bending and axial loading environments following the appropriate ASTM standards for plastic parts. The results demonstrated that the high bending to axial stiffness ratio is maintained irrespective of manufacturing method and material used and in some cases the ratio can be even higher. Moreover, it was shown that the cactus fibre hierarchical structure is responsible for the mechanical characteristics demonstrated while also enabling the generation of a novel cactus-based material platform that maintains high bending to axial stiffness ratios irrespective of the material and the manufacturing method used. In order to assess the application potential of this cactus based material platform the 3D printed cactus analogues were compared to equivalent beams having the same overall dimensions and it was proven that the cactus based analogues provide significant benefits in terms of weight saving in flexural loading scenarios as well as in preliminary impact energy work. The generation of the 3D rendered models of the cactus structure also prompted the generation of a finite element beam generated based on the cross-sectional areas of the cactus 3D rendered structure. The generated finite element beam was simulated under bending and axial loading scenarios and gave unique insight on the mechanical behaviour of the 3D printed cactus-based analogues. Besides the varied cross section area of the cactus structure the topology of the macro-pores is of vital importance both for the bending and tensile properties demonstrated from the cactus structure. In addition, the finite element simulations provided an evaluation on novel equivalent cactus based non-porous materials in terms of their mechanical properties and their bending to

axial stiffness ratio. Overall, we have demonstrated the ability to use 3D printing for the explanation of the unique structural characteristics observed in a biological material while also developing a novel bioinspired material platform with unusual high bending to axial stiffness ratios that could be utilized in flexural energy dissipation applications.

## **6 Cactus Based Thermoplastic and Hydrogel composites**

---

### **Relevant Publication:**

Deller RC, Richardson T, Richardson R, Bevan L, **Zampetakis I**, Scarpa F, et al. **Artificial cell membrane binding thrombin constructs drive in situ fibrin hydrogel formation**. Nature Communications. 2019;10(1):1887.

### ***6.1 Chapter Overview***

The overall focus of this chapter is to understand the potential of the cactus fibre as a biological material in different settings. The cactus fibres are utilized as a structural reinforcement both for a hydrogel bioink system as well as a thermoplastic matrix system. The mechanical benefits obtained are assessed and compared to other common natural fibres widely utilized across the open literature. The composite hydrogel bioink system is further evaluated in order to assess the potential of utilizing natural plant fibres and specific cactus fibres as a potential biomedical material to structurally enhance the properties of hydrogel matrices *via* cytotoxicity and bone tissue engineering experiments.

## 6.2 Results & Discussion

### 6.2.1 Natural Fibre Characterization

Cactus fibres have previously demonstrated their potential when implemented as composite reinforcement yielding novel composite materials with exciting flexural and energy dissipating properties<sup>9</sup>. However, natural fibres are used in various formats when implemented as composite reinforcements, and there are various reports of using natural fibres as fillers or weaves, for the generation of novel composite materials<sup>197-200</sup>. Thus, it was important to assess the potential of the cactus natural fibre being used as a composite reinforcement for different matrix composites in different formats. Initial work<sup>10</sup> demonstrated the potential of using the cactus fibre in a powder format for the generation of bio-composites with quite interesting results. In our case however, we are focusing on significantly smaller weight percentages as well as on a hydrogel matrix besides a thermoplastic matrix for our composite material. It was important to determine the potential of the cactus fibre in as a composite matrix and compare its reinforcement potential with other natural fibres commonly used<sup>93-97</sup>. Since the cactus fibres we use are not chemically processed it was important to utilize non chemically processed natural fibres for all the composites manufactured and FTIR measurements (Fig. 6.1) demonstrated that all the natural fibres used had not been through chemical modification.

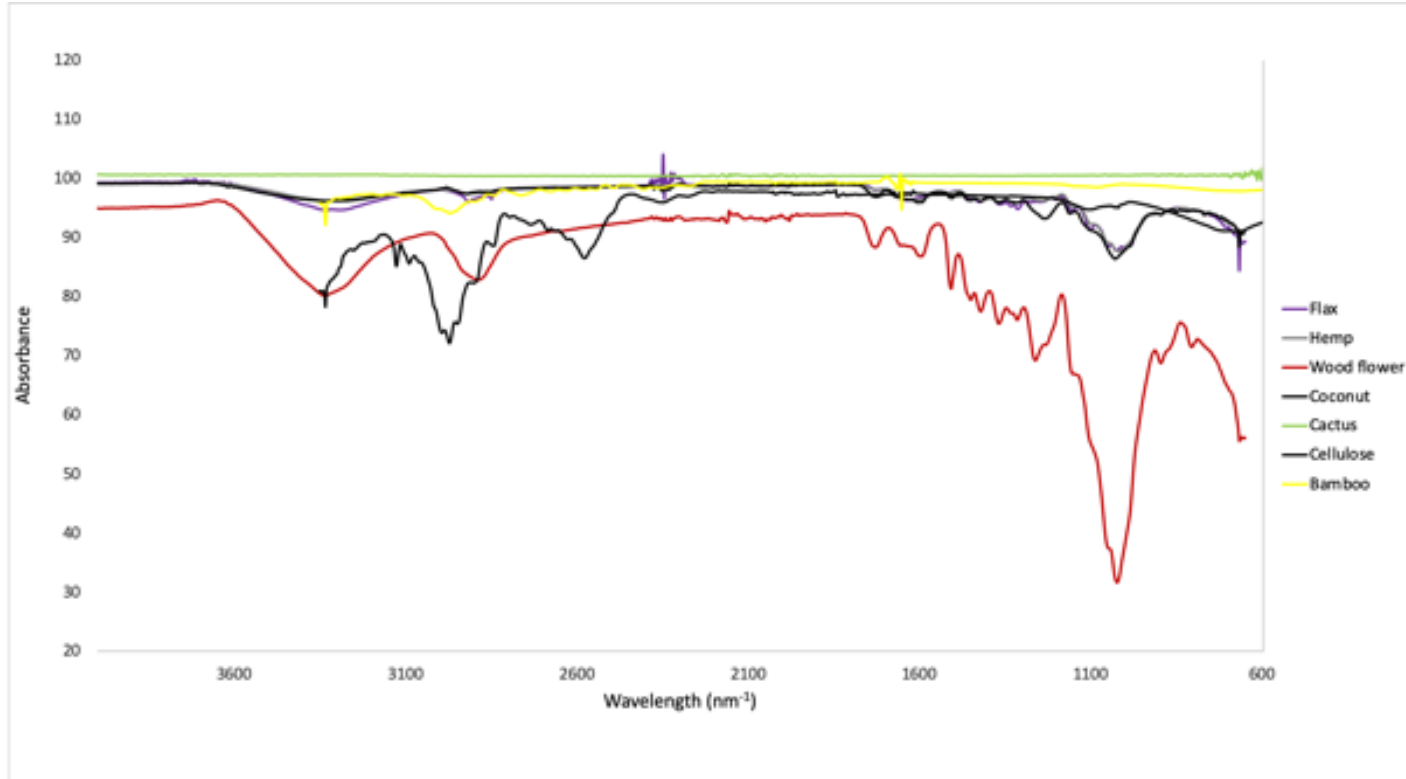


**Fig. 6.1** The Fourier Transform Infrared Spectroscopy (FTIR) results of all the natural fibres used for this work demonstrating that there is no chemical modification present as all natural fibres present peaks in the same regions. Characteristic peaks are observed at  $3700 \text{ cm}^{-1}$  for the OH groups, at  $1600 \text{ cm}^{-1}$  for

the C=C, and from 1000-1700 cm<sup>-1</sup> for the cellulose crystals. Fourier Transform Infrared Spectroscopy results reveal that the chemical components of all natural fibres are the same but the chemical composition of each fibre is different, while it was verified that no chemical modification is present. More specifically, looking at Figure 6.1 it is clear that all the natural fibres used exhibit peaks in similar regions which is to be expected as their constituent materials are similar, but the discrepancy in the strength of each peak is directly correlated to the source of the fibre as fibres from different sources exhibit a different spectra<sup>201,202</sup>. With regards to the peaks, specifically it is evident that there is a peak at around 3300 cm<sup>-1</sup> signifying the presence of lignocellulose via the existence of hydroxyl groups, a double bond carbonyl peak at around 1650 cm<sup>-1</sup> and various peaks in the region of 1000 cm<sup>-1</sup>-1700 cm<sup>-1</sup> signifying the presence of the cellulose crystallites<sup>10,201</sup>. As evidenced, the same peaks are observed in all the natural fibres tested signifying that no chemical modification has been carried out on these materials. It is also important to note that the differences between the intensity of the peaks between the natural fibres observed signifies that even though the fibres are primarily consisting of the same constituents, the amount of each constituent varies for each fibre, which is a phenomenon that is to be expected, since those fibres originate from different plant sources<sup>201,202</sup>.

### **6.2.2 Natural fibres Hydrogel bioink composites**

Once it was established that the natural fibres have not undergone any chemical modification, they were ball milled to generate the natural fibres powders. The first attempt of making a composite material with those natural fibre powders focused on generating a composite hydrogel material due to the small size of the fillers achieved via the ball milling process. Hydrogel systems are mainly developed for biomedical applications and thus are generally manufactured at significantly smaller scales, meaning that small amounts of fillers introduced in the system amount for a significant weight percentage of the entire specimen. Moreover, hydrogels are primarily comprised of a polymeric network swelling in water and thus any additional solid material could introduce significant mechanical reinforcements within the polymeric network. The high-water content of the hydrogels is simultaneously one of the disadvantages of using hydrogels, since it has been shown that water uptake deteriorates the properties of natural fibres over time<sup>203</sup>. That could be one of the main reasons why even though commercial natural fibres such as flax, hemp and bamboo have found their way into commercial composite applications<sup>93-196</sup>, their use as hydrogel reinforcement has been severely limited in literature. Cellulose, the primary chemical component of all natural fibres, is being used for hydrogel formation and as a hydrogel reinforcement yielding improved mechanical results<sup>117</sup> but fibres directly from plants are not widespread as a hydrogel filler despite being

widely available and cost effective. We hypothesized that the natural fibres obtained directly from plants could provide significant mechanical reinforcement in hydrogel systems and thus developed a methodology of introducing the natural fibres as a filler for the generation of hydrogel composite systems. We focused on a previously developed hydrogel system that had been used for bioprinting applications<sup>103</sup> with the aim to not only generate hydrogel composite systems but simultaneously develop a composite bioink system comprising of natural fibres. We were initially able to introduce the natural fibres through a simple mixing methodology using a dual asymmetric centrifuge. Through rheology the hydrogel properties of the composite systems were evaluated to determine if significant differences are observed between the original hydrogel system and the new composite hydrogel system before crosslinking. As evident in Fig. 6.2, rheology analysis demonstrated that as the cactus fibre content increased there is a distinct increase in both the storage and loss moduli, which is to be expected as we are adding a filler for mechanical reinforcement of the hydrogel matrix. The storage modulus describes the solid-state behaviour of the specimen, while the loss modulus its liquid state behaviour. Thus, by adding more solid content, it is expected that both moduli will increase in value as the whole specimen becomes more solid. In other words, storage modulus describes the stored energy deformation during flow, while the loss modulus describes the energy lost during flow. Thus, viscoelastic solids, such as the one in our case, are expected to have a higher storage modulus as compared to loss modulus<sup>103</sup>. As evident in Fig. 6.2 this holds true for all our specimens while the introduction of the cactus fillers increases the values of the storage and loss moduli as additional solid material is added. The values of the storage and loss moduli are utilized in the calculation of the flow indexes shown in Table 6.1, where flow indexes between 0 and 1 demonstrate Non-Newtonian fluid behaviour similar to the behaviour of honey for instance where the flow pattern changes under shear stress. The distinct difference observed between the flow index of Cactus\_20% as compared to the other specimen is attributed to the rheometer of some samples coming into direct contact with the cactus fibres thus resulting in a higher value however the value is well within the accepted range to allow for extrusion of the hydrogel.

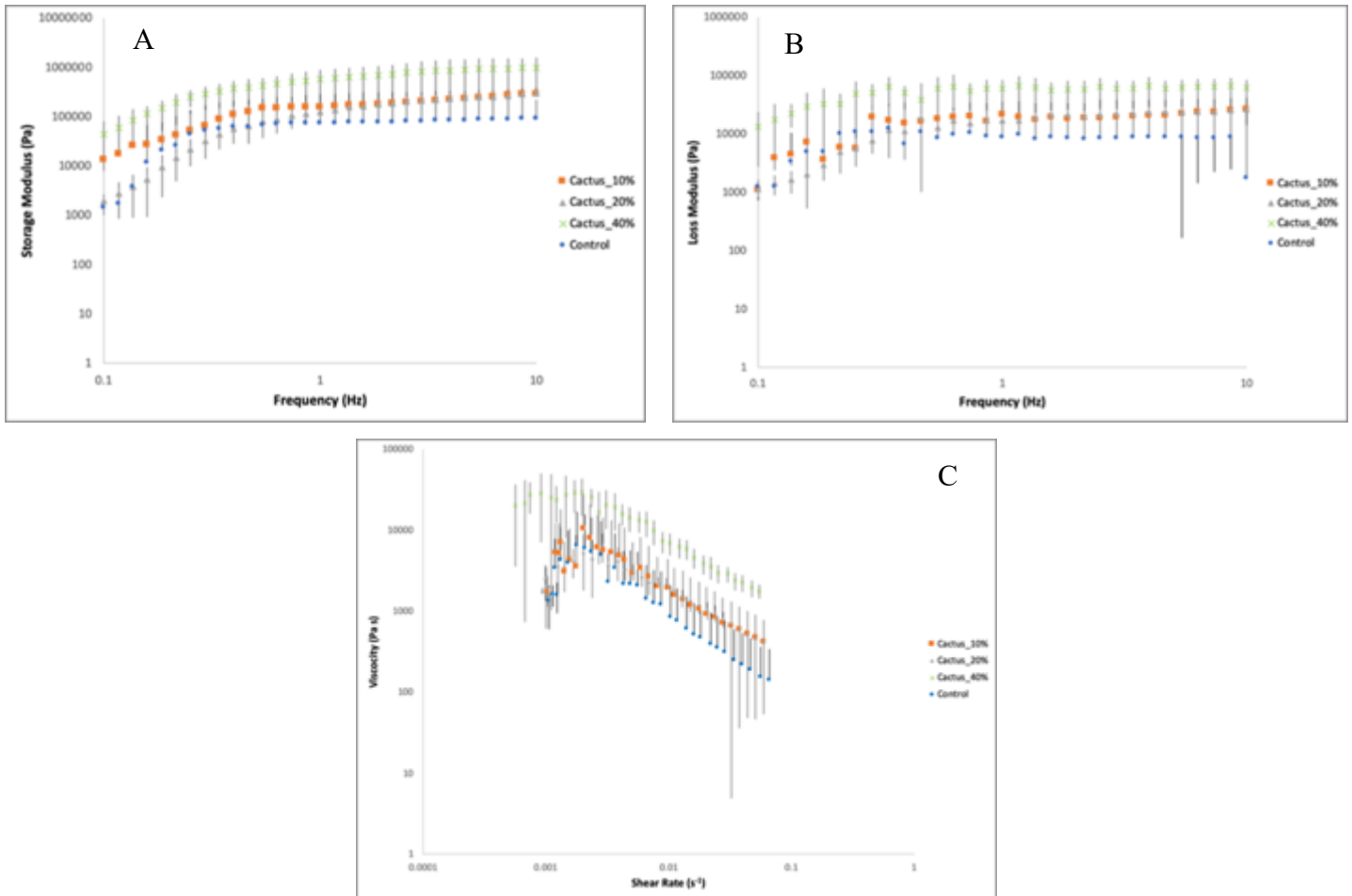


**Fig.6.2** Storage Modulus (a), loss Modulus (b) and viscosity (c) of all the hydrogel and hydrogel composites to ensure the extrudability of the cactus-based gels ( $n=5$ ). Increase in the storage and modulus with the addition of the fillers is observed which is an expected result due to the addition of a solid component. The viscosity graph was used for the determination of the flow indexes demonstrating the non-Newtonian nature of the hydrogels. Observing all three figures it is demonstrated that the addition of the filler does not alter the flow properties of the original hydrogel significantly thus the composite hydrogel inks can still be utilized for extrusion.

**Table 6.1** Flow indexes calculated via the Ostwald–de Waele relationship. Flow indexes between 0 and 1 demonstrate Non-Newtonian fluid behaviour as evident in all hydrogel specimens. All four hydrogels tested demonstrate very similar flow indexes indicating that the filler addition does not alter the flow properties.

	Flow index
Control	$0.12 \pm 0.08$
Cactus_10%	$0.13 \pm 0.08$
Cactus_20%	$0.2 \pm 0.04$
Cactus_40%	$0.13 \pm 0.04$

The most important finding from the rheology measurements is the fact that the flow properties observed in the cactus hydrogels still render the hydrogel extrudable and thus we are still able to use the composite natural fibre system for 3D printing to generate our specimens and for potential bioprinting applications. More specifically, the viscosity seems to decrease in all cases as the shear rate is increasing signifying shear thinning behaviour. Moreover, the calculation of flow indexes via Ostwald-de Waele power law model (Table 6.1) demonstrates that all the gels have very similar flow index values and all around 0.1. This result signifies shear thinning behaviour as values between 0 and 1 describe non-Newtonian fluids with Newtonian fluids having a value of 1<sup>204</sup>. Furthermore, no crossover point was observed between the storage and loss modulus which signifies a rigid gel network<sup>205</sup>.

The next step of the characterization of the hydrogel composite systems included the assessment of the mechanical reinforcement achieved with natural fibres when they are incorporated in the hydrogel system after the specimens are extruded and crosslinked. As evident in Fig. 6.3, significant mechanical reinforcement was achieved with all of the natural fibres implemented in this study at 2.5% w/w as described in method section.

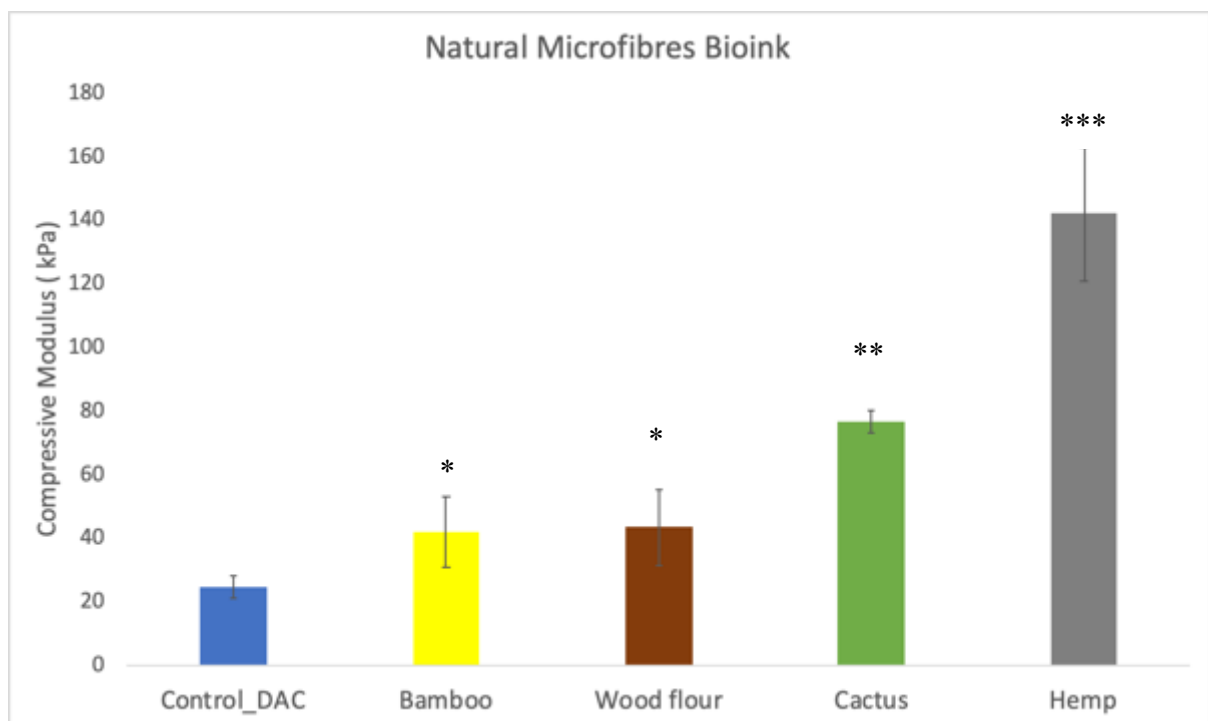


**Fig. 6.3** Compressive modulus comparison between control hydrogels and different hydrogel composites. The structural reinforcement is evident across all the natural fillers used with cactus and hemp fibres providing the more significant compressive modulus increase. The addition of solid particles in a hydrogel network is expected to mechanically reinforce the specimens as it is observed.

To the author's knowledge this is the first attempt at the utilization of this type of filler in a hydrogel system. (\*) shows significant difference), (ANOVA, p<0.05,n=5)

The increase in the Young's modulus was not unexpected, as natural fibre powders have been shown to provide significant mechanical reinforcement in composite systems<sup>195-197</sup>. However, to the author's knowledge, this is the first attempt at implementing ball milled natural fibre powders directly into a hydrogel system as a mechanical reinforcement, as well as the first 3D printing hydrogel ink system with this type of natural fibre reinforcement. From our results, it was also evident that the cactus and hemp reinforcements provided the most significant mechanical reinforcement and it is significantly higher compared to all the other natural fibres utilized.

### ***6.2.3 Thermoplastic natural fibre Composites***

The fact that mechanical reinforcement is achieved at such small weight percentages in hydrogels prompted the idea of preliminary testing of these natural fibres at these mass fractions of 3.3 % w/w in a more composite relevant matrix (PLA), as well to assess its potential as a thermoplastic filler. Moreover, this approach provided the added benefit of exploring whether the reinforcement in the hydrogel was a result of intrinsic properties of the fibres, and not simply *via* changes in the hydrogel structure through defects formation and gel nucleation. The natural fibres were implemented as a filler reinforcement of thermoplastic PLA *via* thermomixing and thermoforming. The resulting specimens were tested to assess their dynamic mechanical properties. µCT measurements (Fig. 6.4) revealed the dispersion achieved within those composite specimens demonstrating that despite the rudimentary method used for the composite mixing, good dispersion is achieved. The ball milling did, however, introduce some size polydispersity in the cactus powder particles.

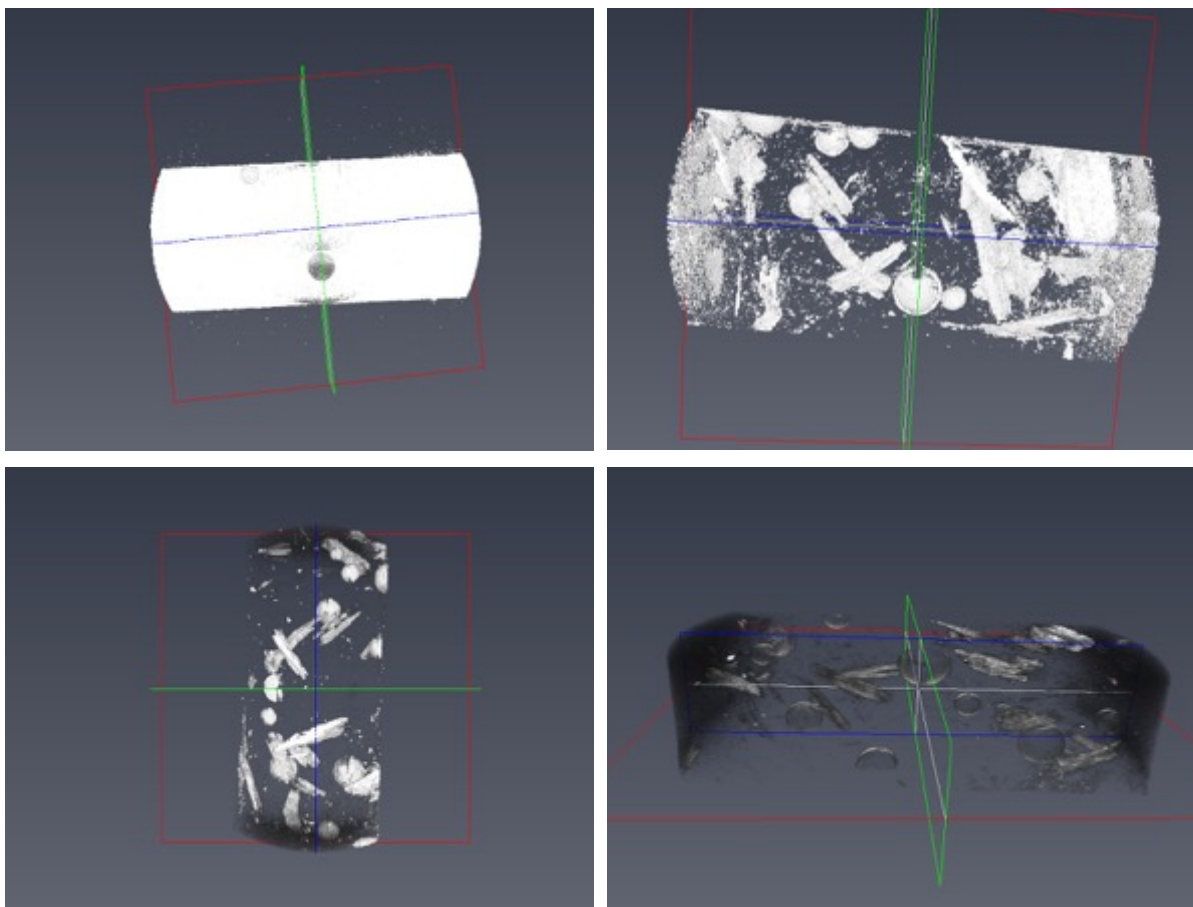


**Fig. 6.4** Micro-Computed Tomography ( $\mu$ CT) results of the PLA thermoplastic composites manufactured. The images are demonstrating the distribution of the cactus natural fibre within the composite. It is evident that a good dispersion is achieved within the thermoplastic matrix via the manufacturing method utilized. The size of the specimens was optimized for in situ Micro-Computed Tomography ( $\mu$ CT) 3 point bending tests to be carried out.

3-point bending to failure of the cactus thermoplastic composite specimens compared to control specimens in situ revealed that some mechanical reinforcement is achieved even at very low weight percentages of 3.3% w/w (Fig. 6.5). These specimens were tested at a small scale however the mechanical property increase observed is interesting in terms of the filler potential of the cactus fibres.

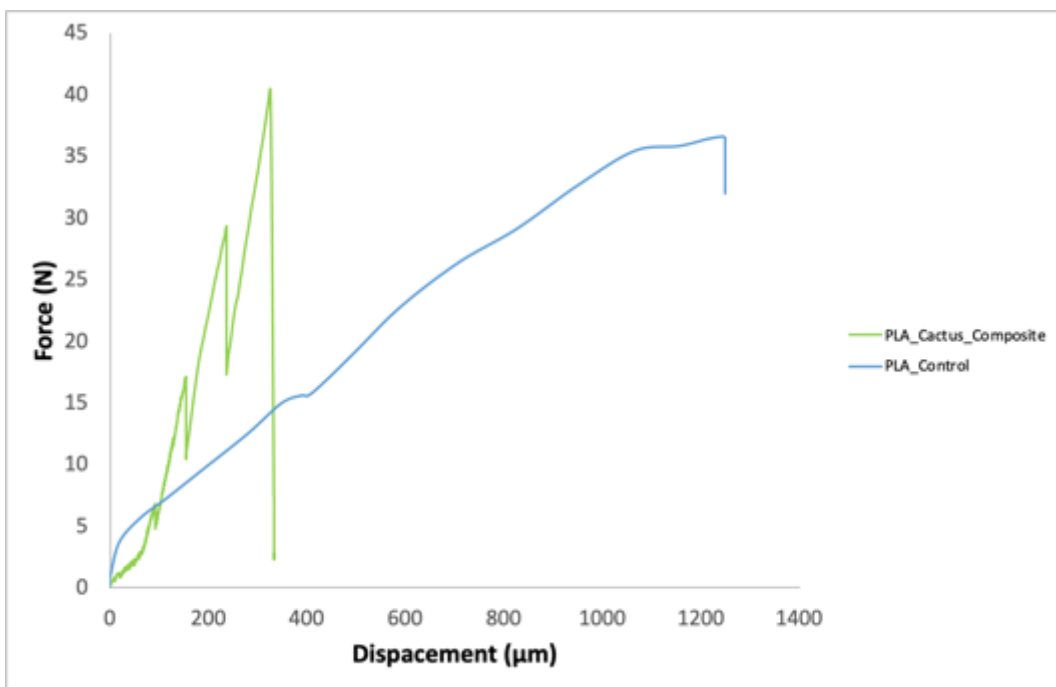


**Fig. 6.5** In situ 3 point bending tests of PLA and PLA cactus composites. It is observed that mechanical reinforcement is achieved in flexural loading at a significantly low weight percent of cactus fibre filler at 3% w/w. The mechanical reinforcement is attributed to the presence of the cactus filler increasing the material strength both in compression and tensile loading.

In terms of assessing the cactus fibre potential as a natural filler and where it stands in comparison to other natural fibres under DMA testing, it is evident in Fig. 6.6 that the cactus fibres provide some mechanical reinforcement comparable to most natural fibres used with the exception of hemp, which clearly shows a rather significant increase in comparison to other natural fibres.

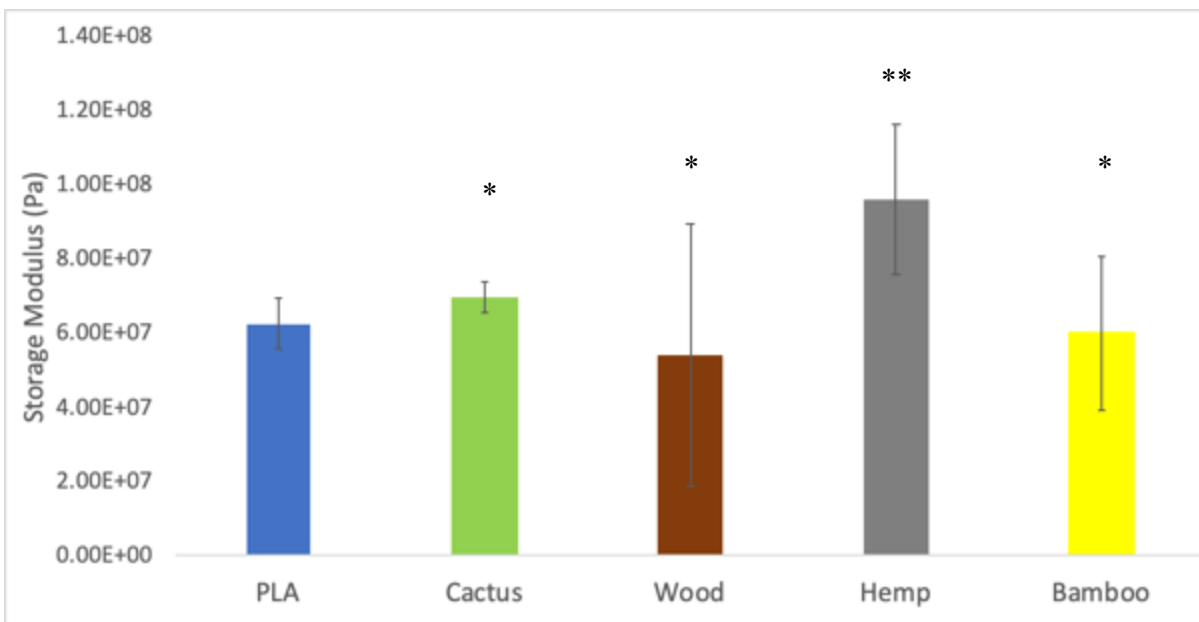


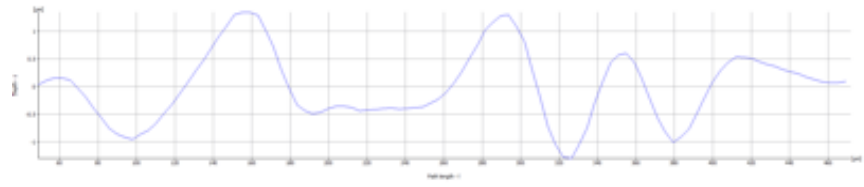
**Fig. 6.6** Storage Modulus Dynamic Mechanical Analysis (DMA) results of PLA and PLA natural fibre composites in 3 point bending. The structural reinforcement is evident across all the natural fillers used with cactus and hemp fibres providing the more significant storage modulus increase. Natural fibre fillers have been previously utilized for mechanical reinforcement of thermoplastic matrices and the increase in storage modulus is to be expected. (\* shows significant difference), (ANOVA,  $p<0.05, n=5$ )

These results demonstrate that the cactus fibre is able to compete with the industry standard natural fibres such as flax, hemp and bamboo as a composite reinforcement something that was expected<sup>9,10</sup>. Moreover, it was again observed that the cactus and hemp fibres provide the most significant matrix reinforcement. Thus, it was decided to carry out further investigation with specific focus on these two types of natural fibre with the aim to explain this phenomenon further as well as to assess their potential as materials for biomedical applications.

#### **6.2.4 Alicona Surface Measurements**

In order to get a deeper understanding of how the cactus and hemp fibres interact with a matrix material, preliminary surface measurements were carried out Fig. 6.7 and table 6.2

A



B

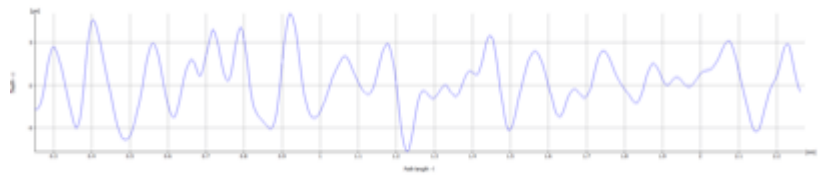


**Fig. 6.7** (a)Cactus and (b) Hemp Alicona surface measurements results demonstrating the differences in roughness demonstrated by these two types of natural fibres. Significant differences in the surface roughness are observed which could allow for the explanation of the different mechanical properties observed. The roughness is quantified as the difference between the peaks and the valleys in the graphs shown. It is shown that the hemp fibres have a significantly smaller difference between its peaks and valleys as compared to the cactus fibre, this significantly smaller roughness which could allow for better impregnation within a composite matrix yielding better mechanical properties.

**Table 6.2** Roughness Profile of Cactus and Hemp determined by Alicona surface measurements. The quantitative information obtained from the roughness profile demonstrated in the figure above. As anticipated, the roughness of the cactus fibres is significantly higher than of the hemp fibres.

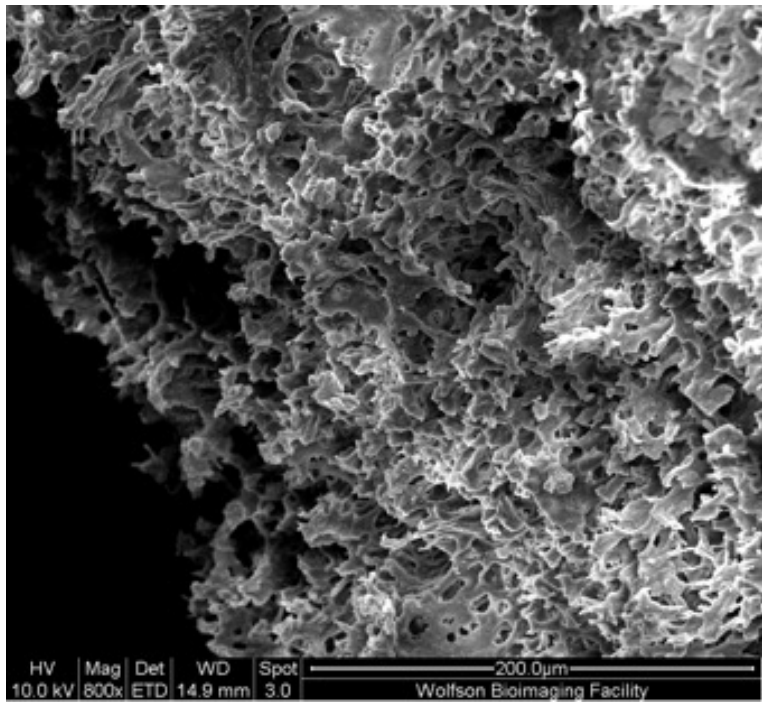
	Roughness Profile (um)
Cactus	520.8
Hemp	2.7

Those measurements were carried out using an Alicona microscope based on the focus variation approach of a vertical object as explained in detail in the methodology section 2.16. Those revealed there are significant differences in terms of the surface topology and surface roughness between the different natural fibres, specifically cactus and hemp fibres. This could lead to a different adhesion between the fibres and the matrix leading to the significant differences observed in the mechanical behaviour of the composite systems. **Potential future measurements could be carried out across all the natural fibres to determine if there is a trend between the surface properties observed and the adhesion composite properties in composite manufacturing.**

#### **6.2.5 Bioinks Morphological Characterization**

Once the mechanical properties were characterized and initial surface information was obtained, it was important to determine the internal structure of the composite hydrogels generated through SEM images. It is evident as seen in Fig. 6.8 that micro-porosity is prevalent throughout the natural fibre hydrogel composite which is a key factor enabling cell viability in these 3D specimens<sup>206,207</sup>.

*Control Hydrogels*



*Cactus Hydrogels*

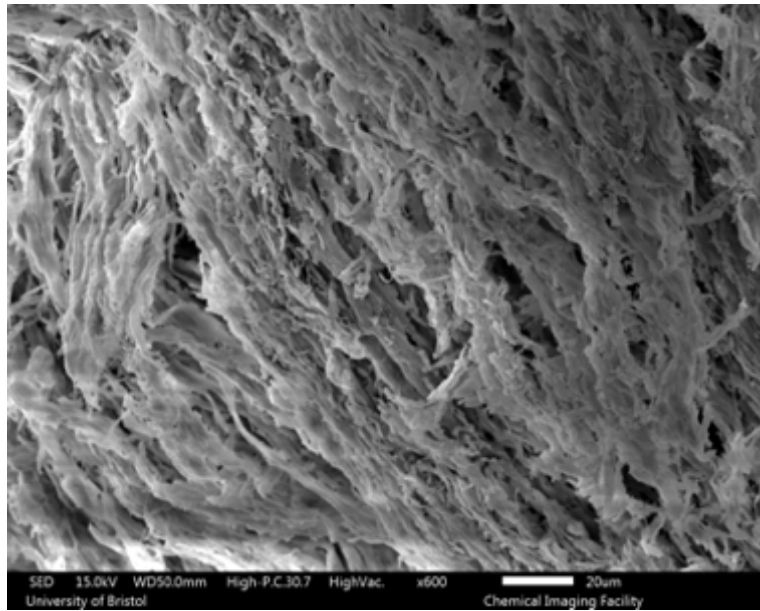
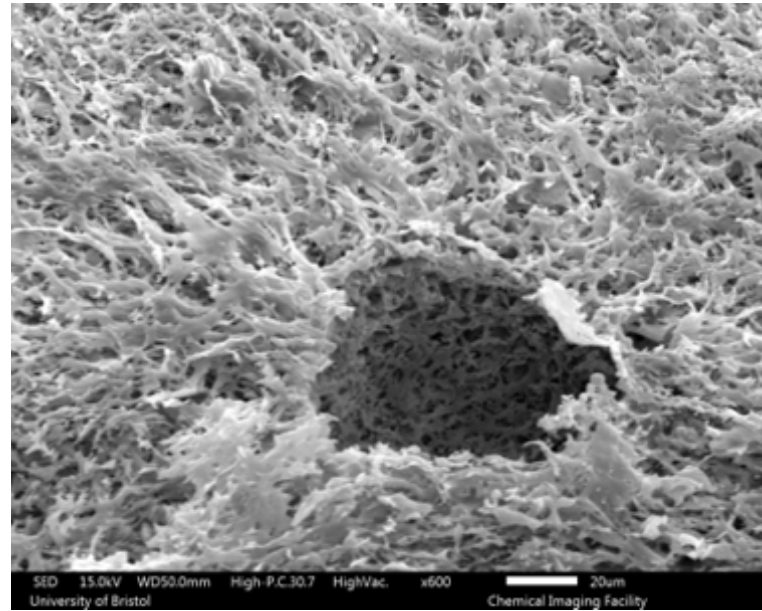
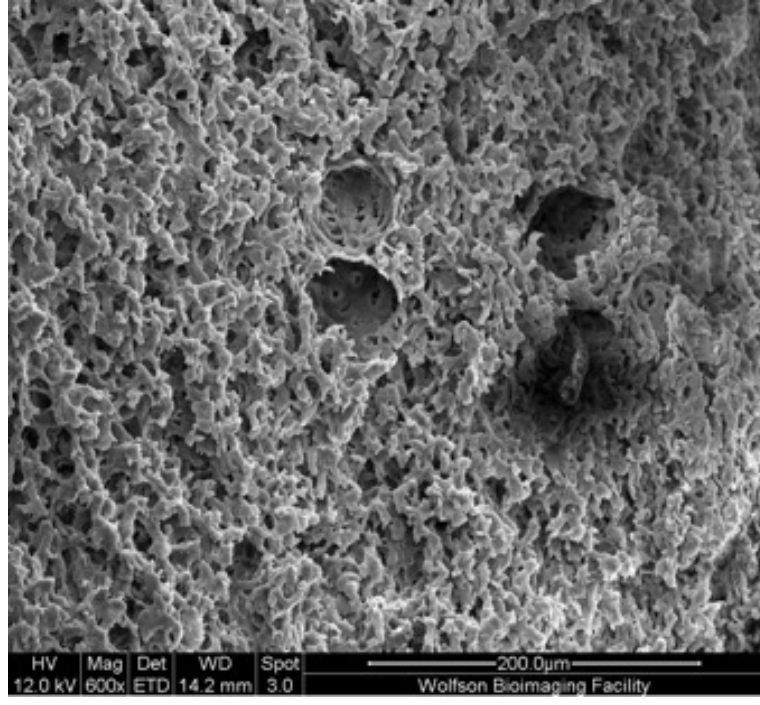


**Fig. 6.8** Comparison of Scanning Electron Microscopy (SEM) Micrographs between Control Hydrogels and Cactus Hydrogel composites. It is evident that in both cases significant micro-porosity is maintained throughout the hydrogel networks. Thus, the cactus fibre is embedded within the porous hydrogel matrix without significantly altering the morphology of the original system signifying that they are able to enhance the hydrogel mechanical properties without causing significant changes in its internal morphology.

Moreover, it is evident that the natural fibres are seamlessly integrated within the hydrogel matrix as it is evident if Figure 6.8 t is seen that on the surface of the hydrogel composite specimens the natural fibre is acting as a template for the gel to attach on the same direction

something that could be attributed on the shear alignment achieved *via* extrusion. It is also evident that the integration of the natural fibres leads to the loss of some of the porosity, as it can be seen in the cross sectional images that the fibres are blocking section of the inner structure of the gels, however, we hypothesized that the existing porosity should be adequate for cell viability. After the hydrogel composite specimens were fully characterized, our attention shifted to generating a biomedical application using this novel hybrid gel system. Since the main benefit observed in the system was the mechanical reinforcement of the original hydrogel, bone tissue engineering was pursued as an initial target for a biomedical application.

#### **6.2.6 Cell viability and Cytotoxicity**

The first step towards a successful bone tissue engineering scaffold is cell viability, i.e., it was paramount to ensure that the cactus fibres specifically do not induce any cell cytotoxicity. A preliminary study of seeding cells directly on the cactus fibres was carried out demonstrating that cell viability is not affected by the presence of the cactus fibres Fig. 6.9.

*Green-Live*

*Red-Cactus*

*Composite Image*

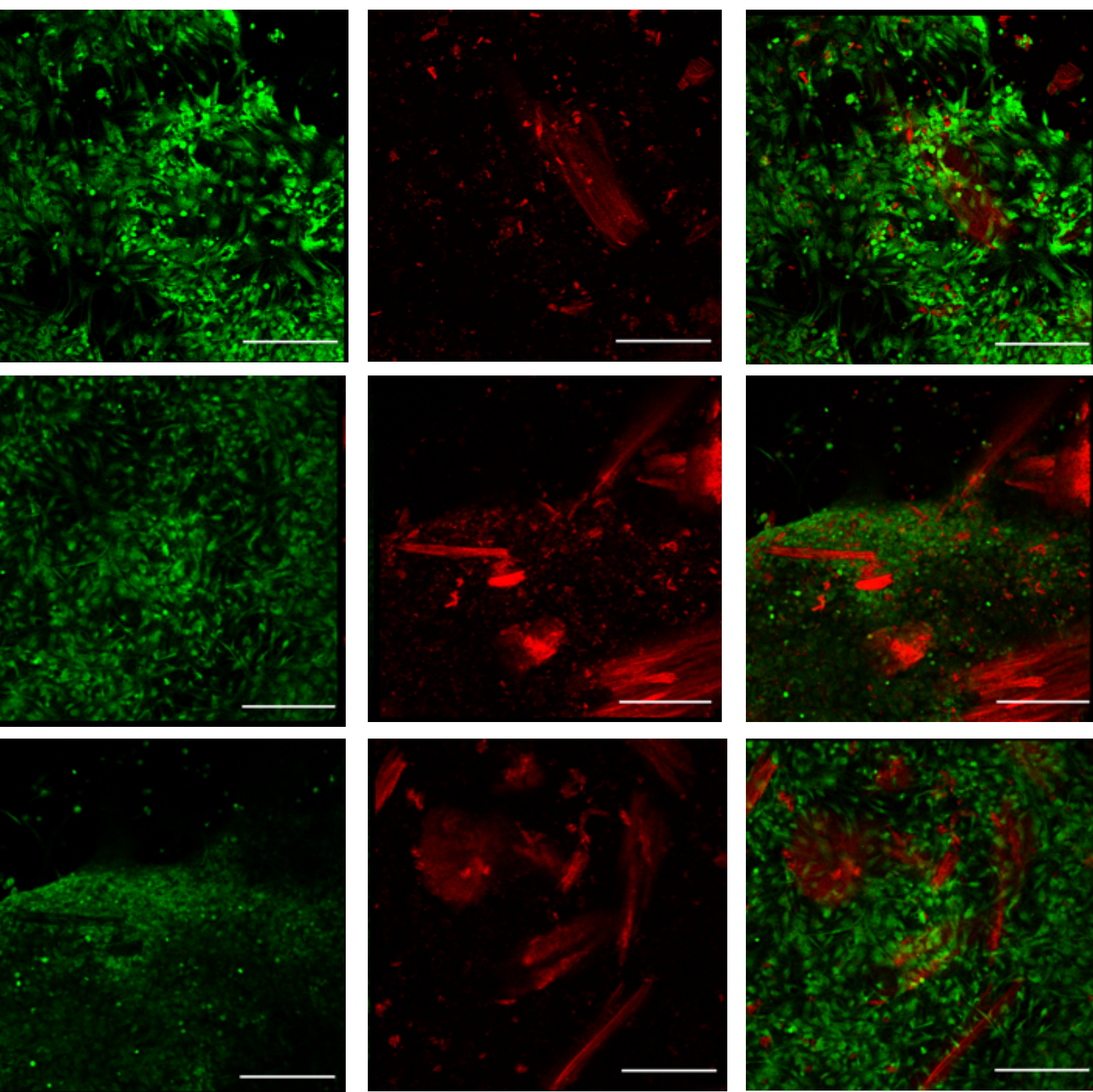
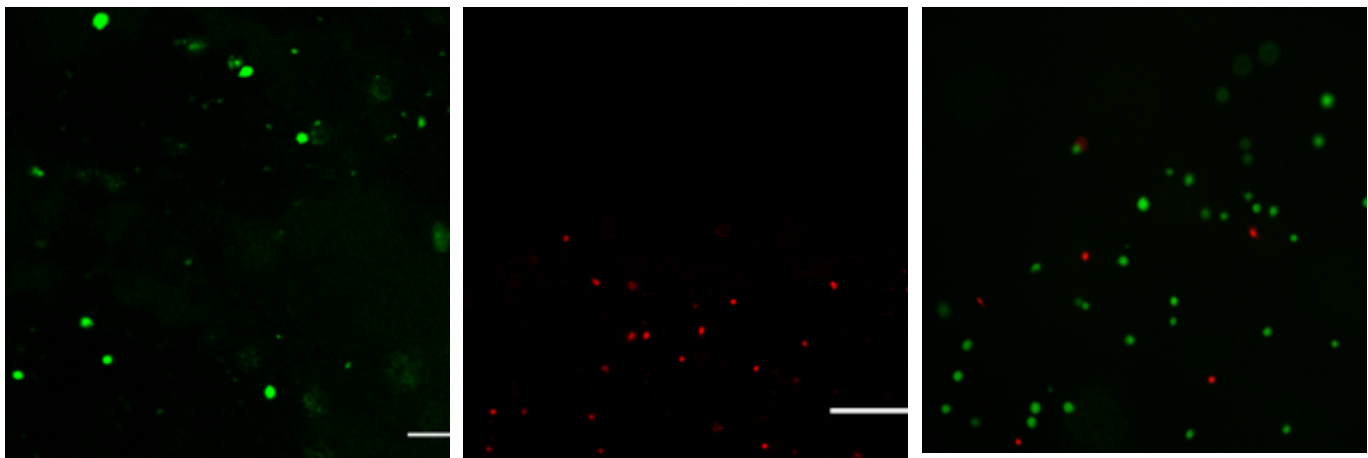


**Fig. 6.9** Confocal Images demonstrating the interaction of the cactus fibres with stem cells showing no effect on cell viability ( Day 7). Live-dead staining was achieved using calcein-AM (live cells, green stain) and propidium iodide (dead cells, red stain).It is evident that the cell viability and fibroblast morphology is unaffected by the presence of the cactus fibres. The direct interaction of the stem cells

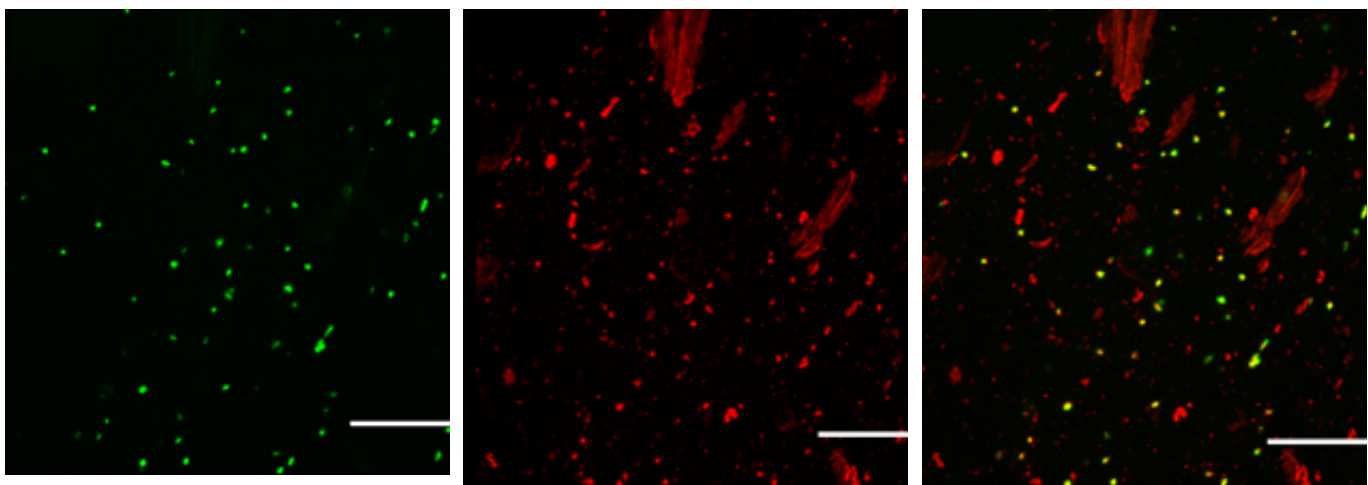
with the cactus fibre could provide added benefits for further tissue engineering applications. (Scale bar 150  $\mu\text{m}$ )

With regards to the hydrogel scaffold cytotoxicity, due to the fact that this a three-dimensional scaffold, a confocal microscopy imaging protocol as described in section 3.6.10 was used to assess the cell viability throughout the material. However, an issue arose as the natural fibres tend to emit autofluorescence in the same wavelength region as the dead cells as evidenced in Fig. 6.9 and Fig. 6.10. Thus, a true representation of the percent viability could not be determined *via* this method. However, we were able to conclude that for the same cell density implemented the amount of viable cells between the control hydrogel (without any natural fibres) and the amount of viable cells on all the hydrogel composite systems is not significantly different as evidenced in Fig. 6.10, thus the cell viability is adequate to pursue tissue engineering<sup>103</sup>.

(a) Control Hydrogel



(b) Cactus Hydrogel Composite



(c) Hemp Hydrogel Composite

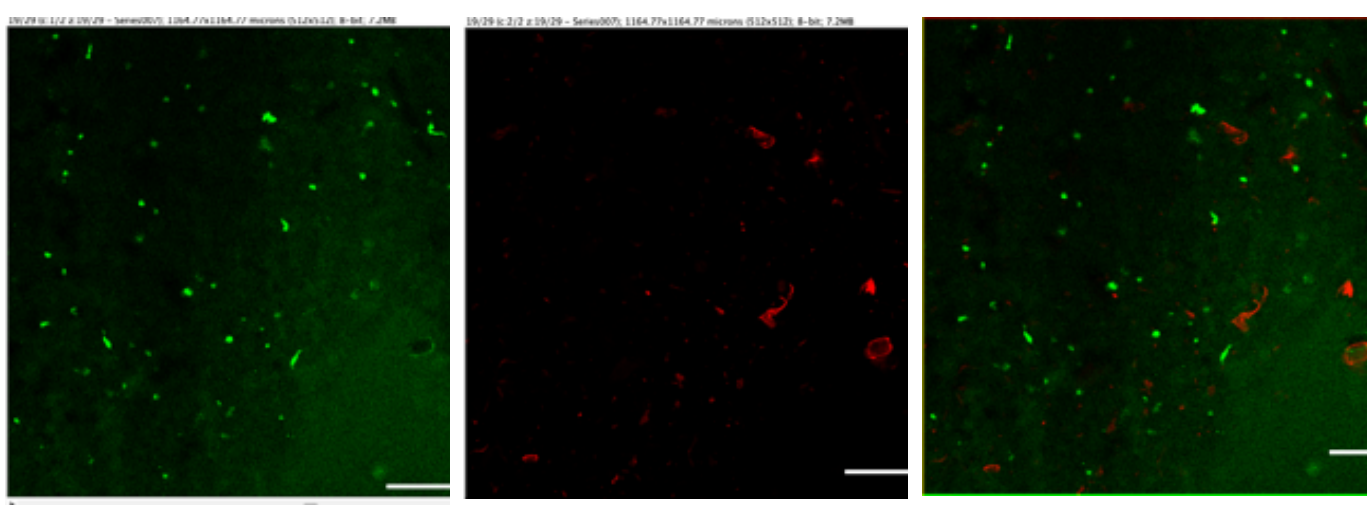


**Fig. 6.10** Confocal images assessing the cell viability at Day 7 on (a) Control Hydrogels, (b) Cactus Hydrogel Composites, (c) Hemp Hydrogel Composites extruded through a 21- gauge needle via a syringe. Live-dead staining was achieved using calcein-AM (live cells, green stain) and propidium iodide (dead cells, red stain).For the Cactus (b) and Hemp (c) hydrogels autofluorescence of the cactus and the hemp is observed in red wavelength region inhibiting the assessment of the dead cells. Overall at same cell density no significant difference is observed in the number of live cells between the control(a) and the composite systems(b), (c). (Scale bar 150  $\mu$ m)

### **6.2.7 Bone Tissue Engineering Evaluation**

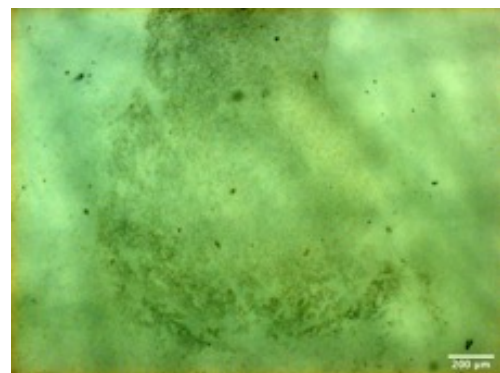
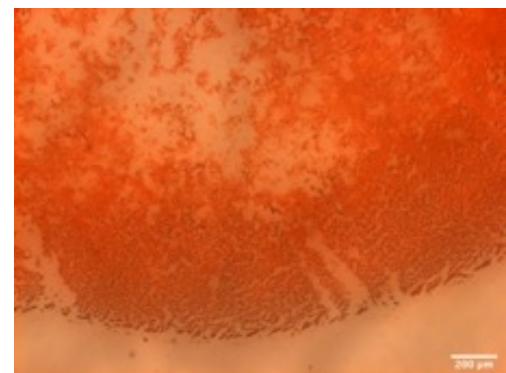
Once adequate cell viability was established, we focused on the two stiffest matrices - the cactus and hemp hydrogels. Here, the bone tissue engineering potential was compared to the control hydrogel that had been utilized previously<sup>103</sup>. After the 21 day differentiation cycle was completed, histological analysis was performed (Fig. 6.11) on all the differentiated specimens. Initially, it is evident that with regards to the hemp hydrogel composites, the differentiation was not successful, as none of the dyes utilized that are specific to the generation of bone Extracellular Matrix (ECM) are present in the sample. Those dyes include Alizarin Red (AR) an indicator of phosphate deposition, Safranin O (SO) an indicator of Glycosaminoglycan (GAG) deposition and Von Kossa (VK) an indicator of calcium deposition, as described in the methodology section 3.6.13. It is evident that both for the control and the cactus hydrogel cases the results demonstrate a clear generation and deposition of bone ECM. **It is important to note in this case that Safranin O will also stain alginate control hydrogels due to the presence of GAGs in alginate itself, thus the staining is to be expected.** However, the histological analysis is still beneficial as the presence of calcium and phosphate deposition combined with the mechanical stiffness increase observed are strong indicators of successful bone tissue differentiation.

Safranin O

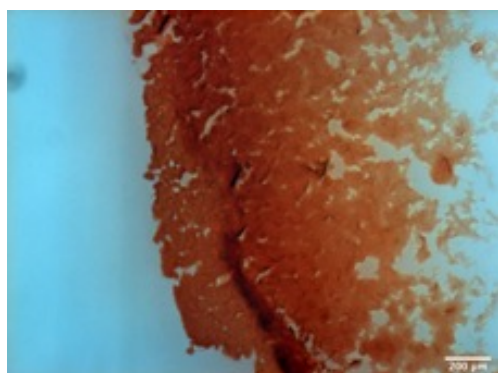
Alizarin Red

Von Kossa

(a) Control Hydrogel



(b) Cactus Hydrogel Composite



(c) Hemp Hydrogel Composite

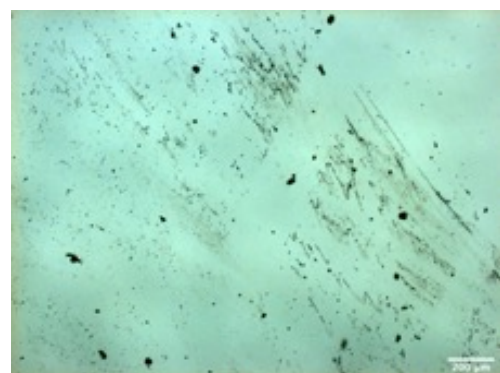
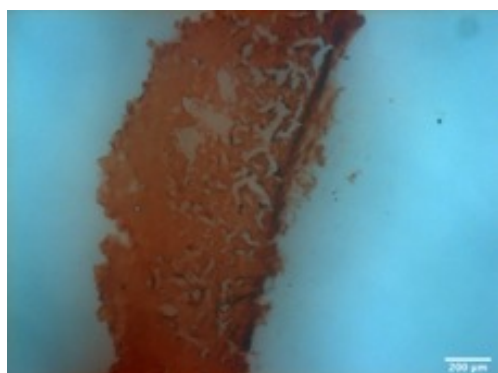
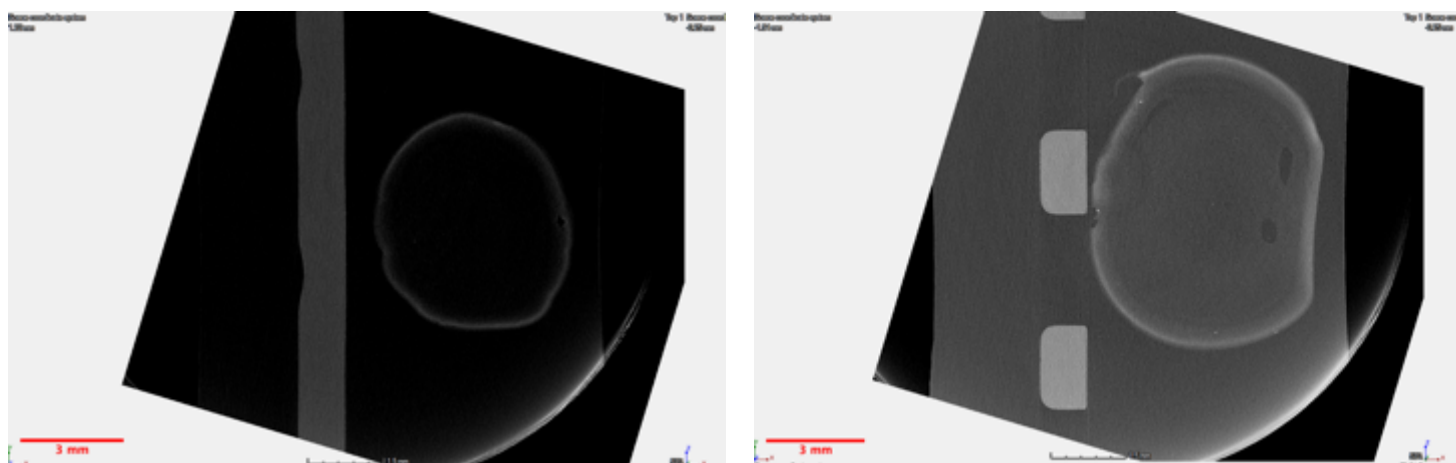


**Fig. 6.11** Histology results for Control (a), Cactus Hydrogel Composites (b) and Hemp Hydrogel composites (c) after 21 days of differentiation. Safranin O (SO) staining for the presence of glycosaminoglycans within the systems stained positive for the Control (a) and Cactus (b) systems but not for the Hemp (c) system, demonstrating some collagen deposition present. Inorganic calcium mineral deposits via Alizrin Red (AR) staining and phosphate and Von Kossa (VK) staining were primarily observed in the control (a) and Cactus (b) systems but not in the Hemp (c) system. It is concluded that bone tissue engineering differentiation was more successful in the control (a) and Cactus (b) systems yielding more widespread deposition of minerals within the matrix with the highest deposition of phosphate observed in the Cactus (b) system.

As the study was focussed on demonstrating an extrudable 3D hydrogel system, it was important to determine whether the differentiation is achieved through the scaffold or just in the surface of the hydrogel composite scaffold. Accordingly,  $\mu$ CT measurements were carried out on the differentiated tissue engineered hydrogel samples and were compared to undifferentiated control specimens (Fig. 6.12). It is evident that in the undifferentiated control specimen case there is no contrast difference observed between the wax, in which the samples are embedded, and the sample itself. On the contrary, in the cactus bone case there is a clearer contrast difference that is attributed to the calcium phosphate generation due to the bone differentiation and the bone ECM deposition. It is important to note that in the control gel where no cells or cactus fibres are present the gel was also subjected to the same differentiation media for 21 days before imaging and the differences between the two cases is easily discernible. Further imaging needs to be carried out to obtain  $\mu$ CT measurements of the cactus hydrogels without cells at day 21. This will allow for the evaluation of the morphological differences that occur when the cells are present within the cactus hydrogel. It is also important to compare measurements between the control hydrogel and the cactus hydrogel after 21 days of cell differentiation to determine what differences occur in the calcium deposition. However, those preliminary results of the cactus hydrogel specimens are quite encouraging demonstrating calcium deposition occurs in these novel natural fibre hydrogel systems, enhancing the potential for utilizing these systems in tissue engineering applications.

(a) Undifferentiated Hydrogel



(b) Differentiated Cactus Hydrogel

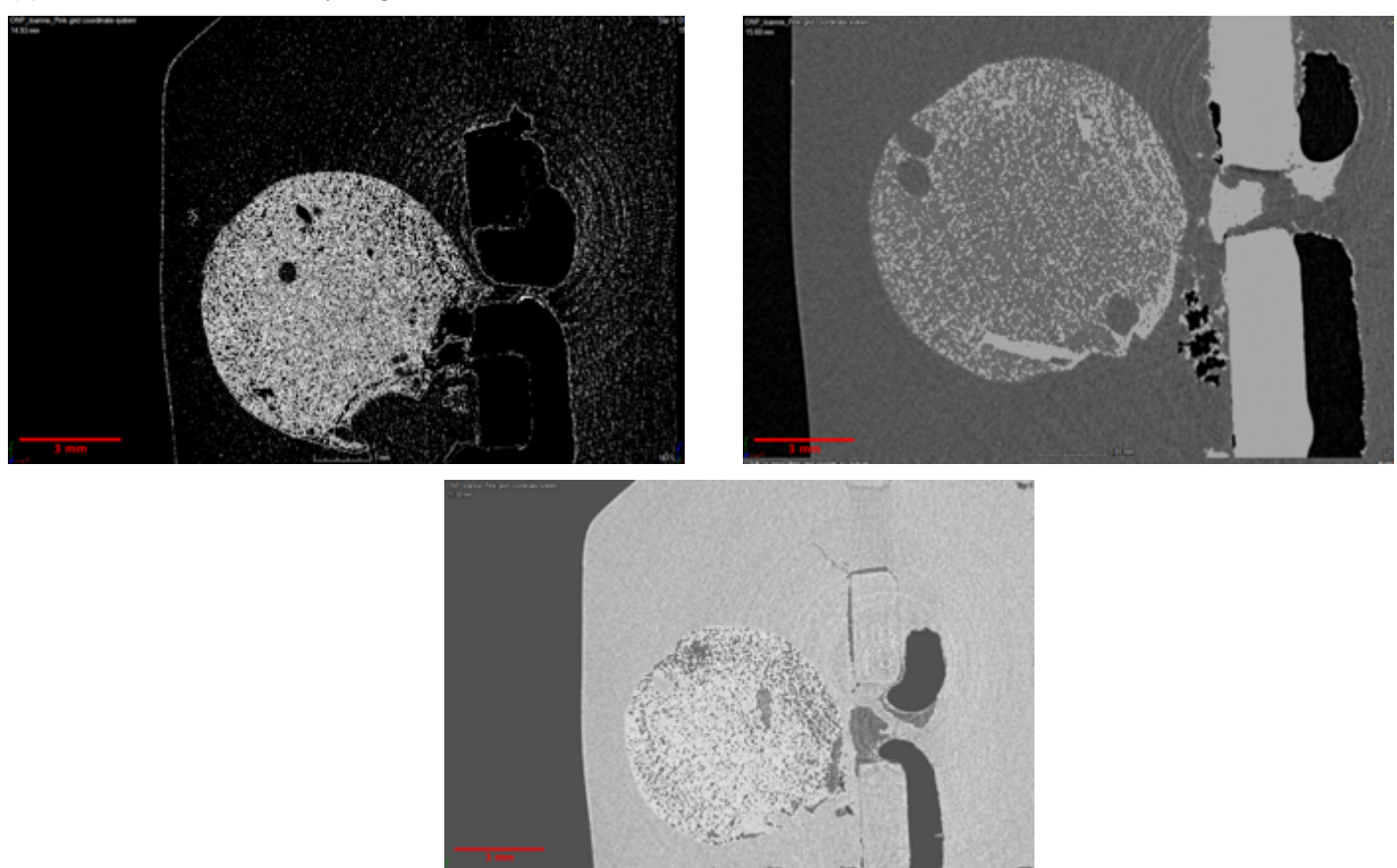


**Fig. 6.12** Micro-Compusted ( $\mu$ CT) results for Non-cell containing Hydrogel (a) and Cell containing Cactus hydrogel after 21 days of differentiation (b). The enhanced contrast observed in the bone tissue engineered samples (b) is attributed to the calcium phosphate deposition throughout the cactus composite hydrogel system. As this is a 3D culture system it is important to observe differentiation achieved throughout the specimen and not just in the surface thus the presence of enhanced contrast in the tissue engineered specimens reveals calcium phosphate deposition occulting across the structure. The black spots observed within the cactus differentiated system (b) are attributed to the presence of the cactus fibres.

Mechanical testing on the differentiated hydrogel systems was carried out and as it is evident in Fig. 6.13 and Fig. 6.14 that a significant increase in the mechanical stiffness was observed for both the control ( from 25 KPa to 76 KPa) and the cactus specimens ( from 77 KPa to 120 KPa) , while the increase in the hemp specimens (from 142 KPa down to 122 KPa) was insignificant. Increase in the mechanical stiffness of bone tissue engineered hydrogel specimen is a factor previously reported<sup>105</sup> to demonstrate successful bone ECM formation leading to improved mechanical properties. Moreover, our results showed that the cactus fibre reinforced hydrogels can provide significant benefits in terms of bone tissue engineering, yielding a significantly stiffer matrix that is attributed to the bone ECM being laid out efficiently throughout the 3D scaffold. The fact that the hemp specimens do not yield significant increase in the mechanical stiffness after differentiation can be attributed to the fact that the initial stiffness of the specimen was too high. It has been shown that 3D specimen stiffness has to be at an optimal range of between 60 KPa and 100 KPa to achieve efficient bone differentiation<sup>208</sup>, and the stiffness of the hemp hydrogel systems falls outside that range. **However, it is important to note that with an optimization of the hemp hydrogel composite formulation it is entirely possible to develop a system that falls within the required range for successful bone tissue engineering.** The significant mechanical stiffness increase after a bone differentiation protocol is implemented is strong evidence of the successful differentiation achieved within the hydrogel specimens, which demonstrates the novelty of this work as to the author's knowledges this is the first extrudable natural fibre hydrogel system able to achieve successful bone differentiation.

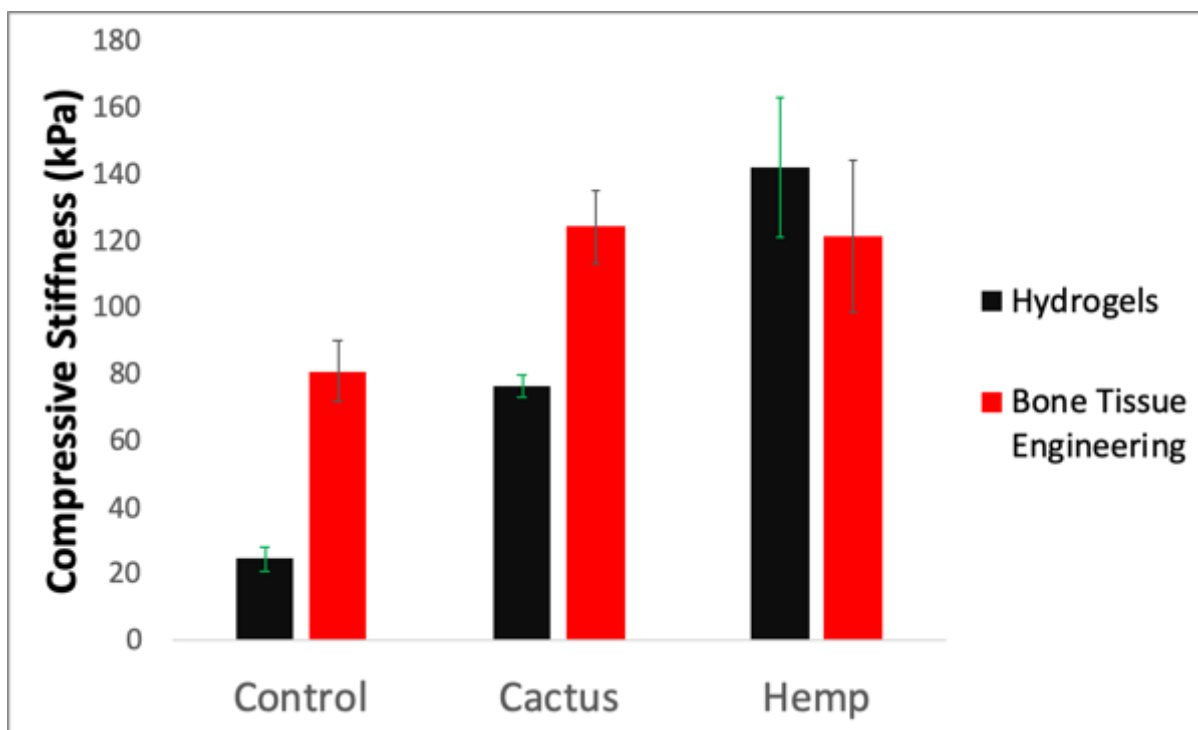


**Fig. 6.13** Compressive modulus comparison between control hydrogels and different hydrogel composites differentiated and undifferentiated. After 21 days of differentiation it is observed that in both the controls and the cactus hydrogel system a significant increase in the compressive modulus is achieved that is not present in the hemp system. Again, it can be concluded that no significant hydrogel degradation is observed within the systems as the modulus does not deteriorate in culture. The increase is attributed to efficient calcium phosphate deposition occurring via the osteogenic differentiation pathways and in the cases of the control and the cactus systems. In the case of the hemp system a small decrease in the modulus is observed which is attributed to the fact that osteogenic differentiation is not occurring homogeneously, and stem cells are not able to lay down calcium phosphate minerals.

The mechanical stiffness increase combined with the histological and  $\mu$ CT results provide significant evidence that the bone tissue differentiation was successful and that cactus natural fibres can be a novel hydrogel filler for biomedical applications. It is concluded that the bone differentiation is occurring through the entirety of the matrix and not just in localized areas. The complete analysis of the hydrogel composites revealed that natural fibres have the potential to provide significant benefits as a cheap easily accessible filler to mechanically modify hydrogel matrix systems in an effort to achieve optimal stiffnesses for tissue engineering applications. Specifically, cactus fibres are a novel natural fibre filler that could yield further applications in tissue differentiation.

### **6.2.8 Osteogenic Potential of Composite Bioinks**

In an effort to further assess the application potential of these natural fibres preliminary differentiation potential data was obtained via an Alkaline phosphatase assay that was carried out without the presence of osteogenic growth factors to determine the potential of osteogenesis as described in method 3.6.12. ALP is an indicator of early onset bone differentiation<sup>209,210</sup> and thus ALP results could provide indication as to whether the cactus fibres themselves and the cactus fibre hydrogel systems lead to osteogenic behaviour. **The cactus fibres were sterilized via UV irradiation for 1 hour similarly to the way they are sterilized before they are implemented in the hydrogel system.**

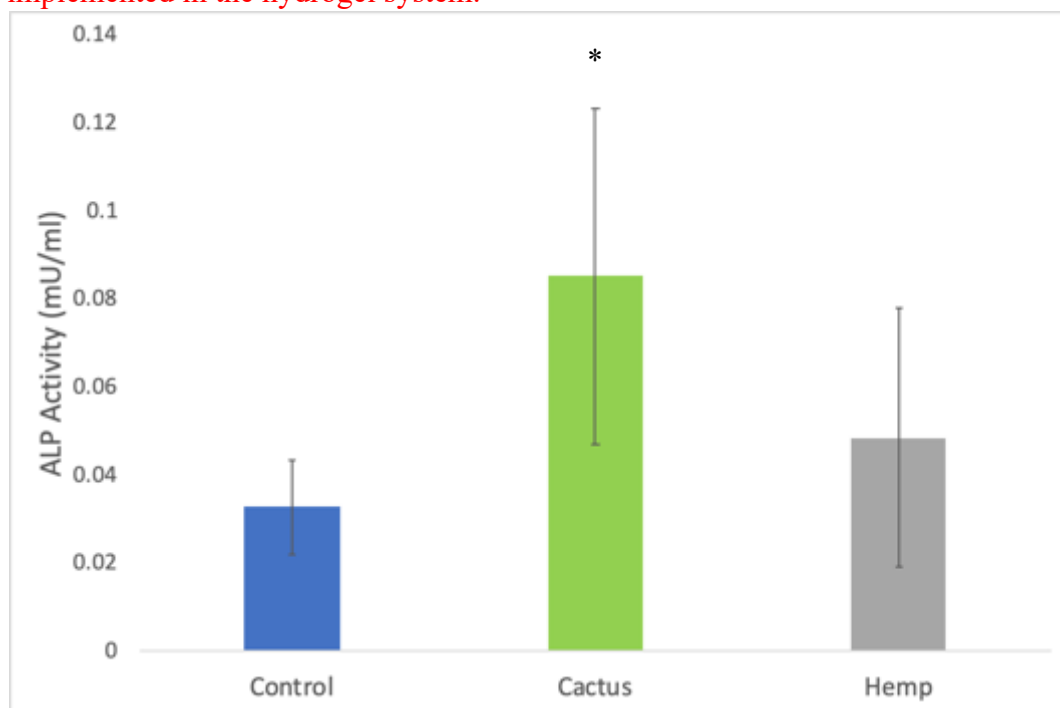


**Fig. 6.14** Alkaline Phosphatase (ALP) assay results comparison between tissue culture plastic (control) cactus fibres and hemp fibres. It is important to note that the ALP assay was carried out without the presence of any osteogenic growth factors in all cases. It is observed that the cactus fibres increase the production of Alkaline Phosphatase (ALP) activity significantly. This could signify that the properties of the cactus fibres elucidate a higher osteogenic response as compared to their hemp counterparts and tissue plastic. This could be attributed to their surface roughness present in the cactus fibres among other factors and further investigation would be required to investigate this result. (\* denotes significant difference), (ANOVA, p<0.05, n=9).

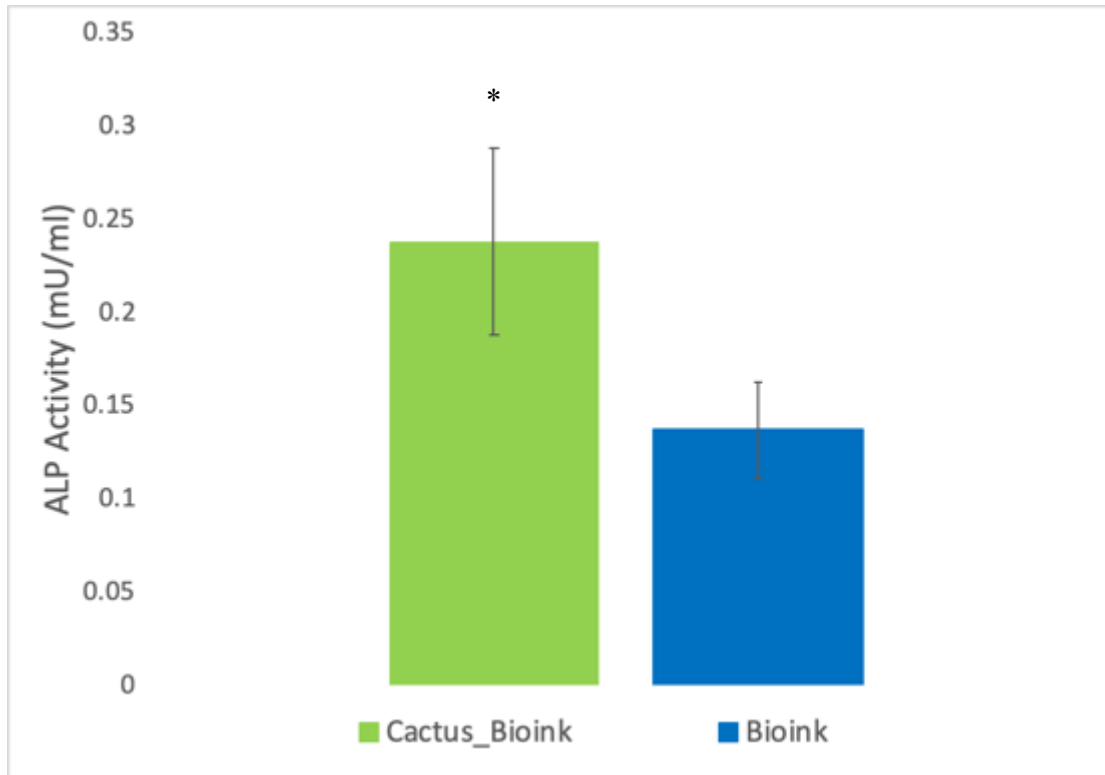


**Fig. 6.15** Alkaline Phosphatase (ALP) assay results comparison between the hydrogel and the cactus composite hydrogel. It is important to note that the Alkaline Phosphatase (ALP) assay was carried out without the presence of any osteogenic growth factors in both cases. The cactus bioink demonstrates increased Alkaline Phosphatase (ALP) activity which could be attributed to the enhanced mechanical properties achieved in the cactus composite system. The increased stiffness achieved with the introduction of the cactus fibre fillers potentially provides mechanical signals in the stem cells enabling them to recognize their stiffer surrounding and follow an osteogenic lineage without the presence of growth factors, which is property that is not observed in the control system. (\* denotes significant difference), (t-test,  $p<0.05$ ,  $n=9$ ).

As evident in Fig. 6.14 the ALP activity is significantly increased on the cactus fibre system when compared to the control (tissue culture plastic) as well as hemp fibres. This result is quite astonishing and implies that the cactus fibres have unique osteogenic activity. In terms of the hydrogel systems, it is evident in Fig. 6.15 that the cactus hydrogel system has significantly increased ALP activity, when compared to the control hydrogel, which could be attributed to the mechanical stiffness of the composite gel as it has been demonstrated in other systems<sup>208</sup> as the assay was carried out without the presence of osteogenic growth factors.

### ***6.3 Conclusions***

Natural fibres have been emerging over the last decade as an exciting material reinforcement for modern composite manufacturing as they are cost effective, lightweight, biodegradable and easily accessible. Previous work on the cactus fibres demonstrated that cactus fibre sheaths have interesting and unusual potential as reinforcement for a composite matrix. In an effort to expand the work a focus was maintained on the potential of these cactus fibres as a composite reinforcement in various formats similarly to the way other commonly used industrial natural fibres are used. Thus, the cactus fibres were initially transformed into a fibre powder, were characterized and then were implemented as a matrix filler reinforcement at small mass fractions to determine the mechanical benefits. It was observed that when the cactus fibres are implemented as a thermoplastic matrix filler, they yield significant mechanical reinforcement. The mechanical advantages obtained are comparable to most natural fibres at the same weight percentage, demonstrating that cacti fibres could have a place in the bio-composite industry. In terms of expanding the potential applications of the natural fibres, the same powders were implemented as a hydrogel matrix reinforcement to assess the mechanical and biomedical benefits demonstrated. It was shown that the implementation of various natural fibres as a hydrogel filler reinforcement yielded novel composite hydrogel systems with significantly different mechanical properties, with cactus and hemp fibres generating the stiffest systems in terms of mechanical properties. Moreover, the natural fibre developed systems all demonstrated good cell viability and extrudability, expanding their application potential as novel hydrogel reinforcements. The good cell viability is primarily inferred due to the successful bone tissue engineering experiments since the cell viability protocols need to be further optimized to account for the natural fibres autofluorescence. Further biomedical evaluation of the cactus and hemp systems revealed that there is significant potential in utilizing natural fibres in the biomedical sector for tissue engineering applications. Specifically, cactus fibre yielded hydrogel composite systems that are biocompatible, while also generating a significantly stiffer neonatal bone matrix and demonstrating some initial traits of osteoinductive behaviour. Overall, we presented a novel natural fibre composite hydrogel system that could provide significant benefits in terms of biomedical applications. Specifically, cactus fibres demonstrate unique potential as a hydrogel filler reinforcement for biomedical applications as well as a novel natural fibre for thermoplastic composite reinforcement.

## 7 Conclusions

---

The overall scope of the thesis is to investigate the natural fibres obtained from the cactus species of *Opuntia Ficus Indica* and their potential in material science as a platform used for bioinspiration as well as a natural fibre reinforcement. To this aim, an extensive morphological characterization of the cactus fibres, a mechanical assessment of bioinspired materials and an evaluation of cactus fibre biocomposites materials was carried out.

Initially in Chapter 4 an extensive morphological evaluation of the cactus fibres was presented. The cactus fibres were imaged with a variety of imaging modalities to get an appreciation of their structure across scales and to understand how their mechanical behaviour can be correlated with this structure. A fractal geometry approach was deemed the best way to characterize the structure and thus a fractal dimension methodology approach was developed and utilized. The fractal analysis revealed that there is structural hierarchy and self-similarity present in the cactus fibre structure at a finite amount of scales. It was demonstrated that the cactus structure can be reduced to a single structural subunit that has the same fractal dimension as the whole structure and that fractal dimension is maintained across imaging modalities as well as after digital self-replication. However, it was observed that at the smaller scales such as the micro and nano scales the fractality of the structure is not maintained and a different structural motif is present. Further analysis and comparison of the cactus fibre fractal dimension with other commonly used natural fibres revealed that there are morphological similarities present in the fractality of natural fibres at smaller scales. It was also observed that the single cactus structural subunit's mechanical behaviour is equivalent to that of the whole structure maintaining the high 7:1 bending to axial stiffness ratio providing additional proof that the fractal geometry present is directly correlated with the mechanical properties observed.

The wealth of imaging and morphological information obtained from the fractal characterization of the cactus fibres enabled the generation of artificial 3D printed cactus analogue specimens in Chapter 5. The first aim of the development of these 3D printed cactus analogues was to provide additional information of how the fractal morphology is responsible for the interesting high bending to axial stiffness ratio observed. The 3D printed cactus analogue specimens were characterized in terms of tensile and bending modulus and it was revealed that the high ratio is maintained in those artificially manufactured specimens,

demonstrating that the fractality of the structure is directly responsible for its mechanical properties. The second aim of the development of these artificial cactus bioinspired materials was to evaluate their potential as compared to their equivalent beams as well as in dynamic loading environments. It was shown that the cellular materials generated from the cactus bioinspiration can provide significant benefits in terms of specific flexural modulus as compared to their equivalent beam counterparts. The morphological information obtained from Chapter 4 also enabled the generation of finite element simulations of the artificial cactus structure in Chapter 5 enabling a better characterization and understanding of the mechanical behaviour of the cactus structure. Even though the simplified model used did not accurately match our experimental predictions in terms of the ratio observed, it still provided us with significant insight for the mechanical behaviour of the cactus structure. It highlighted the importance of the topology of the pores present in the structure, something attributed to its fractal nature, while also demonstrating that equivalent beams based on the cactus structure can generate materials with still a significantly high bending to axial stiffness ratio.

Last but not least, in Chapter 6 the cactus fibre as a biological material structural reinforcement was utilized for the generation of hydrogel and thermoplastic composites. It was demonstrated that the cactus fibres in a powder format can provide significant mechanical benefits both in a hydrogel and a thermoplastic matrix as compared to other commonly used fibres demonstrating the potential of these cactus biocomposites. In terms of the hydrogel composite systems a biomedical application route through bone tissue engineering was explored yielding interesting results for the use of cactus and other plant fibres as structural reinforcement for biomedical materials. It was demonstrated that the cactus fibre hydrogel bioinks developed demonstrated no traits of cytotoxicity, which is attributed to the successful tissue engineering experiments since the cell viability protocols need to be further optimized, while yielding efficient bone ECM formation. These platforms also demonstrated some initial traits of potential osteoinduction mainly attributed to the significant modulus increase achieved by the use of the cactus fibres as filler materials.

All in all, this thesis aimed to explore the potential of the biological fibres obtained from the cactus species of *Opuntia Ficus Indica* both as a bioinspiration platform as well as a composite reinforcement. The morphological evaluation carried out through a novel methodology developed demonstrated the presence of fractality at the macro scale of the structure which can be reduced to a single structural unit with similar mechanical behaviour. The morphological

information enabled the development of cactus bioinspired materials that maintain the interesting properties observed, reinforcing the fractality argument, while also introducing a novel material platform with materials that show a high bending to axial stiffness ratio irrespective of the manufacturing method utilized. Additionally, the cactus fibres as a biological material structural reinforcement demonstrated significant potential as a filler for biomedical applications such as bone tissue engineering scaffolds. Cactus based solids have demonstrated significant potential in various applications according to this thesis.

## **8 Future Work**

---

The preliminary work on cactus based solids originating from the extensive morphological study as well as the generation of cactus based materials has provided some interesting starting points for these materials to be further advanced into industrial applications. However, significant additional work needs to be carried out in order to evaluate the true potential of these materials and understand their properties and potential applications better. The additional work required to achieve this goal is discussed below.

### **8.1 Fractal Morphology Characterization**

The morphological information obtained from the cactus fibres and the development of the fractal characterization algorithm provided a unique insight in the properties of the cactus fibres. However, there is still significant work to be carried out to further advance this work and the use of this algorithm. With regards to the cactus morphology and the algorithm itself it would be interesting to explore further fractal order estimation methodologies apart from the box-counting method and determine if any differences are observed. Furthermore, in our methodology the images utilized are in two dimensions for the fractal characterization and it would be beneficial to develop an algorithmic approach that can be implemented in three-dimensional objects and assess the fractality in 3D to observe morphological features. However, this algorithmic fractal approach could also provide significant benefits and potential applications in the material industry as presented. Initially, it would be interesting to implement this fractal characterization approach on other materials and structures that demonstrate such interesting bending to axial stiffness ratios and determine whether the fractal order observed in the cactus is a universal number present in all structures that demonstrate this mechanical behaviour. This would provide an excellent tool for characterizing materials and correlating their mechanical properties directly with this number in order to be able to assess their application space. Moreover, this fractal characterization could be expanded for the characterization of the morphology of other biological materials. Potentially, a fractal map could be developed where biological materials are characterized by a fractal order value that could reveal their mechanical properties and that fractal value could be utilized as a guide to generate synthetic materials replicating the morphology observed in nature to generate novel materials with interesting properties.

## **8.2 Artificial Cactus Inspired Reinforcement Materials**

Initial work on the development of cactus bioinspired analogues generated some quite intriguing results, however, there is a lot of further work to be carried out to expand the reach and the potential of these materials. To begin with, the rendered models obtained for the generation of these analogues were isolated from a single part of the cactus structure. It would be useful to repeat the whole design and manufacturing process from a different section of the cactus structure to verify that the mechanical properties are maintained irrespectively of the cactus part used which could also further verify our fractal hypothesis. The initial approach of using two different 3D printing modalities yielded very good results in terms of robustness and reproducibility of the bioinspired structures but it is still important to test the feasibility of printing these structures with various others 3D printing modalities to expand further their application potential. Moreover, a systematic study is required to determine the optimal printing parameters of these materials as so far only a few have been investigated. It is important to determine the infill effect on the mechanical properties as well as what is the optimal way of generating these structures to obtain materials with the best mechanical properties possible. It is also important to investigate other manufacturing routes of these structures apart from 3D printing, perhaps through casting of the structure, and see if the properties are maintained as well as enabling a mass production of these materials at a larger scale. Another idea that would expand the scope of this work significantly would be to implement these novel cactus-based structures as composite reinforcements in various composite matrices. The ability to generate a cactus structure with the mechanical properties maintained across any material used could lead to the development of various composite materials with good interfacial adhesion yielding perhaps quite interesting materials. Another important experimental consideration is to generate even bigger structures than the ones presented and see if the mechanical properties are maintained even at a larger industrial size expanding the application potential of these cactus-based solids. In terms of characterizing and testing these novel cactus-based analogues it is important to further investigate the energy dissipation and impact dissipation potential. The initial work does show some encouraging results however it is important to perform cyclic testing over multiple cycles on these manufactured specimens to determine their application potential as a vibration damping platform. Additionally, it would be interesting to perform 3 point bending tests *in situ* with  $\mu$ CT to determine how the load is distributed across the structure to get a better understanding of the mechanical properties observed. Last but not least, significant additional work is required

on the finite element simulation and the modelling of the structure. It is important to find ways to incorporate the topology of the porosity of the structure more efficiently in the finite element beam in order to generate a model that can accurately model the experimental mechanical behaviour observed.

### **8.3 Cactus Based Thermoplastic and Hydrogel composites**

The encouraging results obtained from this initial preliminary work on the biocomposites with cactus fibres provide significant inspiration of further work to be carried out. Initially, with regards to the thermoplastic composite reinforcement it is important to further investigate a wider range of mass percentages of natural fibres filler implemented. The initial results obtained at a low weight percentage are encouraging however to get a full understanding of the utilization of the cactus fibres as a natural fibre filler a wider range needs to be investigated while also additional mechanical tests need to be carried out. It is important that the fibre filler range is increased and the ranges of 5%, 10%, 15% and 20% w/w are investigated while besides 3 point bending it is important to assess the mechanical properties of these composites in tensile tests as well as dynamic loading tests. The dynamical analysis presented gives an indication on the storage modulus difference observed however it is important to further assess the mechanical properties of the cactus fibre composites in terms of energy dissipation and impact mechanics as well as for the evaluation of the tensile and compressive properties of these materials. In terms of the novel biomedical materials developed with the utilization of natural plant fibres, the initial data demonstrating the successful *in vitro* bone tissue engineering are extremely encouraging however significant further investigation needs to be carried out. Initially, similarly to the thermoplastic composite case, it is vital that a wider ranges of natural fibre fillers is investigated in a systematic fashion to determine a correlation between the amount of fibre and the increase in mechanical properties as well as the effect of the filler content in the biomedical potential of these materials. It is also important to carry out further adhesion assays on the natural plant fibres to further understand how the hMSCs behave at the presence of the natural fibres if they are able to adhere and how their behaviour changes. Moreover, in terms of cytotoxicity it is important to find a way to quantify the exact cell viability in the hydrogel composite systems developed without the autofluorescence of the natural fibres hindering the process. One way to achieve that would be through the utilization of a DAPI stain that stains the nucleus of all cells and then through the use of Calcein-AM stain determine the number of live cells and thus get a quantifiable quantity of cell viability on the

composite systems. With regards to the bone tissue engineering aspect the *in vitro* work presented is very encouraging as there are a lot of elements demonstrating that bone tissue engineering is achieved in these systems. It is important however to move to an *in vivo* model for such tissue engineering applications to get a true understanding of how these materials would behave in a living system like a mouse model. As far as osteoinduction is concerned the preliminary data from the ALP assay are encouraging combined with the fact that the increase in the stiffness of the specimens should have a beneficial effect in the hMSCs producing bone ECM without the presence of growth factors. It is of paramount importance that these initial findings are followed by quantitative Polymerase Chain Reaction (qPCR) experiments. Those experiments enable the quantification of the expression of a specific DNA molecule evaluating whether specific genes are expressed leading to molecules being produced related to the tissue being engineered, in the case of bone molecules that are usually upregulated include Bone morphogenic protein-2 (BMP-2), Alkaline Phosphatase (ALP) and osteopontin<sup>217-219</sup>. This would enable to get a clear understanding of the gene expression that takes place in those systems without the presence of growth factors and assess if the gene expression corresponds to bone ECM being produced, verifying that this system does indeed possess osteoinductive traits. Another property of these novel hydrogel systems that needs to be investigated is their biodegradability to determine their potential as tissue engineering materials. The degradability of alginate is known and has been studied<sup>103</sup> however the biodegradability of the cactus remains unknown and protocols need to be developed in order to assess the time of life of the cactus within a biological system. Overall, the preliminary work on the cactus fibre biocomposites presented in this chapter has yielded quite interesting results enabling a wider pursuit of significant additional experiments to fully understand the potential of these novel materials.

## 9 Bibliography

---

1. Feugang, J. M., Konarski, P., Zou, D., Zou, C. & Stintzing, F. C. Nutritional and medicinal use of Cactus pear (*Opuntia* spp.) cladodes and fruits. *Frontiers in Bioscience* 11, 2574-2589, doi:10.2741/1992 (2006).
2. Azucena Nazareno M, Phytochemicals of nutraceutical importance from cactus and their role in human health, in *Phytochemicals f Nutraceutical Importance*, Prakash D and Sharma G (Eds). Cabi, Wallingford (2014); Chapter 7.
3. Ciriminna, R., Chavarría-Hernández, N., Rodríguez-Hernández, A. I. & Pagliaro, M. Toward unfolding the bioeconomy of nopal (*Opuntia* spp.). *Biofuels, Bioproducts and Biorefining* 0, doi:10.1002/bbb.2018 (2019).
4. Angulo-Bejarano PI, Martínez-Cruz O and Paredes-López O, Phytochemical content, nutraceutical potential and biotechnological applications of an ancient Mexican Plant: Nopal (*Opuntia ficus-indica*). *Curr Nutr Food Sci* 10:19 6 – 217 (2014).
5. Trombetta, D. et al. Effect of polysaccharides from *Opuntia ficus-indica* (L.) cladodes on the healing of dermal wounds in the rat. *Phytomedicine* 13, 352-358, doi:<http://dx.doi.org/10.1016/j.phymed.2005.06.006> (2006).
6. McGarvie, D. & Parolis, H. The mucilage of *Opuntia ficus-indica*. *Carbohydrate Research* 69, 171-179, doi:[http://dx.doi.org/10.1016/S0008-6215\(00\)85762-6](http://dx.doi.org/10.1016/S0008-6215(00)85762-6) (1979).
7. Malainine, M. E., Mahrouz, M. & Dufresne, A. Thermoplastic nanocomposites based on cellulose microfibrils from *Opuntia ficus-indica* parenchyma cell. *Composites Science and Technology* 65, 1520-1526, doi:<http://dx.doi.org/10.1016/j.compscitech.2005.01.003> (2005).
8. Greco, A., Gennaro, R., Timo, A., Bonfantini, F. & Maffezzoli, A. A Comparative Study Between Bio-composites Obtained with *Opuntia ficus indica* Cladodes and Flax Fibers. *Journal of Polymers and the Environment* 21, 910-916, doi:10.1007/s10924-013-0595-x (2013).
9. Bouakba, M., Bezazi, A., Boba, K., Scarpa, F. & Bellamy, S. Cactus fibre/polyester biocomposites: Manufacturing, quasi-static mechanical and fatigue characterisation. *Composites Science and Technology* 74, 150-159, doi:<http://dx.doi.org/10.1016/j.compscitech.2012.10.009> (2013).

10. Scaffaro, R., Maio, A., Gulino, E. F. & Megna, B. Structure-property relationship of PLA-Opuntia Ficus Indica biocomposites. *Composites Part B: Engineering* **167**, 199-206, doi:<https://doi.org/10.1016/j.compositesb.2018.12.025> (2019).
11. Mandelbrot, B. B. *The fractal geometry of nature*. Vol. 173 (WH freeman New York, 1983).
12. Lopes, R. & Betrouni, N. Fractal and multifractal analysis: A review. *Medical Image Analysis* **13**, 634-649, doi:<http://dx.doi.org/10.1016/j.media.2009.05.003> (2009).
13. Harrison, A. Fractals in chemistry. (Oxford University Press New York, 1995).
14. Carpinteri, A. Special Issue on Microstructure and Strain Localization in Geomaterials Fractal nature of material microstructure and size effects on apparent mechanical properties. *Mechanics of Materials* **18**, 89-101, doi:[http://dx.doi.org/10.1016/0167-6636\(94\)00008-5](http://dx.doi.org/10.1016/0167-6636(94)00008-5) (1994).
15. Kruger, A. Implementation of a fast box-counting algorithm. *Computer Physics Communications* **98**, 224-234, doi:[https://doi.org/10.1016/0010-4655\(96\)00080-X](https://doi.org/10.1016/0010-4655(96)00080-X) (1996).
16. Tolle, C. R., McJunkin, T. R. & Gorsich, D. J. An efficient implementation of the gliding box lacunarity algorithm. *Physica D: Nonlinear Phenomena* **237**, 306-315, doi:<https://doi.org/10.1016/j.physd.2007.09.017> (2008).
17. A. Costa, Hausdorff (box-counting) fractal dimension  
(<http://uk.mathworks.com/matlabcentral/fileexchange/30329-hausdorff--box-counting--fractal-dimension>)
18. Bisoi, A. K. & Mishra, J. On calculation of fractal dimension of images. *Pattern Recognition Letters* **22**, 631-637, doi:<http://dx.doi.org/10.1016/>
19. Foroutan-pour, K., Dutilleul, P. & Smith, D. L. Advances in the implementation of the box-counting method of fractal dimension estimation. *Applied Mathematics and Computation* **105**, 195-210, doi:[https://doi.org/10.1016/S0096-3003\(98\)10096-6](https://doi.org/10.1016/S0096-3003(98)10096-6) (1999).
20. Posadas, A. N. D., Giménez, D., Quiroz, R. & Protz, R. Multifractal Characterization of Soil Pore Systems. *Soil Science Society of America Journal* **67**, doi:[10.2136/sssaj2003.1361](https://doi.org/10.2136/sssaj2003.1361) (2003).
21. Guarino, V., Guaccio, A., Netti, P. A. & Ambrosio, L. Image processing and fractal box counting: user-assisted method for multi-scale porous scaffold characterization. *Journal of Materials Science: Materials in Medicine* **21**, 3109-3118,

22. Fazzalari, N. L. & Parkinson, I. H. FRACTAL DIMENSION AND ARCHITECTURE OF TRABECULAR BONE. *The Journal of Pathology* **178**, 100-105, doi:10.1002/(SICI)1096-9896(199601)178:1<100::AID-PATH429>3.0.CO;2-K (1996).
23. Lakes, R. Materials with structural hierarchy. *Nature* **361**, 511-515, doi:10.1038/361511a0 (1993).
24. Murr, M. M. & Morse, D. E. Fractal intermediates in the self-assembly of silicatein filaments. *Proceedings of the National Academy of Sciences of the United States of America* **102**, 11657-11662 (2005).
25. Smith Jr, T. G., Lange, G. D. & Marks, W. B. Fractal methods and results in cellular morphology — dimensions, lacunarity and multifractals. *Journal of Neuroscience Methods* **69**, 123-136, doi:[http://dx.doi.org/10.1016/S0165-0270\(96\)00080-5](http://dx.doi.org/10.1016/S0165-0270(96)00080-5) (1996).
26. Schaefer, D. W. Polymers, fractals, and ceramic materials. *Science* **243**, 1023-1027 (1989).
27. Reznikov, N., Bilton, M., Lari, L., Stevens, M. M. & Kröger, R. Fractal-like hierarchical organization of bone begins at the nanoscale. *Science* **360** (2018).
28. Al-Kadi, O. S. & Watson, D. Texture analysis of aggressive and nonaggressive lung tumor CE CT images. *IEEE transactions on biomedical engineering* **55**, 1822-1830 (2008).
29. Picu, R. C. *et al.* Composites with fractal microstructure: The effect of long range correlations on elastic–plastic and damping behavior. *Mechanics of Materials* **69**, 251-261, doi:<http://dx.doi.org/10.1016/j.mechmat.2013.11.002> (2014).
30. Meza, L. R. *et al.* Resilient 3D hierarchical architected metamaterials. *Proceedings of the National Academy of Sciences* **112**, 11502, doi:10.1073/pnas.1509120112 (2015).
31. Billon, K. *et al.* Mechanics and band gaps in hierarchical auxetic rectangular perforated composite metamaterials. *Composite Structures* **160**, 1042-1050, doi:<http://dx.doi.org/10.1016/j.compstruct.2016.10.121> (2017).
32. Bhushan, B. Biomimetics: lessons from nature—an overview. *Philosophical Transactions of the Royal Society A: Mathematical, Physical and Engineering Sciences* **367**, 1445 (2009).
33. Fratzl, P. Biomimetic materials research: what can we really learn from nature's structural materials? *Journal of The Royal Society Interface* **4**, 637 (2007).
34. Wegst, U. G. K., Bai, H., Saiz, E., Tomsia, A. P. & Ritchie, R. O. Bioinspired

- structural materials. *Nat Mater* **14**, 23-36, doi:10.1038/nmat4089 (2015).
35. Chen, P.-Y., McKittrick, J. & Meyers, M. A. Biological materials: Functional adaptations and bioinspired designs. *Progress in Materials Science* **57**, 1492-1704, doi:<https://doi.org/10.1016/j.pmatsci.2012.03.001> (2012).
36. Smith, B. L. *et al.* Molecular mechanistic origin of the toughness of natural adhesives, fibres and composites. *Nature* **399**, 761-763, doi:10.1038/21607 (1999).
37. Munch, E. *et al.* Tough, Bio-Inspired Hybrid Materials. *Science* **322**, 1516, doi:10.1126/science.1164865 (2008).
38. du Plessis, A. & Broeckhoven, C. Looking deep into nature: A review of micro-computed tomography in biomimicry. *Acta Biomaterialia* **85**, 27-40, doi:<https://doi.org/10.1016/j.actbio.2018.12.014> (2019).
39. Weinkamer, R. & Fratzl, P. Mechanical adaptation of biological materials — The examples of bone and wood. *Materials Science and Engineering: C* **31**, 1164-1173, doi:<https://doi.org/10.1016/j.msec.2010.12.002> (2011).
40. Tan, T. *et al.* Mechanical properties of functionally graded hierarchical bamboo structures. *Acta Biomaterialia* **7**, 3796-3803, doi:<https://doi.org/10.1016/j.actbio.2011.06.008> (2011).\\
41. Meza, L. R. *et al.* Resilient 3D hierarchical architected metamaterials. *Proceedings of the National Academy of Sciences* **112**, 11502, doi:10.1073/pnas.1509120112 (2015).
42. Bouville, F. *et al.* Corrigendum: Strong, tough and stiff bioinspired ceramics from brittle constituents. *Nature Materials* **16**, 1271, doi:10.1038/nmat4982 (2017).
43. Eadie, L. & Ghosh Tushar, K. Biomimicry in textiles: past, present and potential. An overview. *Journal of The Royal Society Interface* **8**, 761-775, doi:10.1098/rsif.2010.0487 (2011).
44. Yoo, S. C., Park, Y. K., Park, C., Ryu, H. & Hong, S. H. Biomimetic Artificial Nacre: Boron Nitride Nanosheets/Gelatin Nanocomposites for Biomedical Applications. *Advanced Functional Materials* **0**, 1805948, doi:10.1002/adfm.201805948 (2018).
45. Mirkhalaf, M., Dastjerdi, A. K. & Barthelat, F. Overcoming the brittleness of glass through bio-inspiration and micro-architecture. *Nature Communications* **5**, 3166, doi:10.1038/ncomms4166 (2014).
46. Fernandez, J. G. & Ingber, D. E. Unexpected Strength and Toughness in Chitosan-Fibroin Laminates Inspired by Insect Cuticle. *Advanced Materials* **24**, 480-484, doi:10.1002/adma.201104051 (2011).
47. Wu, Z. *et al.* Biomimetic structure design and construction of cactus-like MoS<sub>2</sub>/Bi<sub>19</sub>Cl<sub>3</sub>S<sub>27</sub> photocatalysts for efficient hydrogen evolution. *Journal of*

- Materials Chemistry A*, doi:10.1039/C8TA08834A (2018).
- 48. Porter, M. M., Ravikumar, N., Barthelat, F. & Martini, R. 3D-printing and mechanics of bio-inspired articulated and multi-material structures. *Journal of the Mechanical Behavior of Biomedical Materials* **73**, 114-126,
  - 49. Dimas, L. S., Bratzel, G. H., Eylon, I. & Buehler, M. J. Tough Composites Inspired by Mineralized Natural Materials: Computation, 3D printing, and Testing. *Advanced Functional Materials* **23**, 4629-4638, doi:10.1002/adfm.201300215 (2013).
  - 50. Studart, A. R. Additive manufacturing of biologically-inspired materials. *Chemical Society Reviews* **45**, 359-376, doi:10.1039/C5CS00836K (2016).
  - 51. Hull, C. W. (Google Patents, 1986).
  - 52. Lee, J.-Y., An, J. & Chua, C. K. Fundamentals and applications of 3D printing for novel materials. *Applied Materials Today* **7**, 120-133, doi:<http://dx.doi.org/10.1016/j.apmt.2017.02.004> (2017).
  - 53. Khoo, Z. X. et al. 3D printing of smart materials: A review on recent progresses in 4D printing. *Virtual and Physical Prototyping* **10**, 103-122 (2015).
  - 54. Espalin, D., Muse, D. W., MacDonald, E. & Wicker, R. B. 3D Printing multifunctionality: structures with electronics. *The International Journal of Advanced Manufacturing Technology* **72**, 963-978 (2014).
  - 55. Compton, B. G. & Lewis, J. A. 3D-printing of lightweight cellular composites. *Advanced materials* **26**, 5930-5935 (2014).
  - 56. Chia, H. N. & Wu, B. M. Recent advances in 3D printing of biomaterials. *Journal of biological engineering* **9**, 4 (2015)
  - 57. Porter, M. M., Ravikumar, N., Barthelat, F. & Martini, R. 3D-printing and mechanics of bio-inspired articulated and multi-material structures. *Journal of the Mechanical Behavior of Biomedical Materials* **73**, 114-126,
  - 58. Dimas, L. S., Bratzel, G. H., Eylon, I. & Buehler, M. J. Tough Composites Inspired by Mineralized Natural Materials: Computation, 3D printing, and Testing. *Advanced Functional Materials* **23**, 4629-4638, doi:10.1002/adfm.201300215 (2013).
  - 59. Studart, A. R. Additive manufacturing of biologically-inspired materials. *Chemical Society Reviews* **45**, 359-376, doi:10.1039/C5CS00836K (2016).
  - 60. Dimas, L. S., Bratzel, G. H., Eylon, I. & Buehler, M. J. Tough Composites Inspired by Mineralized Natural Materials: Computation, 3D printing, and Testing. *Advanced Functional Materials* **23**, 4629-4638, doi:10.1002/adfm.201300215 (2013).
  - 61. de Obaldia, E. E., Jeong, C., Grunenfelder, L. K., Kisailus, D. & Zavattieri, P.

- Analysis of the mechanical response of biomimetic materials with highly oriented microstructures through 3D printing, mechanical testing and modeling. *Journal of the Mechanical Behavior of Biomedical Materials* **48**, 70-85,
- 62. Kokkinis, D., Bouville, F. & Studart, A. R. 3D Printing of Materials with Tunable Failure via Bioinspired Mechanical Gradients. *Advanced Materials* **30**, 1705808, doi:10.1002/adma.201705808 (2018).
  - 63. Martin, J. J., Fiore, B. E. & Erb, R. M. Designing bioinspired composite reinforcement architectures via 3D magnetic printing. *Nature Communications* **6**, 8641,doi:10.1038/ncomms9641https://www.nature.com/articles/ncomms9641#supplementary-information (2015).
  - 64. Zorzetto, L. & Ruffoni, D. Wood-Inspired 3D-Printed Helical Composites with Tunable and Enhanced Mechanical Performance. *Advanced Functional Materials* **29**, 1805888, doi:10.1002/adfm.201805888 (2019).
  - 65. Mayandi, K., Rajini, N., Manojprabhakar, M., Siengchin, S. & Ayrilmis, N. in *Durability and Life Prediction in Biocomposites, Fibre-Reinforced Composites and Hybrid Composites* (eds Mohammad Jawaid, Mohamed Thariq, & Naheed Saba) 1-13 (Woodhead Publishing, 2019).
  - 66. Vasiliev, V. V. & Morozov, E. V. in *Advanced Mechanics of Composite Materials and Structures (Fourth Edition)* (eds Valery V. Vasiliev & Evgeny V. Morozov) 1-73 (Elsevier, 2018).
  - 67. Gay, D. *Composite materials: design and applications.* (CRC press, 2014).
  - 68. Mangalgiri, P. D. Composite materials for aerospace applications. *Bulletin of Materials Science* **22**, 657-664 (1999).
  - 69. Ramakrishna, S., Mayer, J., Wintermantel, E. & Leong, K. W. Biomedical applications of polymer-composite materials: a review. *Composites science and technology* **61**, 1189-1224 (2001).
  - 70. Sathishkumar, T. P., Satheeshkumar, S. & Naveen, J. Glass fiber-reinforced polymer composites – a review. *Journal of Reinforced Plastics and Composites* **33**, 1258-1275, doi:10.1177/0731684414530790 (2014).
  - 71. Yao, S.-S., Jin, F.-L., Rhee, K. Y., Hui, D. & Park, S.-J. Recent advances in carbon-fiber-reinforced thermoplastic composites: A review. *Composites Part B: Engineering* **142**, 241-250, doi:https://doi.org/10.1016/j.compositesb.2017.12.007 (2018).
  - 72. Faruk, O., Bledzki, A. K., Fink, H.-P. & Sain, M. 2012. Biocomposites reinforced with natural fibers: 2000–2010. *Progress in Polymer Science*, **37**, 1552-1596.

73. DeArmitt, C. & Rothon, R. Particulate Fillers, Selection, and Use in Polymer Composites. *Fillers for Polymer Applications*, 3-27 (2017).
74. Yang, H.-S. *et al.* Rice-husk flour filled polypropylene composites; mechanical and morphological study. *Composite Structures* **63**, 305-312, doi:[https://doi.org/10.1016/S0263-8223\(03\)00179-X](https://doi.org/10.1016/S0263-8223(03)00179-X) (2004).
75. Liu, H. *et al.* Compatibilizing and toughening bamboo flour-filled HDPE composites: Mechanical properties and morphologies. *Composites Part A: Applied Science and Manufacturing* **39**, 1891-1900, doi:<https://doi.org/10.1016/j.compositesa.2008.09.011> (2008).
76. Chun, K. S., Husseinsyah, S. & Osman, H. Properties of coconut shell powder-filled polylactic acid ecocomposites: Effect of maleic acid. *Polymer Engineering & Science* **53**, 1109-1116 (2013).
77. Mohanty, A. K., Drzal, L. T. & Misra, M. Novel hybrid coupling agent as an adhesion promoter in natural fiber reinforced powder polypropylene composites. *J Mater Sci Lett* **21**, 1885-1888, doi:[10.1023/A:1021577632600](https://doi.org/10.1023/A:1021577632600) (2002).
78. Cheung, H.-Y., Ho, M.-P., Lau, K.-T., Cardona, F. & Hui, D. 2009. Natural fibre-reinforced composites for bioengineering and environmental engineering applications. *Composites Part B: Engineering*, **40**, 655-663
79. Wambua, P., Ivens, J. & Verpoest, I. 2003. Natural fibres: can they replace glass in fibre reinforced plastics? *Composites Science and Technology*, **63**, 1259-1264.
80. Saheb, D. N. & Jog, J. P. 1999. Natural Fiber Polymer Composites: A Review. *Advances in Polymer Technology*, **18**, 351–363.
81. Pandey, J. K., Ahn, S. H., Lee, C. S., Mohanty, A. K. & Misra, M. 2010. Recent advances in the application of natural fiber based composites. *Macromolecular Materials and Engineering*, **295**, 975-989.
82. John, M. J. & Thomas, S. Biofibres and biocomposites. *Carbohydrate Polymers* **71**, 343-364, doi:<http://dx.doi.org/10.1016/j.carbpol.2007.05.040> (2008)
83. Peças, P., Carvalho, H., Salman, H. & Leite, M. Natural Fibre Composites and Their Applications: A Review. *Journal of Composites Science* **2**, doi:[10.3390/jcs2040066](https://doi.org/10.3390/jcs2040066) (2018).
84. Sanjay, M. R., Arpitha, G. R., Naik, L. L., Gopalakrishna, K. & Yugesha, B. Applications of natural fibers and its composites: An overview. *Natural Resources* **7**, 108 (2016).
85. Li, Y., Yi, X., Yu, T. & Xian, G. An overview of structural-functional-integrated composites based on the hierarchical microstructures of plant fibers. *Advanced Composites and Hybrid Materials*, doi:[10.1007/s42114-017-0020-3](https://doi.org/10.1007/s42114-017-0020-3) (2018).
86. A.Komuraiah, N. S. K., B.Durga Prasad. Chemical Composition Of Natural Fibers

- An Its Influence On Their Mechanical Properties. *Mechanics of Composite Materials* **30** (2014).
- 87. Valadez-Gonzalez, A., Cervantes-Uc, J. M., Olayo, R. & Herrera-Franco, P. J. 1999. Effect of fiber surface treatment on the fiber–matrix bond strength of natural fiber reinforced composites. *Composites Part B: Engineering*, **30**, 309-320.
  - 88. Mohanty, A. K., Misra, M. & Drzal, L. T. Surface modifications of natural fibers and performance of the resulting biocomposites: an overview. *Composite Interfaces* **8**, 313-343 (2001).
  - 89. Yuanjian, T. & Isaac, D. H. 2007. Impact and fatigue behaviour of hemp fibre composites. *Composites Science and Technology*, **67**, 3300-3307
  - 90. Bledzki, A. K., Zhang, W. & Chate, A. Natural-fibre-reinforced polyurethane microfoams. *Composites Science and Technology* **61**, 2405-2411, doi:[http://dx.doi.org/10.1016/S0266-3538\(01\)00129-4](http://dx.doi.org/10.1016/S0266-3538(01)00129-4) (2001).
  - 91. López-Alba, E., Schmeer, S. & Díaz, F. Energy Absorption Capacity in Natural Fiber Reinforcement Composites Structures. *Materials* **11**, doi:[10.3390/ma11030418](https://doi.org/10.3390/ma11030418) (2018).
  - 92. Ho, M.-p. *et al.* Critical factors on manufacturing processes of natural fibre composites. *Composites Part B: Engineering* **43**, 3549-3562, doi:<https://doi.org/10.1016/j.compositesb.2011.10.001> (2012).
  - 93. Oksman, K., Skrifvars, M. & Selin, J. F. Natural fibres as reinforcement in polylactic acid (PLA) composites. *Composites Science and Technology* **63**, 1317-1324, doi:[http://dx.doi.org/10.1016/S0266-3538\(03\)00103-9](http://dx.doi.org/10.1016/S0266-3538(03)00103-9) (2003).
  - 94. Okubo, K., Fujii, T. & Thostenson, E. T. Multi-scale hybrid biocomposite: Processing and mechanical characterization of bamboo fiber reinforced PLA with microfibrillated cellulose. *Composites Part A: Applied Science and Manufacturing* **40**, 469-475, doi:<http://dx.doi.org/10.1016/j.compositesa.2009.01.012> (2009).
  - 95. Silva, L. J. *et al.* Statistical design of polymeric composites reinforced with banana fibres and silica microparticles. *Journal of Composite Materials* **47**, 1199-1210 (2013).
  - 96. Arib, R. M. N., Sapuan, S. M., Ahmad, M. M. H. M., Paridah, M. T. & Zaman, H. M. D. K. 2006. Mechanical properties of pineapple leaf fibre reinforced polypropylene composites. *Materials & Design*, **27**, 391-396.
  - 97. Amroune, S., Bezazi, A., Belaadi, A., Zhu, C., Scarpa, F., Rahatekar, S. & Imad, A. 2015. Tensile mechanical properties and surface chemical sensitivity of technical

- fibres from date palm fruit branches (*Phoenix dactylifera* L.). *Composites Part A: Applied Science and Manufacturing*, 71, 95-106.
98. Kalia, S., Kaith, B. S. & Kaur, I. Pretreatments of natural fibers and their application as reinforcing material in polymer composites—A review. *Polymer Engineering & Science* 49, 1253-1272, doi:10.1002/pen.21328 (2009).
99. Ahmed, E. M. Hydrogel: Preparation, characterization, and applications: A review. *Journal of Advanced Research* 6, 105-121, doi:<https://doi.org/10.1016/j.jare.2013.07.006> (2015).
100. Huglin, M. R. *Hydrogels in medicine and pharmacy* Edited by N. A. Peppas, CRC Press Inc., Boca Raton, Florida, 1986 (Vol. 1), 1987 (Vols 2 and 3). Vol. 1 Fundamentals, pp. vii + 180, £72.00, ISBN 0-8493-5546-X; Vol. 2 Polymers, pp. vii + 171, £72.00, ISBN 0-8493-5547-8; Vol. 3 Properties and Applications, pp. vii + 195, £8000, ISBN 0-8493-5548-6. *British Polymer Journal* 21, 184-184, doi:10.1002/pi.4980210223 (1989).
101. Takeda, H. & Taniguchi, Y. (Google Patents, 1985).
102. Drury, J. L. & Mooney, D. J. Hydrogels for tissue engineering: scaffold design variables and applications. *Biomaterials* 24, 4337-4351, doi:[https://doi.org/10.1016/S0142-9612\(03\)00340-5](https://doi.org/10.1016/S0142-9612(03)00340-5) (2003).
103. Armstrong, J. P. K., Burke, M., Carter, B. M., Davis, S. A. & Perriman, A. W. 3D Bioprinting Using a Templatized Porous Bioink. *Advanced Healthcare Materials*, n/a-n/a, doi:10.1002/adhm.201600022 (2016).
104. Kim, J. et al. Bone regeneration using hyaluronic acid-based hydrogel with bone morphogenic protein-2 and human mesenchymal stem cells. *Biomaterials* 28, 1830-1837, doi:<https://doi.org/10.1016/j.biomaterials.2006.11.050> (2007).
105. Deller, R. C. et al. Artificial cell membrane binding thrombin constructs drive in situ fibrin hydrogel formation. *Nature Communications* 10, 1887, doi:10.1038/s41467-019-09763-0 (2019).
106. Hinton, T. J. et al. Three-dimensional printing of complex biological structures by freeform reversible embedding of suspended hydrogels. *Science Advances* 1 (2015).
107. Nöth, U. et al. Chondrogenic differentiation of human mesenchymal stem cells in collagen type I hydrogels. *Journal of Biomedical Materials Research Part A* 83A, 626-635, doi:10.1002/jbm.a.31254 (2007).
108. Raucci, M. G., Alvarez-Perez, M. A., Demitri, C., Sannino, A. & Ambrosio, L. Proliferation and Osteoblastic Differentiation of hMSCs on Cellulose-Based Hydrogels. *Journal of Applied Biomaterials & Functional Materials* 10, 302-307,

- doi:10.5301/JABFM.2012.10366 (2012).
109. Jungst, T., Smolan, W., Schacht, K., Scheibel, T. & Groll, J. Strategies and Molecular Design Criteria for 3D Printable Hydrogels. *Chemical Reviews* 116, 1496-1539, doi:10.1021/acs.chemrev.5b00303 (2016).
110. Vats, K. et al. Nanoscale physicochemical properties of chain- and step-growth polymerized PEG hydrogels affect cell-material interactions. *Journal of Biomedical Materials Research Part A* 105, 1112-1122, doi:10.1002/jbm.a.36007 (2017).
111. Schmedlen, R. H., Masters, K. S. & West, J. L. Photocrosslinkable polyvinyl alcohol hydrogels that can be modified with cell adhesion peptides for use in tissue engineering. *Biomaterials* 23, 4325-4332, doi:[https://doi.org/10.1016/S0142-9612\(02\)00177-1](https://doi.org/10.1016/S0142-9612(02)00177-1) (2002).
112. Chiang, C.-Y. & Chu, C.-C. Synthesis of photoresponsive hybrid alginate hydrogel with photo-controlled release behavior. *Carbohydrate Polymers* 119, 18-25, doi:<https://doi.org/10.1016/j.carbpol.2014.11.043> (2015).
113. Xu, G. et al. Injectable biodegradable hybrid hydrogels based on thiolated collagen and oligo(acryloyl carbonate)-poly(ethylene glycol)-oligo(acryloyl carbonate) copolymer for functional cardiac regeneration. *Acta Biomaterialia* 15, 55-64, doi:<https://doi.org/10.1016/j.actbio.2014.12.016> (2015).
114. Kenry, Lee, W. C., Loh, K. P. & Lim, C. T. When stem cells meet graphene: Opportunities and challenges in regenerative medicine. *Biomaterials* 155, 236-250, doi:<https://doi.org/10.1016/j.biomaterials.2017.10.004> (2018).
115. Visser, J. et al. Reinforcement of hydrogels using three-dimensionally printed microfibres. *Nature Communications* 6, 6933, doi:10.1038/ncomms7933<https://www.nature.com/articles/ncomms7933#supplementary-information> (2015).
116. Ziv, K. et al. A tunable silk-alginate hydrogel scaffold for stem cell culture and transplantation. *Biomaterials* 35, 3736-3743, doi:<https://doi.org/10.1016/j.biomaterials.2014.01.029> (2014).
117. Markstedt, K. et al. 3D Bioprinting Human Chondrocytes with Nanocellulose-Alginate Bioink for Cartilage Tissue Engineering Applications. *Biomacromolecules* 16, 1489-1496, doi:10.1021/acs.biomac.5b00188 (2015).
118. Nayak, T. R. et al. Graphene for controlled and accelerated osteogenic differentiation of human mesenchymal stem cells. *ACS nano* 5, 4670-4678 (2011).
119. Shin, S. R. et al. Carbon nanotube reinforced hybrid microgels as scaffold materials

- for cell encapsulation. *ACS nano* **6**, 362-372 (2011).
120. Meyers, M. A. Dynamic behavior of materials. (John Wiley & Sons, 1994).
  121. Qiao, P., Yang, M. & Bobaru, F. Impact Mechanics and High-Energy Absorbing Materials: Review. *Journal of Aerospace Engineering* **21**, 235-248, doi:10.1061/(ASCE)0893-1321(2008)21:4(235) (2008).
  122. Jang, B. Z., Chen, L. C., Hwang, L. R., Hawkes, J. E. & Zee, R. H. The response of fibrous composites to impact loading. *Polymer Composites* **11**, 144-157, doi:10.1002/pc.750110303 (1990).
  123. Avalle, M., Belingardi, G. & Montanini, R. Characterization of polymeric structural foams under compressive impact loading by means of energy-absorption diagram. *International Journal of Impact Engineering* **25**, 455-472, doi:[http://dx.doi.org/10.1016/S0734-743X\(00\)00060-9](http://dx.doi.org/10.1016/S0734-743X(00)00060-9) (2001).
  124. Hufenbach, W., Gude, M. & Ebert, C. Hybrid 3D-textile reinforced composites with tailored property profiles for crash and impact applications. *Composites Science and Technology* **69**, 1422-1426, doi:<http://dx.doi.org/10.1016/j.compscitech.2008.09.033> (2009).
  125. Justo, J., Osuna, S. & París, F. Design of composite materials with improved impact properties. *Composites Part B: Engineering* **76**, 229-234, doi:<http://dx.doi.org/10.1016/j.compositesb.2015.02.025> (2015).
  126. Cantwell, W. J. & Morton, J. The impact resistance of composite materials — a review. *Composites* **22**, 347-362, doi:[http://dx.doi.org/10.1016/0010-4361\(91\)90549-V](http://dx.doi.org/10.1016/0010-4361(91)90549-V) (1991).
  127. Chandra, R., Singh, S. P. & Gupta, K. Damping studies in fiber-reinforced composites – a review. *Composite Structures* **46**, 41-51, doi:[http://dx.doi.org/10.1016/S0263-8223\(99\)00041-0](http://dx.doi.org/10.1016/S0263-8223(99)00041-0) (1999).
  128. Holbery, J. & Houston, D. Natural-fiber-reinforced polymer composites in automotive applications. *Jom* **58**, 80-86 (2006).
  129. Heo, H., Ju, J. & Kim, D.-M. Compliant cellular structures: Application to a passive morphing airfoil. *Composite Structures* **106**, 560-569, doi:<https://doi.org/10.1016/j.compstruct.2013.07.013> (2013).
  130. DiPalma, M. & Gandhi, F. in *24th AIAA/AHS Adaptive Structures Conference AIAA SciTech Forum* (American Institute of Aeronautics and Astronautics, 2016).

131. Sofla, A. Y. N., Meguid, S. A., Tan, K. T. & Yeo, W. K. Shape morphing of aircraft wing: Status and challenges. *Materials & Design* **31**, 1284-1292, doi:<https://doi.org/10.1016/j.matdes.2009.09.011> (2010).
132. Viola, J., Lal, B. & Grad, O. *The Emergence of Tissue Engineering as a Research Field* (2003); available at <<http://www.nsf.gov/pubs/2004/nsf0450/start.htm>>.
133. Peppas, N. A. & Langer, R. New challenges in biomaterials. *Science* **263**, 1715, doi:[10.1126/science.8134835](https://doi.org/10.1126/science.8134835) (1994).
134. Place, E. S., Evans, N. D. & Stevens, M. M. Complexity in biomaterials for tissue engineering. *Nature Materials* **8**, 457, doi:[10.1038/nmat2441](https://doi.org/10.1038/nmat2441) <https://www.nature.com/articles/nmat2441#supplementary-information> (2009).
135. Henkel, J. *et al.* Bone Regeneration Based on Tissue Engineering Conceptions — A 21st Century Perspective. *Bone Research* **1**, 216, doi:[10.4248/BR201303002](https://doi.org/10.4248/BR201303002) (2013).
136. Chagastelles, P. C. & Nardi, N. B. Biology of stem cells: an overview. *Kidney Int Suppl (2011)* **1**, 63-67, doi:[10.1038/kisup.2011.15](https://doi.org/10.1038/kisup.2011.15) (2011).
137. Athanasiou, K. A., Eswaramoorthy, R., Hadidi, P. & Hu, J. C. Self-organization and the self-assembling process in tissue engineering. *Annu Rev Biomed Eng* **15**, 115-136, doi:[10.1146/annurev-bioeng-071812-152423](https://doi.org/10.1146/annurev-bioeng-071812-152423) (2013).
138. Roach, P., Eglin, D., Rohde, K. & Perry, C. C. Modern biomaterials: a review—bulk properties and implications of surface modifications. *Journal of Materials Science: Materials in Medicine* **18**, 1263-1277, doi:[10.1007/s10856-006-0064-3](https://doi.org/10.1007/s10856-006-0064-3) (2007).
139. Elloumi-Hannachi, I., Yamato, M. & Okano, T. Cell sheet engineering: a unique nanotechnology for scaffold-free tissue reconstruction with clinical applications in regenerative medicine. *Journal of internal medicine* **267**, 54-70 (2010).
140. Haraguchi, Y., Shimizu, T., Yamato, M. & Okano, T. Scaffold-free tissue engineering using cell sheet technology. *Rsc Advances* **2**, 2184-2190 (2012).
141. Norotte, C., Marga, F. S., Niklason, L. E. & Forgacs, G. Scaffold-free vascular tissue engineering using bioprinting. *Biomaterials* **30**, 5910-5917 (2009).
142. Hutmacher, D. W. & Cool, S. Concepts of scaffold-based tissue engineering—the rationale to use solid free-form fabrication techniques. *Journal of cellular and molecular medicine* **11**, 654-669 (2007).
143. Moroni, L. *et al.* Biofabrication strategies for 3D in vitro models and regenerative medicine. *Nature Reviews Materials* **3**, 21 (2018).

144. Yunus Basha, R., T.S, S. K. & Doble, M. Design of biocomposite materials for bone tissue regeneration. *Materials Science and Engineering: C* **57**, 452-463, doi:<http://dx.doi.org/10.1016/j.msec.2015.07.016> (2015).
145. Amini, A. R., Laurencin, C. T. & Nukavarapu, S. P. Bone Tissue Engineering: Recent Advances and Challenges. *Critical reviews in biomedical engineering* **40**, 363-408 (2012).
146. Weiner, S. & Wagner, H. D. THE MATERIAL BONE: Structure-Mechanical Function Relations. *Annual Review of Materials Science* **28**, 271-298, doi:[10.1146/annurev.matsci.28.1.271](https://doi.org/10.1146/annurev.matsci.28.1.271) (1998).
147. Rho, J.-Y., Kuhn-Spearing, L. & Ziopoulos, P. 1998. Mechanical properties and the hierarchical structure of bone. *Medical Engineering & Physics*, **20**, 92-102.
148. Hutmacher, D. W. 2000. Scaffolds in tissue engineering bone and cartilage. *Biomaterials*, **21**, 2529-2543.
149. Hutmacher, D. W., Schantz, J. T., Lam, C. X. F., Tan, K. C. & Lim, T. C. State of the art and future directions of scaffold-based bone engineering from a biomaterials perspective. *Journal of Tissue Engineering and Regenerative Medicine* **1**, 245-260, doi:[10.1002/term.24](https://doi.org/10.1002/term.24) (2007).
150. Henkel, J. *et al.* Bone Regeneration Based on Tissue Engineering Conceptions — A 21st Century Perspective. *Bone Research* **1**, 216, doi:[10.4248/BR201303002](https://doi.org/10.4248/BR201303002) (2013).
151. LeGeros, R. Z. Calcium Phosphate-Based Osteoinductive Materials. *Chemical Reviews* **108**, 4742-4753, doi:[10.1021/cr800427g](https://doi.org/10.1021/cr800427g) (2008).
152. Albrektsson, T. & Johansson, C. Osteoinduction, osteoconduction and osseointegration. *European spine journal* **10**, S96-S101 (2001).
153. Kim, S.-S., Sun Park, M., Jeon, O., Yong Choi, C. & Kim, B.-S. Poly(lactide-co-glycolide)/hydroxyapatite composite scaffolds for bone tissue engineering. *Biomaterials* **27**, 1399-1409, doi:<https://doi.org/10.1016/j.biomaterials.2005.08.016> (2006).
154. Wang, H. *et al.* Biocompatibility and osteogenesis of biomimetic nano-hydroxyapatite/polyamide composite scaffolds for bone tissue engineering. *Biomaterials* **28**, 3338-3348, doi:<https://doi.org/10.1016/j.biomaterials.2007.04.014> (2007).
155. Liu, X., Smith, L. A., Hu, J. & Ma, P. X. Biomimetic nanofibrous gelatin/apatite composite scaffolds for bone tissue engineering. *Biomaterials* **30**, 2252-2258, doi:<https://doi.org/10.1016/j.biomaterials.2008.12.068> (2009).
156. Lee, K. Y. & Mooney, D. J. Hydrogels for tissue engineering. *Chemical reviews* **101**, 1869-1880 (2001).

157. Alsberg, E., Anderson, K. W., Albeiruti, A., Franceschi, R. T. & Mooney, D. J. Cell-interactive Alginate Hydrogels for Bone Tissue Engineering. *Journal of Dental Research* **80**, 2025-2029, doi:10.1177/00220345010800111501 (2001).
158. Burdick, J. A. & Anseth, K. S. Photoencapsulation of osteoblasts in injectable RGD-modified PEG hydrogels for bone tissue engineering. *Biomaterials* **23**, 4315-4323, doi:[https://doi.org/10.1016/S0142-9612\(02\)00176-X](https://doi.org/10.1016/S0142-9612(02)00176-X) (2002).
159. Karoly Jakab And Cyrille Norotte And Francoise Marga And Keith Murphy And Gordana Vunjak-Novakovic And Gabor, F. 2010. Tissue engineering by self-assembly and bio-printing of living cells. *Biofabrication*, **2**, 022001.
160. Derby, B. Printing and Prototyping of Tissues and Scaffolds. *Science* **338**, 921 (2012).
161. Nguyen, D. *et al.* Cartilage Tissue Engineering by the 3D Bioprinting of iPS Cells in a Nanocellulose/Alginate Bioink. *Scientific Reports* **7**, 658, doi:10.1038/s41598-017-00690-y (2017).
162. Gao, T. *et al.* Optimization of gelatin-alginate composite bioink printability using rheological parameters: a systematic approach. *Biofabrication* **10**, 034106-034106, doi:10.1088/1758-5090/aacdc7 (2018).
163. Zheng, Z. *et al.* 3D Bioprinting of Self-Standing Silk-Based Bioink. *Advanced Healthcare Materials* **7**, 1701026, doi:[doi:10.1002/adhm.201701026](https://doi.org/10.1002/adhm.201701026) (2018).
164. Behera, B. K. & Dash, B. P. Mechanical behavior of 3D woven composites. *Materials & Design* **67**, 261-271, doi:<https://doi.org/10.1016/j.matdes.2014.11.020> (2015).
165. Currey, J. D. The Mechanical Properties of Bone. *Clinical Orthopaedics and Related Research* **73** (1970).
166. de Obaldia, E. E., Jeong, C., Grunenfelder, L. K., Kisailus, D. & Zavattieri, P. Analysis of the mechanical response of biomimetic materials with highly oriented microstructures through 3D printing, mechanical testing and modeling. *Journal of the Mechanical Behavior of Biomedical Materials* **48**, 70-85, doi:<https://doi.org/10.1016/j.jmbbm.2015.03.026> (2015).
167. Herrera-Franco, P. J. & Valadez-González, A. A study of the mechanical properties of short natural-fiber reinforced composites. *Composites Part B: Engineering* **36**, 597-608, doi:<http://dx.doi.org/10.1016/j.compositesb.2005.04.001> (2005).
168. Kokkinis, D., Bouville, F. & Studart, A. R. 3D Printing of Materials with Tunable Failure via Bioinspired Mechanical Gradients. *Advanced Materials* **30**, 1705808, doi:10.1002/adma.201705808 (2018).

169. Chua, C. K., Wong, C. H. & Yeong, W. Y. in *Standards, Quality Control, and Measurement Sciences in 3D Printing and Additive Manufacturing* (eds Chee Kai Chua, Chee How Wong, & Wai Yee Yeong) 95-137 (Academic Press, 2017).
170. Saba, N., Jawaid, M. & Sultan, M. T. H. in *Mechanical and Physical Testing of Biocomposites, Fibre-Reinforced Composites and Hybrid Composites* (eds Mohammad Jawaid, Mohamed Thariq, & Naheed Saba) 1-12 (Woodhead Publishing, 2019).
171. Campo, E. A. in *Selection of Polymeric Materials* (ed E. Alfredo Campo) 41-101 (William Andrew Publishing, 2008).
172. Licari, J. J. & Swanson, D. W. in *Adhesives Technology for Electronic Applications* (eds James J. Licari & Dale W. Swanson) 393-430 (William Andrew Publishing, 2005)
173. Ahearne, M., Yang, Y. & Liu, K. K. Mechanical characterisation of hydrogels for tissue engineering applications. *Topics in tissue Engineering* **4**, 1-16 (2008).
174. Augst, A. D., Kong, H. J. & Mooney, D. J. Alginate hydrogels as biomaterials. *Macromolecular bioscience* **6**, 623-633 (2006).
175. Maire, E. et al. On the Application of X-ray Microtomography in the Field of Materials Science. *Advanced Engineering Materials* **3**, 539-546, doi:10.1002/1527-2648(200108)3:8<539::AID-ADEM539>3.0.CO;2-6 (2001).
176. Salvo, L. et al. X-ray micro-tomography an attractive characterisation technique in materials science. *Nuclear Instruments and Methods in Physics Research Section B: Beam Interactions with Materials and Atoms* **200**, 273-286, doi:[http://dx.doi.org/10.1016/S0168-583X\(02\)01689-0](http://dx.doi.org/10.1016/S0168-583X(02)01689-0) (2003).
177. Bensadoun, F. et al. Challenges of X-Ray Tomography Technique on Natural Fibre-Based Composites. (2014).
178. du Plessis, A. & Broeckhoven, C. Looking deep into nature: A review of micro-computed tomography in biomimicry. *Acta Biomaterialia* **85**, 27-40, doi:<https://doi.org/10.1016/j.actbio.2018.12.014> (2019).
179. Maire, E. et al. X-ray tomography applied to the characterization of cellular materials. Related finite element modeling problems. *Composites Science and Technology* **63**, 2431-2443, doi:[http://dx.doi.org/10.1016/S0266-3538\(03\)00276-8](http://dx.doi.org/10.1016/S0266-3538(03)00276-8) (2003).
180. Youssef, S., Maire, E. & Gaertner, R. Finite element modelling of the actual structure of cellular materials determined by X-ray tomography. *Acta Materialia* **53**, 719-730, doi:<http://dx.doi.org/10.1016/j.actamat.2004.10.024> (2005).

181. Finnemore, A. *et al.* Biomimetic layer-by-layer assembly of artificial nacre. *Nature Communications* **3**, 966, doi:10.1038/ncomms1970  
<https://www.nature.com/articles/ncomms1970#supplementary-information> (2012).
182. Gibson, R. F. *Principles of composite material mechanics*. (CRC press, 2016).
183. Bledzki, A. K. & Jaszkiewicz, A. Mechanical performance of biocomposites based on PLA and PHBV reinforced with natural fibres – A comparative study to PP. *Composites Science and Technology* **70**, 1687-1696, doi:<http://dx.doi.org/10.1016/j.compscitech.2010.06.005> (2010).
184. Caló, E. & Khutoryanskiy, V. V. Biomedical applications of hydrogels: A review of patents and commercial products. *European Polymer Journal* **65**, 252-267, doi:<https://doi.org/10.1016/j.eurpolymj.2014.11.024> (2015).
185. Wielage, B., Lampke, T., Utschick, H. & Soergel, F. Processing of natural-fibre reinforced polymers and the resulting dynamic-mechanical properties. *Journal of Materials Processing Technology* **139**, 140-146, doi:[https://doi.org/10.1016/S0924-0136\(03\)00195-X](https://doi.org/10.1016/S0924-0136(03)00195-X) (2003).
186. Macdonald, D. A. The application of focus variation microscopy for lithic use-wear quantification. *Journal of Archaeological Science* **48**, 26-33, doi:<https://doi.org/10.1016/j.jas.2013.10.003> (2014).
187. Li, Y., Yi, X., Yu, T. & Xian, G. An overview of structural-functional-integrated composites based on the hierarchical microstructures of plant fibers. *Advanced Composites and Hybrid Materials*, doi:[10.1007/s42114-017-0020-3](https://doi.org/10.1007/s42114-017-0020-3) (2018).
188. Liu, H. *et al.* Compatibilizing and toughening bamboo flour-filled HDPE composites: Mechanical properties and morphologies. *Composites Part A: Applied Science and Manufacturing* **39**, 1891-1900, doi:<https://doi.org/10.1016/j.compositesa.2008.09.011> (2008).
189. Mohanty, A. K., Drzal, L. T. & Misra, M. Novel hybrid coupling agent as an adhesion promoter in natural fiber reinforced powder polypropylene composites. *J Mater Sci Lett* **21**, 1885-1888, doi:[10.1023/A:1021577632600](https://doi.org/10.1023/A:1021577632600) (2002).
190. Bhushan, B. & Caspers, M. An overview of additive manufacturing (3D printing) for microfabrication. *Microsystem Technologies* **23**, 1117-1124, doi:[10.1007/s00542-017-3342-8](https://doi.org/10.1007/s00542-017-3342-8) (2017).
191. Meza, L. R. *et al.* Resilient 3D hierarchical architected metamaterials. *Proceedings of the National Academy of Sciences* **112**, 11502, doi:[10.1073/pnas.1509120112](https://doi.org/10.1073/pnas.1509120112) (2015).
192. Kim, S.-J., Moon, J.-B., Kim, G.-H. & Ha, C.-S. Mechanical properties of polypropylene/natural fiber composites: Comparison of wood fiber and cotton fiber. *Polymer Testing* **27**, 801-806, doi:<https://doi.org/10.1016/j.polymertesting.2008.06.002> (2008).
193. Reis, J. M. L., Lima, R. P. & Vidal, S. D. Effect of rate and temperature on the mechanical properties of epoxy BADGE reinforced with carbon nanotubes. *Composite Structures* **202**, 89-94, doi:<https://doi.org/10.1016/j.compstruct.2017.11.081> (2018).

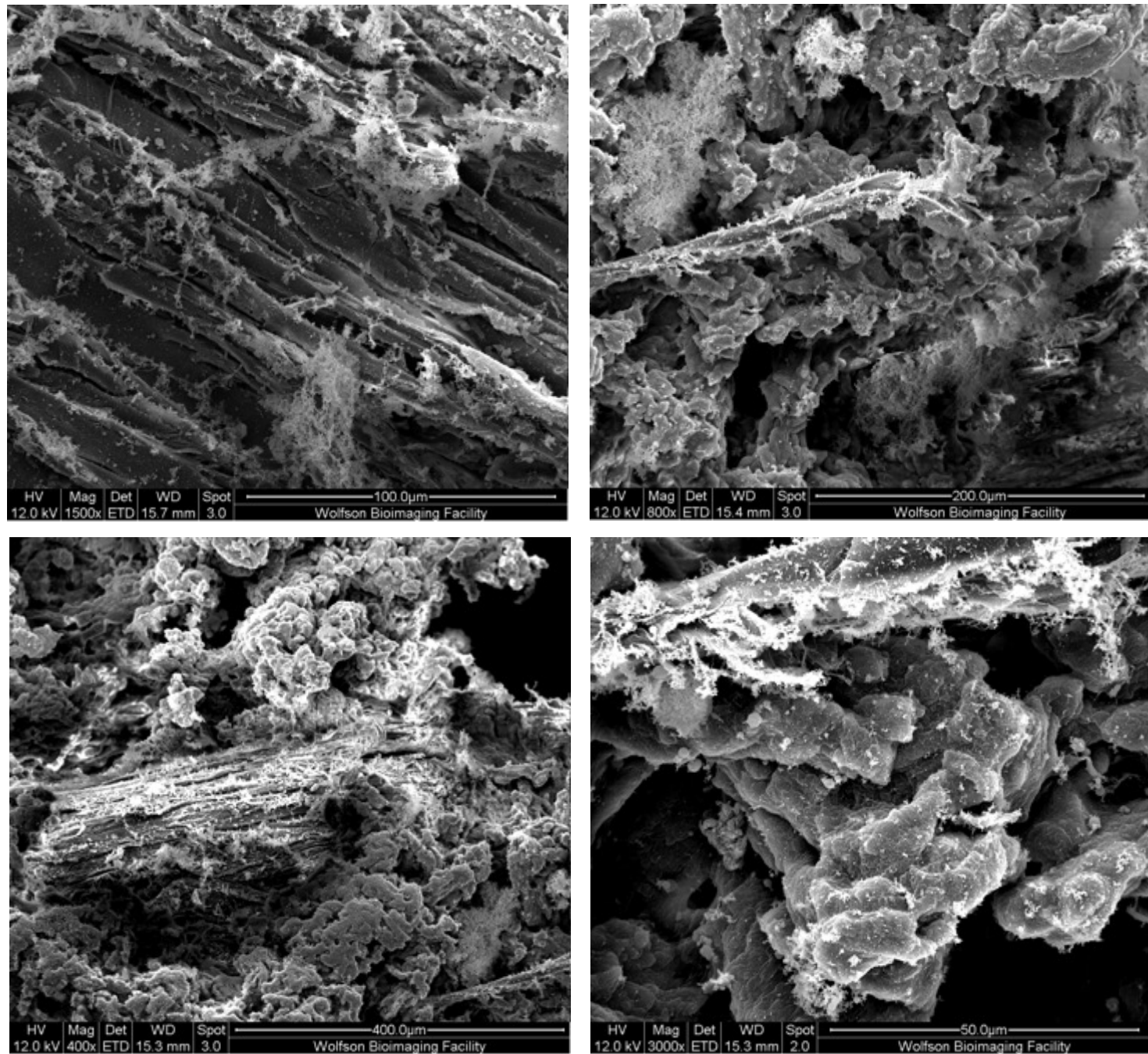
194. Vijaya Ramnath, B. *et al.* Evaluation of mechanical properties of abaca–jute–glass fibre reinforced epoxy composite. *Materials & Design* **51**, 357-366, doi:<https://doi.org/10.1016/j.matdes.2013.03.102> (2013).
195. L.J. Gibson, M.F. Ashby, B.A. Harley Cellular materials in nature and medicine Cambridge University Press, Cambridge (UK) (2010)
196. Ronan, W., Deshpande, V. S. & Fleck, N. A. The tensile ductility of cellular Solids: The role of imperfections. *International Journal of Solids and Structures* **102-103**, 200-213, doi:<https://doi.org/10.1016/j.ijsolstr.2016.10.004> (2016).
197. Goutianos, S., Peijs, T., Nystrom, B. & Skrifvars, M. Development of Flax Fibre based Textile Reinforcements for Composite Applications. *Applied Composite Materials* **13**, 199-215, doi:[10.1007/s10443-006-9010-2](https://doi.org/10.1007/s10443-006-9010-2) (2006).
198. Liu, H. *et al.* Compatibilizing and toughening bamboo flour-filled HDPE composites: Mechanical properties and morphologies. *Composites Part A: Applied Science and Manufacturing* **39**, 1891-1900, doi:<https://doi.org/10.1016/j.compositesa.2008.09.011> (2008).
199. Mohanty, A. K., Drzal, L. T. & Misra, M. Novel hybrid coupling agent as an adhesion promoter in natural fiber reinforced powder polypropylene composites. *J Mater Sci Lett* **21**, 1885-1888, doi:[10.1023/A:1021577632600](https://doi.org/10.1023/A:1021577632600) (2002).
200. Yang, H.-S. *et al.* Rice-husk flour filled polypropylene composites; mechanical and morphological study. *Composite Structures* **63**, 305-312, doi:[https://doi.org/10.1016/S0263-8223\(03\)00179-X](https://doi.org/10.1016/S0263-8223(03)00179-X) (2004).
201. Mizi Fan, Dasong Dai and Biao Huang (2012). Fourier Transform Infrared Spectroscopy for Natural Fibres, Fourier Transform - Materials Analysis, Dr Salih Salih (Ed.), ISBN: 978-953-51-0594-7, InTech, Available from: <http://www.intechopen.com/books/fourier-transform-materials-analysis/fourier-transform-infrared-spectroscopy-for-natural-fibres>
202. Liang, C. Y. & Marchessault, R. H. Infrared spectra of crystalline polysaccharides. II. Native celluloses in the region from 640 to 1700 cm<sup>-1</sup>. *Journal of Polymer Science* **39**, 269-278, doi:[10.1002/pol.1959.1203913521](https://doi.org/10.1002/pol.1959.1203913521) (1959).
203. Wang, W., Sain, M. & Cooper, P. A. Study of moisture absorption in natural fiber plastic composites. *Composites Science and Technology* **66**, 379-386, doi:<http://dx.doi.org/10.1016/j.compscitech.2005.07.027> (2006).
204. Rudman, M., Blackburn, H. M., Graham, L. J. W. & Pullum, L. Turbulent pipe flow of shear-thinning fluids. *J. Nonnewton. Fluid Mech.* **118**, 33–48 (2004).
205. Dash, J., Patil, A. J., Das, R. N., Dowdall, F. L. & Mann, S. Supramolecular hydrogels

- derived from silver ion-mediated self-assembly of 5'-guanosine monophosphate. *Soft Matter* **7**, 8120 (2011).
- 206. Burg, K. J. L., Porter, S. & Kellam, J. F. 2000. Biomaterial developments for bone tissue engineering. *Biomaterials*, **21**, 2347-2359.
  - 207. Byrne, D. P., Lacroix, D., Planell, J. A., Kelly, D. J. & Prendergast, P. J. Simulation of tissue differentiation in a scaffold as a function of porosity, Young's modulus and dissolution rate: Application of mechanobiological models in tissue engineering. *Biomaterials* **28**, 5544-5554, doi:<http://dx.doi.org/10.1016/j.biomaterials.2007.09.003> (2007).
  - 208. Huebsch, N. et al. Matrix elasticity of void forming hydrogels controls transplanted-stem-cell-mediated bone formation. *Nature Materials* **14**, 1269, doi:[10.1038/nmat4407](https://doi.org/10.1038/nmat4407) <https://www.nature.com/articles/nmat4407#supplementary-information> (2015).
  - 209. Kim, S.-S., Sun Park, M., Jeon, O., Yong Choi, C. & Kim, B.-S. Poly(lactide-co-glycolide)/hydroxyapatite composite scaffolds for bone tissue engineering. *Biomaterials* **27**, 1399-1409, doi:<https://doi.org/10.1016/j.biomaterials.2005.08.016> (2006).
  - 210. Lao, L., Wang, Y., Zhu, Y., Zhang, Y. & Gao, C. Poly(lactide-co-glycolide)/hydroxyapatite nanofibrous scaffolds fabricated by electrospinning for bone tissue engineering. *Journal of Materials Science: Materials in Medicine* **22**, 1873-1884, doi:[10.1007/s10856-011-4374-8](https://doi.org/10.1007/s10856-011-4374-8) (2011).
  - 211. Karnesis, N. & Burriesci, G. Uniaxial and buckling mechanical response of auxetic cellular tubes. *Smart Materials and Structures* **22**, 084008, doi:[10.1088/0964-1726/22/8/084008](https://doi.org/10.1088/0964-1726/22/8/084008) (2013).
  - 212. Provaggi, E., Capelli, C., Rahmani, B., Burriesci, G. & Kalaskar, D. M. 3D printing assisted finite element analysis for optimising the manufacturing parameters of a lumbar fusion cage. *Materials & Design* **163**, 107540, doi:<https://doi.org/10.1016/j.matdes.2018.107540> (2019).
  - 213. Scarpa, F., Smith, F. C., Chambers, B. & Burriesci, G. Mechanical and electromagnetic behaviour of auxetic honeycomb structures. *The Aeronautical Journal (1968)* **107**, 175-183, doi:[10.1017/S0001924000013269](https://doi.org/10.1017/S0001924000013269) (2003).
  - 214. Ghanbari, H. et al. The anti-calcification potential of a silsesquioxane nanocomposite polymer under in vitro conditions: Potential material for synthetic leaflet heart valve. *Acta Biomaterialia* **6**, 4249-4260, doi:<https://doi.org/10.1016/j.actbio.2010.06.015> (2010).
  - 215. Ghanbari, H. et al. Polymeric heart valves: new materials, emerging hopes. *Trends in Biotechnology* **27**, 359-367, doi:<https://doi.org/10.1016/j.tibtech.2009.03.002> (2009).

216. Kidane, A. G. *et al.* A novel nanocomposite polymer for development of synthetic heart valve leaflets. *Acta Biomaterialia* **5**, 2409-2417,  
doi:<https://doi.org/10.1016/j.actbio.2009.02.025> (2009).
217. Frank, O. *et al.* Real-time quantitative RT-PCR analysis of human bone marrow stromal cells during osteogenic differentiation in vitro. *Journal of Cellular Biochemistry* **85**, 737-746,  
doi:[10.1002/jcb.10174](https://doi.org/10.1002/jcb.10174) (2002).
218. Ignatius, A. *et al.* Tissue engineering of bone: effects of mechanical strain on osteoblastic cells in type I collagen matrices. *Biomaterials* **26**, 311-318,  
doi:<https://doi.org/10.1016/j.biomaterials.2004.02.045> (2005).
219. Yang, X. *et al.* Bone to pick: the importance of evaluating reference genes for RT-qPCR quantification of gene expression in craniosynostosis and bone-related tissues and cells. *BMC Res Notes* **5**, 222-222, doi:[10.1186/1756-0500-5-222](https://doi.org/10.1186/1756-0500-5-222) (2012).
220. BOXCOUNT Box-Counting of a D-dimensional array (with D=1,2,3). Copyright (c) 2008, Frederic Moisy. All rights reserved.).  
(<https://www.mathworks.com/matlabcentral/fileexchange/13063-boxcount>) All Copyrights Reserved
221. 1<sup>st</sup> Year Progress Review Report, 2016, Ioannis Zampetakis
222. 2<sup>nd</sup> Year Progress Review Report, 2017, Ioannis Zampetakis
223. 3<sup>rd</sup> Year Progress Review Report, 2018, Ioannis Zampetakis
224. 4<sup>th</sup> Year Progress Review Report, 2019, Ioannis Zampetakis
225. Cactus bone: a new bioink for osteogenic tissue engineering, Undergraduate Dissertation, Edward Blackburn, 08/03/2018
226. Stintzing, F. C. & Carle, R. Cactus stems (*Opuntia* spp.): A review on their chemistry, technology, and uses. *Molecular Nutrition & Food Research* **49**, 175-194,  
doi:[10.1002/mnfr.200400071](https://doi.org/10.1002/mnfr.200400071) (2005).
227. Anderson, E. F., The Cactus Family, Timber Press, Portland, OR 2001, pp. 15 –72.

## 10 Appendix

### SEM Hydrogels With Cells



**Appendix Fig. 1** SEM Micrographs of stem cell containing Cactus Hydrogel composites demonstrating the cactus fibre embedded within the porous hydrogel matrix, demonstrating good cell adhesion while the porosity is maintained. The initial traits of stem cell adhesion on the cactus fibres initially observed in the confocal imaging are further observed here within the cactus composite hydrogel matrix showing the cells adhering on the cactus surface.

### **Impact Specimen Manufacturing and Testing**

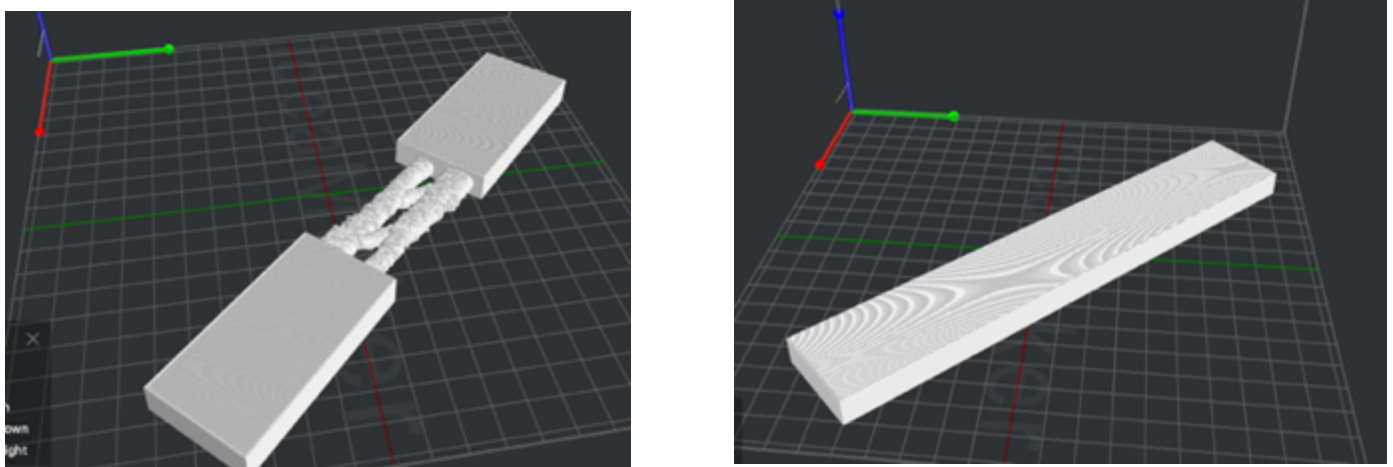
Dynamic bending measurements were obtained through performing impact drop tower tests on 3D printed cactus analogue specimens. The specimens manufactured for this test were designed so that the control and the cactus analogue specimens had the same boundary conditions and only the impact area was specific for cactus and control specimens (figure). Printer bed limitations did not allow to build bigger cactus samples thus the specimen dimensions were as follows:

Control: L=200 mm, W=35mm, T=10 mm

Cactus: L=200 mm, W=35mm (maximum width), T=10 mm

All impact tests were carried out on Instron Dynatup 9250HV at a total energy of 2 J. For these experiments only PLA printing was used with the 3D printer described above and due to the printed bed limitations, it was not possible to generate control samples that conformed with ASTM D5420 – 16 thus the comparison was only made with the equivalent beam control specimens.

An example of a dynamic bending loading scenario is an impact tower test. In order to perform this test specimens were designed with the same boundary conditions and thus an equivalent beam was designed with a beam impact area whereas the cactus specimens had the cactus as the impact area as shown on Fig.5.16. As it was briefly described in the methods due to manufacturing constraints the samples generated did not conform with ASTM standards for drop weight impact tests (ASTM D5420-16) and our comparison was limited between a cactus and equivalent beam impact area. **Additionally, printer bed limitations did not allow us for the generation of bigger and thus more reliable samples for testing this is why the work presented here is preliminary.** It is important to note that this is preliminary data with regards to impact and energy absorption of these cactus bioinspired materials however the initial data is encouraging.

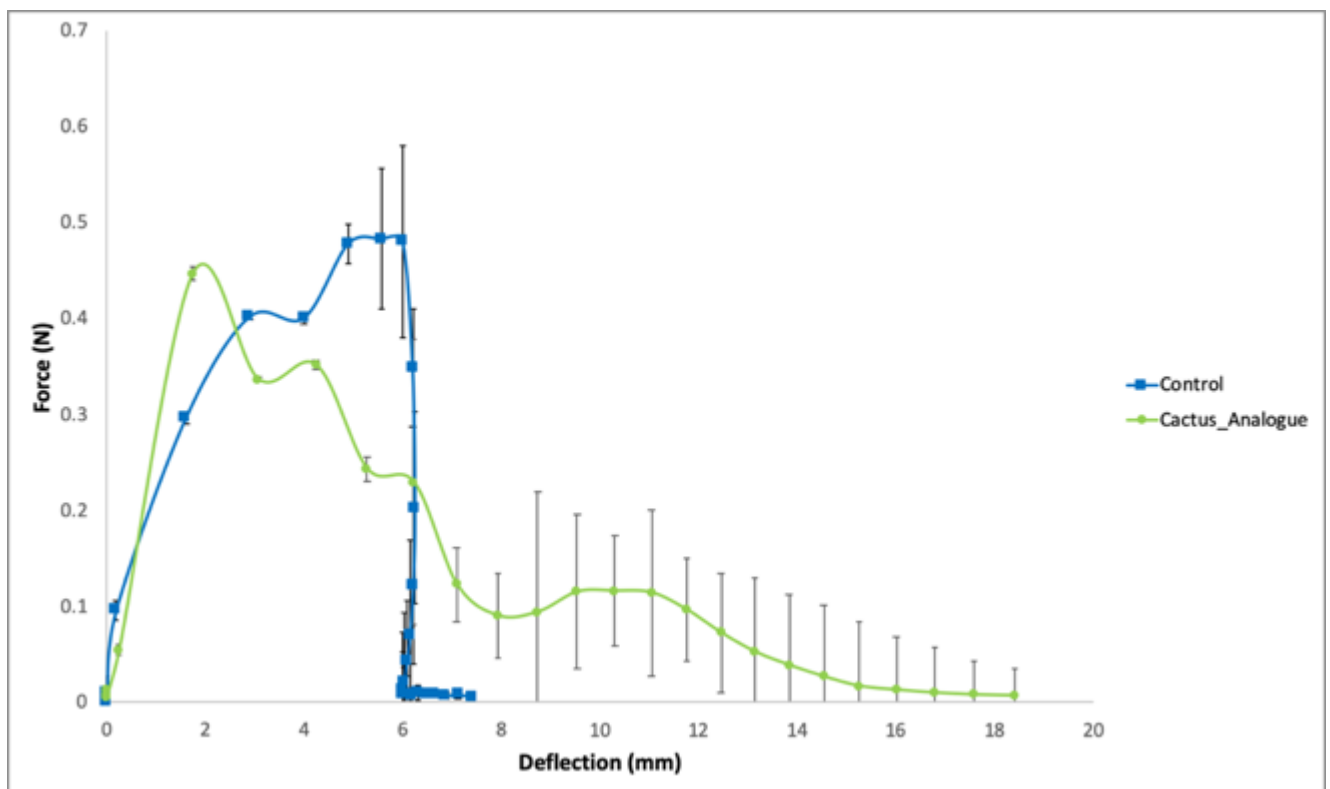


**Appendix Fig.2** (A) 3D Printed Impact specimen of the Cactus Analogue architecture, (B) Equivalent beam impact specimens.

As it is evidenced in Appendix Fig.2 and Appendix Table 1 the total energy of the cactus bioinspired specimens is comparable to the total energy absorbed from the control equivalent beam specimens. This combined with the fact that the cellular nature of the cactus bioinspired materials provides significant benefits in terms of weight saving there is potential demonstrated in the use of this novel bioinspired material in dynamic energy dissipation applications.

**Appendix Table 1** Impact Testing results and comparison between 3D Printed Control equivalent beams and cactus analogues (n=5).

	Total Energy (J)	Impact Energy (J)
Control	$2.28 \pm 0.02$	$1.92 \pm 0.01$
Cactus_Analogue	$1.83 \pm 0.27$	$2.1 \pm 0.003$



**Appendix Fig.3** Impact Testing Force vs Displacement results and comparison between 3D Printed Polylactic Acid (PLA) Control Equivalent beams and Cactus analogues. **This is solely experimental data and no simulation data is present.** (n=5)